# Biofilm formation under industrially-relevant conditions


Wendy Charlotte Allan

A thesis submitted to the University of Birmingham for the degree of DOCTOR OF PHILOSOPHY (PhD)

School of Chemical Engineering
College of Engineering and Physical Sciences
University of Birmingham
June 2021

# Abstract

Biofilms are considered to be one of the most prevalent and successful modes of life on Earth, and the prevailing lifestyle for microorganisms. Enabling bacteria to adapt to an incredibly diverse array of environments and extreme conditions, biofilms are a major contaminant of both medical and industrial settings. Indeed, approximately 80% of microbial infections are associated with biofilm formation, whilst the damage caused by biofilms in industry is estimated at between 2 – 3% of global GDP per annum. In this body of work, the effect of two industrially-relevant shear conditions on biofilm formation by the reference *Pseudomonas aeruginosa* (*Ps. a.*) strains PA01 and PA14 was investigated, as well as the effect of growth conditions and growth medium components on curli gene expression in *E. coli* K12 PHL644.

The CBC biofilm reactor was used to model low and high shear conditions at 75 RPM and 350 RPM respectively, and biofilms grown over a time period of 96 hours. High levels of the intracellular second messenger c-di-GMP are regarded as the determining factor for *Ps. a.* sessility and progression of the biofilm phenotype, thus the c-di-GMP-responsive *cdrA::gfp* reporter was used to measure intracellular c-di-GMP levels of PA01 and PA14 under low and high shear conditions. Biofilms were analysed via confocal laser scanning microscopy and staining of extracellular DNA (eDNA) and the exopolysaccharides Psl and Pel, which are all form crucial components of a self-produced and protective extracellular matrix that surrounds and enmeshes *Ps. a.* within a biofilm. Under high shear at 350 RPM, intracellular c-di-GMP levels of initially adhered (at 24 hours) bacteria were increased, resulting in increased production of

exopolysaccharides and formation of early aggregative structures. Shear conditions were shown to impact upon biofilm development and maturation of three-dimensional structures: crucially, mushroom-shaped macrocolonies, which are archetypal of *Ps. a.* biofilm formation, did not form under high shear. Under low shear at 75 RPM, Psl and Pel were organised into networks of fibre-like structures that penetrated throughout well-established basal biofilms (> 72 hours), which is in agreement with the work of others (with respect to Psl), but is a novel observation of Pel morphology as produced by PA14. The work presented in this thesis therefore provides further insight on the variety of Psl and Pel morphologies that exhibit different structures, spatial and temporal organisation, and function across PA01 and PA14 biofilms in response to either low or high shear conditions. Whilst similarities were observed between the two strains, PA01 and PA14 exhibited distinct responses to the imposed shear regime, in terms of initial surface colonisation, time taken for mature structures to emerge, and exopolysaccharide production.

Biofilms produced by *E. coli* PHL644 were grown using the Duran bottle model, via a method previously developed by the Overton laboratory. High levels of the transcriptional regulator CsgD are regarded as 'master switch' that determines biofilm formation in *E. coli*, thus the CsgD-responsive *csgB::gfp* reporter was used to measure curli gene expression in response to growth in LB broth (a rich medium) versus M63+ minimal medium, different concentrations of glucose (at 0 mM, 1 mM, 10 mM and 100 mM), and incubation at different temperatures (at 25 $^{o}$C, 28 $^{o}$C, 30 $^{o}$C and 37 $^{o}$C), and identify parameters which resulted in maximal expression of curli. Planktonic cell samples were taken from the tops of the Duran bottles, and sedimented cell samples

taken from the bottom of the Duran bottles for comparative analysis of growth via spectrophotometry at $OD_{600}$ and *csgB::gfp* fluorescence by flow cytometry. Curli gene expression was found to be highest in cultures grown in M63+ minimal medium, with a glucose concentration of 10 mM and at an incubation temperature of 30 $^{o}$C, which is in agreement with comparable studies in the literature. Of interest was the fact that an inverse relationship between biomass concentration (as defined by $OD_{600}$ values) and *csgB::gfp* fluorescence was observed. Curli gene expression in sedimented cell samples was consistently lower than that of planktonic cell cultures across all experimental subsets, suggesting that planktonic cells are physically more capable of surface attachment, and curli expression may be downregulated when in a sediment; exemplifying the importance and function of curli as the initial adhesin of *E. coli* K12.

Overall, this body of work concludes that different shear conditions can impact upon *Ps. a.* biofilm development and induce distinct organisation of the ECM, and that the CBC biofilm reactor is a suitable experimental model for assessing the impact of turbulent flow regimes, akin to those experienced in industrial manufacturing plants, on biofilm formation and composition. Additionally, this body of work also demonstrated that the Duran bottle model is also a suitable method for biofilm formation, and for investigating the effect of a wide array of growth conditions on *E. coli* K12 biofilm formation and curli gene expression. Parameters that resulted in maximal curli gene expression in *E. coli* K12 PHL644 cultures grown via the Duran bottle method under the conditions tested were identified, and could be further used to optimise production of a physically robust *E. coli* biofilm for use in biocatalysis or certain industrial settings.

*Dedicated to M.G.A, my beloved Grun*

# Acknowledgements

I would like to thank my primary supervisor, Dr Tim Overton for all of his support and guidance over the past four and a half years, both academically and pastorally. Tim, thank you for mentoring me over the course of the PhD project, your patience and wisdom have been absolutely invaluable, as have our conversations about the pampered lives of our cats and exploring places on Google maps. I have been so lucky to be a part of the Overton laboratory, and definitely could not have done this without you. To my secondary supervisors Dr Mark Webber (at the Quadram Institute in Norwich) and Dr Kevin Wright (at Procter and Gamble in Reading), thank you both for hosting me on visits to the laboratories, all the shared laughter and for all of your help and insights during the course of the PhD. Having the three of you as my supervisory team has been fantastic – I will always be incredibly grateful.

I would like to also extend thanks to Procter and Gamble, for part-funding this PhD, and to both the BBSRC and MIBTP, for the opportunity and for all that I have learnt about myself, both as a researcher and as an individual. Thank you to the Birmingham MIBTP directors, Professor Chris Thomas and Dr Tim Knowles, for all their help and assistance, especially during the pandemic.

To past technical staff in Biochemical Engineering, my lab 'moms' Elaine Mitchell and Ronnie Baglin, none of the work in this thesis would have been possible if not for all of your help and support. No query or problem was ever too much to ask of either of you to solve, and all of our impromptu chats in the prep. room and offices, setting the world to rights and fantasising about holiday destinations post-pandemic, will always mean so much to me. To the current technical staff – David, Angelica and Zoe, thank you for all of the help and assistance you have provided, especially David who always helped to fix and source numerous components of my reactor set up. I would also like to extend heartfelt thanks to Dr Alex Di Maio in Biosciences, for guidance on the confocal microscopes, and all of the kind words of encouragement and support.

Thanks are also due for fellow members of the Overton laboratory, whom I have had the pleasure of working alongside for the past four and a half years. To past members – Ikhlaas, Stacey, Maria C., and present – Pav, John, Dario, Ana, Parisa, Nasim, Terri-Anne and Alex O. – thank you for all of the chats, the laughter, shared tales of successes and woes, sanity checks and times at Staff House (as well as morning pilgrimages to McDonald's Alex!). To other students in Biochemical Engineering, Alex (aka Brean), Maria M., Nellie, Martin, Paolo, Ines and Anna – thank you for your friendship and help – Brean, maybe one day we'll finally use our voucher at The Country Girl in Selly! To my best squirrel-friends Jenny, Sel, Sophie, Georgie, Ben, Mark and Jaz, thanks for all your continued love, support and encouragement (I think I'm finally finished with higher education now, after nearly nine continuous years!)

## Acknowledgements (continued)

I would not have been able to complete this PhD without the unending love and encouragement of my family. Mom, Dad, Simon, Nan and Uncle Steve – words will never express how thankful I am for all of the support and Skype calls during the numerous lockdowns! I shall always be eternally grateful for the belief you all have in me. Thank you, for everything. To my parents-in-law, Sue and John, thank you for your love, encouragement and help over the past four and a half years, I could not have finished it without support from you both. Renn, thank you for all of the pep talks, the movie nights and heart-to-heart chats – I am so lucky to be able to call you my sibling, and would have been lost without you during the numerous lockdowns.

Finally, my greatest thanks are reserved for Dave, who has been with me every step of the way – from first meeting at our MIBTP induction in Warwick, to us becoming husband and wife – what an adventure we've had thus far! For bringing me snacks during all of my late nights in the laboratory on weekends, for teaching me how to use 'jazzy' software and code, and all the times you drove me to and from campus, no matter the weather or time, I thank you. For becoming my cheerleader and biggest fan during my write-up, supporting me through my ups and downs, I will always be eternally grateful – I love you, forever and always.

# Table of Contents

## Chapter 1: Introduction

## Table of Contents (continued)

### Chapter 1: Introduction (continued)



### Chapter 2: Material and methods

## Table of Contents (continued)

### Chapter 2: Material and Methods (continued)



### Chapter 3: Biofilm formation by PA14 under low shear conditions at 75 RPM versus high shear conditions at 350 RPM

## Table of Contents (continued)

# List of Figures

## Chapter 1: Introduction



## Chapter 2: Materials and methods



## Chapter 3: Biofilm formation by PA14 under low shear conditions at 75 RPM versus high shear conditions at 350 RPM

## List of Figures (continued)

### Chapter 3: Biofilm formation by PA14 under low shear conditions at 75 RPM versus high shear conditions at 350 RPM (continued)

## List of Figures (continued)

### Chapter 3: Biofilm formation by PA14 under low shear conditions at 75 RPM versus high shear conditions at 350 RPM (continued)



### Chapter 4: Biofilm formation by PA01 under low shear conditions at 75 RPM versus high shear conditions at 350 RPM

## List of Figures (continued)

### Chapter 4: Biofilm formation by PA01 under low shear conditions at 75 RPM versus high shear conditions at 350 RPM (continued)



### Chapter 5: Analysis of curli gene expression in the *Escherichia coli* strain K-12 PHL644

## List of Figures (continued)

### Chapter 5: Analysis of curli gene expression in the *Escherichia coli* strain K-12 PHL644

# List of Tables

## Chapter 2: Materials and methods



## Chapter 5: Analysis of curli gene expression in the *Escherichia coli* strain K-12 PHL644

## List of Abbreviations

| | |
|---|---|
| **Ag43** | Antigen 43 |
| **AHL** | *N*-acetylated homoserine lactone |
| **AI2** | Autoinducer II |
| **AI3** | Autoinducer III |
| **ALI** | Air-liquid interface |
| **BALM** | Biosciences Advanced Light Microscopy |
| **cAMP** | 3',5'-cyclic adenosine monophosphate |
| **CBR** | CDC biofilm reactor |
| **c-di-GMP** | Cyclic dimeric guanosine monophosphate |
| **CF** | Cystic fibrosis |
| **CFU** | Colony forming units |
| **ConA-TRITC** | Concanavalin A conjugated to tetramethylrhodamine |
| **CRP** | cAMP-receptor protein |
| **Dam** | Deoxyadenosine methylase |
| **DFR** | Drip flow biofilm reactor |
| **DGC** | Diguanylate cyclase |
| **dTDP** | Deoxythymidine diphosphate |
| ***E*** | RNA polymerase core enzyme |
| ***E. coli*** | *Escherichia coli* |
| **ECM** | Extracellular matrix |
| **eDNA** | Extracellular DNA |
| **EPS** | Extracellular polymeric substances |
| **FCM** | Flow cytometry |
| **FSC** | Forward scatter detector |
| **GDP** | Guanosine-diphosphate |
| **GTP** | Guanosine-5'-phosphate |
| **LB** | Luria-Bertani |
| **NA** | Nutrient agar |
| **$OD_{600}$** | Optical density at 600 nm |

## List of Abbreviations (continued)

| | |
|---|---|
| **PBS** | Phosphate buffered saline |
| **PDE** | Phosphodiesterase |
| **PE** | Polyethylene |
| ***pel*** | Pellicle gene locus |
| **pGpG** | 5'-phosphoguanylyl-(3'-5')-guanosine |
| **PNAG** | Poly-β-1,6-N-acetylglucosamine |
| **PQS** | *Pseudomonas* Quinolone Signal |
| ***Ps. a.*** | *Pseudomonas aeruginosa* |
| ***psl*** | Polysaccharide synthesis **l**ocus |
| **P&G** | Procter and Gamble |
| **QS** | Quorum sensing |
| **QscR** | Quorum sensing control repressor |
| **RD** | Robbins device |
| **SSC** | Side scatter detector |
| **TFP** | Type IV pili |
| **TPS** | Two-partner secretion |
| **TSA** | Tryptic soy agar |
| **TSB** | Tryptic soy broth |
| **UDP** | Uridine-diphosphate |
| **Vfr** | Virulence factor regulator |
| **VqsR** | Virulence quorum sensing regulator |
| **WCB** | Working cell bank |
| **WGA** | Wheat Germ Agglutinin conjugated to Alexa Fluor 633 |
| $\sigma^s$ | Sigma factor encoded by *rpoS* |
| **3-oxo-$C_{12}$-HSL** | *N*-(3-oxo-dodecanoyl)-L-homoserine-lactone |
| **$C_4$-HSL** | *N*-(butanoyl)-L-homoserine-lactone |
| **$C_4H_4Na_2O_4$** | Sodium succinate |
| **$FeSO_4$** | Ferrous sulfate |
| **$KH_2PO_4$** | Potassium phosphate monobasic |
| **$MgSO_4$** | Magnesium sulfate |

# Chapter 1: Introduction

# Chapter 1: Introduction

Throughout nature, cooperation of individuals within a community is known to beneficial for a variety of advantages that solitary life does not provide, including protection from predation, starvation and adverse environmental conditions (Mann and Wozniak, 2012). Whilst this notion is easily spotted in a variety of animal species (including flocks of birds, herds of mammals, schools of fish and colonies of insects), it may be surprising to note that there is evidence in the early fossil record of putative community organisation by microorganisms over 3.2 billion years ago, forming structures now referred to as biofilms (Costerton, 1978; Rasmussen *et al.,* 2000; Westall, *et al.* 2001). Analogous biofilm structures can still be found in contemporary hydrothermal environments such as deep-sea vents and hot springs (Taylor *et al.,* 1999; Reysenbach and Cady, 2001), and the visual characteristics of biofilms that form under various natural and artificial environmental conditions are notably similar to one another (Hall-Stoodley *et al.,* 2004). Similarly to the advantages acquired by *Animalia* communities, the convergence of community organisation within microbial biofilms enables bacteria to adapt to an incredibly diverse array of environments and extreme conditions.

## 1.1.1. Definition of a biofilm

A biofilm can be described as an assemblage of bacterial cells that are encased in a protective extracellular matrix (ECM) that is self-produced and can be composed of polysaccharide material or lipids (Donlan, 2002; Hall-Stoodley *et al.*, 2004; Branda *et al.,* 2005; Ma *et al.,* 2009). Whilst the term biofilm predominantly refers to a solid,

surface-attached structure, it can also be used in reference to suspended filamentous structures (known as streamers) or biofilms that have formed at the air-liquid interface of standing cultures, termed pellicles (Rusconi *et al.,* 2010). Able to form on both abiotic and biotic surfaces, the ECM creates a niche environment that facilitates cell-cell interaction and communication; providing a reservoir of metabolites for promotion of growth in addition to protection of bacteria from their external, surrounding environment outside of the biofilm (Flemming and Wingender, 2010). Biofilms can be composed of a single species of bacteria, or a collective of multiple species and other microorganisms including fungi (Beloin *et al.,* 2008; Flemming *et al.,* 2016).

Geesey *et al.,* (1977), revealed that in both natural environments and those under human influence, over 99% of resident bacteria are surface-attached, with the ratio of sessile to planktonic cells often greater than $10^3$ – $10^4$:1. Indeed, biofilms are considered to be one of the most prevalent and successful modes of life on Earth (Stoodley *et al.,* 2002), and the prevailing lifestyle for microorganisms (Watnik and Kolter, 2000). Microbial cells encased within the ECM are able to withstand multiple environmental pressures, including UV radiation; extremes in both temperature and pH; high salinity; high pressure; mechanical and shear forces; nutrient depravation; the risk of desiccation, and chemical agents including antibiotics and anti-fouling compounds (Harrison *et al.,* 2007; Hostacká *et al.,* 2010; Yang *et al.* 2011; Kim and Chong, 2017; Hathroubi *et al.,* 2017; Marsden *et al.,* 2017; Singh *et al.,* 2017; Hou *et al.,* 2018).

### 1.1.2. Bacterial biofilms in medical settings

According to the National Institute of Health (Davies, 2003; Karatan and Watnick, 2009; Joo and Otto, 2012; Jamal *et al.,* 2018), up to 80% of microbial infections are associated with biofilm formation, including but not limited to native-valve endocarditis, periodontitis, osteomyelitis, pyelonephritis and otis media (Donlan, 2002; Hall-Stoodley *et al.,* 2004; Bjarnsholt, 2013; Chau *et al.,* 2014; Veerachamy *et al.,* 2014; Gupta *et al.,* 2016). Formation of biofilms is also archetypal of chronic infections, such as non-healing wounds, cystic fibrosis and chronic prostatitis; indicative of disease progression, long-term persistence and increased morbidity and mortality for affected patient populations (Spoering and Lewis, 2001; Donlan, 2002; Kiedrowski and Horswill, 2011; Majik and Parvatkar, 2014).

Of further concern is the fact that biofilm formation is also associated with nosocomial (hospital-acquired) infections, which are demarcated as the fourth leading cause of death in the USA; resulting in 2 million cases annually and an additional cost of $5 billion per annum to the medical sector (Wenzel, 2007). An estimated 60 – 70% of nosocomial infections are correlated to the use of implanted medical devices, of which in the USA alone, approximately 5 million are used per annum (Spoering and Lewis, 2001; Bryers, 2008; Majik and Parvatkar, 2014). Catheter-associated urinary tract infections are the most prevalent nosocomial infection, accounting for 40% of all nosocomial infections globally (Hooton *et al.,* 2010).

Contamination of prosthetic and implantable devices can occur during surgery or during recovery, with factors such as biomaterial composition, implant surface

hydrophilicity, surface charge and surface energy associated with the increasing rate of infection of devices (Ribeiro *et al.,* 2012; Koseki *et al.,* 2014; Tran *et al.,* 2015; Roehling *et al.,* 2017). Furthermore, there is always an inherent chance of bacteria re-colonising new implantable surfaces (Oliveira *et al.,* 2018) or being transmitted from patient to patient (Russotto *et al.,* 2015), as the bacterial load required to colonise such surfaces is up to $10^4$ less than in comparison to native tissue surfaces (Zimmerli *et al.,* 2004; Vergidis and Patel, 2012; Nowakowska *et al.,* 2014). In spite of the $180 billion per annum industry relating to the worldwide production of prostheses, implants and materials related to tissue-engineering, all medical devices or tissue-engineered constructs remain at risk of microbial colonisation, and thus biofilm formation (Bryers and Ratner, 2004; Castelli *et al.,* 2006; Bryers, 2008).

### 1.1.3. Bacterial biofilms in industrial settings

Biofouling in industry is defined by the undesired formation of organic deposits upon a surface (Characklis, 1981). Microbial biofouling occurs as a result of biofilm formation and development, whilst macrobial biofouling involves the subsequent deposition and growth of organisms such as barnacles and mussels (Characklis, 1981). Many industries are affected by microbial biofouling, including but not limited to bottling or wine industries, food production, the dairy industry, production plants, power plants, water and marine industries, and even construction (Vishwakarma, 2019).

In industry, the consequences of uncontrolled microbial fouling are numerous: it can negatively affect the energetic efficiency of processes; cause surface corrosion and material deterioration; decrease product quality due to contamination, and can

eventually release opportunistic or pathogenic microorganisms (such as *Legionella* in aerosol form, from biofilms in cooling towers), leading to their dissemination in the environment and the promotion of disease (Characklis, 1981; Costerton *et al.,* 1999; Ludensky, 2003; Srey *et al.,* 2013; Liu *et al.*, 2014; Lemos *et al.,* 2015). Indeed, the damage caused by biofilms in industry is estimated at between 2 – 3% of global GDP per annum (http://engage.innovateuk.org/technologystrategyboardlz/lz.aspx?p1=050 46241S4354&CC=&w=7804&cID=0&cValue=1).

Biofilm control in industry is maintained through the use of biocides to disinfect surfaces and incapacitate microorganisms, but this is often ineffective as removal of the biomass itself is neglected (Cloete *et al.,* 1998; Mah and O'Toole, 2001; Faille *et al.,* 2013). Mechanical cleaning, illustratively by either pigging to remove deposits in pipelines (Flemming, 2011) or through the use of ultrasonic treatment of surfaces in the food industry (Boulangé-Petermann, 1996), whilst successful, is dependent upon system design, as some pipelines can only be reached via chemical cleaning (Cloete, 2003). In areas of industrial plants where the flow rate is low, such as in crevices, corners of tubing and pipelines, dead zones and surrounding valves, stagnation can occur; promoting accumulation of bacteria and persistence of the biofilm, as well colonisation of other surfaces if parts of the biofilm become detached and transported downstream through the plant (Brooks and Flint, 2008; Manuel *et al.,* 2009). Due to their self-produced and protective ECM, bacteria sequestered within biofilm structures are known to exhibit resistance and increased tolerance to biocidal treatments, including disinfectants and antimicrobial compounds (Stewart and Costerton*,* 2001; Høiby *et al.,* 2010).

### 1.1.4. General biofilm formation and lifestyle

The transition from a planktonic to sessile mode of growth in a biofilm occurs in response to environmental changes, and requires the collective effect of multiple regulatory networks and concerted changes in gene expression to facilitate the spatial and temporal reorganisation of the bacterial cell (Pratt and Kolter, 1998; O'Toole *et al.,* 2000; Prigent-Combaret *et al.,* 2001; Parsek and Singh, 2003; Monds and O'Toole, 2009). Whilst the precise mechanism of biofilm formation and the resultant biofilm architecture and ECM components vary between different bacterial species, the process of surface-associated biofilm formation can be summarised by five principal stages: initial and reversible attachment, irreversible attachment, colonisation, maturation and finally detachment or dispersal (Figure 1.1) (O'Toole *et al.,* 2000; Palmer *et al.,* 2007; Taylor *et al.,* 2014).

When a bacterium comes into contact with a surface, it can become loosely adhered to the substratum via one pole of the cell, and is able to detach and re-attach to the surface (Agladze *et al.,* 2005; Petrova and Sauer, 2012). During this stage (known as reversible attachment), bacteria are subject to Brownian motion, and may spin, vibrate or move rapidly across a surface (Sauer *et al.*, 2002; Toutain *et al.*, 2007). The boundary layer above a surface is hydrodynamic, and can repel bacteria due to the net negative electrostatic forces present (Pratt and Kolter, 1999; Goulter *et al.*, 2009). Additionally, there are drag and frictional forces that have to be overcome in order for a bacterium to make contact with a surface (Goulter *et al.*, 2009; Petrova and Sauer, 2012). Local nutrient levels, pH, ionic strength and temperature can result in the presence of attractive or repulsive forces that are able to affect the velocity and

direction of bacteria either moving toward or away from a contact surface (Donlan, 2002; Kostakiotki *et al.,* 2013). Furthermore, physical conditions such as the presence of a conditioning film upon a surface, surface topography and roughness, and weak interactive forces such as van der Waals also mediate initial surface attachment (Tuson and Weibel, 2013).

**Figure 1.1**
**The general formation of a biofilm can be summarised by five distinct stages**

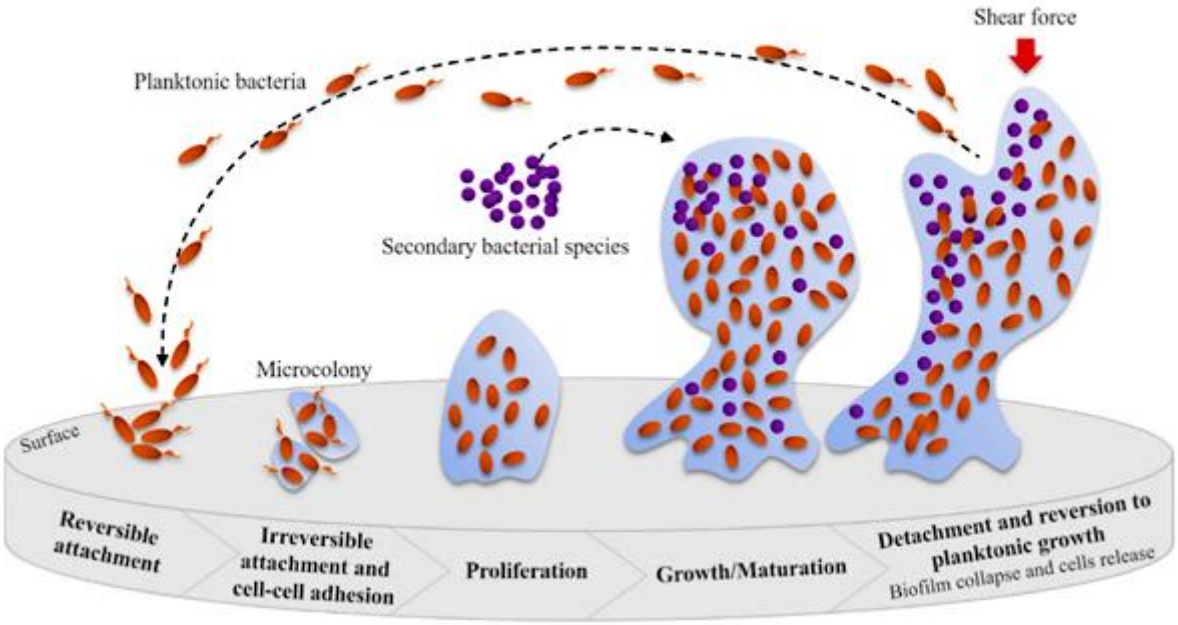


The five stages of biofilm development can be summarised as follows: planktonic bacteria that come into contact with a suitable surface will detach and re-attach reversibly, until maintained cell-surface and cell-cell interactions result in sessility via irreversible attachment. The production of a protective extracellular matrix (shown in blue) enables the biofilm to grow and mature, forming complex three-dimensional structures such as macrocolonies by either a single or multiple species of bacteria. Finally, detachment (which limits the overall accumulation of biomass by the structures) occurs: either passively, as a result of increased shear force causing erosion or sloughing of parts of the biofilm, or actively via dispersion, enabling the translocation of bacteria to new surfaces for colonisation and thus continuation of the biofilm lifestyle.

Figure taken from Pinto *et al.,* (2020)

Motile bacteria can additionally utilise flagella to overcome both repulsive and hydrodynamic forces (Kostakioti *et al.,* 2013). Within the literature the importance of flagellar motility for initial attachment has been documented in a variety of species, including *Pseudomonas aeruginosa* (*Ps. a.*), *Vibrio cholerae*, *Listeria monocytogenes* and *Escherichia coli* (*E. coli*) (O'Toole and Kolter, 1998; Watnick and Kolter, 1999; Lemon *et al.,* 2007; Toutain *et al.,* 2007). In some bacterial species, chemotaxis can also be used to direct attachment. Mutations in the CheR1 methyltransferase were shown by Schmidt *et al.,* (2010), to result in impaired surface sensing by *Ps. a.*, whilst Hadjifrangiskou *et al.,* (2012), demonstrated that disruption to the methyl-accepting chemotaxis protein II in uropathogenic *E. coli* results in perturbed biofilm phenotypes.

The transition from reversible to irreversible attachment can be defined by the ability of surface-associated bacteria to withstand shear forces and maintain contact with the surface (Kostakioti *et al.,* 2013). Attachment of a bacterium to a surface via the long axis of its cell, as well as the use of extracellular appendages and secreted adhesins, results in irreversible attachment (Zobell, 1943; Jensen *et al.,* 1992; O'Toole and Kolter, 1998b). More stable than reversible attachment, irreversible attachment is regarded as the first phase in biofilm formation, and is associated with the establishment of a monolayer of colonising cells upon a surface (Monds and O'Toole, 2009). Whilst surface motility facilitates exploration of an environment, downregulation of motile elements has to occur in order to support sessility and surface colonisation. Gram negative bacteria, including *Ps. a.*, *Neisseria meningitidis* and enterotoxigenic *E. coli* are known to undergo transcriptional changes that are contact-dependent (Dietrich *et al.*, 2003; Kansal *et al.*, 2013; Siryaporn *et al.*, 2014). Such changes can

illustratively affect the production of virulence factors or toxins, as well as Type IV pili tension on a surface (Moorthy *et al.*, 2016; Newman *et al.,* 2017; Floyd *et al.*, 2017).

Maturation of the biofilm leads to the development of microcolonies (and subsequently macrocolonies) that result in a more distinctive, three-dimensional structure with pronounced architectural features. Mature biofilm colonies are densely packed with bacterial cells embedded in the ECM, and can result in the development of pillar- and mushroom-shaped masses that project outwards, and can reach several hundreds of microns in height (Hall-Stoodley *et al.,* 2004). This stage of the biofilm lifestyle is characterised by the upregulation of genes involved in the synthesis of extracellular polymeric substances (EPS) such a polysaccharides, proteins, lipids and DNA (Flemming *et al.,* 2007; da Costa Lima *et al.,* 2018; Di Martino, 2018). EPS exhibit both diverse structures and functions, but all are highly hydrated polymers that are fundamental to ECM formation during biofilm maturation (Flemming *et al.,* 2007). EPS are distributed through the biofilm in a heterogenous pattern (Houari *et al.,* 2008), interacting with one another to form the encompassing ECM, as well as with bacterial cells to confer both cohesion and viscoelastic properties to the biofilm structure (Shaw *et al.,* 2004; Payne and Boles, 2016).

A passive process, detachment is regarded as the principal mechanism that limits overall accumulation of biofilm biomass, and refers to the release of parts of the biofilm as a result of mechanical or shear stress (van Loosdrecht *et al.,* 1997; Kaplan, 2010). Erosion and sloughing are two distinct forms of detachment that both denote loss of biofilm cells due to fluid frictional forces: erosion refers to the removal of small amounts

of the biofilm, whilst sloughing may result in the loss of intact pieces of biofilm or the whole structure itself (Bryers, 1988; Telgmann *et al.,* 2004; Flemming *et al.,* 2011). By contrast, dispersion (the final stage of the biofilm lifestyle) demarcates the process of bacteria leaving the biofilm, through the en-masse transition of formerly sessile, matrix-encased cells to the planktonic mode of growth (Rumbaugh and Sauer, 2020). A dynamic process, dispersal results in the active 'escape' of either matrix-encased or single cells from the biofilm; leaving behind biofilms with visible cavities or central voids (Sauer *et al.,* 2002; Stoodley *et al.,* 2005; Petrova and Sauer, 2007). Often referred to as 'seeding dispersal', dispersion contributes to bacterial survival; enabling the translocation of bacteria to new surfaces for colonisation, and thus continuation of the biofilm lifestyle (Purevdorj-Gage *et al.,* 2005).

## 1.2. *Pseudomonas aeruginosa* and biofilm components

### 1.2.1. *Pseudomonas aeruginosa*

*Ps. a.* is a Gram negative bacillus of unipolar motility that ubiquitously inhabits the soil and surfaces of aqueous environments; also forming a constituent part of the normal skin flora of humans (Sousa and Pereira, 2014). *Ps. a.* is one of the most important model organisms regarding the study of biofilms, due to the relative ease of growing structured biofilms under laboratory conditions that are both consistent and reproducible (Taylor *et al.*, 2014). In addition, *Ps. a.* is of great clinical significance as the causal agent of both acute and chronic infections in a variety of patient populations (Gellatly and Hancock, 2013).

### 1.2.2. Surface organelles

#### *1.2.2.1. Flagellum*

Flagella are long, helical and rotatable extracellular appendages that enable bacterial dissemination in liquid, across semi-solid surfaces and at surface interfaces (Haiko and Westerlund-Wilkström, 2013). Over 80% of known bacterial species possess flagella and in Gram negative bacteria, such as *Ps. a.* and *E. coli*, the flagellum machinery spans across both the inner and outer membranes (Moens and Vanderleyden, 1996). Whilst the structure and arrangement of flagella on the cell-surface is both species- and environment- dependent (Joys, 1988; Wilson and Beveridge, 1993), flagellar motility is advantageous; enabling bacteria to move either towards or away from favourable or detrimental conditions, colonise surfaces and to successfully compete with other microorganisms (Fenchel, 2002; Soutourina and Bertin, 2003). In *Ps. a.*, flagella-mediated swimming can overcome surface repulsion, and cell spinning is indicative of flagella attachment to a surface (Toutain *et al.*, 2007; Petrova and Sauer, 2012).

*Ps. a.* expresses a single, polar flagellum that is a polymer, composed of flagellin subunits: the helical N- and C-termini of the flagellin monomers form the inner core and enable polymerisation into a filament, whilst the outer surface of the flagellum is composed of the middle residues (Vonderviszt and Namba, 2013). The flagellum of *Ps. a.* is a motorised structure composed of a rotor, two stators, a flagella hook and filament proteins; anchored into the cell membrane via several ring structures (Figure 1.2) (Ha and O'Toole, 2015). Powered by a transmembrane proton (or sodium ion) gradient (Hirota and Imae, 1983; Blair 2003; Toutain *et al.*, 2005), the rotor unit dictates

the directional movement of the flagella (clockwise or anticlockwise), and sits within the stator (Francis *et al.*, 1994; Kojima and Blair, 2004).

**Figure 1.2**
**Structure of the flagellar apparatus**

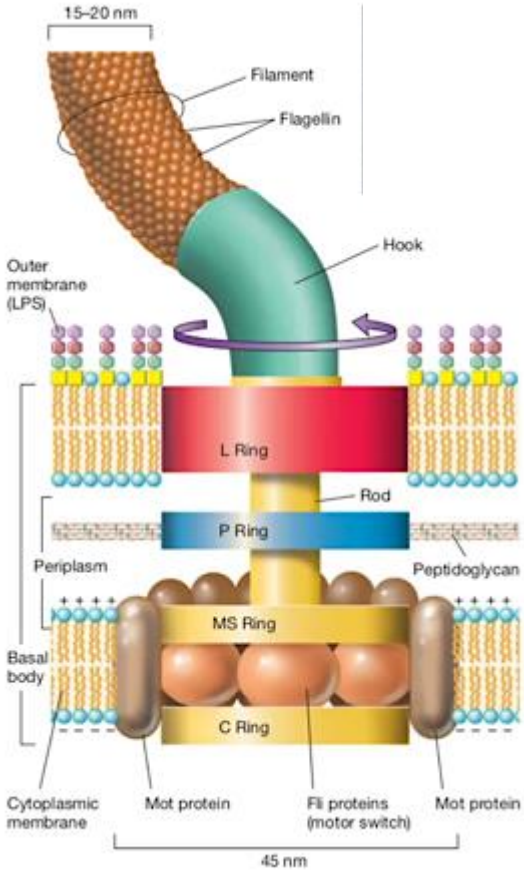


Scaled representation of the conserved flagellar apparatus in Gram negative bacteria. The hook (green) connects the filament structure (composed of flagellin subunits) to the motor area of the apparatus, known as the basal body. The basal body is a rod-shaped structure anchored into three layers of the cell wall by several encompassing rings: the L ring located within the outer membrane (red), the P ring anchored within the peptidoglycan layer (blue), and the MS and C rings (yellow), which are anchored in the inner (cytoplasmic) membrane and to the cytoplasm respectively. Mot proteins surround the MS and C rings, and act as the stators for the motorised part of the flagellar apparatus, complexed to the C ring which acts as the rotor, resulting in movement of the extracellular filament structure. The motor switch is comprised of Fli proteins, which can reverse rotation of the flagellum upon interactions with intracellular signalling molecules or in response to chemotaxis.

Figure taken from https://microbeonline.com/bacterial-flagella-structure-importance-and-examples-of-flagellated-bacteria/

The genome of *Ps. a.* contains single copies of the *fliC* and *fliD* genes, encoding for flagellin subunits and a cap protein respectively (Toutain *et al.*, 2007; Petrova and Sauer, 2012). Comparison of the amino acid sequences of *fliC* genes from a variety of *Ps. a.* strains revealed that two distinctive flagellin protein types of differing molecular weights and structures (classified as type-a and type-b) are synthesised, with type-a flagellins being more heterogenous than type-b flagellins (Allison *et al.*, 1985; Arora *et al.*, 2001). *Ps. a.* strain PA01 for example expresses type-b flagellin, whilst the majority of clinical isolates encode type-a flagellin (Arora *et al.,* 2001). FliD is an important structural component of the *Ps. a.* flagellum: a flagellar cap protein located at the tip of the flagellum, FilD is a mucin-specific adhesin that is exposed to a bacterium's external surroundings and its selective environmental pressures (Toutain *et al.,* 2007).

The two stator units, MotAB and MotCD, are both required for initial polar attachment to a surface (Toutain *et al.*, 2005; Petrova and Sauer, 2012). First reported by Kato *et al.*, (1999), mutations in either stator resulted in retarded attachment of *Ps. a.* PA01, and deletion of MotAB and/or MotCD results in strains that, whilst able to synthesise a flagellum (Enomoto, 1966; Dean *et al.*, 1984), were unable to rotate properly and only able to move via swimming motility, albeit at a reduced speed compared to wild-type PA01 and PAK strains (Doyle *et al.*, 2004). MotAB (but not MotCD) additionally facilitates irreversible attachment, which is the first step in progression toward sessility and biofilm formation (Petrova and Sauer, 2012; Ha and O'Toole, 2015). Toutain *et al.*, (2005), showed that downregulation of *motAB* results in a significant proportion of cells attaching via their axis to a surface (rather than the cap protein FliD); transitioning into the irreversible attachment phase.

#### *1.2.2.2. Type IV pili*

Type IV pili (TFP) are an additional motile appendage that mediates bacterial cell attachment to both abiotic and biotic surfaces, and initiation of biofilm formation in *Ps. a.* (O'Toole and Kolter, 1998). Similarly to the flagellum being composed of flagellin subunits, TFP are composed of polymers of the PilA protein (known as pilin) that can be reversibly assembled and disassembled to propel bacteria laterally across semi-solid surfaces (Sastry *et al.,* 1985; Mattick, 2002; Dasgupta *et al.*, 2003). In Gram negative bacteria, pilin subunits are held together by non-covalent interactions, whilst Gram positive pili are polymers composed of pilin subunits that are covalently bonded together via a sortase enzyme (Beaussart *et al.*, 2014). *Ps. a.* expresses several TFP located at the same pole of the cell (Rashid and Kornberg, 2000), with Skerker and Berg (2001), observing that individual pili on the same cell were able to extend and retract rapidly and independently of one another, at an average rate of 0.5 μm per second, with an estimated retraction force of 10 pN.

Beaussart *et al.*, (2014), used different force microscopy techniques (atomic, chemical and single-cell force microscopies) to discern how *Ps. a.* TFP adhere to surfaces. Chemical force microscopy revealed that *Ps. a.* TFP are mechanically robust, with individual pili able to withstand mechanical forces of up to 250 pN each (Beaussart *et al.*, 2014). By comparison, TFP on *Neisseria gonorrheae* have been observed to withstand forces of up to 100 pN, with pili becoming narrower and longer in structure under such conditions (Biais *et al*., 2008). Atomic force microscopy has also been used to show that P-pili and Type I pili from Gram negative bacteria such as *E. coli* are able to readily become longer when under mechanical stress to yield constant force

plateaus, as a result of confirmational changes to the protein's quaternary structure (Miller *et al.*, 2006; Dufrêne *et al.,* 2014). In response to mechanical or shear stress, *Ps. a.* TFP are able to transition into an extended quaternary structure through protein unfolding, which in turn exposes previously-hidden amino acid residues that are thought to either promote adhesion, or to act as a signal that demarcates strong attachment to the surface (Beaussart *et al.*, 2014). Furthermore, evidence presented by Anyan *et al.,* (2014), suggests that TFP can promote cell-cell associations, and control the collective movement of *Ps. a.* cell populations through TFP-TFP interactions. Such interactions may occur as a precursor to biofilm formation, as observed in *Vibrio cholerae* (Jude and Taylor, 2011), enabling *Ps. a.* to quickly colonise new surfaces through fast and synchronised translocation of the bacterial population (Shrout *et al.,* 2006; Caiazza *et al.*, 2007; Barken *et al.,* 2008; Burrows, 2012).

### 1.2.3. EPS and matrix composition

#### *1.2.3.1. Psl*

In 1989, a neutral EPS was purified from a clinical *Ps. a.* immunotype 4 isolate, and found to contain D-mannose, D-glucose and L-rhamnose residues (Kocharova *et al.,* 1989). The same constituents were identified by Rocchetta *et al.,* (1998), and Wozniak *et al.,* (2003), during analysis of an EPS derived from *Ps. a.* PA01, and recognised by several other research groups through the use of *Ps. a.* strains incapable of synthesising alginate, but still able to colonise solid glass substrata and form biofilms (Friedman and Kolter, 2004a; Jackson *et al.,* 2004; Mastukawa and Greenberg, 2004). The first 3 genes of the polysaccharide synthesis locus (*psl*) were identified in 1998, and their role in the production of a putative polysaccharide originally intimated based

on sequence similarity to genes involved in the synthesis of the polysaccharides colonic acid (in *E. coli* and *Salmonella spp.*) and xanthan gum (in *Xanthomonas campestris*) (Chou *et al.,* 1997; Rocchetta *et al.,* 1998; Stevenson *et al.,* 2000).

Psl has a distinct chemical structure, composed of a pentameric repeat of D-mannose, D-glucose and L-rhamnose moieties (Figure 1.3) (Byrd *et al.,* 2009). The Psl polymer is made from the sugar-nucleotide precursors guanosine diphosphate (GDP)-D-mannose, uridine diphosphate (UDP)-D-glucose and deoxythymidine diphosphate (dTDP)-L-rhamnose from the sugar nucleotide pool (Byrd *et al.,* 2009). Each sugar-nucleotide precursor is synthesised via its own distinct pathway, and the precursors can either be directly incorporated into the elongating polymer chain, or modified before incorporation (Rocchetta *et al.,* 1998; Whitfield and Roberts, 1999).

**Figure 1.3**
**Chemical structure of the Psl polysaccharide**

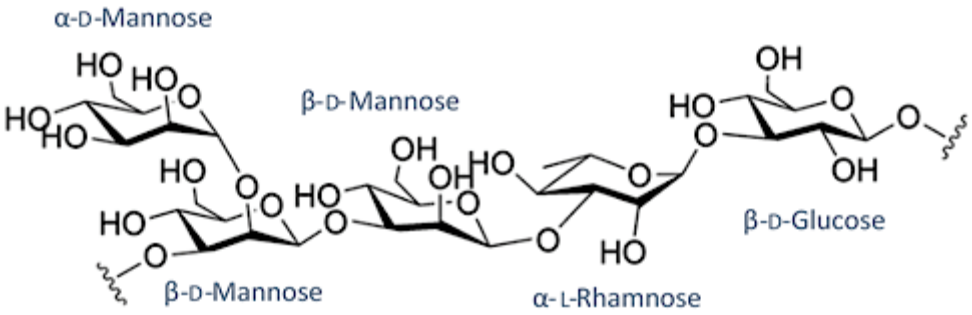


Figure adapted from Liang, 2015

The *psl* locus consists of 15 genes (*pslA* to *pslO*, gene cluster PA2231 – PA2245) spanning an 18.8 kb region of the *Ps. a.* PA01 genome (Friedman and Kolter, 2004a; Jackson *et al.,* 2004; Mastukawa and Greenberg, 2004). Of these, 11 genes

(*pslACDEFGHIJKL*) are co-transcribed and requisite for the synthesis and export of Psl, whilst the remaining 4 (*pslB*, *pslM*, *pslN* and *pslO*) are not required (Byrd *et al.,* 2009; Franklin *et al.,* 2011). Data from transcriptional profiling revealed that the *pslMNO* genes are not co-transcribed with *pslABCDEFGHIJKL* genes (Goodman *et al.,* 2004; Starkey *et al.,* 2009). Furthermore, the gene products of *pslMNO* have no known homologs in *Ps. a.*, nor are functionally associated with synthesis of a polysaccharide (Stover *et al.,* 2000; Friedman and Kolter, 2004b; Jackson *et al.,* 2004). The second gene in the *psl* locus, *pslB*, is not essential for Psl production as it shares functional redundancy with *wbpW* (Rocchetta *et al.,* 1998; Jackson *et al.,* 2004; Lee *et al.,* 2008). In *Ps. a.* PA01, *pslB* and *wbpW* encode for bifunctional phosphomannose isomerase/GDP-D mannose pyrophosphorylases that are functionally interchangeable for production of the GDP-D-mannose precursor necessary for Psl synthesis (Byrd *et al.,* 2009; Franklin *et al.,* 2011).

Psl is essential for initial attachment to abiotic and biotic surfaces by several *Ps. a.* strains, and is able to form a primary scaffold upon which development of a biofilm can occur (Ma *et al.,* 2006; Byrd *et al.,* 2009; Byrd *et al.,* 2010). *Ps. a.* can additionally deposit trails of Psl upon a surface which influences the motility of subsequent bacterial cells attaching to the surface, further initiating biofilm formation (Zhao *et al.,* 2013). PslA and PslD have been shown to be essential for biofilm formation in *Ps. a.* PA01, with comparative attachment analyses demonstrating that a PA01Δ*pslA* mutant was significantly attenuated with respect to both initial attachment and biofilm development (Overhage *et al.,* 2005; Campisano *et al.,* 2006).

Through the use of Psl-specific lectins, Ma *et al.,* (2009), were able to directly visualise Psl formation and localisation at different stages of biofilm formation. During initial surface attachment, Psl was found to associate with the bacterial cell surface, anchored in a helical pattern around the cell; stabilising Psl-Psl interactions between adjacent bacteria, and resultantly enhancing cell-surface and intercellular interactions (Ma *et al.*, 2009; Wei and Ma, 2013). Mature biofilms were observed to have two distinct architectures: a flat monolayer with equal distribution of the cell-associated Psl matrix, or three-dimensional microcolonies with Psl accumulation at the periphery of structures, and minimal amounts of Psl in the interior cavities of the microcolonies (Ma *et al.,* 2009). Crucially, Psl is the primary EPS produced by *Ps. a.* PA01, whilst PA14 is incapable of producing Psl, due to a deletion of *pslA* to *pslD* in its genome (Friedman and Kolter, 2004a; 2004b).

#### *1.2.3.2. Pel*

In addition to forming biofilms on solid surfaces, *Ps. a.* is able to form biofilms at the air liquid interface (ALI) of standing cultures, forming structures known as pellicles (Ryder *et al.,* 2007). *Ps. a.* strain PA14 is capable of forming robust pellicles at the ALI, with Friedman and Kolter, (2004a), observing the development of a distinct architecture of bacterial cells embedded in an opaque matrix (visible with the naked eye) within 48 hours. After 120 hours of incubation, due to the rigidity of the pellicle, this matrix could not be dispersed by either forceful vortexing, boiling or enzymatic treatments (Friedman and Kolter, 2004a). Through screening of a PA14 transposon library for pellicle-deficient mutants, the *pel* operon was identified, and hypothesised to have involvement in the production of an ECM constituent (Friedman and Kolter, 2004a).

The pellicle gene locus (*pel*) consists of seven genes (*pelA* to *pelG*, gene cluster PA3058 – PA3064), spanning a 12.2 kb region of the *Ps. a.* PA01 genome (Freidman and Kolter, 2004a). The corresponding region of the *Ps. a.* PA14 genome shares 98% nucleotide sequence similarity with PA01, whilst the protein products from the *pel* gene cluster are identical in both PA01 and PA14 (Friedman and Kolter, 2004a). All seven genes in the *pel* operon are required for Pel-dependent biofilm phenotypes (Vasseur *et al.,* 2005; Franklin *et al.,* 2011), with five of the predicted protein products exhibiting amino acid sequence similarities with known carbohydrate processing proteins from other bacterial species (Friedman and Kolter, 2004a). In contrast to the *psl* operon, the *pel* operon is poorly conserved in *Pseudomonas syringae*, *Pseudomonas putida* and *Pseudomonas mendocina* (Mann and Wozniak, 2015).

Although the structure of Pel has yet to be elucidated, early carbohydrate and linkage analyses suggested that *pel* encodes for a glucose-rich, linear EPS (Friedman and Kolter, 2004a; 2004b). Pel is believed to be a cationic polymer, composed of partially acetylated, 1,4-linked *N*-acetylglucosamine and *N*-acetylgalactosamine moieties (Friedman and Kolter, 2004a; Jennings *et al.,* 2015). Similarly to Psl, Pel can serve as a primary scaffold during early biofilm formation through the maintenance of cell-cell interactions, and is essential for the development of mature biofilm structures by *Ps. a.* PA14 (Colvin *et al.,* 2011; Ghafoor *et al.,* 2011; Yang *et al.,* 2011). In the non-piliated *Ps. a.* strain PAK, there is evidence to suggest that Pel can also compensate as an initial attachment factor in the absence of other adhesins such as TFP (Vasseur *et al.,* 2005).

Initially, PA14 biofilms develop as small microcolonies that become increasingly complex during maturation, resulting in the formation of large, multicellular aggregates (Colvin *et al.,* 2011; Yang *et al.,* 2011). Pel facilitates the differentiation of mature biofilm structures: compared to the wild-type, a PA14Δ*pelB* mutant is unable to develop a three-dimensional architecture; capable of only producing a dense monolayer of cells on the surface (Colvin *et al.,* 2011). Conversely, overexpression of *pel* results in the formation of larger cell aggregates with increased biofilm biomass (Colvin *et al.,* 2011). Furthermore, localisation of Pel in PA14 is analogous to that of Psl localisation in PA01, with Jennings *et al.,* (2015), revealing that Pel accumulates at the periphery, rather than within the interior, of mature biofilm structures. In the archetypal mushroom-shaped masses of PA14 biofilms, Pel has been observed to localise to the stalk of such structures, forming intertwined Pel fibres that extend from the surface substratum and around the mushroom-shaped microcolonies, tethering them in place (Jennings *et al.,* 2015).

#### *1.2.3.3. Alginate*

Unlike Psl and Pel which are aggregative exopolysaccharides, alginate is defined as a capsular polysaccharide that forms a protective layer around a bacterium (Mann and Wozniak, 2015). Alginate is a high molecular weight polymer, composed of non-repeating monomeric units of β-1,4-linked, selectively O-acetylated D-mannuronic acid and its C5' epimer α-L-guluronic acid (Evans and Linker, 1973; Chitnis and Ohman, 1990; Ryder *et al.,* 2007; Franklin *et al.*, 2011). In *Ps. a.*, alginate is firstly synthesised as a linear homopolymer of D-mannuronic acid residues, and then modified in the periplasm through selective O-acetylation by AlgI, AlgJ and AlgF and epimerised by

AlgG (Franklin and Ohman, 1993; Franklin and Ohman, 2002; Franklin *et al.,* 2011). AlgG converts D-mannuronic acid to L-guluronic acid at the polymer level, and acetylation occurs at the hydroxyl groups at either the C2' and/or the C3' positions. Thus, alginate is an EPS with a more irregular and distinctive structure than other polysaccharides that are composed of regularly repeating monomeric units (Figure 1.4) (Boyd and Chakrabaty, 1995; Franklin *et al.,* 2011).

**Figure 1.4**
**Chemical structure of alginate**

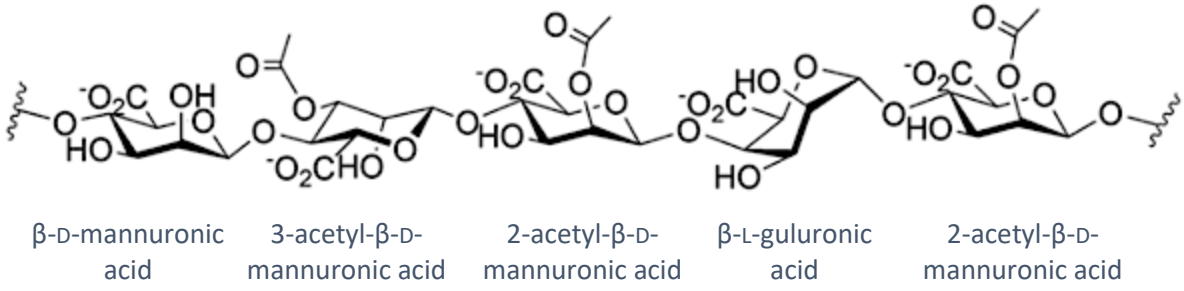


Figure adapted from Liang, 2015

Alginate biosynthesis has been extensively studied due to its function as a major virulence factor in *Ps. a.* strains that opportunistically infect the lungs of cystic fibrosis (CF) patient populations (Govan and Deretic, 1996; Pier, 1998; Stapper *et al.,* 2004). Non-mucoid strains of *Ps. a.* initially colonise the CF lung, producing little or no alginate (Nivens *et al.,* 2001). This happens early in life, with a study by Burns *et al.,* (2001), reporting that over 97% of children with CF have evidence of *Ps. a.* infection by the age of 3. Over time however, mucoid variants, characterised by their overproduction of alginate emerge and eventually dominate as the principal pulmonary pathogen, with the transition from non-mucoid to mucoid phenotypes associated with the increased

morbidity and mortality of CF patients (Høiby, 1975; Govan and Deretic, 1996; Ramsay and Wozniak, 2005).

Colonisation of pulmonary surfaces by *Ps. a. in vivo* results in the formation of a biofilm composed of microcolonies, each encapsulated in a glycocalyx of alginate (Lam *et al.,* 1980; Nivens *et al.,* 2001). In an early study by Fick *et al.,* (1992), approximately 85% of *Ps. a.* strains isolated from the lungs of CF patients had the archetypal mucoid phenotype, whilst by comparison, only 1% of *Ps. a.* strains isolated from other sites of infection display mucoidy (Doggett *et al.,* 1966). Mucoidy in the CF lung environment therefore confers a distinct advantage in terms of *Ps. a.* survival, persistence, immune evasion and resistance to antimicrobial treatments (Stapper *et al.,* 2004; Leid *et al.,* 2005). In the laboratory, the mucoid phenotype of *Ps. a.* is unstable, resulting in the frequent and spontaneous conversion of mucoid cells to non-mucoid during culturing (Govan, 1975; Flynn and Ohman, 1988). In non-mucoid strains of *Ps. a.*, such as PA14 and PA01 (the bacterial strains used in Chapters 3 and 4 respectively), alginate itself is not fundamentally required during biofilm formation (Nivens *et al.,* 2001; Mathee *et al.,* 2002; Wozniak *et al.,* 2003; Stapper *et al.,* 2004).

#### *1.2.3.4. Extracellular DNA*

Extracellular DNA (eDNA) has also been shown to be an principal constituent of the ECM of *Ps. a.* (Whitchurch *et al.,* 2002; Allesen-Holm *et al.,* 2006). The eDNA is generated by the lysis of bacterial subpopulations, and has been shown to further facilitate cell-cell interactions within the biofilm (Whitchurch *et al.,* 2002; Nemoto *et al.,* 2003; Montanaro *et al.,* 2011). There is contention in early literature regarding the role

of eDNA: whilst some suggest eDNA is not required for normal biofilm formation (Nemoto *et al.,* 2003; Matsukawa and Greenberg, 2004), others have proposed that eDNA is a vital component of *Ps. a.* biofilms and those formed by other species; promoting the formation of the biofilm through ECM production and providing stability to the developing structure (Whitchurch *et al.,* 2002; Moscoso and Claverys, 2004; Allensen-Holm *et al.,* 2006; Qin *et al.,* 2007; Lappann *et al.,* 2010; Zweig *et al.,* 2014).

The work of Allesen-Holm *et al.,* (2006), originally demonstrated the role of eDNA in promoting distinct interactions between subpopulations of bacteria and mature biofilm differentiation in PA14. Analysis of mushroom-shaped microcolonies grown in flow chambers revealed that eDNA was primarily localised to the stalks of these three-dimensional structures, with most of the eDNA concentrated at the outermost part of the stalk, separating the sessile, 'stalk-forming' bacteria of the biofilm from the migrating, 'cap-forming' cells that give rise to the distinctive mushroom-like architecture (Allesen-Holm *et al.,* 2006; Montanaro *et al.,* 2011). It has since been established that eDNA co-localises with Pel in the stalks of PA14 mushroom-shaped microcolonies, and is able to crosslink with Pel via ionic interactions in a pH-dependent manner (Jennings *et al.,* 2015). At a pH of 6.3, Pel is a cationic polymer capable of aggregating with anionic eDNA *in vitro*: increasing the pH to 7.3 (the isoelectric point of Pel) results in Pel carrying no net charge, rendering it unable to crosslink with eDNA (Jennings *et al.,* 2015). eDNA also co-localises with Psl, resulting in the formation of a thick, 'rope-like' and radial web of eDNA-Psl fibres at the centre of pellicle biofilms to provide structural support to cell aggregates (Wang *et al.,* 2015). Furthermore, eDNA-Psl fibres can function as a biofilm 'skeleton', facilitating further attachment of bacteria through

the provision of a supporting matrix that also enables biofilm expansion, by trafficking cells to the leading edge of the structure (Wang *et al.,* 2014; Wilton *et al.,* 2016) .

#### *1.2.3.5. Additional components*

The first biofilm matrix protein to be identified in *Ps. a.*, CdrA is an adhesin and structural component of the ECM in *Ps. a.* biofilms (Borlee *et al.,* 2010). Encoded by the *cdrAB* operon, CdrA is the product of a two-partner secretion (TPS) system, in which the outer membrane pore CdrB is required for the export of CdrA from the periplasm to the cell surface (Reichhardt *et al.,* 2018). The structure of CdrA is predicted to be similar to other TPS proteins (such as filamentous haemagglutinin), with a β-helical motif that comprises an elongated fibrillar protein core (Borlee *et al.,* 2010). Purported to be a rod-shaped adhesin, CdrA increases the structural stability of *Ps. a.* biofilms through mediation of both CdrA-Psl and CdrA-CdrA interactions (Borlee *et al.,* 2010; Reichhardt *et al.,* 2018). Crosslinking between CdrA and Psl enables Psl to be tethered to, or more tightly associated with, bacterial cells within the ECM; promoting cell aggregation and thus contributing to the integrity of the biofilm (Borlee *et al.,* 2010). Stability of the biofilm is further mediated through CdrA-CdrA interactions, which enable auto-aggregation of bacteria in the absence of exopolysaccharides (Reichhardt *et al.,* 2018). Whilst CdrA-deficient biofilms are able to accumulate biofilm biomass, ensuing bacterial aggregates are loosely-associated with one another and matrix integrity is compromised, resulting in the easy removal of the biofilm from the surface and susceptibility to proteolytic degradation (Borlee *et al.,* 2010; Reichhardt *et al.,* 2018). Recently, Reichhardt *et al.,* (2020), demonstrated that CdrA is also able to

bind to the exopolysaccharide Pel, and is required for the stability and maintenance of Psl-deficient matrices, such as those produced by PA14.

Assembled at the bacterial cell-surface through the chaperone-usher pathway, *Ps. a.* Cup fimbriae are another class of appendages involved in surface attachment, cell-cell interactions and microcolony formation (Vallet *et al.,* 2001; Ruer *et al.,* 2007). Three *cup* gene clusters (*cupA, cupB* and *cupC*) are involved in the assembly of Cup fimbriae in *Ps. a.* strains PA01 and PAK, whilst an additional gene cluster, *cupD*, is found in PA14 and thought to contribute to the increased virulence of this strain (He *et al.,* 2004; Mikkelson *et al.,* 2009). The products of the *cupA* gene cluster were shown by Vallet *et al.,* (2001), to be requisite for initial adhesion to abiotic surfaces, whilst the protein products of *cupB* and *cupC* were not required for surface adherence under the conditions tested. However, Kulasekara *et al.,* (2004), demonstrated that expression of all three *cup* gene clusters was important for the formation of pellicle biofilms at the ALI: in the absence of *cup* genes, pellicle formation did not occur, and the bacteria growing at the ALI were resultantly unicellular, or only associated in small microcolony clusters.

## 1.3. *Escherichia coli* and biofilm components

### 1.3.1. *Escherichia coli*

*E. coli* is a Gram-negative, peritrichous bacillus and facultative anaerobe, that is a principal commensal of the mammalian gastrointestinal tract (Ping, 2010; Blount, 2015). A constituent of the gut microbiomes in birds, reptiles and fish, *E. coli* can also

inhabit the soil, plants, food and aqueous environments (Hartl and Dykhuizen, 1984; Leimbach *et al.,* 2013; Blount, 2015). Due to the ease and low costs associated with its growth and maintenance, *E. coli* is considered a model organism and has widespread use in research and industry, particularly in molecular biology, genetics, physiology and biotechnology (Huang *et al.,* 2012; Son and Taylor, 2012; Cronan, 2014). Able to form robust biofilms on both abiotic and biotic surfaces, *E. coli* is a highly diverse species able to occupy an array of environmental and ecological niches (Katouli, 2010; Blount, 2015).

### 1.3.2. Surface organelles

#### *1.3.2.1. Curli fimbriae*

Curli fimbriae, also referred to as thin aggregative fimbriae, are a type of extracellular amyloid fibre produced by *E. coli* and other *Enterobacteriaceae* including *Shigella* and *Citrobacter* (Smyth *et al.,* 1996). Curli fimbriae are hydrophobic and aggregate at the cell surface, producing structures of diameter 6 – 12 nm, and ranging from 0.5 – 1 μm in length (Beloin *et al.,* 2008). Curli are classified as a type of 'functional amyloid' and are crucial for mediation of initial cell-surface interactions during attachment, as well as succeeding cell-cell interactions during biofilm and pellicle formation (Vidal *et al.,* 1998; Prigent-Combaret *et al.,* 2001; Cookson *et al.,* 2002; Hung *et al.,* 2013). There is also evidence to suggest that curli fimbriae can also influence the three-dimensional structure and differentiation of mature biofilms (Kikuchi *et al.,* 2005). Curli fimbriae are exceptionally robust: able to withstand boiling in detergent or incubation in solvents, biofilms containing curli are thought to be more resistant to stresses imposed by mechanically-demanding environments (Hammar *et al.,* 1995; Nguyen *et al.,* 2014).

Two operons, *csgBAC* and *csgDEFG*, are required for curli production in *E. coli* (Hammar *et al.,* 1995).

The *csgBAC* operon encodes for the major structural subunit of curli (CsgA) and the minor subunit CsgB, which induces nucleation of CsgA monomers into a fibre before assembly on the cell surface (Hammar *et al.,* 1995; Hammar *et al.,* 1996; Barnhart and Chapman, 2006). In the absence of CsgB, CsgA is secreted from the bacterial cell unpolymerised, and curli fimbriae are not assembled (Hammar *et al.,* 1996; Chapman *et al.,* 2002). Co-expressed with CsgA and CsgB is CsgC, which prevents the detrimental misfolding of CsgA in the cytoplasm (Evans *et al.,* 2015). The *csgDEFG* operon encodes for accessory proteins that are requisite for curli assembly (Hammar *et al.,* 1995). CsgE is localised to the periplasm, and mediates the export of stable CsgA and CsgB through CsgG, a nonameric protein complex that forms a diffusion channel in the outer membrane and shares structural similarities to other outer membrane channel-forming proteins (Brok *et al.,* 1999; Thanassi and Hultgren, 2000).

At the outer membrane, CsgE directly interacts with CsgG and the periplasmic protein CsgF (Robinson *et al.,* 2006), enabling secretion of CsgA and localisation of CsgB on the cell surface and subsequent polymerisation to produce curli fimbriae, via a process known as Type VIII (or precipitation-nucleation) secretion (Figure 1.5) (Nenninger *et al.,* 2009; Evans and Chapman, 2014). CsgD is a transcriptional regulator in the FixJ/UhpA family: regarded as a master biofilm regulator in *E. coli*, CsgD positively regulates the *csgBA* operon and thus curli production (Barnhart and Chapman, 2006; Beloin *et al.,* 2008).

**Figure 1.5.**
**Assembly of the surface organelle curli**

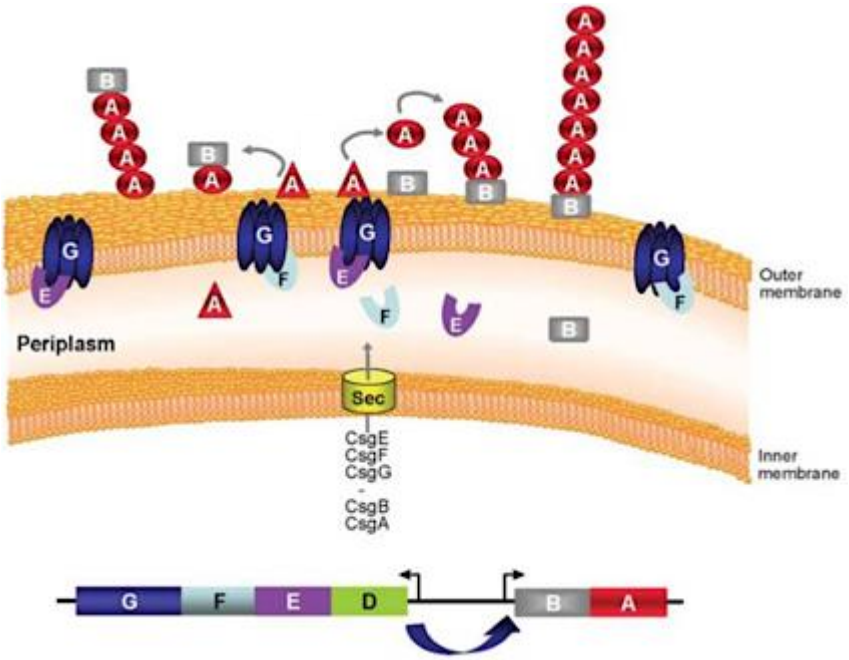


The *csgDEFG* and *csgBA* operons, required for curli synthesis and assembly, are shown in the lower schematic. CsgD is known to positively regulate transcription of the *csgBA* operon. All proteins encoded by these operons, apart from CsgD, are translocated through the periplasm to the outer membrane via Sec apparatus (yellow). CsgE, CsgF and CsgG interact with one another at the outer membrane, and ensure proficient assembly of curli major (CsgA) and minor (CsgB) subunits, that are polymerised to form curli fimbriae.

Figure taken from Barnhart and Chapman, 2006

### *1.3.2.2. Antigen 43*

Antigen 43 (Ag43) is a self-recognising adhesin that mediates cell aggregation and biofilm formation in *E. coli* (Klemm *et al.,* 2004; Ulett *et al.,* 2007). A representative member of the autotransporter family (Henderson and Owen, 1999), Ag43 is a multidomain protein, composed of a β domain that forms a β-barrel pore in the outer membrane, through which the passenger (α) domain is translocated and then anchored to the cell surface via non-covalent interactions (Caffery and Owen, 1989; Henderson *et al.,* 2004; Ulett *et al.,* 2007; van der Woude and Henderson, 2008). X-ray crystallography has revealed that Ag43 is structured distinct in a ‘L-shape’, which

results in the α domain protruding approximately 10 nm from the cell surface (Heras *et al.,* 2014). This enables self-recognition and subsequent auto-aggregation of Ag43 proteins on adjacent bacterial cells, in a head-to-tail 'Velcro-like' mechanism (Heras *et al.,* 2014; Ageorges *et al.,* 2019). Cells express Ag43 in large quantities (estimated at 50,000 copies per cell), promoting biofilm formation through cell-cell interactions in a similar way to curli-mediated aggregation (Danese *et al.,* 2000; Reisner *et al.,* 2003; Schembri *et al.,* 2003; Klemm *et al.,* 2004; Ulett *et al.,* 2007).

Encoded by the *flu* gene, Ag43 exhibits phase variation within a bacterial population, whereby it can be found in either an 'ON' or 'OFF' state for individual cells (Correnti *et al.,* 2002; Ulett *et al.,* 2007). Phase-variable expression of Ag43 occurs at switching rates of circa $10^3$ per cell per generation, as a result of the concerted actions of the enzyme deoxyadenosine methylase (Dam) and the transcriptional regulator OxyR (Henderson *et al.,* 1997; Henderson and Owen, 1999; Ulett *et al.,* 2007). Dam and OxyR compete for sites within the *flu* promoter: binding of Dam to the promoter results in methylation of GATC motifs within the OxyR binding site, resulting in positive regulation of the *flu* gene that results in an 'ON' state (Haagmans and van der Woude, 2000; Waldron *et al.,* 2002; Wallecha *et al.,* 2003). If the OxyR binding site is unmethylated, OxyR binds to the *flu* promoter; preventing transcription of the *flu* gene and Dam-mediated methylation, resulting in an 'OFF' state that is only relieved once a bacterial cell (and its DNA) undergo replication (Waldron *et al.,* 2002; Wallecha *et al.,* 2003; De Luna *et al.,* 2008). Whilst individual cells in any population of *E. coli* will exist in either an 'ON' or 'OFF' state, biofilms have been shown to contain a significant

proportion of ‘ON’ cells; exemplifying the role of Ag43 in *E.* coli biofilm formation (Chauhan *et al.,* 2013).

#### *1.3.3.3. Type 1 fimbriae, F fimbriae and flagella*

Type 1 fimbriae (also referred to as pili) are filamentous adhesins expressed by a variety of both commensal and pathogenic *E. coli* strains (Sauer *et al.,* 2000). Type 1 fimbriae have tubular structures that can be 5 – 7 nm in diameter, and of lengths ranging from 0.2 – 3 μm (Beloin *et al.,* 2008). Composed of repeating FimA monomers with a tip composed of FimF, FimG and mannose-specific FimH, Type 1 fimbriae are able to bind to numerous receptors on eukaryotic cell surfaces in a mannose-dependent manner, as well to mannose moieties of EPS in biofilms (Duncan *et al.,* 2005; Beloin *et al.,* 2008). Indeed, numerous studies in the literature have confirmed the importance of Type 1 fimbriae during attachment of *E. coli* cells to abiotic surfaces and subsequent biofilm formation (Harris *et al.,* 1990; Cookson *et al.,* 2002; Moreira *et al.,* 2003; Orndorff *et al.,* 2004). Pratt and Kolter, (1998), suggested that Type 1 fimbriae are imperative for the non-specific binding activity of *E. coli*, as *fimA* and *fimH* mutant strains experienced reduced rates of initial attachment to abiotic surfaces. Furthermore, expression of Type 1 fimbriae has been shown to be induced in both early and succeeding stages of biofilm formation; potentially altering the physiochemical properties of the outer membrane of *E. coli* cells to increase adhesive properties (Schembri *et al.,* 2003; Beloin *et al.,* 2004; Orndorff *et al.,* 2004). The *fimAICDFGH* operon encodes for structural units of the fimbriae, and is regulated by the recombinases FimB and FimE (Gally *et al.,* 1996; Schilling *et al.,* 2001). FimB and FimE additionally regulate the inversion of a 314 bp section of DNA that precedes *fimA*,

resulting in phase variability of the *fimA* promoter and the ability to switch between 'ON' and 'OFF' states in a clonal cell population, similarly to Ag43 expression (Klemm, 1986; Gally *et al.,* 1996).

F fimbriae, or conjugative F pili, are found in many commensal isolates of *E. coli* and facilitate the rapid sharing of DNA between individual cells via horizontal gene transfer (Silverman and Clarke, 2009; Wang *et al.,* 2009). F fimbriae are helical polymers composed of repeats of a single subunit, F-pilin (Firth *et al.,* 1996), and have been shown to undergo cycles of structural extension and retraction during DNA transfer between donor and recipient cells (Helmuth and Achtman, 1978). Facilitating initial adhesion through non-specific attachment to abiotic surfaces and succeeding cell-cell interactions, F fimbriae bind via a 'catch-bond' mechanism that increases their adhesive strength in response to external, tensional forces that act upon the fimbria (Forero *et al.,* 2006; Aprikian *et al.,* 2011; Berne *et al.,* 2015). F fimbriae are able to stabilise maturing biofilm structure via this mechanism (Ghigo, 2001; Molin and Tolker-Nielsen, 2003), with Reisner *et al.,* (2003), suggesting that the fimbriae can also functionally substitute for other adhesins including curli and Ag43. It is worth noting that most laboratory strains of *E. coli* (such as *E. coli* K-12) do not express F fimbriae due to loss of the F plasmid (Blattner *et al.,* 1997). However, transforming such strains with the F plasmid has been shown to result in the production of thicker and more differentiated biofilms, through stimulation of curli production and colonic acid synthesis (*subsection 1.3.3.1.*) (Domka *et al.,* 2007; May and Okabe, 2008).

In contrast to *Ps. a.*, *E. coli* is a peritrichous bacterium that has multiple flagella expressed on its cell surface (McNab, 1999). It has been demonstrated that *E. coli* flagella have an affinity for hydrophobic surfaces, and can enhance bacterial attachment to rough surfaces, as a result of the flagella being able to penetrate into surface crevices, thus increasing the overall surface area available for bacterial adhesion (Friedlander *et al.,* 2013; Freidlander *et al.,* 2015). In addition to facilitating motility and initial attachment, the flagella of *E. coli* are also associated with maintaining biofilm architecture during growth (Wood *et al.,* 2006; Serra *et al.,* 2013). The work of Serra *et al.,* (2013), demonstrated that flagellar expression at the cell-surface interface resulted in the formation of 'cellular ropes' composed of entangled flagellar filaments, forming a dense mesh that could tether bacterial cells to the surface and provide a stable base upon which macrocolony formation could occur.

### 1.3.3. EPS and matrix composition

#### *1.3.3.1. Colanic acid*

Colanic acid is a capsular exopolysaccharide produced by most strains of *E. coli* and other bacterial species in the *Enterobacteriaceae* family (Stephenson *et al.,* 1996). A negatively charged heteropolymer composed of glucose, galactose, fucose and glucuronic acid moieties, colanic acid forms a protective capsule around a bacterial cell under defined growth or environmental conditions, and its synthesis is upregulated during biofilm formation (Prigent-Combaret *et al.*, 1999; Danese *et al.,* 2000; Beloin *et al.,* 2008). Expression of colanic acid has been shown to be essential during the development of mature *E. coli* biofilms, increasing the strength of the ECM through maintenance of its three-dimensional architecture (Prigent-Combaret and Lejeune,

1999; Danese *et al.,* 2000). Initial attachment events have been shown to stimulate colanic acid synthesis (Prigent-Combaret *et al.,* 1999), although common consensus in the literature is that expression of capsular colanic acid has an inhibitory effect on early biofilm formation, due to the concealment of surface adhesins such as Ag43 (Hanna *et al.,* 2003; Schembri *et al.,* 2004).

The *wca* (formely *cps*) gene cluster is involved in colanic acid production, comprising of at least 19 genes that encode for the synthesis, assembly and transport of the exopolysaccharide (Stevenson *et al.,* 1996). Induced by the RcsC/RcsD/RcsB three-component system and the positive transcription regulator RcsA (Majdalani and Gottesman, 2005), colanic acid synthesis can be upregulated in response to desiccation, osmotic stress, growth on a solid surface and periplasmic glucan levels (Ophir and Gutnick, 1994; Sledjeski and Gottesman, 1996; Ferrieres and Clarke, 2003). Sailer *et al.,* (2003), demonstrated that production of colanic acid is also induced by near-lethal levels of certain β-lactam antibiotics, which further exemplifies the role of colanic acid in biofilm formation (and persistence of the biofilm lifestyle in a host).

#### *1.3.3.2. PNAG*

Poly-β-1,6-N-acetylglucosamine (PNAG) is a highly conserved exopolysaccharide widely expressed by a range of bacterial, fungal and protozoan microorganisms, and is the major virulence factor of the pathogen *Staphylococcus epidermis* (Fitzpatrick *et al.,* 2005; Roux *et al.,* 2015). A linear and positively charged homopolymer (Figure 1.6), PNAG is necessary for the formation of *E. coli* biofilms through mediation of cell-surface and cell-cell interactions (Pratt and Kolter, 1998; Wang *et al.,* 2005). The

increased structural cohesion provided by PNAG is critical during initial attachment of *E. coli* to abiotic surfaces (Agladze *et al.,* 2005), and has a stabilising effect on the mature biofilm structures produced by *E. coli*, *Bacillus subtilis* and *Staphylococci* (Gotz, 2002; Wang *et al.,* 2004; Roux *et al.,* 2015). Degradation of PNAG by metaperiodate or Dispersin B treatment has been shown to depolymerise PNAG and detrimentally affect *E. coli* biofilm structure; disrupting its three-dimensional architecture and resulting in dispersion of the biofilm (Wang *et al.,* 2004; Itoh *et al.,* 2005).

**Figure 1.6**
**Chemical structure of poly-β-1,6-N-acetylglucosamine (PNAG) exopolysaccharide**

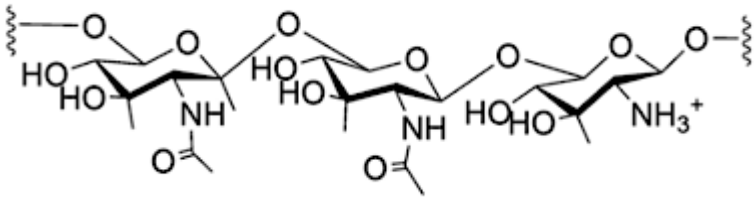

Figure taken from Liang, 2015

The *pgaABCD* operon encodes four proteins required for PNAG synthesis and export: PNAG is polymerised and partially deacetylated in the periplasm, before being translocated to the cell surface (Wang *et al.,* 2004; Itoh *et al.,* 2008). PgaC, which shares homology with family 2 glycosyltransferases, polymerises PNAG with assistance from the membrane protein PgaD, before partial de-*N*-acetylation by the putative lipoprotein PgaB (Wang *et al.,* 2004; Itoh *et al.,* 2008). Secretion of PNAG is then facilitated by PgaA, an outer membrane protein containing a tetratricopeptide repeat motif of which the N-terminal is periplasmic, and the C-terminal forms a β-barrel pore through which PNAG is exported across the bacterial membrane (Wang *et al.,*

2004; Itoh *et al.,* 2008) Partial de-*N*-acetylation of PNAG is necessary to produce the functional form of the cationic polymer: catalytically inactive PgaB (or deletion of *pgaB*) results in the retention of fully-acetylated PNAG in the periplasm, and complete loss of biofilm formation (Little *et al.,* 2012; Little *et al.,* 2014). In *E. coli*, expression of the *pgaABCD* operon is tightly controlled, with positive regulation via the transcriptional activator NhaR in response to sodium binding, and negative regulation by the RNA-binding protein CsrA and OmpR, the response regulator protein of the EnvZ/OmpR two-component regulatory system involved in osmoregulation (Cai and Inouye, 2002; Wang *et al.,* 2005; Pannuri *et al.,* 2012).

#### *1.3.3.3. Cellulose*

Cellulose is a neutral exopolysaccharide that consists of β-1-4-linked glucose moieties (Ross *et al.,* 1991). As a result of hydrogen bond formation between the chains of linear glucose that form the structure of cellulose, fibres can be produced to form an arrangement of structurally-stable cellulose sheets (Lembre *et al.,* 2012). Although not essential for biofilm formation, cellulose can bind with aggregative fimbria on the cell-surface as a structural component of the ECM (Zogaj *et al.,* 2001; White *et al.,* 2003). Cellulose production involves the operons *yhjR-bscQABZC* and *bcsEFG* (Römling and Galperin, 2015). In the common laboratory strain *E. coli* K-12 however, a point mutation exists that results in the presence of a premature stop codon in the *bscQ* gene; ceasing transcription and thus expression of the downstream *bscA* and *bscB* genes, which encode for the subunits of cellulose synthase (Serra *et al.,* 2013). Consequently, *E. coli* K-12 (the bacterial strain used in Chapter 5) does not produce cellulose.

## 1.4. Quorum sensing

Quorum sensing (QS) is an intercellular communication system mediated by the production and detection of small, diffusible signalling molecules, known as autoinducers (Fuqua *et al.,* 1994; Venturi, 2006; Chang, 2018). The QS system was first described in the marine bacterium *Vibrio fischeri*, in which it regulates bioluminescence of the bacteria that colonise the light organ of the squid *Euprymna scolopes* (Nealson and Hastings, 1979; Waters and Bassler, 2005).

QS thusly enables a population of bacterial cells to behave like a community, in order to maximise survival potential through coordinated gene expression and enable selective benefits (that would not arise in individual cells) to be conferred throughout the population (Raina *et al.,* 2009). In general, QS is defined as a cell density-dependent regulatory system, modulated by environmental stimuli and relying on the self-generation of autoinducers in order to activate or repress target gene expression (Williams, 2007; von Bodman *et al.,* 2008).

### 1.4.1. QS in *Ps. a.*

QS controls approximately 10% of genes in *Ps. a.*, including those involved in virulence factor production; mature biofilm development and dispersal; swarming motility, and the expression of antimicrobial efflux pumps (Wagner *et al.,* 2003; Williams and Cámara, 2009). QS in *Ps. a.* is dependent upon three systems regulated in a hierarchical series: the *N*-acetylated homoserine lactone (AHL)-based LasIR and RhlIR systems, and the *Pseudomonas* Quinolone Signal (PQS)-based system

(Williams and Cámara, 2009; Nadal Jiminez *et al.,* 2012; Fazil *et al.,* 2014). The LasIR system is first, and positively regulates the RhlIR system, whilst the PQS system is linked between both AHL-based systems (Chugani *et al.,* 2001; McGrath *et al.,* 2004; Wade *et al.,* 2005).

#### *1.4.1.1. The LasIR system*

LasI catalyses synthesis of the autoinducer *N*-(3-oxo-dodecanoyl)-L-homoserine-lactone (3-oxo-$C_{12}$-HSL), which then binds to its cognate receptor, LasR, a transcription factor that regulates the expression of numerous genes including *rhlI* and *rhlR*, as well as *lasI* in a positive feedback loop to further activate the system (Waters and Bassler, 2005; Williams and Cámara, 2009; Kostylev *et al.,* 2019). Increased cell density results in a corresponding increase in intracellular concentrations of 3-oxo-$C_{12}$-HSL: when a threshold is reached, the autoinducer binds to LasR, resulting in Las-controlled expression of genes related to virulence factor production and biofilm formation (Davies *et al.,* 1998; Hentzer *et al.,* 2003). *Ps. a. las* mutants form biofilms that are undifferentiated and flat, and unable to form the mushroom-shaped macrocolony structures archetypal of mature biofilms produced by this species (Davies *et al.,* 1998).

The LasIR QS system is directly regulated by two LuxR homologues, VqsR (virulence quorum sensing regulator) and QscR (quorum sensing control repressor), which respectively lead to positive and negative regulation of *las* (Juhas *et al.,* 2004). QscR represses *lasI* expression during early growth, as the intracellular concentration of 3-oxo-$C_{12}$-HSL is beneath the threshold for activation of QS (Raina *et al.,* 2009). QscR

repression is purported to occur through the formation of inactive heterodimeric complexes with both LasR and RhlR (Chugani *et al.,* 2001; Ledgham *et al.,* 2003). Accumulation of AHLs results in the threshold level being reached, enabling 3-oxo-$C_{12}$-HSL and *N*-(butanoyl)-L-homoserine-lactone ($C_4$-HSL) to competitively bind to their respective cognate response regulators – dissociation of the heterodimers subsequently enables the formation of active LasR and RhlR homodimers, relieving QscR-mediated repression (Ledgham *et al.,* 2003). Positive regulation of QS pathways occurs by VqsR, via an as-yet uncharacterised mechanism (Raina *et al.,* 2009). Mutant strains of *Ps. a.* that lack a *vqsR* gene were shown to have loss of both AHLs and virulence factor determinant production, further supported by the transcriptomic analysis of Juhas *et al.,* (2004), that revealed VqsR is involved in regulation of both virulence and QS-related gene expression in *Ps. a*.

#### *1.4.1.2. The RhlIR system*

RhlI directs synthesis of the autoinducer $C_4$-HSL which in turn binds to its cognate receptor RhlR which then activates the expression of *rhlI* and other target genes (Waters and Bassler, 2005; Kostylev *et al.,* 2019). As the LasIR system induces both *rhlI* and *rhlR*, the activity of RhlR and subsequent transcription of genes under its control are dependent upon prior induction by LasR (Kostylev *et al.,* 2019). Activation of the RhlIR system results in the production of the surfactant rhamnolipid during biofilm maturation, which crucially maintains the structural integrity of fluid-filled channels (void spaces that separate macrocolonies) and overall three-dimensional biofilm architecture (Pearson *et al.,* 1997; Davey *et al.,* 2003). Increased cell density induces transcription of *rhlI* and *rhlR* and results in QS-dependent rhamnolipid

synthesis (Pearson *et al.,* 1997; De Kievit *et al.,* 2001), which was proposed by Davey *et al.,* (2003), to either prevent colonisation of a pre-formed biofilm by planktonic bacteria, or to prevent accumulation of cellular and EPS material in the channels by triggering dispersion of cells and microcolonies. Other works in the literature are in agreement with the latter suggestion, as rhamnolipids have been shown to reduce the adhesion of cells to one another, resulting in both intraspecies and interspecies biofilm dispersal (Gomes and Nitschke, 2012; Bhattacharjee *et al.,* 2016; Wood *et al.,* 2018).

#### *1.4.1.3. The PQS system*

The PQS-based system is mediated by 2-heptyl-3-hydroxy-4-quinolone (PQS) and its biosynthetic precursor, 2-heptyl-4-quinolone (HHQ) (Gallagher *et al.,* 2002; Déziel *et al.,* 2005; Diggle *et al.,* 2007). The *pqs* operon (*pqsABCDE* and *pqsH*) encodes for numerous 4-quinolones, including HHQ and PQS (Diggle *et al.,* 2006). The gene product of *pqsABCD* directs HHQ synthesis: PqsA is a homologue of a benzoate coenzyme A ligase, whilst PqsB, PqsC and PqsD are similar to β-keto-acyl carrier protein synthases and are all crucial for biosynthesis – mutations in individual genes is enough to completely abolish PQS production (Calfee *et al.,* 2001; Gallagher *et al.,* 2002; Déziel *et al.,* 2005).

HHQ is believed to be an extracellular messenger, released by one *Ps. a.* cell and imported by neighbouring cells, in which HHQ is converted to PQS by PqsH, a predicted FAD-dependent monooxygenase (Déziel *et al.,* 2004). Although Gallagher *et al.,* (2002), suggested that LasR is able to control expression of *pqsH*, significant amounts of PQS can be produced by a *lasR* mutant which may indicate that *pqsH* is

additionally under LasR-independent control, or that there are other enzymes capable of converting HHQ to PQS (Diggle *et al.,* 2003; Diggle *et al.,* 2007).

In contrast to the production of AHL molecules which are cell density-dependent, PQS production is dependent on growth phase, and therefore not involved in sensing cell density (McKnight *et al.,* 2000; Laverty *et al.,* 2014). At the onset of stationery phase, activation of the *pqs* system results in the synthesis of *rhlIR*-dependent exoproducts (Raina *et al.,* 2009). Loss of PQS synthesis was shown by Diggle *et al.,* (2003), to lead to markedly reduced levels of exoproduct formation, even though intracellular $C_4$-HSL concentrations were the same in both wild-type and mutant strains. The PQS system is proposed to link the *las* and *rhl* QS systems: LasR regulates PQS production, whilst RhlR is thought to be important for bioactivity of PQS (Pesci *et al.,* 1999). McKnight *et al.,* (2000), suggested that upregulation of *rhl* by PQS overcomes the inhibitory effect that low intracellular 3-oxo-$C_{12}$-HSL levels have on RhlIR QS; leading to increased $C_4$-HSL synthesis, to a level sufficient enough for $C_4$-HSL to compete with 3-oxo-$C_{12}$-HSL for binding to RhlR.

### 1.4.2. RpoS

Encoded by the *rpoS* gene, RpoS (the sigma factor $\sigma^s$) accumulates inside *Ps. a.* and *E. coli* in response to the onset of stationary phase, or exposure to environmental stress (Evans and Linker, 1973; Hengge-Aronis, 2002; Robbe-Saule *et al.,* 2006). Expression of *rpoS* is under direct control of the *rhl* QS system in *Ps. a.* (and indirectly controlled by *las*), thus $\sigma^s$ production inside the cell enables QS-regulation of genes during stationery phase (Latifi *et al.,* 1996; Jørgensen *et al.,* 1999; Kojic and Venturi,

2001). How the QS systems and $\sigma^s$ interact remains uncharacterised however, although several research groups have observed relationships between them. Schuster *et al.,* (2004), suggested that $\sigma^s$ represses *rhlI* expression (and thus $C_4$-HSL production) until cells reach later logarithmic or stationary growth phases, whilst Medina *et al.,* (2003), proposed that $\sigma^s$ can somewhat activate transcription of *rhlAB* (the genes that control rhamnolipid production), but only in stationary phase of growth. Two lectin adhesins, encoded by *lecA* and *lecB*, are produced as a result of both direct *rhl*-dependent regulation of *lecA*, and indirect regulation by *rhl*, as mediated by $\sigma^s$ (Winzer *et al.,* 2000).

### 1.4.3. QS in *E. coli*

In *E. coli*, there are three different QS systems: the SdiA system, the LuxS/autoinducer-II system, and the autoinducer-III/epinephrine/norepinephrine system (Sperandio *et al.,* 2003; Ahmer, 2004; De Keersmaecker *et al.,* 2006; Walters and Sperandio, 2006). The role of indole as an intercellular QS molecule remains a point of contention within the literature (Hu *et al.,* 2010; Kim and Park, 2011), and indole is generally considered to be an effector of QS-related pathways, rather than a QS autoinducer (Lee *et al.,* 2007).

#### *1.4.3.1. The SdiA system*

The SdiA QS system enables *E. coli* to sense AHL autoinducers produced by other bacterial species, such as *Ps. a.* (Laverty *et al.,* 2014). Whilst *E. coli* lacks the *luxI* gene and thus cannot synthesise its own AHLs, Van Houdt *et al.,* (2006), revealed that the LuxR homologue SdiA can bind to exogenous AHL autoinducers, suggesting that

AHLs can facilitate both intraspecies and interspecies communication. Furthermore, Yao *et al.,* (2006), demonstrated that binding of different AHLs to SdiA results in 'folding switch' behaviour of the LuxR homologue, that may enable identification of AHLs produced by multiple bacterial species.

In the absence of AHLs, expression of *sdiA* results in the formation of insoluble SdiA inclusion bodies; in the presence of AHLs by contrast, the binding of an autoinducer to SdiA 'switches' the protein's structure, leading to the formation of a folded, soluble and monomeric complex (Yao *et al.,* 2006). In agreement with this is the work of Nguyen *et al.,* (2015), who proposed that AHL binding has a stabilising effect on the SdiA protein. SdiA is itself a transcription factor comprised of two functional domains: a C-terminal domain that binds DNA to regulate downstream target genes, and a N-terminal domain that binds autoinducers such as AHL (Henikoff *et al.,* 1990; Van Houdt *et al.,* 2006).

SdiA has been shown by Suzuki *et al.,* (2002), to positively regulate expression of *uvrY*, resulting in activation of the LuxS system and production of autoinducer-II (*subsection 1.4.3.2*). Shimada *et al.,* (2014), further reported that SdiA activation results in a slower rate of cell division, which likely promotes the close proximity of cells preceding biofilm formation (Ren *et al.,* 2004). In mixed *Ps. a.* and *E. coli* biofilms, AHLs produced and secreted by *Ps. a.* are able to bind to SdiA; signalling that another species is nearby on a spatial and temporal level to form a coordinated interspecies biofilm (Culotti and Packman, 2014).

#### *1.4.3.2. The LuxS system*

The LuxS QS system is mediated by autoinducer-II (AI-2), and may be involved in cell metabolism via the up- or downregulation of QS-related genes, and the intracellular activated methyl cycle during exponential growth (March and Bentley, 2004; Vendeville *et al.,* 2005; Laverty *et al.,* 2014). Synthesised via the activity of LuxS, AI-2 concentration peaks during mid- to late-exponential phases of growth, and decreases rapidly at the onset of stationery phase, whilst LuxS protein levels remain relatively constant in comparison (Hardie *et al.,* 2003; Xavier and Bassler, 2005; Laverty *et al.,* 2014). Upon entering stationery phase, AI-2 uptake by *E. coli* cells increases; occurring via the Lsr transporter, an ATP-binding cassette that is itself regulated by *luxS* gene expression (Xavier and Bassler, 2005).

Encoded by the *lsrACDBFG* operon, LsrB is requisite for AI-2 import into cells, with expression of *lsrB* controlled by the QS regulators LsrK and LsrR (encoded by the *lsrKR* operon) (Wang *et al.,* 2005). LsrK is a cytoplasmic kinase, which phosphorylates AI-2 moieties, enabling their subsequent binding to the *lsr* repressor LsrR (Laverty *et al.,* 2014). Mutations to *lsrK* results in repression of the Lsr transporter system, with AI-2 consequently remaining located in the extracellular fluid, whilst mutations of *lsrR* relieve LsrR-mediated repression of the Lsr transporter system; resulting in continuous import of AI-2 into the cell cytoplasm (Taga *et al.,* 2003; Wang *et al.,* 2005; Li *et al.,* 2007).

During early- and mid-exponential phases of *E. coli* growth, intracellular and extracellular concentrations of AI-2 are low, leading to LsrR-mediated repression of the

*lsrACDBFG* and *lsrKR* operons (Wang *et al.,* 2005; Xavier and Bassler, 2005). As extracellular levels of AI-2 increase, active transport and diffusion of the autoinducer occurs, through a yet-to-be elucidated pathway unrelated to Lsr-mediated transport (De Keersmaecker *et al.,* 2006). Non-phosphorylated AI-2 binds to LsrR, resulting in downregulation of a variety of QS and biofilm-related genes, including *lsrR* itself, the *flu* gene (which encodes for production of the auto-aggregative protein Ag43), and the *wza* gene involved in colanic acid synthesis (Laverty *et al.,* 2014). Uptake of AI-2 through the Lsr transport system remains repressed until bacteria enter the late-exponential phase of growth, whereby a threshold concentration of AI-2 (corresponding to nutrient depletion) is reached and leads to increased Lsr-mediated import of AI-2 (Laverty *et al.,* 2014). Intracellular AI-2 is phosphorylated by LsrK: phosphorylated-AI-2 binding to LsrR relieves repression of *lsr* genes, whilst transcription of the *lsrACDBFG* operon acts in a positive feedback loop to increase AI-2 uptake in response to detection of phosphorylated-AI-2 (Taga *et al.,* 2003; Xavier *et al.,* 2007).

In turn, an increase in LsrR/phosphorylated-AI-2 QS results in the expression of genes associated with biofilm formation. Through microarray analysis, DeLisa *et al.,* (2001), observed AI-2-mediated upregulation of the putative fimbrial genes *yadK* and *yadN*, *crl* (a transcriptional regular of *csgA*) and *wzb* and *rscB*, involved in production of fimbriae, curli and colanic acid respectively, and downregulation of *flgN*, required for flagellum synthesis, thus suggesting a switch from a motile to a sessile lifestyle. Furthermore, *E. coli* cells are able to disseminate towards higher concentrations of AI-

2 through chemotaxis, resulting in increased localisation and aggregation of bacterial cells, and greater biofilm formation (Ren *et al.,* 2004; Laganenka *et al.,* 2016).

#### *1.4.3.3. The autoinducer-III/epinephrine/norepinephrine system*

A 4,5-dihdroxy-2,3-pentadione derivative (autoinducer-III, or AI-3) is also produced by LuxS enzymatic activity (Kendall *et al.,* 2007). AI-3 is mainly produced by enterohaemorrhagic *E. coli*, the causative agent of haemorrhagic colitis and haemolytic-uremic syndrome in human hosts (Kaper *et al.,* 2004). Whilst not directly associated with *E. coli* biofilm formation, AI-3 is important with respect to genes relating to virulence factor production, adhesion in the large intestine (as facilitated by the *LEE* operon which causes the formation of attaching and effacing lesions), and motility (via flagella; Sperandio *et al.,* 2001).

Epinephrine and norepinephrine, of the catecholamine class of hormones, are agonists to this system: produced by the colonised host, AI-3 and epinephrine/norepinephrine can bind to the same receptor and enable bacterial-host cell communication (Freestone *et al.,* 2000; Sperandio *et al.,* 2003; Kendall and Sperandio, 2014). The AI-3/epinephrine/norepinephrine QS system is controlled by the activity of a gene regulon which includes the two-component regulatory system QseB/QseC (Walters *et al.,* 2006; Weigel and Demuth, 2016). The kinase receptor QseC undergoes autophosphorylation in the presence of both AI-3 and epinephrine, leading to the successive phosphorylation of QseB, the response regulator that activates the expression of genes involved in flagella biosynthesis and thus motility (Sperandio *et al.,* 2002). Transcription of the *LEE* operon is controlled through the LysR transcription

factors QseA and QseD, whilst formation of the attaching and effacing lesions during intestinal attachment is regulated by QseE and QseF, in a similar manner to the QseB/QseC system (Sperandio *et al.,* 2002; Reading *et al.,* 2009). Bansal *et al.,* (2007), showed that enterohaemorrhagic *E. coli* move via chemotaxis to areas with increased concentration of epinephrine and norepinephrine, leading to the upregulation of virulence genes through binding of the hormones to QseC.

## 1.5. Regulation of biofilm formation

### 1.5.1. cyclic-di-GMP

A universal second messenger in bacteria, cyclic dimeric guanosine monophosphate (c-di-GMP) is believed to be the major determining factor for the motility-sessile switch in *Ps. a* (Henge, 2009; Römling *et al.,* 2013; Chang, 2018). Whilst c-di-GMP is an important factor governing *E. coli* motility and biofilm development, CsgD is regarded as the master regulator of biofilm formation in *E. coli* (*subsection 1.5.3*) (Barnhart and Chapman, 2006), and thus the role of c-di-GMP in *Ps. a.* biofilm formation is discussed.

First identified in *Acetobacter xylinum* to control extracellular cellulose biosynthesis (Ross *et al.,* 1987; Tal, 1998), cellular levels of c-di-GMP have been shown to increase up to fivefold in *Ps. a.* when grown on agar compared to liquid cultures (Chang, 2018), with c-di-GMP promoting biofilm formation and downregulation of motile components such as the flagellum (Kuchma *et al.,* 2012). Indeed, *Ps. a.* biofilms are estimated to contain 75 – 110 pmol of c-di-GMP per mg of total cell extract, whilst planktonic cells contain less than 30 pmol $mg^{-1}$ in comparison (Basu and Sauer, 2014).

#### *1.5.1.1. c-di-GMP metabolism*

Levels of intracellular c-di-GMP are regulated by the enzymatic activity of diguanylate cyclases (DGCs), which synthesise c-di-GMP from guanosine-5'-phosphate (GTP), and phosphodiesterases (PDEs), which degrade c-di-GMP into 5'-phosphoguanylyl-(3'-5')-guanosine (pGpG) (Römling *et al.,* 2013). pGpG is then hydrolysed by the 3'-5' exoribonuclease Orn to yield two molecules of guanosine monophosphate (GMP) (Cohen *et al.,* 2015; Orr *et al.,* 2015).

The catalytic domains of DGCs were found to contain a GGDEF active site motif, whilst PDEs contain either an EAL or a HD-GYP domain (Tal *et al.,* 1998; Ryjenkov *et al.,* 2005; Schmidt *et al.,* 2005). These domains can exist independently in a protein; in association with transmission and receiver domains, or in the case of GGDEF and EAL domains, within the same protein – in the latter, one of the domains will be catalytically active, with the other domain either developing a regulatory function or a third regulatory domain also being present (Chou and Galperin, 2016). Additionally, the works of several research groups have demonstrated that some proteins have both DGC and PDE activities (Boles and McCarter, 2002; Tarutina *et al.,* 2006; Feirer *et al.,* 2015). In *Ps. a.,* one such protein is MucR: in planktonic cells, MucR functions as a DGC and as a positive regulator of alginate synthesis, leading to biofilm formation; in a biofilm, MucR functions as a PDE and positively regulates biofilm dispersal, induced in response to nitric oxide or glutamate (Hay *et al.,* 2009; Valentini and Filloux, 2016).

**Figure 1.7**
**Metabolism and effectors of c-di-GMP**

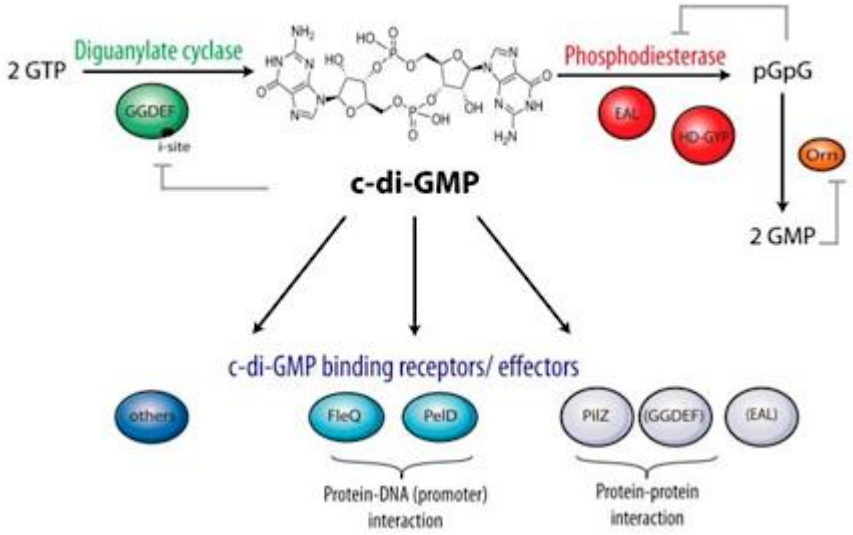


Diguanylate cyclases synthesise the intracellular second messenger c-di-GMP from 2 molecules of GTP via their GGDEF domain-containing active sites, whilst phosphodiesterases (containing either EAL or HD-GYP catalytic domains) degrade c-di-GMP into pGpG. Further hydrolysis of pGpG by Orn results in the formation of 2 molecules of GMP. Increased concentrations of intracellular c-di-GMP lead to its binding (directly or allosterically) to effector proteins; altering their function in response to elevated levels of the second messenger and controlling the transition from planktonic growth and motility to sessility in a biofilm.

Figure taken from Vallentini and Filloux, (2016)

The genome of *Ps. a.* PA01 encodes for 17 proteins with DGC activity; 5 with EAL domain-mediated PDE activity; 3 with predicted HD-GYP domains, and 16 that have both DGC and PDE activity (Galperin *et al.,* 2005; Kulesekara *et al.,* 2006; Valentini and Filloux, 2016). *Ps. a.* PA14 contains most of the same genes but lacks two that encode for a DGC and PDE respectively, and also has an additional PDE-encoding gene (Kulesekara *et al.,* 2006). *Ps. a.* has one of the highest numbers of DGCs and PDEs encoded in its genome, and this could reflect the multiplicity of cellular functions associated with c-di-GMP signalling (Valentini and Filloux, 2016).

#### *1.5.1.2. Modulation and regulation of c-di-GMP*

Five DGCs are known thus far to specifically control the shift from planktonic to surface-associated growth: WspR, SadC, RoeA, SiaD and YfiN/TpbB (Hickman *et al.,* 2005; Güvener *et al.,* 2007; Klebensberger *et al.,* 2009; Malone *et al.,* 2010; Merritt *et al.,* 2010; Bernier *et al.,* 2011; Valentini and Filloux, 2016). Two DGCs (GcbA and NicD) and the PDEs DipA, NbdA and RbdA have been associated with biofilm dispersal (Ueda and Wood, 2009; Li *et al.,* 2013; Petrova *et al.,* 2014; Roy and Sauer, 2014).

The works of Kuchma *et al.*, (2007), and Merritt *et al.*, (2007), respectively demonstrated that the DGC SadC and the PDE BifA can regulate biofilm formation and swarming motility. Using *Ps. a.* PA14, a Δ*sadC* mutant is a hyper-swarming strain that has significantly impaired attachment whilst the Δ*bifA* mutant is the opposite: unable to swarm but exhibiting a hyper-biofilm phenotype (Kuchma *et al.,* 2007; Merritt *et al.,* 2007). Swimming and twitching motilities were not really affected: neither mutant had swimming motilities significantly different from the wild-type, and a slight reduction in twitching motility was only observed in the Δ*bifA* mutant – from this, it was concluded that SadC and BifA principally impact upon swarming but not swimming or twitching behaviours, and that SadC and BifA are important for regulation of intracellular c-di-GMP levels for surface behaviours, including swarming, EPS production and biofilm formation in PA14 (Kuchma *et al.,* 2007; Merritt *et al.,* 2007; Fazil *et al.,* 2014).

Part of the Wsp (wrinkly spreader) chemotaxis-like regulatory system in *Ps. a.*, the WspR response-regulator is a DGC of detailed characterisation in the literature (D'Argenio *et al.,* 2002; Hickman *et al.,* 2005; Güvener and Harwood, 2007; Malone *et*

*al.*, 2007; Chen *et al.*, 2014; Hueso-Gil *et al.,* 2020). The Wsp chemosensory system responds to a sensed surface by regulating intracellular c-di-GMP levels, and is encoded by a cluster of seven genes: *wspA*, *wspB*, *wspC*, *wspD*, *wspE*, *wspF* and *wspR* (Hickman *et al.* 2000; Güvener and Harwood, 2007).

In response to growth on a surface, the chemoreceptor WspA is methylated by WspC, ultimately leading to the activation of WspE, which is able to phosphorylate WspR and result in c-di-GMP synthesis (Güvener and Harwood, 2007; O'Connor *et al.,* 2012). WspR phosphorylation has been shown by Huangyutitham *et al.,* (2013), to prompt subcellular oligomerisation and cluster formation, which further increases the DGC activity of WspR. Wsp-mediated accumulation of c-di-GMP leads to increased EPS production and resultantly, a distinct wrinkly colony morphology (Hickman *et al.,* 2005; Ha and O'Toole, 2015). Work by De *et al.,* (2008), showed that WspR can be inhibited in a phosphate-independent manner through c-di-GMP binding at the DGC's inhibitory site. Furthermore, several groups have shown that WspR can adopt three different forms in solution: as a globular dimer when active; a tetramer with increased DGC activity, and an elongated dimer in response to c-di-GMP binding, which results in decreased enzymatic activity and feedback inhibition (Malone *et al.,* 2007; De *et al.,* 2010).

#### *1.5.1.3. c-di-GMP effectors*

Four proteins in *Ps. a.* have thus far been identified as effectors of c-di-GMP: Alg44, FimX, FleQ and PelD (Hickman *et al.,* 2005; Kazmierzcak *et al.,* 2006; Lee *et al.,* 2007; Merighi *et al.,* 2007). Alg44 is a membrane-associated protein involved in alginate

synthesis (Fazil *et al.,* 2014). Crucially, Alg44 has a cytoplasmic PilZ domain, containing two conserved motifs that can bind c-di-GMP; upon c-di-GMP binding, the activity of Alg44 is modulated and leads to increased alginate production and the characteristic *Ps. a.* mucoid phenotype (Merighi *et al.,* 2007; Høiby *et al.,* 2010). PilZ domains are recognised as the archetypical c-di-GMP binding domain in bacteria (Fazil *et al.,* 2014).

FimX is a cytoplasmic protein with degenerate GGDEF and EAL domains, and was originally thought to have c-di-GMP PDE activity (Huang *et al.,* 2003; Kazmierczak *et al.,* 2006). However, up to 20 – 25% of EAL domains encoded by bacterial genomes are catalytically ineffectual, due to the absence of crucial amino acid residues within their active sites (Rao *et al.,* 2008; Barends *et al.,* 2009). FimX has been shown to have no DGC activity, and only weak PDE activity *in vitro*, although it is able to bind c-di-GMP with high affinity via its EAL domain ($K_D$ ~ 100 nM) (Kazmierczak *et al.,* 2006; Navarro *et al.,* 2009; Qi *et al.,* 2011).

FimX is requisite for TFP biogenesis and twitching motility in *Ps. a.*, with Huang *et al.,* (2003), revealing that unipolar localisation of FimX is critical for its function in TFP assembly. Deletion of FimX, or point mutations within the degenerate GGDEF and EAL domains, results in diminished twitching motility: intracellular pilin subunit levels remain unchanged, but there is a marked diminution in surface pili expression (Huang *et al.,* 2003; Kazmierczak *et al.,* 2006). Current consensus regarding FimX is that it may be crucial in the coupling of TFP-mediated twitching motility and adhesion to c-di-GMP; under low intracellular c-di-GMP levels, FimX localises to the leading pole of the cell,

promoting the spatial and temporal localisation of pili assembly by binding with the PilB ATPase (Qi *et al.,* 2011; Jain *et al.,* 2017).

Identified as novel c-di-GMP-binding protein by Hickman and Harwood, (2008), FleQ is an enhancer-binding protein that regulates flagellum biosynthesis. FleQ contains an N-terminal FleQ domain, an AAA+/ATPase $\sigma^{54}$-interaction domain and a helix-turn-helix DNA binding domain at its C-terminus (Baraquet *et al.,* (2012). Dasgupta *et al.,* (2000), demonstrated that the expression of all FleQ-regulated operons involved in flagellum biosynthesis are dependent on $\sigma^{54}$, and that most of these genes are downregulated under high intracellular c-di-GMP levels. In contract, the expression of FleQ-regulated genes involved in biofilm formation occurs independently of $\sigma^{54}$ (Dasgupta *et al.,* 2000).

Although lacking a PilZ domain, c-di-GMP is able to interact with FleQ via its ATP-binding site, and thus competitively inhibit the ATPase activity of FleQ (Su *et al.,* 2015). Baraquet *et al.,* (2012), demonstrated that FleQ is able to act as both an activator or repressor of *pel* transcription. When intracellular c-di-GMP levels are high, the second messenger binds to FleQ, resulting in its dissociation from a secondary protein, FleN, and conversion of FleQ from a repressor of *pel*, *psl* and *cdr* genes into an activator, leading to increased EPS and adhesin production (Baraquet *et al.,* 2012; Baraquet and Harwood, 2013; Su *et al.,* 2015).

Synthesis of Pel is further controlled by the effector protein PelD. PelD is an inner membrane protein with a GAF domain, a degenerate GGDEF domain and a conserved

inhibitory site, with a RxxD motif (Whitney *et al.,* 2012; Vallentini and Filloux, 2016). Lee *et al.,* (2007), demonstrated that c-di-GMP binds to PelD via the inhibitory site, and can act as a positive allosteric regulator that primarily regulates Pel polymerisation. Mutations in conserved amino acid residues within the C-terminus of PelD were shown to result in the loss of c-di-GMP binding, and consequently lack of Pel synthesis and biofilm formation in PA14 (Lee *et al.,* 2007).

### 1.5.2. CsgD

CsgD, the master regulator of curli expression, is regarded as the 'master switch' of biofilm formation in *E. coli* (Barnhart and Chapman, 2006). Composed of a N-terminal receiver domain and C-terminal DNA-binding domain, CsgD acts as a transcriptional regulator that mediates the expression of approximately 24 genes, including the CsgD-dependent *adrA* gene, which encodes for a DGC that synthesises c-di-GMP and also stimulates the enzymes required for cellulose production (Galperin *et al.,* 2001; Simm *et al.,* 2004; Brombacher *et al.,* 2006). CsgD also modulates expression of *yoaD*, which encodes a protein with an EAL-containing PDE domain that can degrade c-di-GMP; thus enabling tight control of cellulose synthesis via CsgD-dependent *adrA* and *yoaD* expression (Brombacher *et al.,* 2003).

During stationary phase of growth, CsgD is the transcription activator of the *csgBAC* operon, leading to increased curli synthesis (Brombacher *et al.,* 2003). CsgD also stimulates expression of the DGC-encoding *yaiC*, leading to increased c-di-GMP synthesis and promotion of the biofilm phenotype, whilst downregulating expression of *fecR*, *pepD* and *yagS*, the gene products of which all detrimentally affect cell

attachment, aggregation and biofilm formation (Brombacher *et al.,* 2003; Brombacher *et al.,* 2006). Through the activation and repression of multiple genes, CsgD is a positive determinant that is essential for *E. coli* biofilm formation (Brombacher *et al.,* 2003; Brombacher *et al.,* 2006; Liu *et al.,* 2014).

#### *1.5.2.1. Modulation and regulation of cgsD*

Modulation of *csgD* expression occurs through its concerted regulation by a multitude of different transcription factors associated with sensing stressful or adverse environmental conditions, including OmpR (Vidal *et al.,* 1998; Prigent-Combarent *et al.,* 2000; Gerstel *et al.,* 2003), CpxR (Prigent-Combarent *et al.,* 2001; Jubelin *et al.,* 2005), IHF (Gerstel and Römling, 2001; Gerstel *et al.,* 2003), H-NS (Arnqvist *et al.,* 1994; Gerstel *et al.,* 2003) and RstA (Ogasawara *et al.,* 2010). OmpR, CpxR and RstA are all organised in two-component regulatory systems, and only activated when phosphorylated by the sensor kinases EnvZ, CpxA and RstB respectively (Raivio and Silhavy, 1997; Yamamoto *et al.,* 2005; Ogasawara *et al.,* 2010). OmpR and RstA are positive factors that lead to transcription from the *csgD* promoter, and thus synthesis of curli, in response to low osmolarity (OmpR) or under acidic conditions (RstA) (Russo and Silhavy, 1991; Vidal *et al.,* 1998; Ogasawara *et al.,* 2010). IHF is a nucleoid protein and global regulator of transcription when bound near promoters, and is able to form complexes with OmpR and RstA to positively influence *csgD* transcription (Ogasawara *et al.,* 2010).

By contrast, CpxR and the global regulatory protein H-NS are factors that negatively affect *csgD* transcription (Raivio and Silhavy, 1997; Dorel *et al.,* 1999; Jueblin *et al.,*

2005). Activated CpxR is able to bind to several repression sites on the promoters for *csgD* and *csgB* transcription, and repress *csgD* translation via activation of the small RNA RprA, leading to reduced curli synthesis in response to high osmolarity, cell envelope stress and high salt concentrations (Prigent-Combarent *et al.,* 2001; Ogasawara *et al.,* 2010; Hunke *et al.,* 2012). Work by Ogasawara *et al.,* (2010), demonstrated that H-NS is able to cooperatively repress expression of *csgD* through simultaneous binding to the *csgD* promoter; negatively affecting *csgD* transcription.

## 1.6. Multispecies biofilms

Biofilms are considered a distinctive bacterial phenotype, principally characterised in the past through *in vitro* studies focusing on monospecies biofilms (Parsek and Greenberg, 2005). However, the composition of the majority of biofilms in natural habitats is multispecies: containing different species of bacteria and in some cases even algae, fungi and protozoa (Jass *et al.,* 2002). As a result of the increased complexity with respect to interspecies interactions within a multispecies biofilm, and the emergence of multiple functions and capabilities as a result, multispecies biofilms are known to exhibit increased tolerance against antibiotics; increased tolerance to grazing by predatory protozoan; increased virulence in infections, and the ability to degrade more complex organic compounds in comparison to monospecies biofilms (Fux *et al.,* 2005; Bharathi *et al.,* 2011; Lopes *et al.,* 2012; Pastar *et al.,* 2013; Røder *et al.,* 2016). Multispecies biofilms also provide opportunities for horizontal gene transfer and co-metabolism (Molin and Tolker-Nielson, 2003; Jefferson, 2004; Burmølle *et al.,* 2006).

Common consensus in the literature is that there are three forms of bacterial organisation within a multispecies biofilm: microcolonies, which form separate niches in parallel to one another; layered structures, in which different species are located in separate layers, and the formation of multispecies mixing patterns (Tolker-Nielsen and Molin, 2000; Habimana *et al.,* 2010; Liu *et al.,* 2018). The development of multispecies biofilms is believed to occur through a succession of cooperative and competition events, which are themselves influenced by cell-cell and cell-environment interactions (Liu *et al.,* 2016).

For example, biofilms that form in the human oral cavity are complex and well-organised structures, due to the cooperative and successive interspecies interactions they exhibit (Zijnge *et al.,* 2010; Ferrer and Mira, 2016). Coaggregation is defined as a specific cell-cell interaction (facilitated through binding of bacteria in suspension) that often occurs between genetically distinct species or even genera during multispecies biofilm formation, and over 1000 oral bacterial strains are known to co-aggregate (Rickard *et al.,* 2003). In other instances, bacterial species within a multispecies biofilm may be spatially-separated from one another, in order to avoid interspecies competition for substrates or the secretion of toxic compounds by neighbouring cell populations (Kim *et al.,* 2008; Momeni *et al.,* 2013). Spatially-structured multispecies biofilms are thought to facilitate effective co-existence of different bacterial species; enabling co-metabolism, coordinated social activities (including increased virulence during infections) and the negation of localised competition (Harrison *et al.,* 2006; Hansen *et al.,* 2007; Pande *et al.,* 2016).

1.6.1. Biofilm components in multispecies biofilms: cell-surface organelles and EPS

Biofilm components such as curli fimbriae, cellulose, capsular polysaccharides and lipopolysaccharides are believed to improve the biofilm-forming ability of bacteria through mediation of crucial cell-surface and cell-cell interactions, and also promote the viability and resistance of biofilms (Wang, 2019; Li *et al.,* 2021). In multispecies biofilms, non-EPS-producing strains are often at a disadvantage: directly competing against EPS-producing strains for nutrients and space, as EPS-mediated expansion of the biofilm during maturation enables EPS-producing strains to develop into the nutrient-rich areas surrounding the biofilm (Wang *et al.,* 2013). Illustratively, through use of knock-out mutants, Periasamy *et al.,* (2015), observed that the genes involved in Pel and alginate production gave *Ps. a.* a distinct competitive advantage over *Pseudomonas protegens* and *Klebsiella pneumoniae* during multispecies biofilm formation. However, bacteria lacking EPS and cell-surface organelles can still form mixed species biofilms, through interactions with bacteria that do have the ability to produce biofilm components; enabling their proliferation and persistence in the biofilm (Wang, 2019).

The structure of multispecies biofilms formed by *E. coli* O157:H7 and *Salmonella typhimurium* is highly dependent on the presence of curli fimbriae and cellulose (Wang *et al.,* 2013). Whilst Wang *et al.,* (2013), demonstrated that *Salmonella typhimurium* was able to outcompete *E. coli* O157:H7 during planktonic growth, development of the mixed biofilms between the two species was dependent upon EPS production and curli-mediated cell-cell interactions. In mixed species biofilms, mutant strains of either *E. coli* O157:H7 or *Salmonella typhimurium* with EPS-negative phenotypes were found

to exhibit increased resistance against sanitiser treatment in comparison to monospecies biofilms, by forming a multispecies biofilm with the EPS-producing strain of the other species, which offered protection to the non-EPS producing companion strain (Wang *et al.,* 2013). Carter *et al.,* (2019), revealed that curli fimbriae endow *E. coli* O157:H7 with a competitive advantage over spinach-associated microorganisms isolated from foodborne contaminants, by increasing the rate of curli-mediated *E. coli* attachment on spinach leaves and stainless steel surfaces, resulting in increased biofilm formation by *E. coli* O157:H7. *E. coli* O157:H7 mutants deficient in curli production were impaired in both initial surface colonisation and mixed species biofilm formation with the spinach-associated microorganisms (Carter *et al.,* 2019).

The EPS TasA, produced by *Bacillus subtilis*, is able to directly interact with polysaccharides produced by *Streptococcus mutans*; enabling enhanced rates of the initial attachment of both species during dual-species biofilm formation (Duanis-Assaf *et al.,* 2018). Wild-type *Bacillus subtilis* expressing TasA was able to adhere strongly to *Streptococcus mutans* biofilms, whilst a TasA-deficient mutant exhibited reduced adhesive properties, and consequently the mutant strain was less abundant in the dual-species biofilm due to its inability to adhere to *Streptococcus mutans* (Duanis-Assaf *et al.,* 2018). Expression of major *Bacillus subtilis* ECM operons were found to be significantly upregulated in the presence of *Streptococcus mutans* across different stages of biofilm development, suggesting that the two species were interacting with one another and modulating gene expression accordingly, in order to produce a robust dual-species biofilm with increased three-dimensional complexity (Duanis-Assaf *et al.,* 2018).

During the processing of ultrahigh-temperature-sterilised milk, Kives *et al.,* (2005), revealed that *Lactococcus lactis*, a species naturally poor in biofilm formation, benefits from the enhanced attachment conferred through forming a multispecies biofilm with *Pseudomonas fluorescens*; utilising its ECM to form compact biofilms in which both cell types were found in close spatial proximity to one another. Despite *Pseudomonas fluorescens* and *Lactococcus lactis* normally occupying different ecological niches as contaminants in raw milk, both species are able to benefit from forming a multispecies biofilm. *Pseudomonas fluorescens* can utilise lactic acid (which is produced by *Lactococcus lactis*) as a source of carbon and energy, with Kives *et al.,* (2005), suggesting that the rate of lactic acid production is compensated via its consumption by *Pseudomonas fluorescens*, ensuring that pH levels within the biofilm remain constant. In fermented foods, direct cell-cell interactions between a lectin-like protein produced by *Lactococcus plantarum* and mannan produced by the yeast *Saccharomyces cerevisiae* is thought to enable the formation and maintenance of multispecies biofilms (Hirayama *et al.,* 2019), whilst in drinking water distribution systems, *Pseudomonas spp.* and *Basidiobolus* similarly coexist in dual-species biofilms: *Basidiobolus* secretes extracellular enzymes that are able to degrade high-molecular-weight compounds; releasing secondary metabolites which can then be used by other microorganisms (including *Pseudomonas spp.*) for growth and further development of the biofilm (Douterelo *et al.,* 2016).

### 1.6.2. QS in multispecies biofilms

As previously described in section 1.4, QS enables a population of bacterial cells to behave like a community, by sensing cell density and then regulating gene expression

accordingly; maximising the survival of the population through coordinated responses to stimuli (Raina *et al.,* 2009). AHL-mediated QS has been purported by Chandler *et al.,* (2012), to be vital for interspecies competition in multispecies biofilms. Using a dual-species model composed of the soil saphrophytes *Burkholderia thailandensis* and *Chromobacterium violaceum*, Chandler *et al.,* (2012) reported that *Chromobacterium violaceum* can 'eavesdrop' on AHLs produced by *Burkholderia thailandensis* by sensing AHL production via a broad-spectrum, 'promiscuous' AHL receptor; providing a competitive advantage to *Chromobacterium violaceum* through inhibition of growth of *Burkholderia thailandensis*. Competitive interactions have been observed between *Pseudomonas fluorescens* and *Shewanella baltica*, whereby *Shewanella baltica* is thought to either consume the AHL secreted by *Pseudomonas fluorescens*, or inhibit its production altogether in dual-species biofilms (Zhu *et al.,* 2019). In contrast to this, the work of Almeida *et al.,* (2017), demonstrated that *Salmonella enteriditis* is able to form biofilms that are physically stronger and more robust in the prescence of AHL autoinducers from other species under anaerobic conditions, in spite of being unable to produce these autoinducers themselves.

*Ps. a.* and *Burkholderia cepacia* can be found existing in mixed biofilms in the CF lung, with each employing AHL-mediated QS to control both the expression of virulence factors and biofilm formation (Van Delden and Iglewski, 1998; Tummler and Kiewitz, 1999; Elias and Banin, 2012). Through use of an artificial biofilm flow chamber reactor and alginate bead mouse lung infection model, Riedel *et al.,* (2001), demonstrated that *Burkholderia cepacia* is able to recognise several AHLs produced by *Ps. a.*, resulting in close association and the formation of mixed microcolony formation between the two

species. Furthermore, AHL-mediated communication between the two species was observed occurring during co-infection (Riedel *et al.,* 2001). When *Burkholderia cepacian* was grown with non-AHL producing strains of *Ps. a.*, separate microcolonies formed, resulting in the loss of interspecies interactions; indicating the role of AHL-mediated signalling during development of the architecture (and virulence) of these mixed species biofilms (Riedel *et al.,* 2001). Similarly to this, the work of An *et al.,* (2006), in which *Ps. a.* and *Agrobacterium tumefaciens* were co-cultured in a flow-cell system, revealed a competitive fitness imparted to *Ps. a.* via AHL-based QS. When co-cultured with wild-type *Ps. a.*, *Agrobacterium tumefaciens* biofilm biomass was notably reduced compared to the monospecies *Agrobacterium* biofilm; when co-cultured with a *Ps. a.* QS-mutant strain defective in both the LasIR and RhlIR QS systems (and thus unable to respond to the autoinducers 3-oxo-$C_{12}$-HSL and $C_4$-HSL respectively), the amount of *Agrobacterium tumefaciens* biomass remained constant across both the monospecies and mixed biofilms (An *et al.,* 2006).

The AI-2 QS system has been shown to be an important factor governing dual-species biofilm formation between *E. coli* and *Enterococcus faecalis* (Laganenka and Sourjik, 2018). Accumulation of AI-2 in extracellular medium occurs during early growth: once a certain cell density is reached, extracellular AI-2 levels are depleted via import of the autoinducer via the Lsr transport system into the bacterial cell (Xavier and Bassler, 2005). In the dual-species biofilms, *Enterococcus faecalis* secreted greater concentrations of AI-2, enhancing the expression of the *E. coli lsr* operons, promoting coaggregation of both species and increased resistance to stress (Laganenka and Sourjik, 2018). In dual-species biofilms composed of *Pseudomonas fluorescens* and

*Staphylococcus aereus*, regulation of EPS by AI-2 has been shown to result in the formation of more complex biofilm structures (Wang *et al.,* 2020), whilst in multispecies biofilms formed by *Ps. a.*, *Pseudomonas fluorescens* and *Aeromonas hydrophila* on crab surfaces, *Ps. a.* and *Pseudomonas fluorescens* were found to significantly reduce extracellular levels of both AHL and AI-2 autoinducers, resulting in significant inhibition of biofilm formation by *Aeromonas hydrophila* (Jahid *et al.,* 2018).

## 1.7. Hydrodynamic conditions and shear stress

Hydrodynamic conditions within industrial processes are known to influence biofilm formation, development and persistence. Hydrodynamic conditions demarcate the transport of bacterial cells, as well as oxygen and nutrient gradients from the bulk fluid to the biofilm (Bryers and Characklis, 1981; Stoodley *et al.,* 1999; Simões *et al.,* 2007). The hydrodynamics of the bulk fluid can therefore affect the structure and activity of the biofilm, as flow conditions define both the velocity of the bulk fluid and the shear stress that will be exerted upon the surface (Vieira and Melo, 1999; Manz *et al.,* 2003; Gjersing *et al.,* 2005; Lemos *et al.,* 2015). Indeed, within the literature are a plethora of studies that consistently conclude that fluid flow greatly influences biofilm characteristics (Santos *et al.,* 2001; Stoodley *et al.,* 1999; Pereira *et al.,* 2002; Hall-Stoodley *et al.,* 2005; Tsai, 2005; Besemer *et al.,* 2007; Fonseca and Sousa, 2007; Merrit *et al.,* 2007; Simões *et al.,* 2007; Graham *et al.,* 2013; Teodósio *et al.,* 2013).

Shear fluid forces present at the interface between the bulk fluid and the biofilm can influence EPS production; cause mechanical deformation of the biofilm and impact

upon local flow patterns surrounding parts of the biofilm, and lead to increased rates of detachment (Salek *et al.,* 2009). As a result of shear fluid forces, erosion can be continuous and encompass the detachment of either single cells or small clusters of cells from the biofilm surface, whilst detachment by sloughing is more severe, and leads to the precipitous loss of large aggregates or whole areas of the biofilm (Bryers, 1988; Choi and Morgenroth, 2003). If the internal strength of the biofilm cannot withstand sloughing, complete loss of the biofilm can occur (Garny *et al.,* 2008).

Thus, the strength of shear fluid forces is a parameter that crucially influences both microbial adhesion (Bucssher and van der Mei, 2006), and biofilm development (Stoodley *et al.,* 1999; Liu and Tay, 2002). However, there are contrasting views in the literature as to whether shear stress enhances or impedes the formation of a biofilm. During the initial stages of biofilm formation, some contend that high shear forces will increase the residence time of bacterial cells at the substratum's interface with the bulk fluid, resulting in more rapid cell association with the surface (Characklis, 1990; Donlan, 2002; Lecuyer *et al.,* 2011). Others suggest that high shear stress leads to reduced attachment and maintenance of stable interactions with the surface, as a result of weaker adhesion and increased incidences of reversible compared to irreversible attachment (Ramsey and Whitley, 2004; Fonseca and Sousa, 2007; Park *et al.,* 2011).

Common consensus is that high shear forces lead to the development of biofilms that are thinner, denser and stronger (Kwok *et al.,* 1998; Liu and Tay, 2002; Laspidou and Rittmann, 2004), whilst low shear forces result in thicker, multilayer biofilm structures

(Rochex *et al.,* 2008; Rodesney *et al.,* 2017). As fluid shear stress increases, biofilm density has been observed to also increase: leading to the formation of biofilms with higher volumetric density but decreased thickness, mass and microbial diversity (Celmer *et al.,* 2008; Paul *et al.,* 2012).

Mechanosensitive proteins, thought to be expressed on the cell envelope of *Ps. a.*, are thought to enable 'mechanosensing' of changes in surrounding environmental conditions (Kuchma *et al.,* 2010; Luo *et al.,* 2015; Rodesney *et al.,* 2017). Siryaporn *et al.,* (2014), suggested that the cell surface protein PilY1, necessary for TFP biogenesis and pili-mediated attachment in *Ps. a.* (Aim *et al.*, 1996; Heiniger *et al.*, 2010), may act as a mechanosensor, whilst Persat *et al.,* (2015), proposed that TFP are able to act as 'force sensors', modulated by the second messenger 3',5'-cyclic adenosine monophosphate (cAMP). High levels of cAMP are associated with *Ps. a.* virulence, as cAMP can bind to, and in turn activate, the transcription factor Vfr (virulence factor regulator) (Whitchurch *et al.,* 2005). Vfr regulates the expression of over 200 genes, including those involved in type II and III secretion systems and quorum sensing (Whitchurch *et al.,* 2003; McDonough and Rodriguez, 2011).

Rodesney *et al.,* (2017), demonstrated that increased mechanical shear is an environmental 'cue' mechanically-sensed by *Ps. a.* that leads to increased c-di-GMP synthesis; enhancing the transition from a motile to sessile lifestyle. In agreement with Luo *et a*l. (2015), PilY1 was identified as a mechanosensitive protein that upon sensing a surface, signals the inner-membrane bound DGC SadC, resulting in increased c-di-GMP synthesis (Luo *et al.,* 2015; Rodesney *et al.,* 2017). Early enhancement of

intracellular c-di-GMP levels in response to increased shear stress is purported as an adaptation in response to high shear, through greater resilience of cells and increased EPS production; forming biofilms that are more elastic and denser in ECM components than those grown under lower shear regimes (Stewart and Franklin, 2008; Lemos *et al.,* 2015; Araujo *et al.,* 2016).

## 1.8. Experimental models for biofilm growth under flow conditions

Growth of biofilms under flow conditions is used to more accurately imitate real environmental conditions, and evaluate dynamic biofilm formation in response to physiological parameters. Through use of fluid flow regimes, the effect of media composition, oxygen concentration, temperature and pH across all stages of biofilm development can be investigated, as well as the effects of antibiotics and strategies to either control or enhance biofilm formation (Azeredo *et al.,* 2016).

### 1.8.1. The Robbins device

The Robbins device (RD) comprises a pipe, in which there are several threaded holes for the mounting of coupons onto the end of screws to generate submerged biofilms under fluid flow (McCoy *et al.,* 1981; Lappin-Scott and Costerton, 1989). The coupons are aligned in parallel to fluid flow direction, and can be removed independently of one another to provide multiple sampling opportunities. Originally used to evaluate biofilm formation in a ‘simulated drinking water facility’ (McCoy *et al.,* 1981), the RD underwent modification for use in smaller-scale laboratory experiments, as a method of forming biofilms under controlled conditions (Nickel *et al.,* 1985; Azeredo *et al.,* 2016). The

modified RD is composed of a square-shaped pipe, in which there are equally-spaced sampling ports: plugs, comprised of small pistons attached to coupons, align with the inner surface of the device, and can be removed for assessment of biofilm formation (Azeredo *et al.,* 2016). In contrast to the original RD, the modified equipment can operate under both laminar and turbulent flow regimes (Linton *et al.,* 1999), and sustain biofilm growth over a timescale of several weeks or more (Teodosio *et al.,* 2011; Teodosio *et al.,* 2012). The modified RD is typically used to simulate biofilm formation in medical settings on implantable devices and catheters, as well as to evaluate the effects of therapeutic agents on biofilms formed under flow conditions relevant to those *in vivo* (Coenye *et al.,* 2007; Blanc *et al.,* 2014; Magana *et al.,* 2018).

### 1.8.2. The drip flow biofilm reactor

Developed by Goeres *et al.,* (2009), the drip flow biofilm reactor (DFR) is a small device composed of four parallel chambers that contain a surface (most commonly a microscope slide) upon which biofilms can form. Each chamber has a lid, which is vented, and a port through which medium and bacterial inoculum can be added through use of a gauge needle (Goeres *et al.,* 2009; Azeredo *et al.,* 2016). The DFR runs tilted at an angle of 10$^{o}$ (from the horizontal), enabling fluid to 'drip' and pass across the length of the test surface (Buckingham-Meyer *et al.,* 2007; Agostinho *et al.,* 2011). Operating under low shear conditions, the DFR enables evaluation of different surface materials simultaneously in one device with the ability to do so non-invasively (Goeres *et al.,* 2009), and is frequently used in efficacy testing of antimicrobial agents and disinfection methods (Stewart *et al.,* 2001; Buckingham-Meyer *et al.,* 2007; Ammons *et al.,* 2011).

### 1.8.3. The CDC biofilm reactor

The CDC biofilm reactor (CBR) is a type of rotating disk reactor that facilitates the growth of biofilms on removable coupon surfaces, under continuous flow conditions and controlled shear stress regimes (Goeres *et al.,* 2005; Swartz *et al.,* 2010). Shear is created in the reactor through use of a magnetic stir plate rotating a magnetic baffle, the latter of which sits centrally within the CBR; also ensuring that inflowing medium is well-mixed and the imposed shear regime remains constant (Lawrence *et al.,* 2000). Fixed in position through the use of holding rods, coupons are equally-spaced and located at the same radial distance from the rotary apparatus, thus hydrodynamic conditions experienced by biofilms forming on the coupons is uniform (Lawrence *et al.,* 2000).

A limitation of the flow regime generated in the modified RD is that plugs located proximal to the inlet for flow will originally experience increased nutrient consumption in comparison to plugs distal to the inlet, therefore biofilm formation will occur under varying nutritional environments unless a stabilisation period of flow is applied, to ensure full development of shear flow and enable direct comparison of samples, independent of plug location (Azeredo *et al.,* 2016). Heterogeneity of biofilms formed through use of the FDR are similarly limited by device hydrodynamics, and the fact that only low shear regimes can be evaluated; the flows of which are of little relevance industrially (Azeredo *et al.,* 2016). The CBR does not have these limitations.

Coupons for use in the CBR can be made from a variety of materials, including plastics and steel, and can be further modified with coatings to reflect medically-relevant

materials (such as those used in implantable devices) or those with anti-biofilm capabilities. In addition, the dilution rate of the inflowing medium can be adjusted independently of the shear regime, enabling greater manipulation of the model's parameters to influence biofilm structure and cell density (Teodosio *et al.,* 2013b). A limitation of the CBR is the fact that only one experimental group can be used in the reactor at a time, whilst its semi-open design, in contrast to the contained designs of the modified RD and FDR, results in an increased risk of system contamination (Azeredo *et al.,* 2016).

Crucially, the CBR is able to model industrially-relevant shear and nutritional conditions, and was thus chosen by the industrial sponsor of this PhD project, Procter and Gamble (P&G), as the experimental model that would be used to assess the impact of turbulent flow regimes akin to those experienced in P&G manufacturing plants on biofilm formation and composition.

## 1.9. Aims and objectives

There were two overarching aims of this PhD project: the first was to investigate the effect of industrially-relevant shear regimes on biofilm formation by *Ps. a.* strains PA01 and PA14, through use of the CDC biofilm reactor, and the second was to evaluate the effect of different growth conditions and growth medium components on curli gene expression by *E. coli* strain K-12 PHL644, through use of the Duran bottle model.

For *Ps. a.* biofilm studies, biofilm samples grown under low and high shear conditions were subject to analysis by confocal scanning laser microscopy and selective staining of both intracellular and extracellular DNA, as well as the crucial ECM components Psl and Pel, to evaluate the effect of shear stress on biofilm development, maturation and architecture of three-dimensional structures. For *E. coli* biofilm and curli gene expression studies, biofilm samples were taken from the top and bottom of the Duran bottles (composed of planktonic cultures and sedimented cells respectively) and subject to analysis by spectrophotometry at $OD_{600}$ and flow cytometry.

Two reporter genes were used throughout this study: *cdrA::gfp* (in Chapters 3 and 4), and *csgB::gfp* (in Chapter 5) for work on *Ps. a.* and *E. coli* respectively. The *cdrA::gfp* reporter enabled inference of intracellular c-di-GMP levels in *Ps. a.* PA01 and PA14 during biofilm formation under low and high shear conditions. The *csgB::gfp* reporter enabled analysis of curli expression by the *E. coli* strain K-12 in response to different growth medium components, measured by flow cytometry and spectroscopy.

Specific objectives over the course of this PhD were as follows:

1. Calculate two different shear stress regimes for the CDC biofilm reactor of industrial relevance to P&G.
2. Generate a standard operating procedure for running the CDC biofilm reactor that is reproducible and reliable, comprising:
    a. Maintenance of system sterility during reactor operation, sampling and replacement of inflow/outflow vessels;
    b. Maintenance of the operating temperature within a defined range; and
    c. Staining of biofilm samples with multiple lectins and dyes.
3. Characterise the effects that low and high shear conditions have upon:
    a. Initial adhesion of PA01 and PA14 to test surfaces;
    b. Production of the exopolysaccharides Psl and Pel and their respective morphologies in PA01 and PA14 biofilms;
    c. Intracellular concentrations of c-di-GMP at different stages of biofilm development through use of the *cdrA::gfp* reporter; and
    d. The differentiation of three-dimensional biofilm architectures, in particular the mushroom-shaped structures, archetypal of mature *Ps. a.* biofilms.
4. Evaluate the effect of physiological conditions have on curli expression in *E. coli* K-12 through use of an existing and established biofilm model in the Overton laboratory, in order to identify conditions that result in optimal expression of curli.

## 1.10. Thesis outline

This thesis is organised into a total of seven chapters: the first comprises a literature review as an introduction to the research areas relevant to the PhD project, and the second a comprehensive list and description of the materials and methods used throughout this PhD. The third chapter focusses on *Ps. a* .PA14 biofilm formation under low and high shear conditions, whilst the fourth chapter presents results of *Ps. a.* PA01 biofilm formation under the same shear conditions in the preceding chapter. The final results chapter focusses on optimisation of curli expression by *E. coli* K-12, and contains published work. The sixth chapter comprises an overall discussion, conclusions and suggestions for further work, including work that was planned but disrupted by the pandemic. Finally, the last chapter is a list of references used throughout this PhD project.

# Chapter 2: Materials and methods

# Chapter 2: Materials and methods

Unless otherwise stated, all solutions in this project were made with sterile deionised water.

Chemicals, unless otherwise stated, were purchased from Sigma Aldrich.

## 2.1. General Microbial Processes

### 2.1.1. Bacterial Strains

*Pseudomonas aeruginosa* (*Ps. a.*) strains PA01 and PA14 were used throughout this study. Both strains were provided by Dr Mark Webber from the Quadram Institute Biosciences, Norwich, UK. Additionally, the *Escherichia coli* (*E. coli*) K-12 PHL644 strain was used for work in Chapter 5. A derivative of the parental strain *E. coli* MC4100, *E. coli* K-12 PHL644 has a single point mutation in the *ompR234* gene which results in an L43R amino acid change and optimised biofilm-forming phenotype (Vidal *et al.,* 1998). A summary of the species and strains used in this study is presented in Table 2.1.

### 2.1.2. Bacterial Growth Media

*Ps. a.* strains were maintained on Tryptic Soy Agar (TSA) plates, whilst *E. coli* K-12 PHL644 was maintained on Nutrient Agar (NA) plates. Plates were incubated statically at 37 $^{o}$C (*Ps. a.*) or 30 $^{o}$C (*E.* coli) for 20 hours for growth, then stored at 4$^{o}$C for a maximum of two weeks. For long-term storage of stocks, bacterial cultures were frozen

in cryogenic vials at -80 $^{o}$C in 25% glycerol (v/v), for a maximum of eighteen months. Recipes for general bacterial growth media used can be found in Table 2.2.

**Table 2.1. Bacterial species and strains used throughout this study**

| Species and strain | Description of genotype | Reference |
|---|---|---|
| *Pseudomonas aeruginosa* PA01 | Wild-type<br>Accession numbers:<br>GCA_000006765.1 (GenBank)<br>GCF_000006765.1 (RefSeq) | *Reference strain*<br>Stover *et al.,* 2000<br>Winsor *et al.,* 2016 |
| *Pseudomonas aeruginosa* PA14 | Wild-type<br>Accession numbers:<br>GCA_000014625.1 (GenBank)<br>GCF_000014625.1 (RefSeq) | *Reference strain*<br>Rahme *et al.,* 1995<br>Winsor *et al.,* 2016 |
| *Escherichia coli* K-12 PHL644 | *deoC1 ptsF25 rbsR malA-kan ompR234* | Vidal *et al.,* 1998 |

For *E. coli* K-12 PHL644 work, M63+ minimal medium was primarily used in experiments and consisted of 100 mM of potassium phosphate monobasic ($KH_2PO_4$), 17 mM of sodium succinate ($C_4H_4Na_2O_4$) (ThermoFisher), 15 mM of ammonium sulfate ($(NH_4)_2SO_4$), 10 mM of D-glucose (ThermoFisher), 1 mM of magnesium sulfate ($MgSO_4$) (ThermoFisher), and 1.8 μM of ferrous sulfate ($FeSO_4$). To prevent interactions between components during preparation and autoclaving, M63+ minimal medium was made in the following order: a 500 mL 5X stock solution comprised of 500 mM $KH_2PO_4$ (32.02 g), 85 mM $C_4H_4Na_2O_4$ (11.48 g), and 75 mM $(NH_4)_2SO_4$ (4.96 g) was dissolved in water and the pH adjusted to 7.0 through dropwise addition of potassium hydroxide. This solution was then autoclaved and stored at room temperature. The remaining components were made up to the stock solution concentrations outlined in Table 2.3.

**Table 2.2. List of bacterial growth media used throughout this study**

| Medium | Composition | Concentration prepared | Supplier |
|---|---|---|---|
| Nutrient Agar | 15 g/L agar<br>5 g/L peptone<br>5 g/L NaCl<br>2 g/L yeast extract<br>1 g/L 'Lab-Lemco' powder | 28 g/L | Oxoid |
| Tryptic Soy Agar | 15 g/L agar<br>15 g/L casein peptone<br>5 g/L NaCl<br>5 g/L soya peptone | 40 g/L | Sigma Aldrich |
| Luria-Bertani Broth | *Miller formula:*<br>10 g/L tryptone<br>5 g/L yeast extract<br>10 g/L NaCl | 25 g/L | Sigma Aldrich |
| Tryptic Soy Broth | 15 g/L casein peptone<br>5 g/L NaCl<br>3 g/L soya peptone<br>2.5 g/L glucose<br>2.5 g/L dipotassium hydrogen phosphate | Variable; see sections **2.2.** and **2.4.** for details | Sigma Aldrich |

**Table 2.3. Additional components of M63+ minimal medium**

| Component | Concentration of stock solution | Final working solution | Supplier |
|---|---|---|---|
| Magnesium sulfate ($MgSO_4$) | 100 mM<br>*Autoclaved* | 1.5 mM | ThermoFisher |
| D-glucose ($C_6H_{12}O_6$) | 1 M<br>*Filter sterilised* | 10 mM | ThermoFisher |
| Ferrous sulfate ($FeSO_4$) | 1.8 mM<br>*Filter sterilised* | 1.8 μM | Sigma Aldrich |

Magnesium sulfate and D-glucose solutions were aliquoted into sterile 50 mL falcon tubes (Alpha Laboratories) and stored at 4 $^{o}$C. Ferrous sulfate was similarly aliquoted into a sterile 50 mL falcon tube, wrapped in foil to prevent exposure to light and stored at 4 $^{o}$C. D-glucose and ferrous sulfate solutions were filter-sterilised using a 0.22 μM filter.

### 2.1.3. Plasmids

The p*cdrA::gfp* plasmid was predominantly used throughout this study. Kindly donated by Professor Morten Rybtke (Costerton Biofilm Centre, University of Copenhagen), the p*cdrA::gfp* plasmid was used as a reporter to measure intracellular c-di-GMP levels in *Ps. a.* The reporter cassette is shown in Figure 2.1. Briefly, the reporter is composed of the promoter region for *cdrA* (an adhesin); an optimised ribosome binding site to enhance translation of *gfp* mRNA; *gfp* mut3 which encodes for a stable GFP protein, and two downstream transcriptional terminators.

**Figure 2.1**
**Reporter cassette designed by Rybtke *et al.*, 2012**

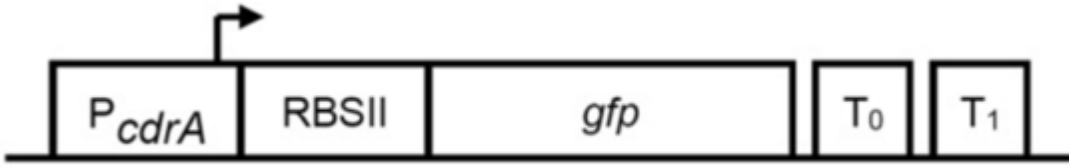


The promoter region for *cdrA* is transcriptionally fused to the ribosome binding site (RBS) and the *gfp* gene, to increase c-di-GMP-responsive transcription from the promoter. T0 and T1 are transcriptional terminators that minimise unnecessary read-through by RNA polymerase.

The plasmid pJTC-L was used in *E. coli* K-12 PHL644 work, as a *csgB::gfp* reporter to measure curli expression levels (Leech, 2017). Using the parental strain MC4100 as the template genome for the reporter sequence, the intergenic sequence (of length

754 base pairs) between the *csgBAC* and *csgDEFG* open reading frames was used as the promoter region for the reporter. The native ribosome binding site of *csgBAC* (AGGGTGACAAC) was replaced with an optimised binding site (AGGAAACAGCT) in order to increase efficiency of translation.

This sequence was fused with eGFP (Zhang *et al.,* 1996), and followed at the C-terminus by an amino acid degradation tag (AANDENYALVA) and two terminator codons. The AANDENYALVA degradation tag was used to reduce the half-life of GFP from 24 hours to approximately 60 minutes (Miller, Leveau and Lindow, 2000).The reporter construct was subcloned into the pPROBE'-TT plasmid (Addgene) using the restriction endonuclease sites flanking the two ends of the construct: EcoRI at the 5' end, and HindIII at the 3' end. pPROBE'-TT has a pBBR1 origin of replication, and a tetracycline resistance marker. Table 2.4 summarises the plasmids used throughout this study.

**Table 2.4. Plasmids used throughout this study**

| Plasmid | Key characteristics | Reference |
|---|---|---|
| p*cdrA::gfp* | pUCP22Not<br>pRO1600 ori<br>$Amp^R$<br>$Gm^R$ | Rybtke *et al.,* 2012 |
| pJCL-T<br>(p*csgB::gfp*) | pPROBE-TT'<br>pBBR1 ori<br>$Tet^R$ | Leech *et al.,* 2020 |

2.1.4. Antibiotics

For *Ps. a.*, selective plates and growth media were supplemented with 200 μg/mL of carbenicillin (Melford). Stock solutions of carbenicillin (at a concentration of 200 mg/mL, in water) were filter-sterilised using a 0.22 μm filter and stored at -20 $^{o}$C. For *E. coli*, selective plates and growth media were supplemented with 10 μg/mL of tetracycline or 100 μg/mL of ampicillin (Roche). Stock solutions of tetracycline and ampicillin (both at a concentration of 100 mg/mL) were dissolved in a 70% (v/v) ethanol solution and water respectively, filter-sterilised using a 0.22 μm filter and stored at -20 $^{o}$C.

2.1.5. Competent Cell Preparation for Electroporation of *Pseudomonas aeruginosa*

The day before electroporation, 300 mM sucrose was prepared and filter-sterilised using a 0.22 μm filter. Sucrose solutions were stored at room temperature in 40 mL aliquots. During competent cell preparation, aseptic technique was followed.

5 mL of Luria-Bertani (LB) broth was used to set up overnight cultures of bacterial strains. Each test tube was inoculated with a single colony and incubated at 42 $^{o}$C at 150 RPM. Cultures were incubated for 18 hours, and then transferred to sterile 2 mL microfuge tubes (2 x 2 mL tubes per strain). Cell cultures were centrifuged at 14,549 g for 15 minutes using a benchtop Eppendorf 5418 centrifuge (Eppendorf, Hamburg, Germany). The supernatants were decanted and discarded, and the pellets each re-suspended in 2 mL of 300 mM sucrose. Cultures were then centrifuged under the same conditions, for a total of three washing stages. After the final wash step, the supernatant was carefully aspirated and discarded, and per strain, the two resultant

pellets re-suspended in a total of 200 μL of 300 mM sucrose solution. Competent cells were used immediately after preparation.

2.1.6. Transformation of Competent *P. aeruginosa* Cells via Electroporation

All steps were performed aseptically and at room temperature unless otherwise stated. From 200 μL aliquots of competent cells, 100 μL was transferred into a sterile 1.5 mL microfuge tube. Per strain, 2 μL of plasmid stock was added gently and allowed to mix for 5 minutes. The other 100 μl of competent cell suspension was transferred to a sterile 1.5 mL microfuge tube, and 2 μL of water added to each negative control. Cell mixtures were then transferred to sterile electroporation cuvettes (Cell Project, blue cap: gap width = 2 mm) and a pulse of 2500 V delivered (Vp 2480, 6 $ms^{-1}$) (BTX Harvard Apparatus).

500 μL of LB broth was immediately added to each cuvette, mixed and the total volume transferred into sterile 1.5 mL microfuge tubes. Tubes were incubated at 37 $^{o}$C at 150 RPM for 4 hours to allow for recovery post-electroporation. After incubation, tubes were removed and the contents gently mixed to re-suspend any sedimented cells. 25 μL of controls and transformants were spread onto LB agar plates (LB broth plus 1.5% (w/v) bacteriological agar (VWR Chemicals)) with 200 μg/mL carbenicillin.

Selective plates were incubated statically at 37 $^{o}$C for 20 hours. Colonies resulting from transformations were subsequently re-streaked onto fresh LB agar plates with 200 μg/mL carbenicillin, to ensure for plasmid selection. Transformation plates were stored at 4 $^{o}$C for a maximum of two weeks.

2.1.7. Competent Cell Preparation for Transformation of *Escherichia coli*

The day before transformation, 100 mM calcium chloride (ThermoFisher) and a solution of 100 mM calcium chloride + 15% (v/v) glycerol was prepared and autoclaved, then stored at 4 $^{o}$C. During competent cell preparation, aseptic technique was followed and all solutions were kept on ice.

5 mL of LB broth was used to set up overnight cultures of bacterial strains. Each test tube was inoculated with a single colony and incubated at 30 $^{o}$C at 150 RPM. Cultures were incubated for 24 hours, and then 400 μL of overnight culture added to 40 mL of LB broth in a 250 mL conical flask, to yield a 1% inoculum. This was incubated for 2 – 4 hours at 30 $^{o}$C at 150 RPM, until an optical density ($OD_{600}$) of 0.3 – 0.5 was reached.

Once the desired $OD_{600}$ was achieved, the 40 mL cell culture was transferred to a sterile 50 mL centrifuge tube (Nalgene), and left on ice for 20 minutes before centrifugation at 1683 g at 4 $^{o}$C for 15 minutes. The supernatant was carefully decanted and discarded, and the pellet resuspended in 4 mL ice-cold 100 mM calcium chloride and left on ice for a further 20 minutes. This was then centrifuged again under the same conditions, and the supernatant decanted and discarded. The resultant pellet was resuspended in 2 mL ice-cold 100 mM calcium chloride + 15% (v/v) glycerol, and transferred into sterile 1.5 mL microfuge tubes in 200 μL aliquots. Competent cell solutions were then stored at -80 $^{o}$C, for a maximum of 12 months.

2.1.8. Transformation of Competent *E. coli* Cells via Heat-Shock

All steps were performed aseptically and on ice unless otherwise stated. An aliquot of chemically competent cells was removed from storage at -80 $^{o}$C and immediately placed onto ice to thaw. 100 μL was transferred to a sterile 1.5 mL microfuge tube, and 1 μL of plasmid stock added gently and allowed to mix for 30 minutes. The other 100 μL of competent cell suspension was transferred to a sterile 1.5 mL microfuge tube, and 1 μL of water added as a negative control, also left on ice to mix. Cell mixtures were then transferred to a heat block, and heat-shocked at 42 $^{o}$C for 1 minute.

Heat-shocked cell mixtures were immediately placed back on ice for 1 minute, and 700 μL of LB added to each. Tubes were then incubated on the heat block at 37 $^{o}$C at 600 RPM for 2 hours, to allow for recovery post-transformation. After incubation, the tubes were centrifuged at 5000 g for 5 minutes, and approximately 750 μL of supernatant removed from each. The remaining 50 μL of supernatant was gently mixed with the pellets, and spread onto NA plates with 10 μg/mL tetracycline or 100 μg/mL ampicillin.

Selective plates were incubated statically at 30 $^{o}$C for 24 hours. Colonies resulting from transformations were subsequently re-streaked onto fresh NA plates with 10 μg/mL tetracycline or 100 μg/mL ampicillin, to ensure for plasmid selection. Transformation plates were stored at 4 $^{o}$C for a maximum of two weeks.

2.1.9. Plasmid Maintenance

Transformed *E. coli* DH5-α cultures were grown in 5 mL of LB broth with appropriate antibiotics. Cultures were incubated at 37 $^{o}$C at 150 RPM for 18 hours. After incubation,

plasmids were extracted from cultures using a QIAprep Spin Mini Kit (QIAGEN) and eluted into molecular biology-grade water. Concentration of DNA was quantified using a NanoDrop 2000 spectrophotometer (Thermo Fisher Scientific, Waltham, Massachusetts). Plasmids were stored in sterile microfuge tubes at -20 $^{o}$C for a maximum of two years.

## 2.2. Biofilm Generation Practices

### 2.2.1 Working Cell Banks for Biofilm Experiments (*P. aeruginosa*)

Per wild-type (plasmid negative) strain, a glycerol stock was removed from -80 $^{o}$C and stabbed once with a sterile, single-use inoculation loop (volume 1μL; Fisher Scientific). This was then subcultured onto a fresh TSA plate and incubated statically at 37 $^{o}$C for 20 hours. For reporter (plasmid positive) strains, glycerol stocks were similarly subcultured onto TSA plates with appropriate antibiotic, and incubated under the same conditions as wild-type plates.

5 mL of 30 g/L Tryptic Soy Broth (TSB) was used to set up overnight cultures of all strains. Each was inoculated with a single colony from the plates generated above, and incubated at 37 $^{o}$C at 150 RPM. Cultures were incubated for 18 hours, and then briefly vortexed to remove any cells from the bottom of culture tubes. 10% (0.5 mL) of each overnight culture was used to inoculate 50 mL of 30 g/L TSB in a 250 mL conical flask, yielding a 1% inoculum. Flasks inoculated with reporter cultures included appropriate antibiotics. Flask cultures were incubated at 37 $^{o}$C at 150 RPM, and grown until an $OD_{600}$ of 0.5 - 0.7 was reached. Once in the desired $OD_{600}$ range, bacterial

cultures were frozen in 2 mL aliquots in cryogenic vials at -80 $^{o}$C in 25% glycerol (v/v) for a maximum of two months, forming the working cell bank (WCB).

### 2.2.2. Cultures for Biofilm Experiments (*P. aeruginosa*)

A vial from a strain's WCB (total volume of 2 mL) was thawed and added to 48 mL of 30 g/L TSB in a 250 mL conical flask to yield a 4% inoculum. Appropriate antibiotics were used when preparing the starter culture of a reporter strain. The flask was incubated at 32.5 $^{o}$C at 150 RPM until an $OD_{600}$ of 0.1 was reached within the 50 mL culture volume (approximately 3.5 – 4.5 hours). Once reached, the total culture volume was transferred to a sterile centrifuge tube and centrifuged at 27,698 g for 25 minutes (Sigma 3K-30). The supernatant was carefully decanted and discarded, and the cell pellet re-suspended in 1 mL of 3 g/L TSB to form the starting culture for biofilm experiments, containing approximately $10^8$ colony forming units (CFU)/mL.

### 2.2.3. Flask cultures of *P. aeruginosa*

1 mL of cell culture (as prepared in subsection 2.2.2) was used to inoculate 48 mL of 3 g/L TSB in a 250 mL conical flask. Flasks were prepared and inoculated in triplicate, and incubated at 25 $^{o}$C at 75 RPM or 350 RPM for 48 hours. At regular timepoints, 1 mL samples from the top and bottom of the flasks were taken and analysed by spectrophotometry ($OD_{600}$) and flow cytometry.

2.2.4. Cultures for Biofilm Experiments (*E. coli*)

Reporter (plasmid positive) strains, a single colony was similarly subcultured onto NA plates with appropriate antibiotic, and incubated under the same conditions as wild-type plates.

From the plates generated above, a single colony was selected and used to inoculate 5 mL of LB which was incubated at 30 $^{o}$C at 150 RPM. Cultures were incubated overnight for 24 hours before centrifugation at 1122 g for 20 minutes. The supernatant was decanted and discarded, and cell pellets gently resuspended in 2.1 mL of M63+ minimal medium.

## 2.3. Biofilm Generation Platforms

2.3.1 Preparation of Coupons for Use in Biofilm Generators

Coupons made of polyethylene (PE) (supplied by Dr Kevin Wright at Procter and Gamble, Reading, UK. Dimensions per coupon: diameter of 30 mm and thickness of 12.7 mm) were boiled in Tween 80 (5% solution in water) for 30 minutes. Coupons were then rinsed in pure water, and sonicated in a sonicating water bath for 30 seconds at a time in pure water until completely free of detergent. Coupons were placed into a 70% ethanol solution for 1 hour before being air-dried. Clean, sterile coupons were stored in petri dishes until use to prevent surface contamination.

After use in biofilm experiments, coupons were autoclaved and once cool, each individually scrubbed to remove any remaining residues. Coupons were then rinsed

with pure water, dried and stored in petri dishes until needed again. Coupons were used in biofilm generators for a maximum of 6 times before being replaced.

### 2.3.2. Use of Duran Bottles as an *E. coli* Biofilm Growth Model

Developed by the Overton laboratory as a method of replicable biofilm generation (Leech *et al.,* 2020, Figure 2.2), a polyurethane bung was inserted into a 100 mL Duran bottle in place of the lid and autoclaved. Table 2.5 outlines the volumes of each M63+ minimal medium component then added to give the desired final concentrations of each, in a total volume of 70 mL. All components were added aseptically in a biological safety cabinet, and antibiotics omitted from growth media to prevent any adverse effects on biofilm formation. All stock solutions were examined daily, and discarded if any signs of contamination or precipitation were present.

**Figure 2.2**
**Schematic of Duran bottle method of biofilm formation developed by the Overton laboratory**

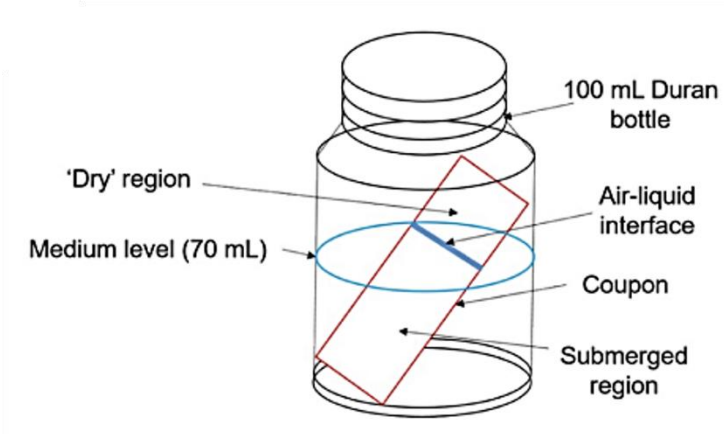


Image taken from Leech *et al.*, 2020.

**Table 2.5. Overview of the M63+ minimal medium 'recipe' for the Duran bottle model**

| Component | Concentration of stock solution | Desired final concentration | Volume added |
|---|---|---|---|
| Water | N/A | N/A | 54.53 mL |
| 5X stock solution | *Comprised of:*<br>500 mM $KH_2PO_4$<br>85 mM $C_4H_4Na_2O_4$<br>75 mM $(NH_2)_4SO_4$ | *For each:*<br>100 mM $KH_2PO_4$<br>17 mM $C_4H_4Na_2O_4$<br>15 mM $(NH_2)_4SO_4$ | 14 mL |
| D-glucose | 1 M | 10 mM | 700 μL |
| $MgSO_4$ | 100 mM | 1 mM | 700 μL |
| $FeSO_4$ | 1.8 mM | 1.8 μM | 70 μL |

700 μL of cell culture (as prepared in subsection 2.2.4.) was used to immediately inoculate the 70 mL M63+ minimal medium. Bottles were prepared and inoculated in duplicate, and incubated at 30 $^oC$ at 70 RPM for 24 – 60 hours, unless otherwise stated in Chapter 5. At regular timepoints, 1 mL samples from the top and bottom of the Duran bottles were taken and analysed by spectrophotometry ($OD_{600}$) and flow cytometry.

## 2.4. Description of the CDC Biofilm Reactor

The CDC Biofilm Reactor (CBR) (BioSurface Technologies, USA) is a glass vessel (capacity 1 L) with an effluent spout positioned to give an approximate operational capacity of 350 mL inside the reactor. The top of the CBR is composed of a polyethylene lid that holds eight independent and removable polypropylene rods in place, as well as an inlet port for media and a gas exchange port (a 0.22 μM bacterial air vent filter, of diameter 50 mm) (Figure 2.3).

2.4.1. Preparation of the CDC Biofilm Reactor

The CBR vessel, head plate, coupon holders and blank rods were washed in laboratory detergent, and then rinsed thoroughly with pure water. Coupons were fitted into their holding rods, and the CBR assembled according to the manufacturer's instructions (Biosurface Technologies Corp.). The nutrient inlet and effluent tubes were clamped prior to medium addition. 350 mL of 3 g/L TSB was prepared and added to the assembled CBR. Exposed tubing ends, and bacterial air vents were foiled, prior to autoclaving for 20 minutes at 121 $^{o}$C to sterilise.

**Figure 2.3**
**Picture of the CDC bioreactor**

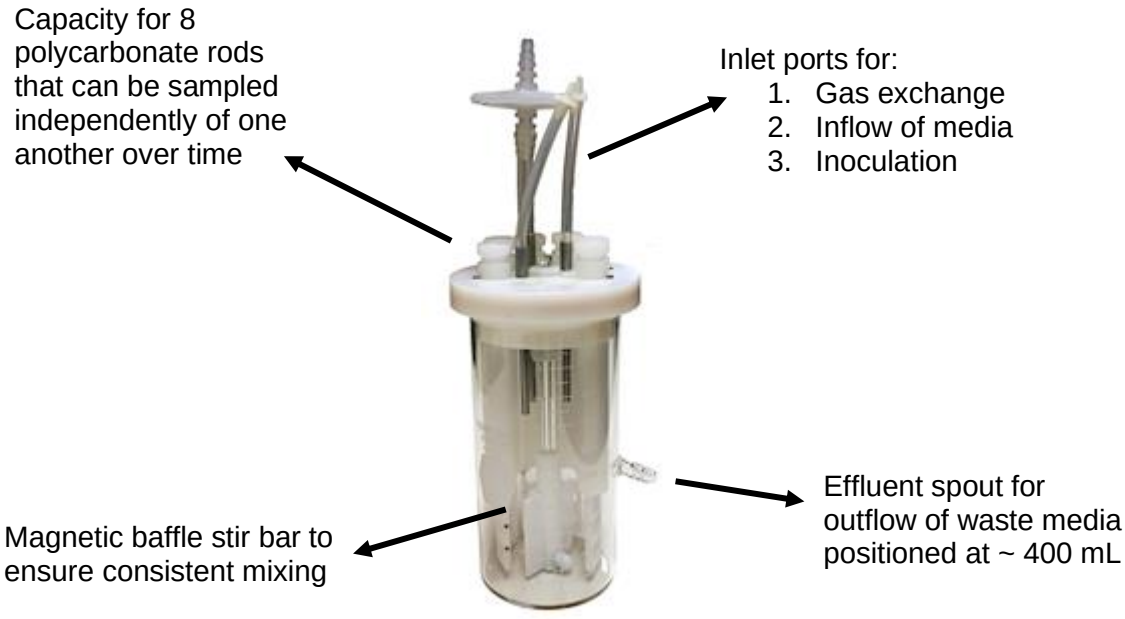


Made of inert materials including Pyrex glass, ultra-high-molecular-weight polyethylene and stainless steel, the CBR facilitates the growth of microorganisms under varying shear stress conditions. A total of 24 sampling opportunities are available, as each rod holds 3 coupons. Image taken from the CDC Bioreactor Operator's Manual, BioSurface Technologies Corp. (2016).

To prepare for the continuous flow phase of the CBR, 3 bottles of 500 mL of 12 g/L TSB were made and autoclaved for 20 minutes at 121 $^{o}$C. Two 20 L carboys were each

filled with 19.5 L of water. Any exposed tubing or air vents on the carboys was covered with foil prior to autoclaving for 20 minutes at 121 $^{o}$C. Carboys were allowed to cool and then stored in a cool dry place until use.

2.4.2. Running the CDC Bioreactor

The CBR was ran in batch phase for 24 hours and then in a continuous flow mode for a total of 72 hours; giving a total run time of 96 hours. To begin the batch phase, the sterile CBR was aseptically inoculated with the previously-prepared 1 mL starting culture (as prepared in subsection 2.2.3.) in a biological safety cabinet. The CBR was then placed onto a magnetic stir plate (IKA RCT basic), and a heat jacket initially wrapped around the reactor to keep the vessel at a constant temperature. The stir plate was set to the desired speed, and the CBR incubated at 25 $^{o}$C for 24 hours.

To run the CBR in continuous flow mode, the ensuing steps were followed and completed aseptically. 500 mL of pre-prepared 12 g/L TSB was added to 19.5 L of water in the inlet carboy, giving a final TSB concentration of 0.3 g/L. The nutrient inlet tube on the CBR was connected to the inlet carboy, and the clamp removed. The effluent tube of the CBR was similarly connected to a waste carboy and the second clamp removed. A peristaltic pump (Watson Marlow) was used to pump a continuous flow of medium into the reactor, with a flow rate of 11.67 $\pm$ 0.2 mL per minute, leading to a residence time of 30 minutes in the CBR. Every 24 hours, the inlet and waste carboys were both replaced to ensure culture volume and nutrient concentration remained constant.

2.4.3. Modifications to the CBR and operating procedures

During initial running of the CBR, several modifications to the standard operating procedure provided by Biosurface Technologies were made. In order to maintain a running temperature of 25 $^{o}$C ($\pm$ 1 $^{o}$C) a recirculating water bath was used, with tubing wrapped around the CBR to the 600 mL mark on the vessel acting as a constant heating jacket. Temperature was monitored digitally via a temperature probe housed in a dip tube and connected to a BioController and BioConsole (Applikon Biotechnologies) to enable constant recording of temperature, accurate to 1 decimal place. As a result of this, the CBR housed 7 rods, giving a total of 21 coupons to sample. The CBR and magnetic stir plate were housed in a containment tray, and carboys sat upon a spill tray with capacity of 40 L (Figure 2.4).

Waste collected in the outlet carboys was neutralised by adding 20% (w/v) of Virkon (LanXESS) and mixed by swirling, before being left for 24 hours in a fume cupboard. After this time, waste medium was disposed of, and outlet carboys rinsed with water before being immediately re-used.

**Figure 2.4**
**Schematic of the CBR set up (A) and modified set up in the laboratory (B)**

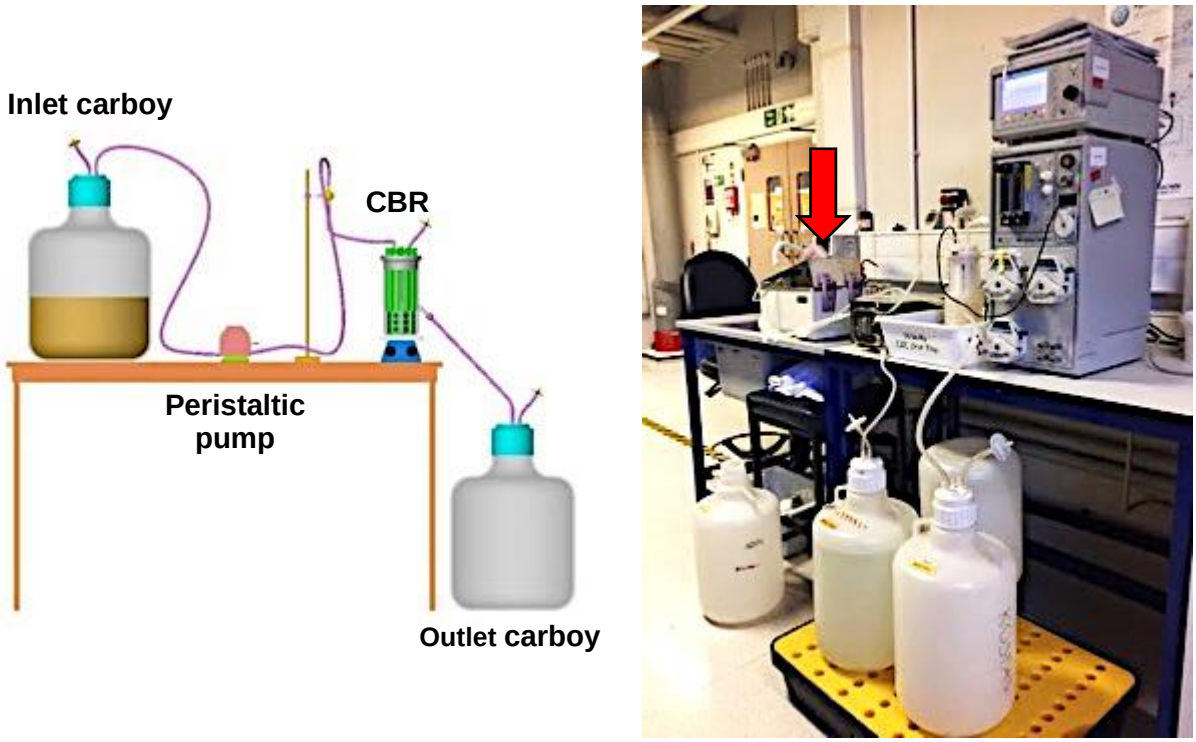


The inlet carboy is connected to a peristaltic pump which feeds medium into the CBR at the desired flow rate. Waste medium leaves the CBR through the effluent spout and is collected into an outlet carboy. In the laboratory (**B**), the carboys sit on the same spill tray and a recirculating water bath (red arrow) is used to keep temperature constant. Schematic (**A**) taken from Norris, 2003.

## 2.4.4. Calculation of Stirring Speeds for Modelling Shear Stress

As the CBR was used to investigate the effect of low and high shear on the growth and morphology of *Ps. a.* biofilms, it was imperative to identify two different stirring speeds that were both relevant to industrial conditions and significantly distinct from one another. To calculate the fluidic wall shear stress that would be exerted onto coupons in the CBR, the reactor was modelled by two concentric cylinders with the assumption that bulk fluid has the properties of water (Table 2.6.). Under hydrodynamic conditions in industry, typical wall shear stresses range from 0.09 – 7.3 Pa with wall shear rates of 86 – 7300 $s^{-1}$ (Saur *et al.,* 2017). Constants for the model were as follows: an outer radius ($R_o$) of 12 cm and an inner radius ($R_i$) of 8cm for the two cylinders, giving a ratio

of the inner to outer cylinder of 0.667; fluid density ($\rho$) of 998.23 kg.m$^{-3}$, and a dynamic viscosity ($\mu$) of 0.001002 kg.(m.s$^{-1}$).

**Table 2.6. Fluid dynamic equations for the CBR**

| Equations | Model assumptions | References |
|---|---|---|
| $\mathcal{R}e = \frac{N.\alpha.R_o^2.\rho}{\mu}$<br>$\mathcal{R}e_{trans} = \frac{41.3}{(1-\alpha)^{1.5}}$<br>$\mathcal{F}_{turb.} = \frac{0.0791}{\mathcal{R}e^{0.25}}$<br>$\mathcal{F}_{lam.} = \frac{16}{\mathcal{R}e}$<br>$\gamma = \frac{\mathcal{F}.\rho.N^2.R_i.R_o}{2}$ | i. The reactor is modelled by two concentric cylinders<br>ii. Reynolds equation as described by Characklis and Marshall (1990), to concentric cylinders<br>iii. Bulk fluid has the properties of water | Goeres (2006)<br>Gomes *et al.* (2014) |

Adapted from Gomes *et al.* (2014), where: $\mathcal{R}e$ = Reynolds number; N = rotational speed; $\alpha$ = the ratio of the inner to outer cylinder; $R_o$ = outer radius; $\rho$ = fluid density; $\mu$ = dynamic viscosity; $\mathcal{F}$ = fanning friction factor; $R_i$ = inner radius and $\gamma$ = shear stress.

Reynolds number ($\mathcal{R}e$) is a dimensionless quantity that is defined by the ratio of inertial to viscous forces in a fluid (Franklin *et al.,* 2015). A low $\mathcal{R}e$ number describes laminar flow of fluids, whilst a high $\mathcal{R}e$ number conversely describes the turbulent flow of fluids. A stirring speed of 75 RPM was selected to represent a low shear, industrially-relevant condition, whilst a stirring speed of 750 RPM was initially selected to represent the high shear condition, being ten-fold greater than the low shear stirring speed. However, during testing of stir speeds, 750 RPM was found to result in instability of the CBR itself with a risk of the reactor breaking, and so an alternative high shear condition, based upon a stirring speed of 350 RPM was selected as this was a five-fold increase in RPM and still of industrial relevance. Calculated parameters are presented in Table 2.7., and are within the range of shear rates described by Saur *et al.,* (2017).

**Table 2.7. Calculated Reynold's numbers and shear stress rates for the stirring speeds selected**

| Stirring speed (RPM) | $\mathcal{R}e$ | Wall shear stress (Pa) | Wall shear rates ($s^{-1}$) |
|---|---|---|---|
| 75 | 6383 | 0.074 | 74.348 |
| 350 | 29,788.807 | 0.690 | 688.626 |
| 750 | 63,833.158 | 2.076 | 2071.424 |

Wall shear stress and wall shear rates were calculated using Taylor-Couette flow equations as outlined by Saur *et al.,* 2017.

Agitation flow is considered laminar if $\mathcal{R}e$ < 10 and turbulent if $\mathcal{R}e$ > $10^4$ (Geankoplis, 1993; Perez *et al.,* 2006). Thus, a stir speed of 75 RPM can be described as transitional flow (with a $\mathcal{R}e$ number of 6383 < $10^4$), whilst stirring at 350 RPM is decidedly turbulent (as the calculated $\mathcal{R}e$ number of 29,788.807 > $10^4$). Additionally, the presence of bubbles during stirring at 350 RPM was observed and absent at 75 RPM, further confirming that the two stirring speeds selected were dynamically distinct from one another and represented two distinctive flow configurations. It is worth noting that the CBR is not a good geometry for generating or testing laminar flow.

### 2.4.5. Sampling of CDC Bioreactor Coupons

Coupons were sampled every 24 hours from the CBR: at the end of the batch phase, and before carboys were replaced during continuous flow mode. Sampling was done under aseptic technique. At each sampling time, the peristaltic pump was stopped and the inlet and effluent tubes on the CBR were clamped, and the reactor disconnected from both carboys. The CBR was then transferred to a biological safety cabinet and samples removed by pulling out the relevant coupon holding rods. Sterile blank rods were inserted to replace sampled rods. The CBR was then transferred back to the stir

plate, water bath tubing re-wrapped around it, and attached to new inlet and waste carboys. Flow rate through the reactor was monitored to ensure that residence time remained the same.

Although biofilms form on both faces of each coupon, only the inner faces (i.e. those that were located "baffle-side" of the holding rods) were subject to analysis. Removed coupons were carefully unscrewed from their holding rods and deposited into a petri dish, inner faces orientated upwards.

1 mL of planktonic culture from the top and the bottom of the CBR was taken using sterile, disposable glass Pasteur pipettes (230 mm in length; Volac), and transferred to a disposable culture tube (made from borosilicate glass, dimensions 13 x 100 mm; FisherScientific) for flow cytometry analysis. 1 mL of phosphate buffered saline (PBS) (Oxoid) was added to the inner faces of both the top and bottom coupons to keep them hydrated until staining. The remaining coupon (from the middle of the holding rod) was held between forceps, and the biomass from the inner face scraped off with a sterile toothpick into a cuvette (Sarstedt), before disaggregation of biofilm from the toothpick into 1 mL of PBS and subsequent transferal of the suspension to a disposable culture tube.

## 2.5. Analytical Techniques

### 2.5.1. Flow Cytometry

Planktonic cell and disaggregated biofilm suspensions were analysed using a BD Accuri C6 Flow Cytometer (FCM) (BD, UK). Samples were diluted as necessary in filter-sterilised PBS to give approximately 2000 events per second. In order to measure GFP fluorescence, a laser of wavelength 488 nm was used to excite samples, and fluorescence emission detected via a 533/30 nm filter. Mean GFP fluorescence (FL1-A) was calculated using Accuri C6 software (BD, UK). No additional staining was required, as FCM was used to solely measure GFP fluorescence.

The FCM was set to record 25,000 events per sample, at a flow rate of 35 μL/min. Cell size was measured using a forward scatter detector (FSC), and cell granularity by a side scatter detector (SSC). A threshold of 12,000 units was applied to the FSC, to reduce background noise (i.e. from non-cellular materials) and ensure events were recorded for average *Ps. a.* and *E. coli* cell sizes. After running samples, the FCM was flushed with 0.5% sodium hypochlorite solution (filter-sterile) for 10 minutes followed by filter-sterilised water and 70% ethanol for 3 minutes at a time, at a flow rate of 66 μL/min.

### 2.5.2. Confocal Laser Scanning Microscopy

The inner faces of the top and bottom coupons were gently rinsed with 1 mL PBS, added dropwise via Pasteur pipette, to remove non-adherent cells before staining. Coupons were carefully transferred to a 6-well plate wrapped in foil for sequential

staining of different biofilm components. An overview of stains and lectins used can be found in Table 2.8.

**Table 2.8. Stain and lectins used to visualise *Ps. a.* biofilm components**

| Stain/lectin | Fluorophore | Stock solution | Working solution |
|---|---|---|---|
| Hoechst 33342 | N/A | 1 mg/mL | 100 μg/mL |
| Concanavalin A | Tetramethylrhodamine | 5 mg/mL | 250 μg/mL |
| Wheat Germ Agglutinin | Alexa Fluor 633 | 10 mg/mL | 100 μg/mL |

All stock solutions were made in sterile deionised water, and stored in the dark at -20 °C. From these, fresh working solutions were made fortnightly, diluted in water and stored at 4 °C.

Hoechst 33342 (ThermoFisher Scientific) binds to double stranded DNA, and was used to stain all cells and eDNA. Concanavalin A conjugated to tetramethylrhodamine (ConA-TRITC) (ThermoFisher Scientific) binds to α-mannopyranosyl and α-glucopyranosyl residues whilst Wheat Germ Agglutinin Alexa Fluor 633 (WGA) binds to *N*-acetylglucosaminyl residues, thus enabling visualisation of the EPS components Psl and Pel respectively. Stains were added to biofilms in the following order: for PA01, Hoechst, ConA-TRITC and then WGA; for PA14, Hoechst and then WGA. 50 μL of each working solution was added to biofilms that were 24 and 48 hours old, and 100 μL added to biofilms that were 72 and 96 hours old. Between addition of each stain, biofilms were incubated at room temperature for 15 minutes, in the dark to prevent photobleaching.

The foil-wrapped 6-well plate containing stained coupons was placed into a polystyrene box for immediate transport to the Biosciences Advanced Light Microscopy (BALM) suite. Stained coupons were placed into sterile polystyrene dishes (of diameter

35 mm and depth 10 mm) (CytoOne), and deionised water added. As PE coupons float, BluTac was used to secure these coupons to the bottom of the dish during imaging. All images in this study were obtained using a Leica TCS SP8 Confocal Scanning Microscope (Leica Microsystems CMS GmbH, Wetzlar, Germany), with a 40X water immersion lens due to the necessity of keeping biofilms hydrated during image acquisition.

The excitation and emission filters used were as follows: for Hoechst, excitation at 410 nm using a UV filter and emission at 483 nm; for ConA, 493/566 nm, and for WGA, 638/775 nm. For GFP, an excitation and emission filter of 493/566 nm was used. When visualising PA01 reporter biofilms, two sequential scans were completed: the first for Hoechst and ConA, and the second for GFP and WGA to reduce the effect of fluorophore overlap.

Per coupon, 5 – 7 separate sample sites across the surface were imaged. A Z-stack scan was taken for each sample site, and a scanning distance between each Z-slice of 1 – 2 μm was employed to capture the visible thickness of the biofilms. For biofilms that had a thickness greater than 150 μm, the scanning distance was increased to 5 μm. Sectional and 3D rendered images of the biofilms were obtained using LasX software (Leica).

### 2.5.3. Image Analysis

Fiji (Schindelin *et al.,* 2012) was used to quantify fluorescent values in individual Z-stack images; line profiles were quantified from horizontal lines drawn across Z-stack

slices of each sample site. Fluorescence signal intensity was normalised to the brightest pixel per coupon, and a five point moving average calculated.

# Chapter 3: Biofilm formation by PA14 under low shear conditions at 75 RPM versus high shear conditions at 350 RPM

# Chapter 3: Biofilm formation by PA14 under low shear conditions at 75 RPM versus high shear conditions at 350 RPM

## 3.1. Introduction

As discussed in Chapter 1, *Ps. a.* is one of the most important model organisms regarding the study of biofilms, due to the relative ease of growing structured biofilms under laboratory conditions that are both consistent and reproducible (Taylor *et al.*, 2014). Furthermore, strains of *Ps. a.* are frequently isolated from a variety of medical and industrial settings, whereby they colonise a variety of biotic and abiotic surfaces; forming persistent biofilms that can have a pronounced and detrimental effect upon affected patient populations and industrial processes.

Work presented in this chapter focusses on the effect of two different shear conditions on biofilm development by the reference strain PA14. Incapable of synthesising Psl as a result of a deletion of *pslA* to *pslD* in its genome, PA14 is reliant on Pel for microcolony and macrocolony development during biofilm maturation (Friedman and Kolter, 2004a; 2004b; Colvin *et al.,* 2011). Therefore, biofilm formation of PA14 under low and high shear regimes was investigated first, to enable more detailed characterisation of observed Pel morphologies in a Pel-dependent strain, rather than initially inferring structural and functional roles of the exopolysaccharide in PA01, a strain which primarily relies on Psl instead.

The CBR was used to investigate the effect of shear on biofilm formation by *Ps. a.* strains PA01 and PA14. Both strains were transformed with the *pcdrA::gfp* plasmid constructed by Rybtke *et al.,* (2012), which expresses GFP under control of the c-di-GMP-responsive *cdrA* promoter (Rybtke *et al.,* 2012; Nair *et al.,* 2016). Use of the *cdrA::gfp* reporter thusly enabled the visualisation of c-di-GMP throughout the biofilm structures as they developed over time, with the fluorescence intensity of GFP correlating directly to intracellular c-di-GMP levels.

## 3.2. Methodology

To generate the biofilms, 1 mL of PA01 *cdr*A::*gfp* or PA14 *cdrA::gfp* cells were inoculated into the CBR to give a starting cell concentration of $10^8$ CFU/mL. The CBR was run in batch phase for 24 hours with 3 g/L TSB as the growth medium, and then in a continuous flow mode for a total of 72 hours feeding 0.3 g/L TSB. Shear conditions were determined through use of a magnetic stir plate (upon which the CBR sat), set to either 75 RPM or 350 RPM for low and high shear conditions respectively (section 2.4.4). During continuous flow mode, the CBR was operated with a flow rate of 11.67 $\pm$ 0.2 mL per minute, leading to a residence time of 30 minutes in the CBR. Every 24 hours, the inlet and waste carboys were both replaced to ensure culture volume and nutrient concentration remained constant.

Biofilms were grown on the surfaces of PE coupons, which were removed at 24, 48, 72 and 96 hours for analysis by CLSM and flow cytometry. For CSLM, a 40X water immersion lens was used, due to the necessity of keeping biofilms hydrated during

image acquisition. Hoechst 33342 was used to stain the DNA of all *Ps. a.* cells (as well as extracellular DNA) and identify those that were not expressing GFP, whilst WGA (which binds to *N*-acetylglucosaminyl residues) conjugated to Alexa Fluor 633 was used to visualise the exopolysaccharide Pel. The excitation and emission filters used were as follows: for Hoechst, excitation at 410 nm using a UV filter and emission at 483 nm; for GFP, an excitation and emission filter of 493/566 nm; and for WGA-Alexa633 excitation at 638 nm and emission at 775 nm.

Per coupon, 5 – 7 separate sample sites across the surface were imaged, with a Z-stack scan taken for each sample site, at a scanning distance of 1 – 2 μm between each Z-slice to capture the visible thickness of the biofilms. Two coupons were imaged per timepoint. Sectional and 3D rendered images of the biofilms were obtained using LasX software, whilst Fiji was used post-image acquisition to quantify fluorescent values in individual Z-stack images and generate fluorescence intensity profiles, enumerated from horizontal lines drawn across Z-stack slices of each sample site.

## 3.3. Results

### 3.3.1. Initial attachment of PA14 *cdrA::gfp* is greater under high shear at 350 RPM

After 24 hours of growth, colonisation of the coupon surfaces was sparse under both low and high shear conditions, with a mixture of adhered single cells, cell clusters and small, three-dimensional features being observed. Under low shear at 75 RPM, surface colonisation was generally more homogenous than at high shear, with the adherence of PA14 *cdrA::gfp* cells either individually or in small, elliptical aggregates of cells being

most predominant (Figure 3.1). As a reflection of this, fluorescence intensity profiles were punctate, with peaks corresponding to areas of cell clustering or increased fluorescence of individual cells, and troughs indicative of areas of the coupon surface with little or no colonisation (Figure 3.1A, yellow arrows). Overall, colonisation of the coupon surface after 24 hours remained sparse in terms of the number of attached cells or clusters, whilst structures formed under low shear remained largely two-dimensional and flat. Height at this stage was very low, with attachment only two cells thick in the z dimension.

**Figure 3.1**

**Early cell-surface adhesion of PA14 *cdrA::gfp* after 24 hours growth under low shear conditions at 75 RPM**

(*figure legend overleaf*)

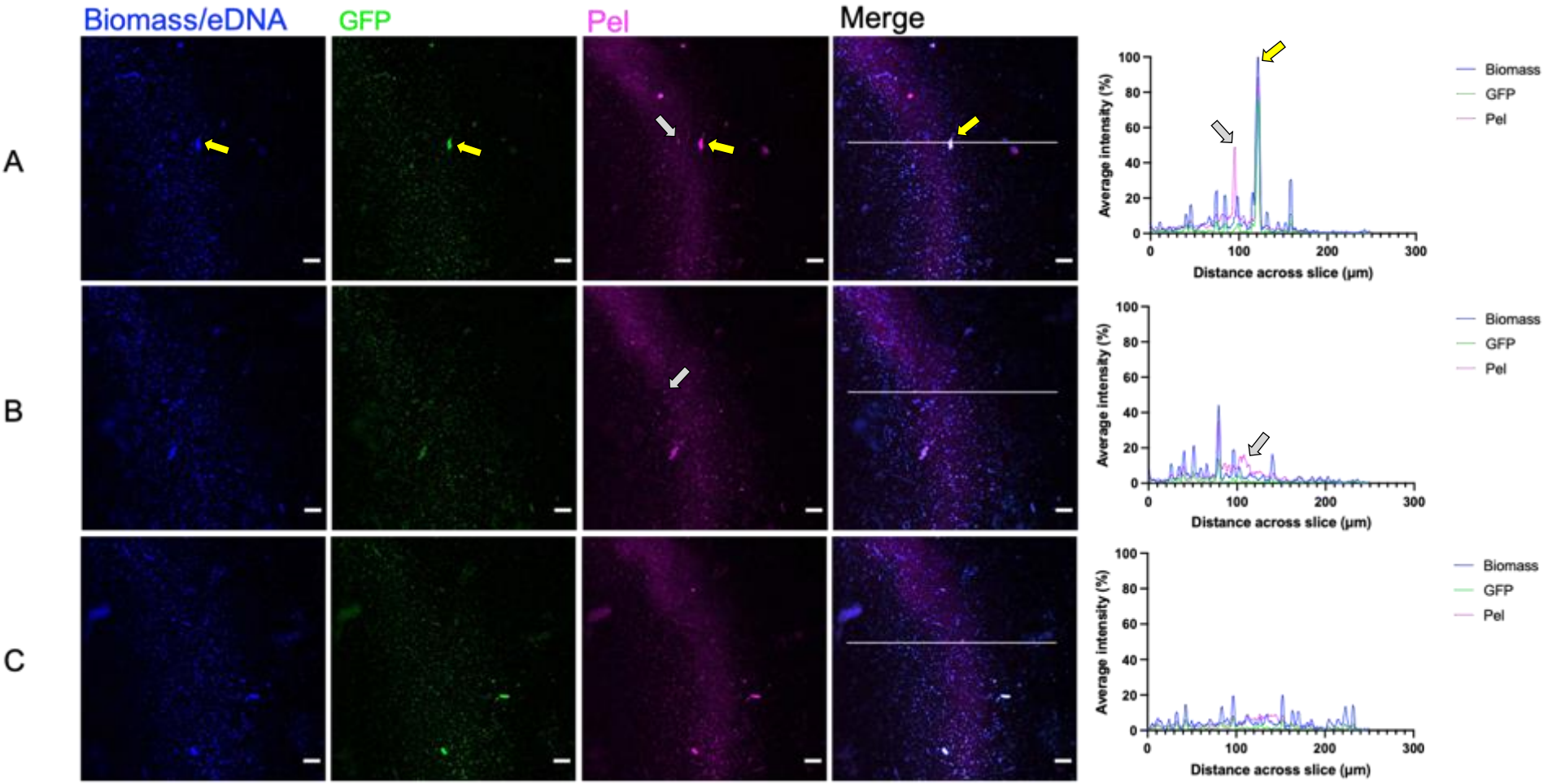

(*figure legend for* Figure 3.1)

Representative confocal images are from PA14 *cdrA::gfp* biofilms (GFP signal is green) cultivated for 24 hours in the CBR under low shear (at 75 RPM) and stained with Hoechst for biomass/eDNA (blue) and the Pel-specific lectin WGA (magenta). A, B and C are each independent sample sites from two different coupon surfaces, and show horizontal optical cross-sections with limited surface colonisation. Scale bar = 20 μm. Fiji was used to quantify fluorescent values in individual z-stack images: fluorescence signal intensity was normalised to the brightest pixel per coupon, and a five point moving average calculated. Yellow arrows show a punctate fluorescence intensity for a small cluster of cells, whilst grey arrows show a punctate signal for Pel, uncorrelated to either Hoechst or GFP fluorescence.

Hoechst fluorescence and GFP expression were found to correlate well with one another, as shown by their respective and similar fluorescence intensity profiles. This suggests that all cells were expressing comparable quantities of *cdrA* and therefore likely had similar c-di-GMP concentrations. Across independent sample sites of the coupon surfaces, colonised areas generally displayed similar fluorescence intensity profiles to one another (Figure 3.1), suggesting homogeneity in Hoechst and *cdrA::gfp* fluorescence across this initially attached cell layer, irrespective of spatial location. In areas with punctate and colocalised fluorescence intensities across all three channels, Hoechst staining of clusters is likely cell-based.

Small multicellular features were observed sporadically as a form of surface colonisation under low shear at 24 hours, composed of three-dimensional, globular structures (Figure 3.2). At this stage, the height of features (in the z dimension) was 5 –10 μm on average, whilst the length and width of the features (in the x and y dimensions) were more variable. Intensity profiles for featureless areas of the surface were similarly punctate to those in Figure 3.1, with Hoechst fluorescence, *cdrA::gfp* fluorescence and Pel fluorescence correlating well with one another (Figure 3.2). By contrast, the relative fluorescence intensity profiles across all three channels for the three-dimensional structures were greater, and dependent upon the individual organisation of the features themselves. The three-dimensional structures had more diffuse Hoechst staining, suggesting eDNA can function an early ECM component.

**Figure 3.2**

**Early feature development by PA14 *cdrA::gfp* cell populations after 24 hours of growth under low shear conditions at 75 RPM**

(*figure legend overleaf*)

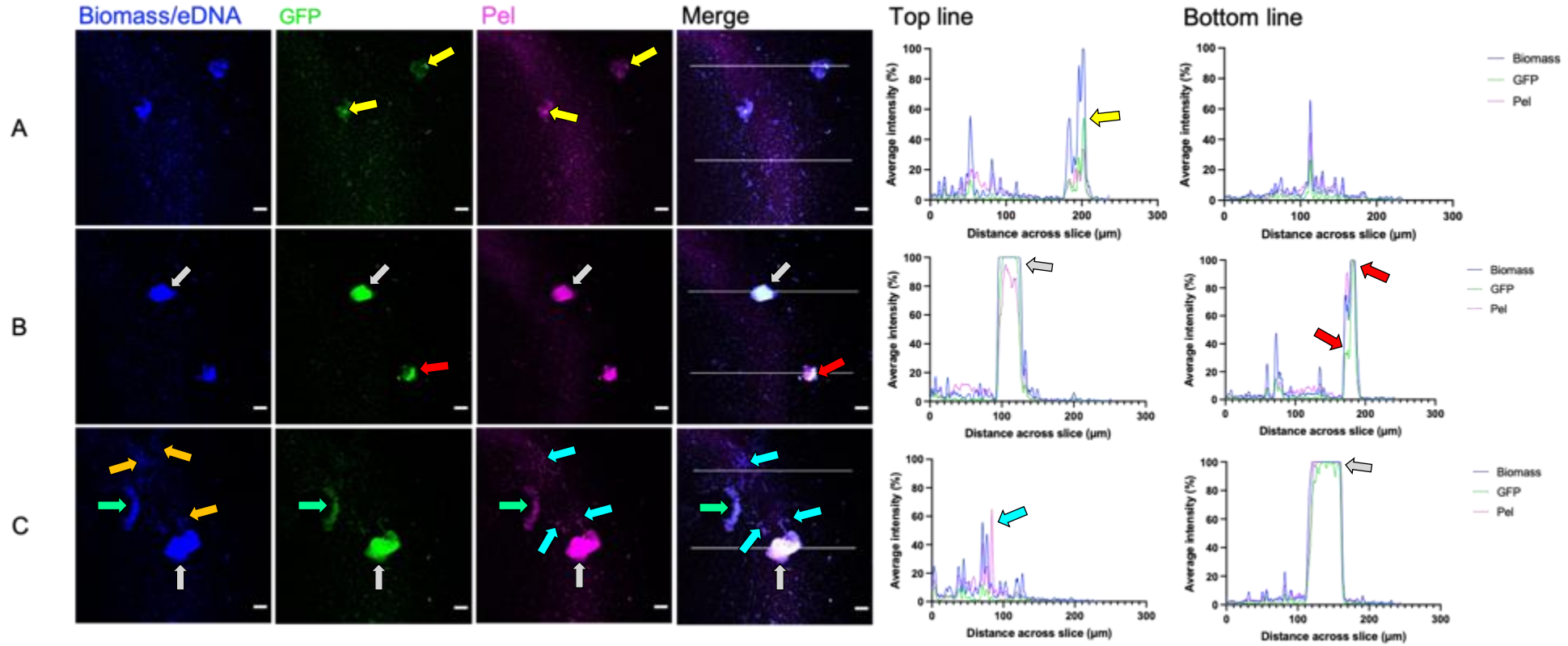

(*figure legend for* Figure 3.2)

Representative confocal images are from PA14 *cdrA::gfp* biofilms (GFP signal is green) cultivated for 24 hours in the CBR under low shear (at 75 RPM) and stained with Hoechst for biomass/eDNA (blue) and the Pel-specific lectin WGA (magenta). A, B and C are each independent sample sites from two different coupon surfaces, and show horizontal optical cross-sections with limited surface colonisation. Scale bar = 20 μm. Fiji was used to quantify fluorescent values in individual z-stack images: fluorescence signal intensity was normalised to the brightest pixel per coupon, and a five point moving average calculated. Yellow arrows show a punctate fluorescence intensities for GFP and Pel within a feature, red arrows show heterogenous GFP fluorescence within the same features, orange and cyan arrows show the formation of an eDNA (orange arrows) and Pel network (cyan arrows) forming upon the coupon surface, green arrows show eDNA and Pel localisation to an elongated feature with lower GFP fluorescence, and grey arrows show plateaus as maximum intensity across the three channels was reached in some features.

For some of the features there was localised variation in the intensity of biomass, *cdrA::gfp* and Pel fluorescence, leading to peaks and troughs observed in the resultant intensity histograms for the features themselves. In Figure 3.2A, the fluorescence intensity of Hoechst was greatest in the feature, with a punctate region of GFP correlating to a similarly punctate Pel expression on the feature's as-viewed right-hand side (yellow arrows). By comparison, the feature captured by the bottom sampling line in Figure 3.2B had well correlated intensities for both Hoechst and Pel fluorescence, but varying *cdrA::gfp* fluorescence which was lower on the feature's as-viewed left-hand side (red arrow). Staining of these features by Hoechst and WGA was colocalised, which could suggest both eDNA and Pel are both important for initial cell-surface and cell-cell interactions during early development of PA14 biofilms.

In Figure 3.2C, a mesh-like network stained by Hoechst can be seen on the coupon surface as well as protruding from the periphery of the spherical feature (orange arrows). Punctate Pel fluorescence was observed to associate with the mesh-like networks, (Figure 3.2, cyan arrows), whilst GFP expression of individual PA14 *cdrA::gfp* cells within the network was lower than that of the features, suggesting the cells have lower intracellular c-di-GMP levels, and may have become recently sessile. In the elongated structural feature (Figure 3.2C, green arrows), punctate Pel production is seen interspersed throughout areas stained by Hoechst, and could be representative of a feature at an earlier stage of formation, whereby eDNA has provided a structural network that PA14 cells can adhere to. Allensen-Holm *et al.,* (2006), showed that eDNA is organised during early PA01 biofilm formation, and entwining of eDNA between cells can result in the development of stable clumps (i.e. within the features shown in Figure 3.2). The work of Gloag *et al.,* (2012), further

supports this, as eDNA was revealed to maintain coherent cell alignments during twitching motility-mediated growth of the biofilm.

The fluorescence intensity profiles for some of the features formed plateaus, displaying maximum intensity across the three channels. Plateau formation may be indicative of overexposure during image acquisition, leading to saturation of the structures within some of the more defined features (Figures 3.2B and 3.2C, grey arrows). After 24 hours of growth under low shear at 75 RPM, it was extremely challenging to expose the image such that small, faint features (i.e. individual PA14 cells) and large, bright features were both visible and not saturated.

Under high shear at 350 RPM, initial attachment of PA14 *cdrA::gfp* was generally characterised by the formation of cell clusters or aggregates (of sizes ranging from 20 μm to > 50 μm in the x and y dimensions) that were spatially separate from one another, leading to sparse colonisation of the coupon surface overall. Compared to low shear at 75 RPM where single cell attachment was typically seen (Figure 3.1), high shear conditions appeared to induce the formation of small clusters of cells (Figure 3.3). For areas of the coupon surfaces colonised by individual cells and clusters under both low and high shear, intensity profiles were similarly very punctate, but the respective fluorescence intensities across all three channels were more variable for the high shear condition. Under high shear at 350 RPM, individual cells and clusters exhibited greater fluorescence intensities, a lack of correlation between channels, and more pronounced punctate profiles as a result of increased PA14 *cdrA::gfp* attachment to the surface (Figure 3.3A, red arrows).

Figure 3.3A shows individual PA14 *cdrA::gfp* cells that are surface-attached, as well as the formation of clustering cell populations of varying sizes, which may be indicative of various stages of localised cluster development (i.e. early versus established clusters) (Figure 3.3A, pink arrows). Hoechst and GFP fluorescence were well correlated with one another in the clusters, which were observed to have increased fluorescence intensities compared to the single attached cells for both Hoechst and GFP, but not Pel (Figure 3.3A, grey arrows). Clustering of PA14 *cdrA::gfp* cells, which appear to be attached to both the surface and to one another, was induced by high but not low shear conditions, and may precede the formation of features and early microcolony development. Lecuyer *et al.,* (2011), previously demonstrated that increased shear stress resulted in a greater frequency of adhesion events for PA14, resulting in cells that were surface-attached for longer, and were less likely to detach from the surface once adhered. In agreement with this is the work of several other groups, who similarly found that higher rates of shear resulted in increased accumulation of bacteria on test surfaces (Thomas *et al.,* 2002; Horn *et al.,* 2003).

**Figure 3.3**

**Increased attachment of PA14 *cdrA::gfp* cells after 24 hours of growth under high shear conditions at 350 RPM**

*(figure legend overleaf)*

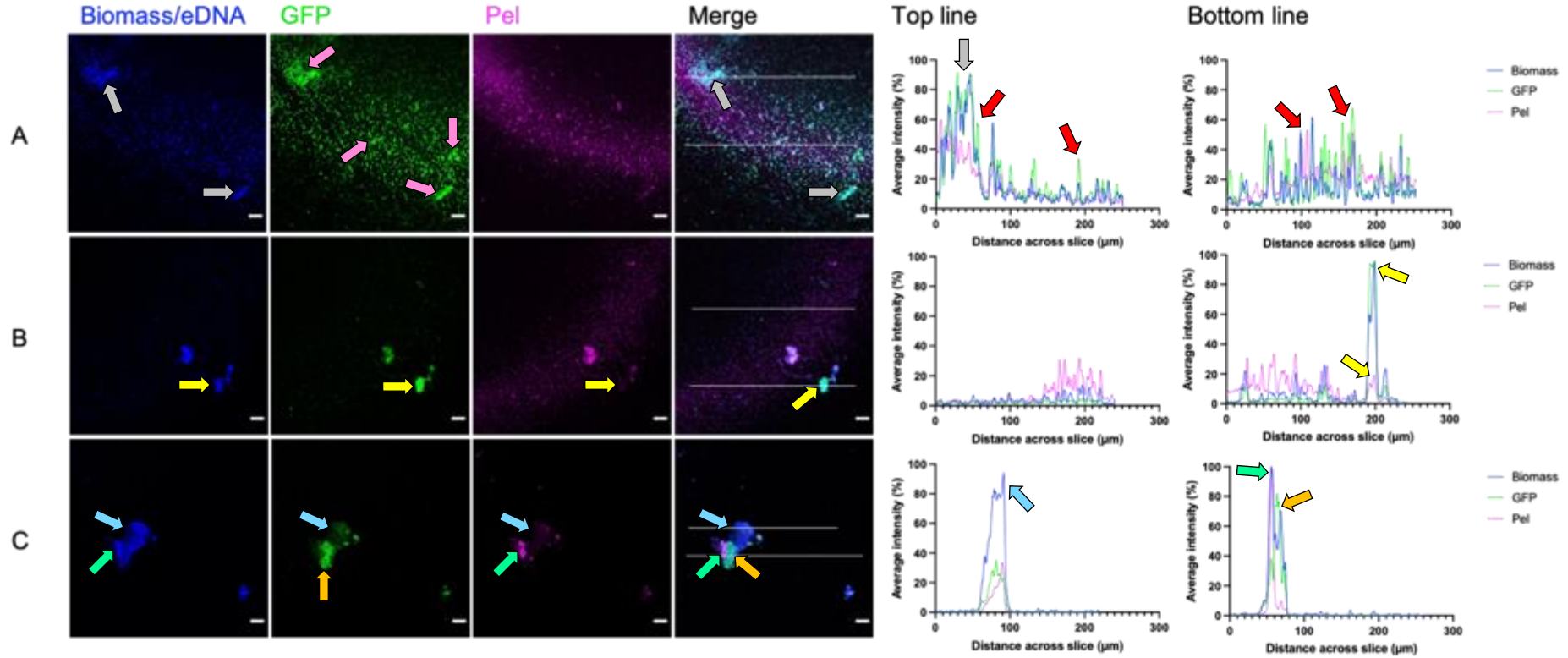

(*figure legend for* Figure 3.3)

Representative confocal images are from PA14 *cdrA::gfp* biofilms (GFP signal is green) cultivated for 24 hours in the CBR under high shear (at 350 RPM) and stained with Hoechst for biomass/eDNA (blue) and the Pel-specific lectin WGA (magenta). A, B and C are each independent sample sites from two different coupon surfaces, and show horizontal optical cross-sections with limited surface colonisation overall. Scale bar = 20 μm. Fiji was used to quantify fluorescent values in individual z-stack images: fluorescence signal intensity was normalised to the brightest pixel per coupon, and a five point moving average calculated. Red arrows show punctate fluorescence intensity profiles across all three channels as a result of increased single cell attachment, pink arrows show population of GFP-expressing cells forming clusters, which had well correlated Hoechst fluorescence as shown by the grey arrows. Light blue, orange and green arrows show areas of a feature displaying heterogenous fluorescence intensities, as a result of variable GFP expression and differential staining of the feature by Hoechst and WGA.

Given that the fluorescence intensity of Pel was lower than and often uncorrelated to Hoechst and GFP fluorescence intensities (Figure 3.3A), clustering of individual cells may have been facilitated by surface-associated behaviours such as swarming and twitching, leading to migration of individual PA14 cells to the same area of the coupon surface (Burrows, 2012; Partridge and Harshey, 2013). Twitching is mediated by TFP, and this type of motility has been previously observed in cellular aggregates (Semmler *et al.,* 1999; Merz *et al.,* 2000; Mattick, 2002). Furthermore, TFP are known to be involved in mediating cell-surface and cell-cell interactions enabling biofilm development, as *Ps. a.* mutants defective in pili biosynthesis are non-motile, do not migrate along surfaces and are unable to form microcolony structures (O'Toole and Kolter, 1998a; Klausen *et al.,* 2003; Barken *et al.,* 2008).

In contrast to the observations of PA14 cells grown under low shear, high shear conditions at 350 RPM resulted in the formation of much more pronounced features, which were more variable with respect to their size (in x, y and z dimensions), shape and relative proportions of Hoechst, GFP and Pel fluorescence. Whilst some of the features were of a comparable size to those formed under low shear, fluorescence intensities within the features differed based upon spatial location. Some features exhibited modest Pel production in comparison to the correspondingly high intensities for Hoechst and *cdrA::gfp* fluorescence (Figure 3.3B, yellow arrows), whilst other features had distinct and spatially-dependent fluorescence intensity profiles for Hoechst, GFP and Pel respectively.

Heterogenous fluorescence intensities within the same feature can be seen in the resulting line profiles in Figure 3.3C. Hoechst fluorescence predominated one area of

the feature (as sampled by the top line), whilst GFP and Pel fluorescence intensities were visibly reduced (Figure 3.3C, light blue arrows). In the part of the feature as sampled by the bottom line, Hoechst and Pel were observed to co-localise in an area of the feature with decreased *cdrA::gfp* fluorescence (Figure 3.3C, orange arrows) whilst the adjacent cell subpopulation exhibited increased GFP fluorescence which was uncorrelated to either Hoechst or Pel fluorescence (Figure 3.3C, green arrows). Taken together, such results indicate that production of Pel during early adhesion may be a stochastic process, given that different degrees of Pel fluorescence were observed in both spatially-separated (and thus independently-formed) features, and within the same feature itself (Figure 3.3).

High shear conditions also resulted in the formation of more developed features after 24 hours of growth, with increased height in the z dimension compared to features grown under low shear, which were on average 10 μm in height. By comparison, larger features under high shear were > 10 μm in height on average, had more irregular peripheries, and were seen in areas where surface colonisation by individual cells or small cell clusters was minimal or absent (as already shown by Figures 3.3B and 3.3C). Such features also had differing morphologies to one another, with some structures appearing more globular; composed of individual cell clusters aggregated together which may represent a more mature feature (Figure 3.4). As a result of this, fluorescence intensity profiles for these features were no longer punctate, and in general Hoechst, GFP and Pel fluorescence correlated well with one another, albeit with different intensities respectively.

Figure 3.4 shows a feature imaged at two heights in the z dimension: at Z+5 and Z+10 μm (with Z defined as the bottom layer closest to the coupon surface). At a height of Z+5 μm, three different features can be seen, labelled i, ii and iii respectively. Fluorescence intensities of Hoechst, GFP and Pel are well-correlated to one another for the largest feature (i), with signal intensity highest across all three channels at the feature periphery, resulting in a concave intensity profile (Figure 3.4, feature i, yellow arrows). Fluorescence intensities at the peripheral edges was heterogenous, particularly with respect to GFP and Pel fluorescence which had greater intensities at the as-viewed left-hand side periphery compared to the as-viewed right-hand side periphery (Figure 3.4, red arrows). Features i and iii appeared to have globular-like morphologies, appearing to be composed of individual cell clusters aggregated together. In feature iii, Pel fluorescence was greatest at the periphery in compassion to the feature interior (Figure 3.4, green arrows), whilst Hoechst and GFP fluorescence was more homogenous across the feature, suggesting that cells were expressing equivalent levels of *cdrA* (pink arrows). Hoechst, GFP and Pel fluorescence intensities were similarly well-correlated in feature ii, although *cdrA* expression was heterogenous, with increased GFP fluorescence at the as-viewed right-hand side of the feature interior and periphery (Figure 3.4, grey arrows).

At a height of Z+10 μm, the apex of feature (i) is seen emerging (Figure 3.4). Hoechst, GFP and Pel fluorescence correlated well with one another overall, although the fluorescence intensity of Pel was lower than that of Hoechst and GFP (Figure 3.4, cyan arrows). Given that the fluorescence intensity of Hoechst was greatest, and staining by Hoechst appeared diffuse rather than punctate, this could suggest the presence of eDNA within the feature. As discussed for features formed under low

shear conditions, eDNA can facilitate cell-cell interactions by acting as an interconnecting ECM matrix component, and is believed to be important during the initial and early development of *Ps. a.* biofilms (Whitchurch *et al.,* 2002; Allensen-Holm *et al.,* 2006; Flemming and Wingender, 2010) .

**Figure 3.4**

**Three-dimension feature formation by PA14 *cdrA::gfp* after 24 hours of growth under high shear conditions at 350 RPM**

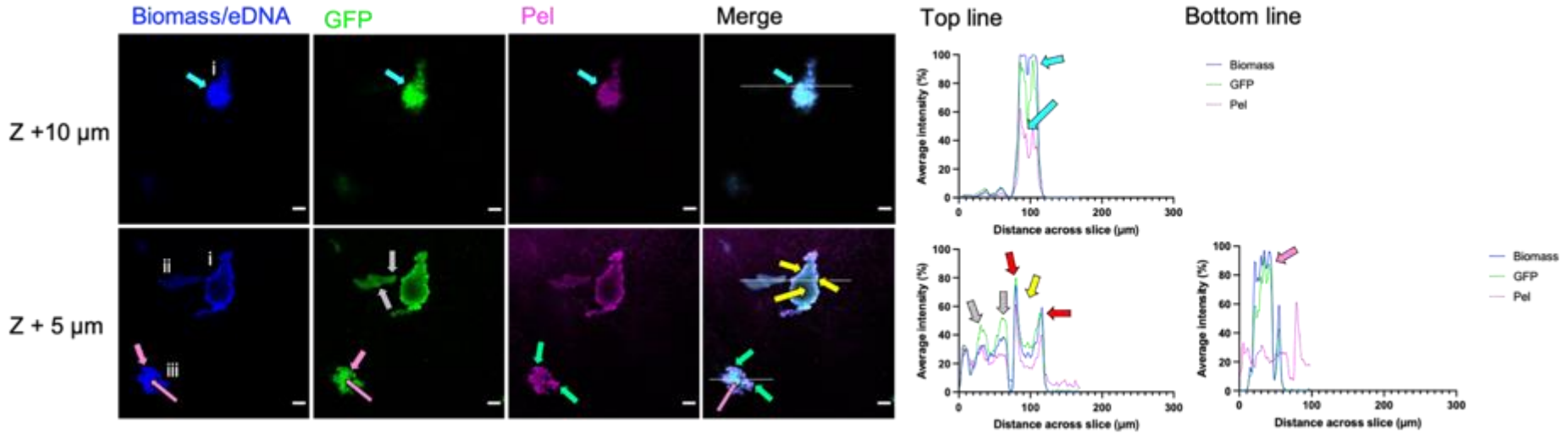


Representative confocal images are from PA14 *cdrA::gfp* biofilms (GFP signal is green) cultivated for 24 hours in the CBR under high shear (at 350 RPM) and stained with Hoechst for biomass/eDNA (blue) and the Pel-specific lectin WGA (magenta). Two different z heights for the same sample location are presented, and show horizontal optical cross-sections of several different features (i, ii and iii). Scale bar = 20 µm. Fiji was used to quantify fluorescent values in individual z-stack images: fluorescence signal intensity was normalised to the brightest pixel per coupon, and a five point moving average calculated. Yellow arrows show a concave fluorescence intensity profile for feature i, indicative of increased GFP expression and staining at the periphery compared to the feature interior. Red arrows show the concave profile is heterogenous, with increased fluorescence intensities at the as-viewed left-hand peripheral edge compared to the as-viewed right-hand side. Green arrows show increased fluorescence of Pel at the periphery of the globular feature iii, and pink arrows show homogenous fluorescence intensities of Hoechst and GFP across the feature's interior. Grey arrows show areas with increased GFP fluorescence in feature ii. Cyan arrows show well-correlated fluorescence intensities in emerging apex of feature i, with Pel fluorescence lower than that of Hoechst and GFP.

3.3.2. Pel production in PA14 is increased during early biofilm development under high shear at 350 RPM

After 48 hours of growth, biofilm formation under low shear at 75 RPM was characterised by the development of a basal biofilm that covered most of the coupon surface (Figure 3.5), with an average height for this layer of 10 – 15 μm. Fluorescence intensity profiles for Hoechst and GFP were well correlated, suggesting most cells were expressing equivalent quantities of *cdrA* to one another throughout the basal biofilm (Figures 3.6 and 3.7).

**Figure 3.5**
**Basal biofilms formed by PA14 *cdrA::gfp* after 48 hours under low shear conditions at 75 RPM are composed of homogenous cell and cell-associated EPS layers**

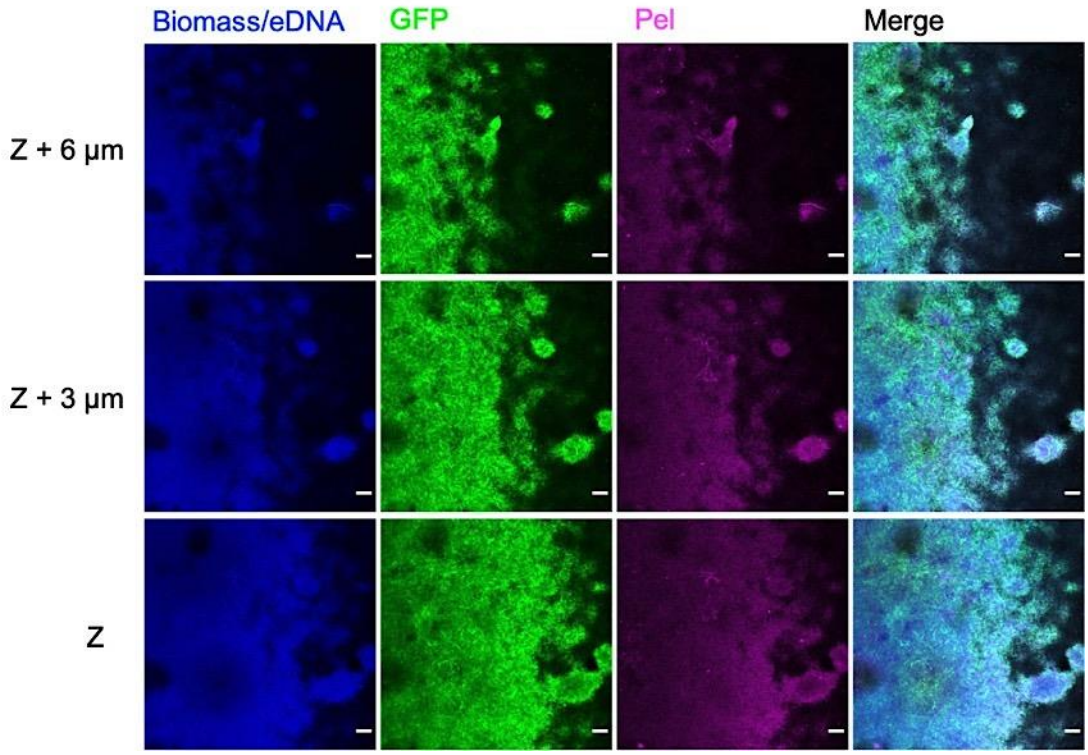


Representative confocal images are from PA14 *cdrA::gfp* biofilms (GFP signal is green) cultivated for 48 hours in the CBR under low shear (at 75 RPM) and stained with Hoechst for biomass/eDNA (blue) and the Pel-specific lectin WGA (magenta). Three different z heights for the same basal biofilm are presented, with Z defined as the bottom layer closest to the coupon surface. Each panel shows horizontal optical cross-sections that display homogeneity with respect to Hoechst, GFP and Pel fluorescence. Scale bar = 20 μm.

Whilst production of Pel, as quantified by WGA, was also well correlated with Hoechst and GFP fluorescence, there were areas within the basal biofilm with increased and localised Pel concentration in lower layers, resulting in more punctate fluorescence intensities (Figure 3.6, yellow arrows). These punctate fluorescence intensities for Pel did not correlate to similarly elevated levels of Hoechst and GFP fluorescence, which suggests that the Pel in this part of the biofilm is not cell-associated (Figure 3.6, from Z to a height of Z+3 μm). This localised area of increased Pel production could indicate that Pel is able to provide structural support to the upper cell layers of that part of the basal biofilm, facilitating their attachment and early development of a three-dimensional architecture.

From a height of Z+6 μm upwards (Figure 3.6), the average fluorescence intensity of Pel decreased with increasing height whilst the fluorescence intensities of both Hoechst and GFP increased, indicating the composition of the biofilm became more cell-based. Work by Vasseur *et al.,* (2005), has previously demonstrated that Pel is required for mediation of initial cell-surface contact, particularly to glass or plastic surfaces. Thus, at the bottom of the basal biofilm where maintenance of irreversible attachment to the surface is vital if maturation of the biofilm is to occur, Pel production may enable increased cell-surface and cell-cell interactions to the PE coupon face.

Using atomic force microscopy and software to enable the tracking of individual bacteria over time, Cooley *et al.,* (2013), revealed that Pel promotes organisation of bacteria lying flat and symmetrically on a surface, with Δ*pel* mutants in comparison forming disorganised piles of cells adhered to the surface and one another asymmetrically (i.e. standing on end rather than lying flat). Therefore, one could

hypothesise that the area of increased Pel concentration as in Figure 3.6 is providing localised, structural organisation to that part of the biofilm; promoting the formation of homogenous cell layers in the same orientation as one another.

By the height Z+15 μm, the basal biofilm is reaching its apex, and populations of cells with increased GFP expression can be seen beginning to protrude above the rest of the biofilm (Figure 3.6, red arrows). Thus, these subpopulations of PA14 *cdrA::*gfp cells can be characterised by their increased *cdrA* expression, as shown by the fluorescence intensity profile for GFP and its more punctate appearance at heights of Z+11 and 15 μm (Figure 3.6, grey arrows).

**Figure 3.6**

**Increased Pel production localised within a basal biofilm formed by PA14 *cdrA::gfp* after 48 hours under low shear conditions at 75 RPM**

*(figure legend overleaf)*

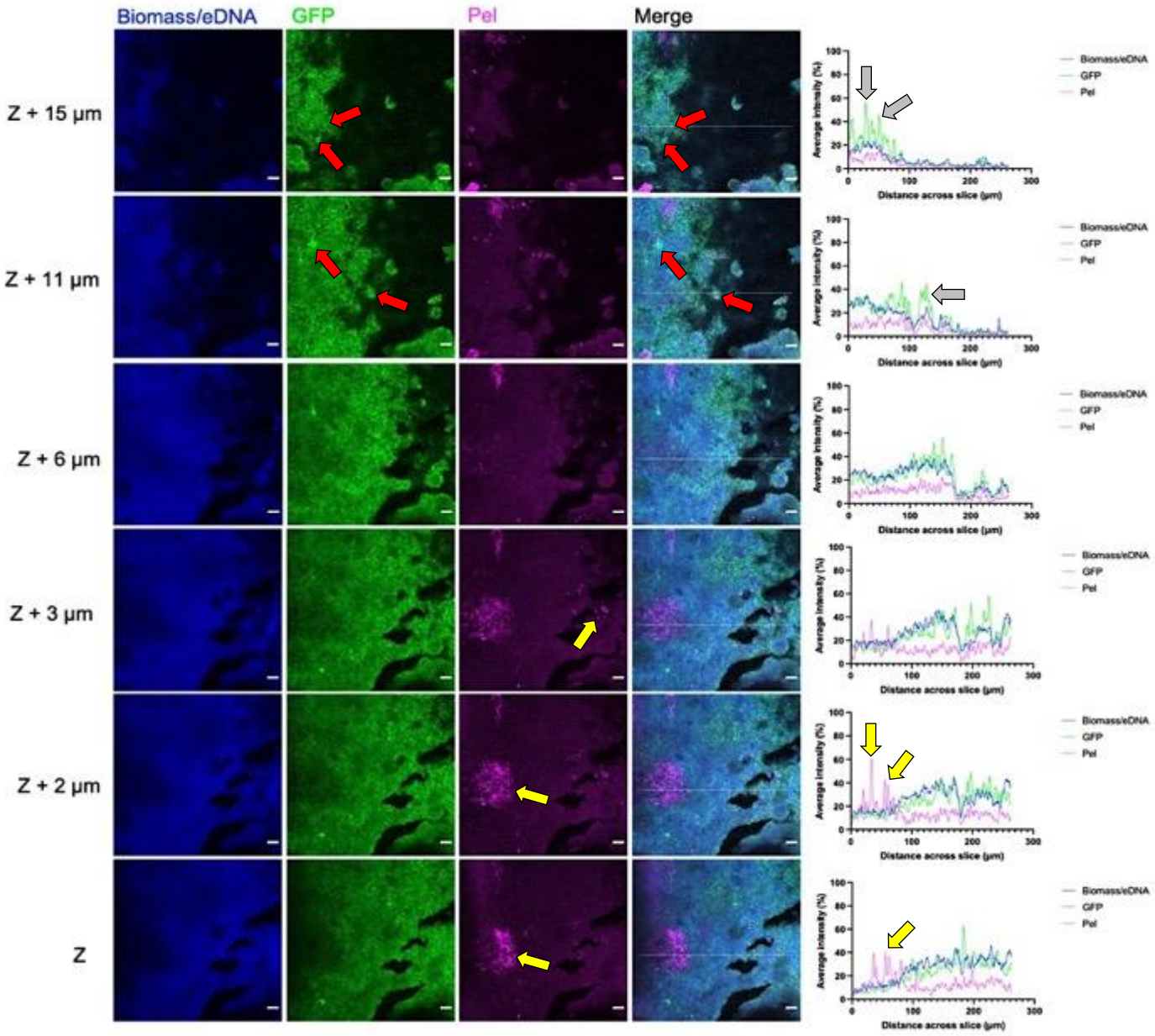

(*figure legend for* Figure 3.6)

Representative confocal images are from PA14 *cdrA::gfp* biofilms (GFP signal is green) cultivated for 48 hours in the CBR under low shear (at 75 RPM) and stained with Hoechst for biomass/eDNA (blue) and the Pel-specific lectin WGA (magenta). Different z heights are shown for the same basal biofilm, with Z defined as the bottom layer closest to the coupon surface. Scale bar = 20 μm. Fiji was used to quantify fluorescent values in individual z-stack images: fluorescence signal intensity was normalised to the brightest pixel per coupon, and a five point moving average calculated. Yellow arrows show regions of punctate Pel fluorescence uncorrelated to Hoechst or GFP fluorescence, red arrows show cell subpopulations within the upper layers of the basal biofilm that have increased GFP fluorescence and therefore *cdrA* expression. Grey arrows show the punctate GFP fluorescence intensities of such cell subpopulations.

Across different sampling sites, localised cell populations were frequently observed to have increased GFP expression in comparison to adjacently located cells (Figure 3.7, pink arrows), that did not appear to correlate with either increased Hoechst or Pel fluorescence. Increased fluorescence intensities for GFP correlate to increased levels of intracellular c-di-GMP, as *cdrA* promoter activation is c-di-GMP-dependent (Rybtke *et al.,* 2012; Nair *et al.,* 2016). Thus, areas composed of PA14 *cdrA::gfp* cells that exhibited increased GFP expression may represent a cell population forming a developing microcolony. Increased intracellular levels of c-di-GMP are known to result in the second messenger binding to FleQ (an enhancer-binding protein that regulates flagellum synthesis), resulting in its dissociation from a secondary protein, FleN, and conversion of FleQ from a repressor of *pel*, *psl* and *cdr* genes into an activator, leading to increased EPS and adhesin production (Baraquet *et al.,* 2012; Baraquet and Harwood, 2013; Su *et al.,* 2015). Areas with increased GFP expression could therefore be nucleation centres for growth and maturation of the biofilm. Microcolony structures emerging from the basal biofilm (Figure 3.7, at Z +13 μm) support this notion, as they were characterised by punctate fluorescence intensity profiles with respect to both GFP and Pel, with Pel observed to localise to either the structure periphery, or the centre of the structure at its apex, emerging above the cells (Figure 3.7, red arrows). Increased and well-correlated fluorescence intensities across all three channels were additionally found across the interior of some structures (Figure 3.7, grey arrows).

At the bottom of the basal biofilm there were ‘shadows’ located directly underneath the microcolony structures with low fluorescence intensities across all three channels (Figure 3.7 at Z, orange arrows). These could represent a limitation in laser penetration to the base of the biofilm.

**Figure 3.7**

**Emergence of developing microcolonies formed by PA14 *cdrA::gfp* after 48 hours under low shear conditions at 75 RPM**

*(figure legend overleaf)*

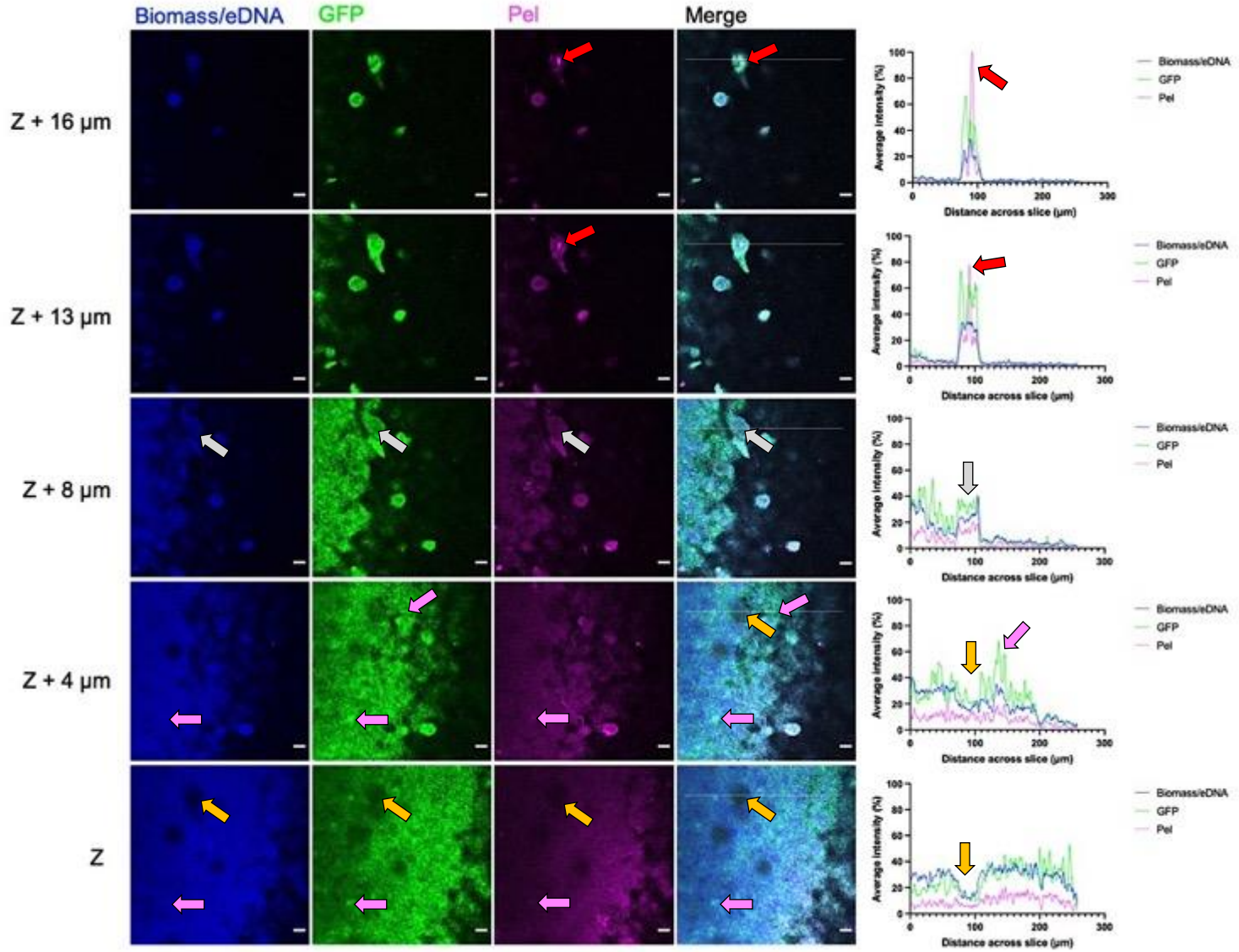

(*figure legend for* Figure 3.7)

Representative confocal images are from PA14 *cdrA::gfp* biofilms (GFP signal is green) cultivated for 48 hours in the CBR under low shear (at 75 RPM) and stained with Hoechst for biomass/eDNA (blue) and the Pel-specific lectin WGA (magenta). Different z heights are shown for the same basal biofilm, with Z defined as the bottom layer closest to the coupon surface. Scale bar = 20 μm. Fiji was used to quantify fluorescent values in individual z-stack images: fluorescence signal intensity was normalised to the brightest pixel per coupon, and a five point moving average calculated. Pink arrows show subpopulations of cells with increased *cdrA* expression in comparison to adjacent cell populations, resulting in increased GFP fluorescence intensities. Red arrows show localisation of punctate Pel fluorescence at the apex of emerging microcolonies, whilst grey arrows show well-correlated Hoechst, GFP and Pel fluorescence intensities across the interior of the microcolony. Orange arrows show cavities with the basal biofilm (including beneath the microcolony identified by the grey and red arrows), with cavities exhibiting negligible fluorescence intensities.

Under low shear conditions at 75 RPM, development of a basal, multi-cell layered PA14 *cdrA::gfp* biofilm appeared to be generally homogenous, irrespective of location on the coupon surface and cell location within the basal layer. Pel fluorescence in the basal biofilm was consistently lowest in terms of its fluorescence intensity when compared to Hoechst and GFP fluorescence intensities, with areas of increased Pel production in the basal biofilm punctate and variable throughout the height of the structure (Figures 3.6 and 3.7). However, some areas of the basal biofilm exhibited greater staining by WGA, indicative of increased and spatially-localised Pel production (Figures 3.8 and 3.9).

In these areas, Pel was observed as either a dense aggregate that encapsulated the spatially-localised PA14 *cdrA::gfp* cells (Figures 3.8 and 3.9, yellow arrows), or as fibre-like projections throughout the lower parts of the basal layer, connecting local populations of adjacent cells to one another (Figures 3.8 and 3.9, grey arrows). Structural cavities were also present in the lower part of the basal biofilm beneath microcolony structures, with Pel seemingly localised to the boundary between the cavity and basal layer (Figure 3.9 at Z and Z+2 μm, red arrows). Previous work by Ma *et al.,* (2009), in *Ps. a.* strain PA01 demonstrated that Psl can either be cell-associated, or located in areas of the biofilm which lacked bacterial cells as free Psl, which was shown to be capable to forming a fibre-like matrix structure that enmeshed bacteria to the test surface (Ma *et al.,* 2009). Zhao *et al.,* (2013), revealed that *Ps. a.* is additionally capable of depositing Psl trails on a surface, which are able to influence the surface motility of subsequently-adhering cells, their migration and initiation of biofilm formation. Given that *Ps. a.* strain PA14 is incapable of making Psl due to a deletion of *pslA* to *pslD* in its genome (Friedman and Kolter, 2004a; 2004b), the observed fibre-

like networks of Pel forming in Figures 3.8 and 3.9 (grey arrows) may be similar to previously-described Psl networks in terms of function; promoting cell-surface and cell-cell interactions via deposition of free Pel on the surface.

**Figure 3.8**

**Aggregative Pel morphologies observed after 48 hours of PA14 *cdrA::gfp* biofilm formation under low shear conditions at 75 RPM**

*(figure legend overleaf)*

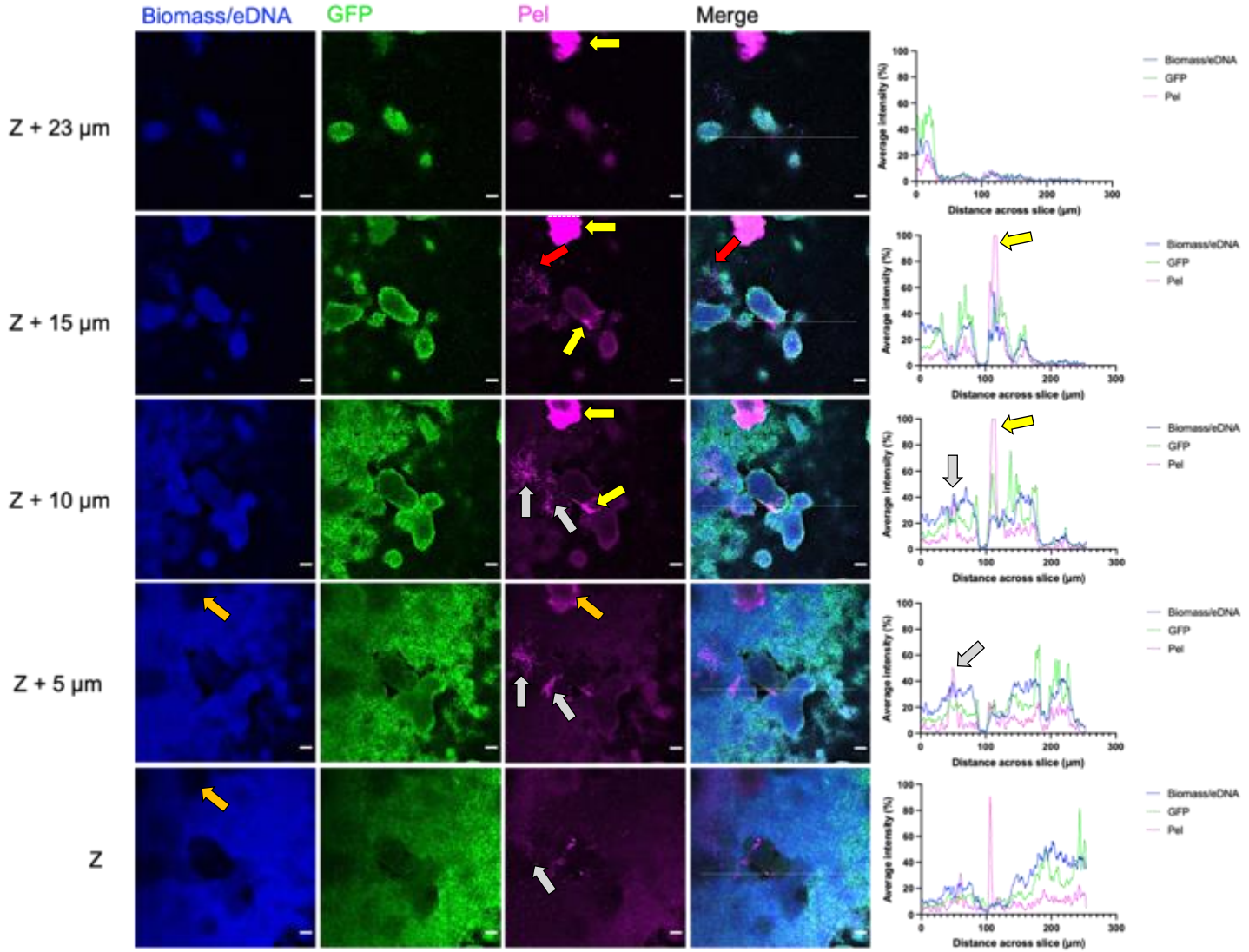

(*figure legend for* Figure 3.8)

Representative confocal images are from PA14 *cdrA::gfp* biofilms (GFP signal is green) cultivated for 48 hours in the CBR under low shear (at 75 RPM) and stained with Hoechst for biomass/eDNA (blue) and the Pel-specific lectin WGA (magenta). Different z heights are shown for the same basal biofilm, with Z defined as the bottom layer closest to the coupon surface. Scale bar = 20 μm. Fiji was used to quantify fluorescent values in individual z-stack images: fluorescence signal intensity was normalised to the brightest pixel per coupon, and a five point moving average calculated. Yellow arrows show dense aggregates of Pel that encapsulated cell populations, whilst grey arrows show Pel as fibre-like projections throughout the basal biofilm, forming a Pel network. Red arrows show a punctate region of Pel production in-between two emerging microcolony apexes. Orange arrows show cavities void in Hoechst fluorescence in the lowest basal layers, at the site of the developing Pel aggregate. White dashed line shows the maximum width reached in the x dimension by the dense Pel aggregate identified by the yellow arrows.

**Figure 3.9**

**Aggregative Pel morphologies within PA14 *cdrA::gfp* basal biofilms observed after 48 hours under low shear conditions at 75 RPM**

*(figure legend overleaf)*

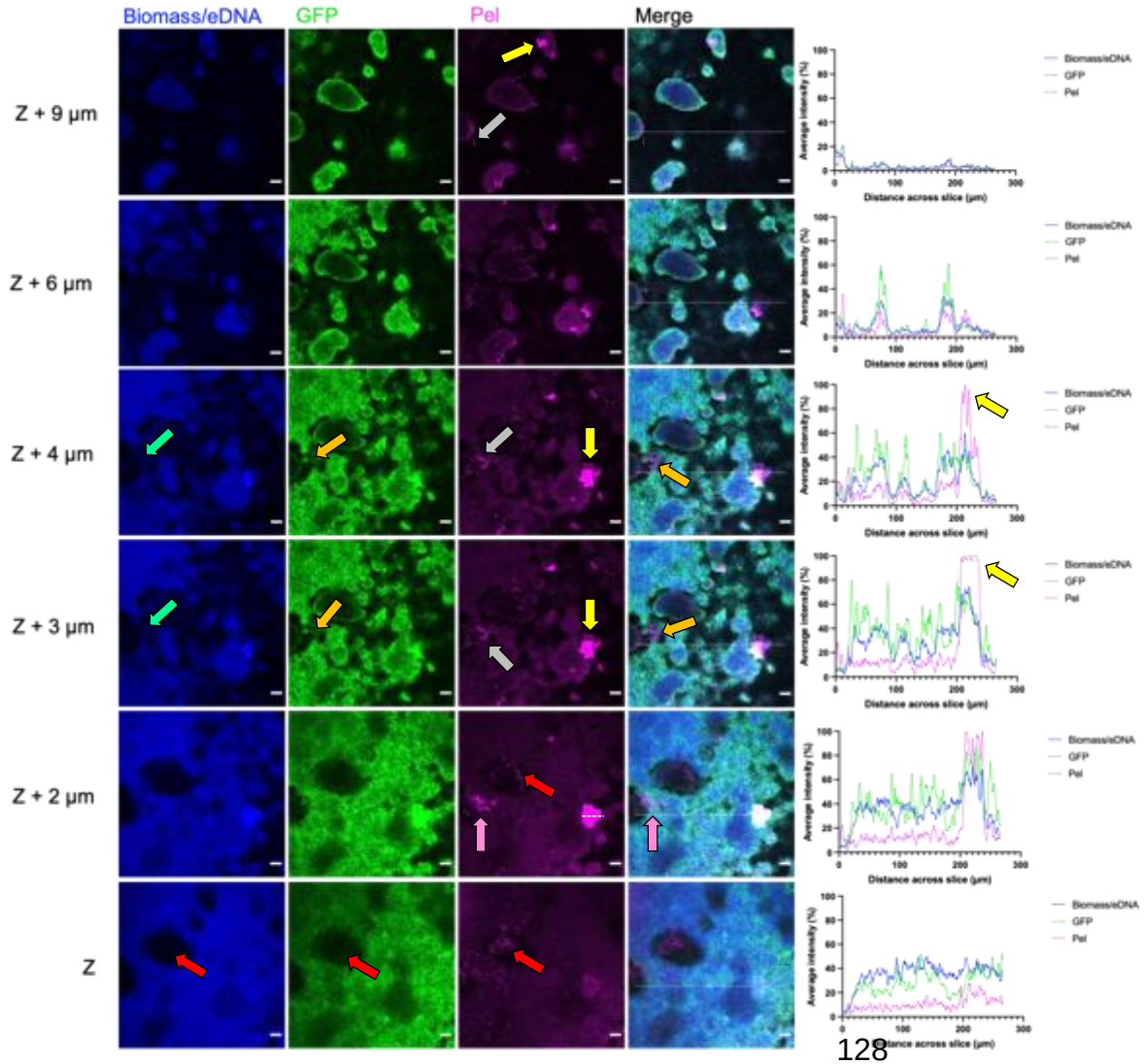

(*figure legend for* Figure 3.9)

Representative confocal images are from PA14 *cdrA::gfp* biofilms (GFP signal is green) cultivated for 48 hours in the CBR under low shear (at 75 RPM) and stained with Hoechst for biomass/eDNA (blue) and the Pel-specific lectin WGA (magenta). Different z heights are shown for the same basal biofilm, with Z defined as the bottom layer closest to the coupon surface. Scale bar = 20 μm. Fiji was used to quantify fluorescent values in individual z-stack images: fluorescence signal intensity was normalised to the brightest pixel per coupon, and a five point moving average calculated. Yellow arrows show dense aggregates of Pel that encapsulated cell populations, whilst grey arrows show Pel as fibre-like projections throughout the basal biofilm, forming a network of Pel. Red arrows show Pel fluorescence localised to the boundary between a microcolony cavity and basal biofilm. Pink arrows show an area of increased fluorescence that is cell-surface and cell-cell associated. Orange arrows show fibre-like projections of Pel connecting to adjacent cell populations to one another. Green arrows show fibre-like projections of eDNA stained by Hoechst, correlating with WGA-stained Pel fibres as identified by the orange arrows. White dashed line shows the maximum width reached in the x dimension by the dense Pel aggregate identified by the yellow arrows.

Chew *et al.,* (2014), suggested that 'younger' biofilms are thinner, less robust structures that are easily disrupted by mechanical forces (such as shear), and that the production of a matrix that is crosslinked or enmeshed prevents detachment of surface-attached cells and centralises growth to these newly-colonised sites. Thus, the Pel fibre-like networks observed could be ensuring neighbouring PA14 *cdrA::gfp* cell populations remain adhered to the surface and to one another, as illustrated in Figure 3.9 at a height of Z+2 μm, whereby increased and cell-associated Pel production can be seen within the initial surface-associated basal layers of the biofilm (pink arrows). This increased and localised concentration of Pel was maintained at heights of Z+3 μm and Z+4 μm, with fibre-like projections of Pel enmeshed together observed forming across an area noticeably devoid of a GFP-expressing cell population; seemingly connecting the two adjacent cell populations to one another until their peripheral edges are seen (Figure 3.9, orange arrows).

As demonstrated in Figure 3.8, an equivalently punctate concentration of Pel can be seen in-between two emerging colony apexes at a height of Z+15 μm (red arrows), as a continuation of the fibre-like Pel structures that initially emerge at Z; extending upwards throughout the basal biofilm, forming a entangled meshwork (Figure 3.8, grey arrows). Maximally produced at a height of Z+10 μm, the meshwork can be seen in a formation akin to a spider's web, with fibres radiating outwards from a central region that exhibits punctate Pel concentration (Figure 3.8, grey arrows). Of further interest is the fact that fibre-like structures stained by Hoechst appear well-correlated to some of the WGA-stained Pel fibres, which could indicate that these structures comprise of Pel-eDNA complexes (Figure 3.9, green arrows). Allesen-Holm *et al.,* (2006), showed that eDNA could promote distinct interactions between subpopulations of bacteria,

thus the formation of Pel-DNA complexes may enhance local interactions between spatially-separated cell populations; in turn ensuring the formation of a stable, more robust basal layer that enables future biofilm development into a more three-dimensional structure.

The dense aggregates of Pel observed in Figures 3.8 and 3.9 (yellow arrows) further suggest that Pel can adopt different structural phenotypes within a developing biofilm. In Figure 3.8, the large Pel aggregate was maximally produced at a height of Z+15 μm, whereby it measured 45 μm in width (in the x dimension, white dashed line) and was observed to be encapsulating a population of cells. In the lower layers of the basal biofilm, at heights of Z and Z+5 μm, formation of the Pel aggregate can be seen in an area that is correspondingly devoid of staining by Hoechst (Figure 3.8, orange arrows), suggesting that this aggregate is composed of more free, rather than cell-associated Pel. By comparison, the aggregate of Pel in Figure 3.9 is much denser: maximally produced at a height of Z+2 μm, whereby it measured 30 μm in width (in the x dimension, white dashed line), the Pel aggregate remained cell-associated throughout the basal biofilm layers, as shown by the well-correlated and increased fluorescence intensities profiles across all three channels.

By contrast, biofilm development under high shear (at 350 RPM) was markedly different, most notably with respect to the formation of the basal biofilm layer. Instead of forming a defined and continuous basal biofilm layer, spatially-separate basal biofilms were distributed across the coupon surface and displayed increased heterogeneity with respect to Hoechst, GFP and Pel fluorescence. Biofilms formed under high shear exhibited noticeably increased Pel production in comparison to those

developing under low shear, with the additional appearance of individual, GFP-expressing cells in the uppermost basal layers (Figure 3.10).

**Figure 3.10**

**Basal biofilm formation by PA14 *cdrA::gfp* under high shear conditions at 350 RPM displays increased heterogeneity**

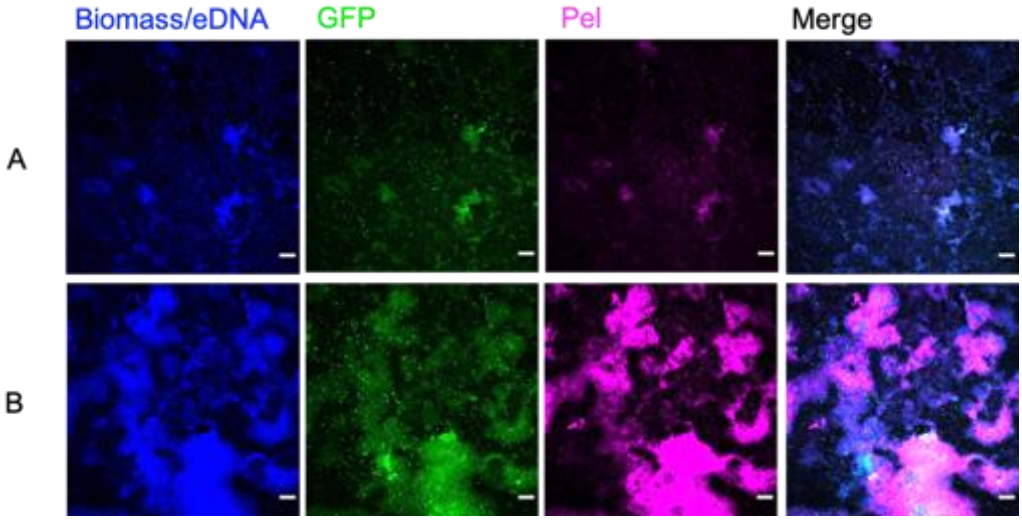


Representative confocal images are from PA14 *cdrA::gfp* biofilms (GFP signal is green) cultivated for 48 hours in the CBR under high shear (at 350 RPM) and stained with Hoechst for biomass/eDNA (blue) and the Pel-specific lectin WGA (magenta). A and B are from two independent sampling sites on the same coupon. Each panel shows horizontal optical cross-sections that display heterogeneity with respect to Hoechst, GFP and Pel fluorescence and biofilm morphology. Scale bar = 20 μm.

Resultantly, fluorescence intensity profiles for GFP were more punctate, and did not strongly correlate with corresponding Hoechst or Pel fluorescence intensity profiles (Figure 3.11). Pel was observed to encapsulate PA14 *cdrA::gfp* cells in certain structures and exist as free, non-cell associated Pel, as demonstrated by the increased fluorescence intensity of Pel in comparison to the equivalent Hoechst and GFP fluorescence intensities (Figure 3.12, red arrows). Individual GFP-expressing cells appeared to localise and associate with such structures and/or the coupon surface.

**Figure 3.11**

**Surface colonisation by PA14 *cdrA::gfp* after 48 hours under high shear conditions at 350 RPM is variable**

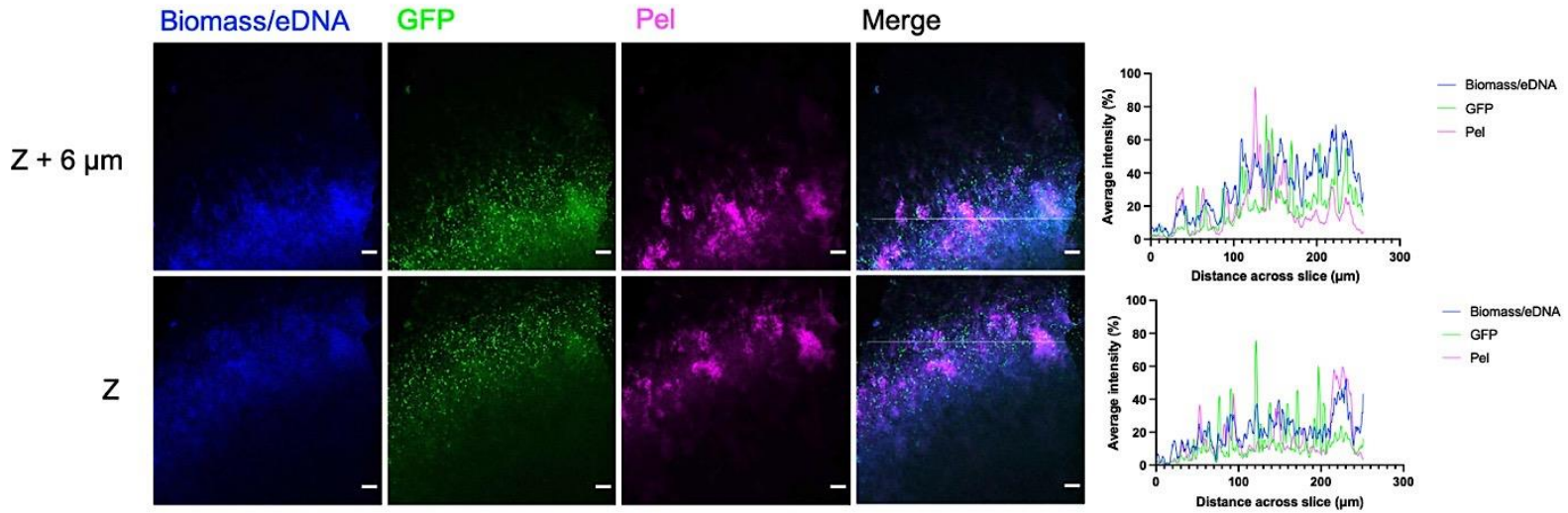


Representative confocal images are from PA14 *cdrA::gfp* biofilms (GFP signal is green) cultivated for 48 hours in the CBR under high shear (at 350 RPM) and stained with Hoechst for biomass/eDNA (blue) and the Pel-specific lectin WGA (magenta). Different z heights are shown for the same basal biofilm, with Z defined as the bottom layer closest to the coupon surface. Scale bar = 20 μm. Fiji was used to quantify fluorescent values in individual z-stack images: fluorescence signal intensity was normalised to the brightest pixel per coupon, and a five point moving average calculated. GFP fluorescence was punctate, and did not correlated to either Hoechst or Pel fluorescence.

**Figure 3.12**

**Increased production of both cell-associated and free Pel structures to increase attachment of PA14 *cdrA::gfp* cells after 48hours under high shear at 350 RPM**

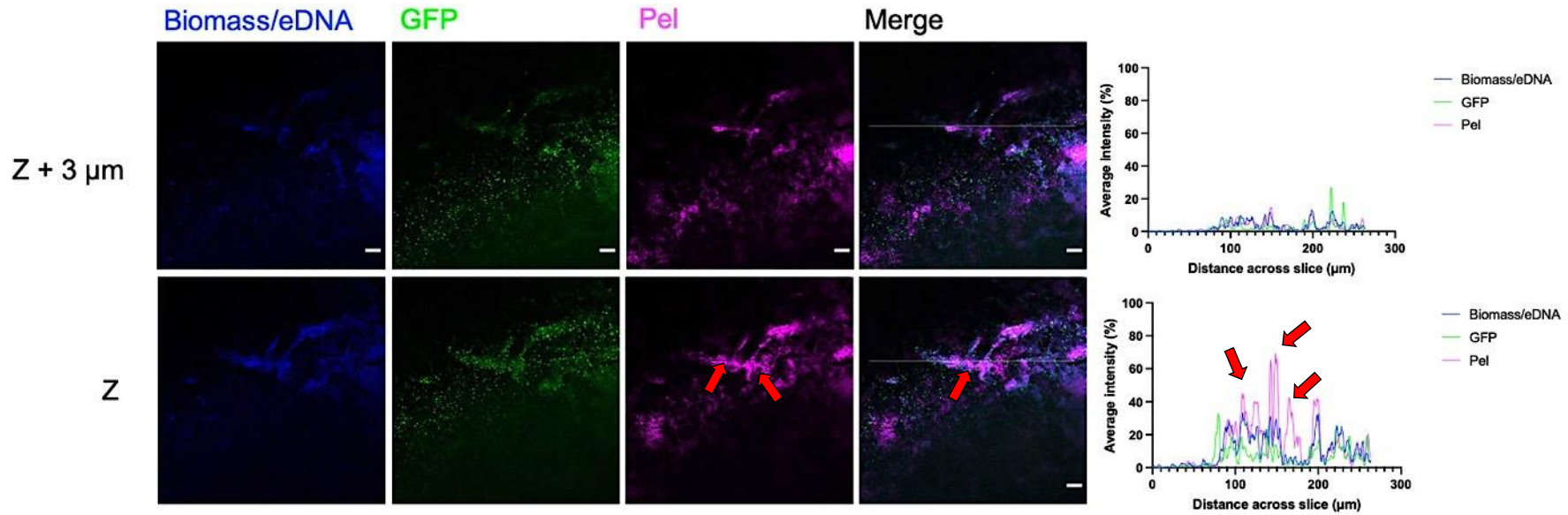


Representative confocal images are from PA14 *cdrA::gfp* biofilms (GFP signal is green) cultivated for 48 hours in the CBR under high shear (at 350 RPM) and stained with Hoechst for biomass/eDNA (blue) and the Pel-specific lectin WGA (magenta). Different z heights are shown for the same basal biofilm, with Z defined as the bottom layer closest to the coupon surface. Scale bar = 20 µm. Fiji was used to quantify fluorescent values in individual z-stack images: fluorescence signal intensity was normalised to the brightest pixel per coupon, and a five point moving average calculated. Red arrows show areas with increased Pel fluorescence intensities and encapsulation of associated cells.

Areas of the coupon surface with a more developed basal biofilm layer exhibited increased Hoechst and WGA staining compared to the basal biofilms formed under low shear, with biomass/eDNA and Pel constituting most of the biofilm structure (Figure 3.13). Some areas of the basal biofilm were composed of layered cell populations separated by channels (of approximate width 20 μm) that were maintained throughout the height of the biofilm (Figure 3.13, red arrows). Although the individual shapes of these basal structures varied, Hoechst and Pel were well correlated with one another with respect to their relevant fluorescence intensities (Figure 3.13, yellow arrows).

GFP fluorescence intensities were also well correlated to both Hoechst and Pel fluorescence intensities, although the average intensities of GFP fluorescence within the basal biofilm were much more variable than they were under low shear, which suggests that under high shear at 350 RPM, *cdrA* expression was more heterogenous.

Other areas of the basal biofilm had increased Pel production, as demonstrated by the Merge channels in Figure 3.13, which show Pel covering the basal layer of cells throughout the height of the biofilm. Compared to low shear, the fluorescence intensities for Pel were much greater, and did not always correlate to Hoechst or GFP fluorescence intensities (Figure 3.13, grey arrows). Furthermore, within the basal biofilm increased Pel concentration was not continuous (as demonstrated by troughs in the intensity profile traces), and some areas had inverse fluorescence intensities for Hoechst and Pel (Figure 3.13, orange arrows).

**Figure 3.13**

**Formation of aggregative clusters and spatially-heterogenous basal biofilms after 48 hours at 350 RPM**

*(figure legend overleaf)*

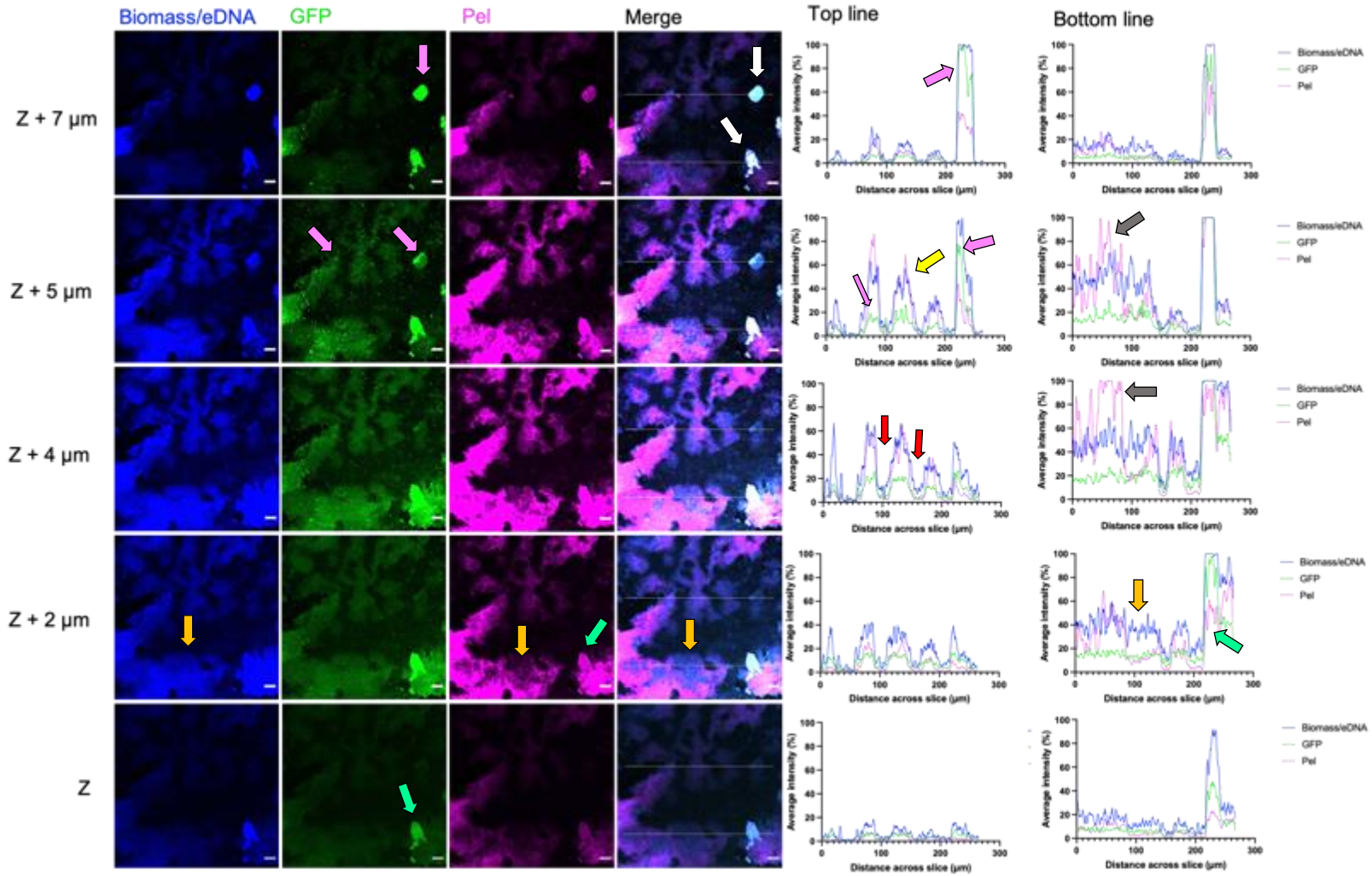

(*figure legend for* Figure 3.13)

Representative confocal images are from PA14 *cdrA::gfp* biofilms (GFP signal is green) cultivated for 48 hours in the CBR under high shear (at 350 RPM) and stained with Hoechst for biomass/eDNA (blue) and the Pel-specific lectin WGA (magenta). Different z heights are shown for the same basal biofilm, with Z defined as the bottom layer closest to the coupon surface. Scale bar = 20 μm. Fiji was used to quantify fluorescent values in individual z-stack images: fluorescence signal intensity was normalised to the brightest pixel per coupon, and a five point moving average calculated. Red arrows show channels separating basal cell populations that were maintained throughout the biofilm. Yellow arrows show well-correlated Hoechst and Pel fluorescence in areas of the basal biofilm with lower GFP fluorescence. Grey arrows show maximal Pel fluorescence intensities in areas with lower Hoechst and GFP fluorescence intensities. Orange arrows show areas of the basal biofilm with increased Hoechst and decreased Pel fluorescence intensities, in contrast to areas identified by the grey arrows. White areas show emergent features with aggregative morphologies. Pink arrows compare increased and heterogenous GFP fluorescence in the features to cells in the basal layer. Green arrows show a globular morphology for Pel punctate fluorescence intensity profiles for GFP and Pel fluorescence, as a result of heterogeneity within the cell aggregates the feature is composed of.

Features projecting upwards from the coupon surface were also observed under high shear conditions (Figures 3.13 and 3.14). Features were often elongated in structure and of an irregular shape, and heterogenous in terms of their respective Hoechst, GFP and Pel fluorescence intensities. Two features are present in Figure 3.13, and emerge from the basal biofilm at differing heights (Figure 3.13, white arrows). The first feature, captured by the top sampling line, emerges at Z+5 μm and has markedly increased Hoechst and GFP fluorescence intensities in comparison to the basal biofilm, indicating that cells within the feature have increased *cdrA* expression in comparison to cells in the basal layer (Figure 3.13, pink arrows). By comparison, Pel fluorescence intensity in this feature is lower than the basal biofilm fluorescence intensity at Z+5 μm.

The second feature, captured by the bottom sampling line in Figure 3.13, emerges at Z and has a more irregular shape. The feature appears to be composed of spherical clusters of cells aggregated together, resulting in localised variation in fluorescence intensities for GFP and Pel, and more punctate intensity profiles (Figure 3.3.13, green arrows). The fluorescence intensities of Hoechst, GFP and Pel are well correlated in the feature, and by Z+5 μm fluorescence intensities are maximal. At heights of Z+4 μm and Z+5 μm, the fluorescence intensities of Pel in the feature are also comparable to the fluorescence intensities of basally-associated Pel, which contrasts with low shear biofilm data in which the basal biofilm is characterised by low concentrations of Pel. Increased Pel production will increase the ‘stickiness’ of bacteria adhering to the coupon surface, and to each other, and reduce the risk of erosion or loss of cell volume due to the increased shear stress.

**Figure 3.14**

**Formation of aggregative clusters of cells and ECM components after 48 hours at 350 RPM**

*(figure legend overleaf)*

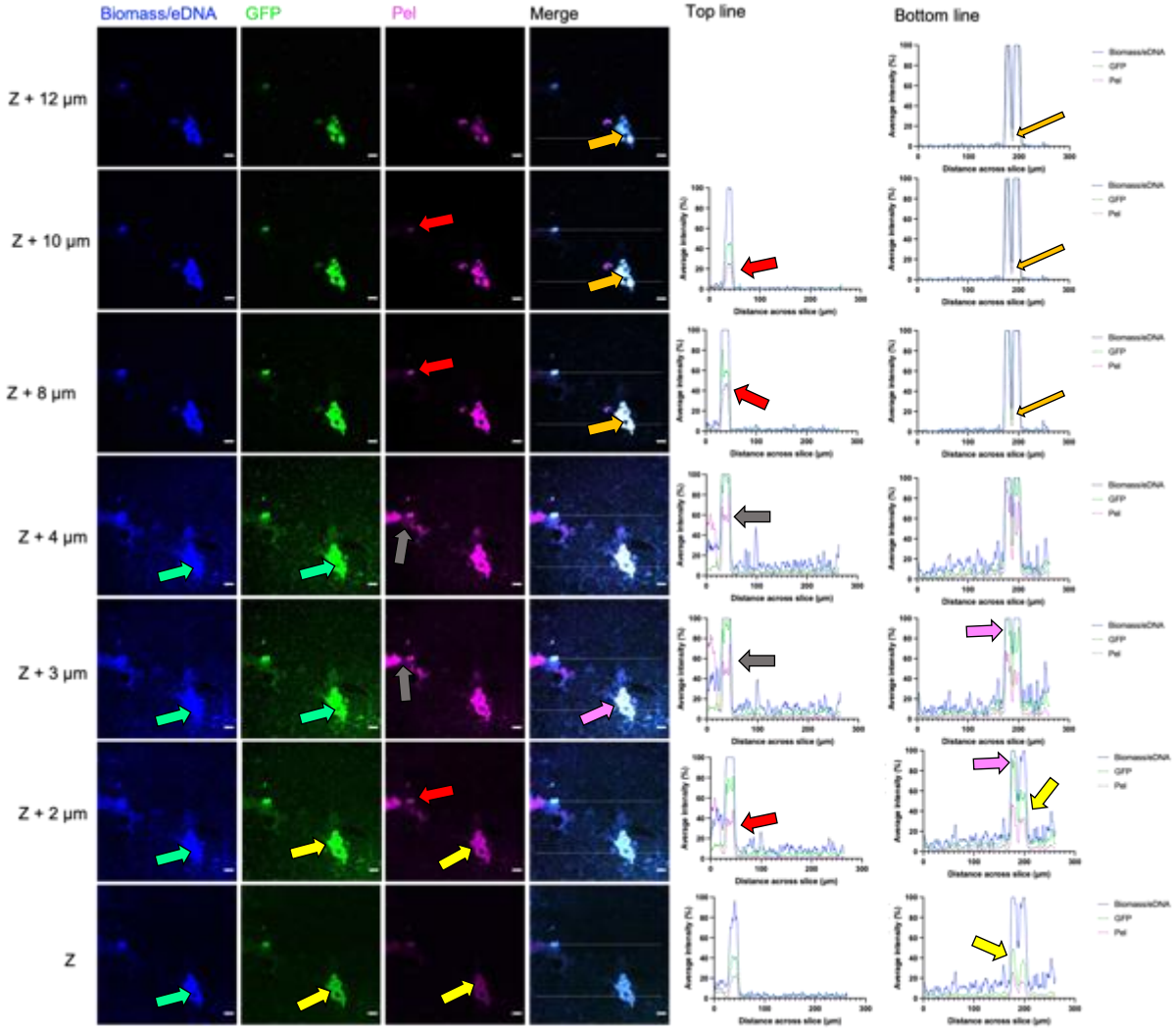

(*figure legend for* Figure 3.14)

Representative confocal images are from PA14 *cdrA::gfp* biofilms (GFP signal is green) cultivated for 48 hours in the CBR under high shear (at 350 RPM) and stained with Hoechst for biomass/eDNA (blue) and the Pel-specific lectin WGA (magenta). Different z heights are shown for the same basal biofilm, with Z defined as the bottom layer closest to the coupon surface. Scale bar = 20 μm. Fiji was used to quantify fluorescent values in individual z-stack images: fluorescence signal intensity was normalised to the brightest pixel per coupon, and a five point moving average calculated. Red arrows show cell aggregates with increased Hoechst and GFP fluorescence but lower Pel fluorescence. Grey arrows show the same cell aggregate emerging from part of a basal layer, in which Pel fluorescence intensities were better correlated to those of Hoechst and GFP. Yellow arrows shows a feature with globular morphology, composed of spherical and aggregative cell clusters that display variable fluorescence intensities for GFP and Pel within the feature. Pink arrows show areas with maximal Hoechst and GFP fluorescence intensities. Green arrows show a pore which is not stained by WGA for Pel, but exhibits staining by Hoechst and the presence of GFP-expressing cells. Orange arrows show exclusion of cells and Hoechst or WGA-stained matrix components from the same pore with increasing z height.

Some features that formed under high shear did not appear to be connected to a well-defined basal biofilm layer, and were spatially isolated from other parts of the developing biofilm (Figure 3.14). In such areas, features were characterised by increased fluorescence intensities of Hoechst, GFP and Pel, although Pel production in these features was once again variable. In the first feature identified in Figure 3.14 by the top sampling line, Hoechst fluorescence intensity is greatest throughout the height of the feature, followed by GFP fluorescence, with Pel fluorescence intensities being lowest in the feature (Figure 3.14, red arrows). This feature appeared to emerge from an area of basal biofilm (from Z+2 μm to a height of Z+4 μm), in which the fluorescence intensities of Pel were comparable to the feature (Figure 3.14, grey arrows).

Of interest are the fluorescence intensity profiles for the second feature (captured by the bottom sampling line in Figure 3.14). Similarly to the feature in Figure 3.13, this feature was composed of spherical clusters of cells aggregated together, with individual cell clusters having localised variation in fluorescence intensities for GFP and Pel once more (Figure 3.14, yellow arrows). Throughout the feature's height, Hoechst and GFP fluorescence intensities were well correlated, with maximal fluorescence intensities reached at a height of Z+4 μm (Figure 3.14, pink arrows). Pel concentration was observed to increase throughout the height of the feature, as shown by the lower fluorescence intensities of Pel at a height of Z+3 μm and below, with maximal Pel fluorescence reached by Z+8 μm. This may suggest that expression of Pel is independent, with different parts of the feature exhibiting different levels of Pel production. Within the centre of the feature, there was a pore that was maintained throughout the height of the biofilm, but exhibited Hoechst staining and the presence

of GFP-expressing cells at heights of Z+2 μm to Z+4 μm (Figure 3.14, green arrows). As the feature increased in height, the trough in fluorescence intensities across all three channels (Hoechst, GFP and Pel) became more pronounced, demonstrating complete exclusion of biofilm components from this pore (Figure 3.14, orange arrows). By a height of Z+8 μm the pore was well defined, and the fluorescence intensities of Hoechst, GFP and Pel surrounding the pore reached a plateau of maximum intensity and correlated well with one another. Given that the pore was maintained throughout the feature's height, it may be an important structural component of the developing biofilm.

Overall, biofilm formation under high shear after 48 hours was characterised by increased but heterogenous Pel production, presumably as a result of the selective pressures conferred by the higher shear condition. Fibres of Pel were also observed at high shear but not low shear. Increased concentrations of Pel throughout the biofilm enables PA14 *cdrA*::*gfp* cells to remain attached to the coupon surface, and by encapsulating the cells Pel and eDNA offers protection from high shear and the risk of sloughing.

3.3.3. Mushroom-shaped macrocolonies do not develop under high shear at 350 RPM

After 72 hours of growth under low shear at 75 RPM, PA14 *cdrA::gfp* biofilms were characterised by the formation of macrocolony structures with defined mushroom cap structures, archetypal of mature *Ps. a.* biofilms (O'Toole *et al.,* 2000; Klausen *et al.,* 2003). The basal biofilm remained on average approximately < 20 μm in height, whilst the mushroom-shaped macrocolonies exhibited more variation in the individual heights they reached, as well as their respective sizes in the x and y dimensions (Figures 3.15 and 3.16).

**Figure 3.15**
**Macrocolony formation by PA14 *cdrA::gfp* after 72 hours under low shear at 75 RPM**

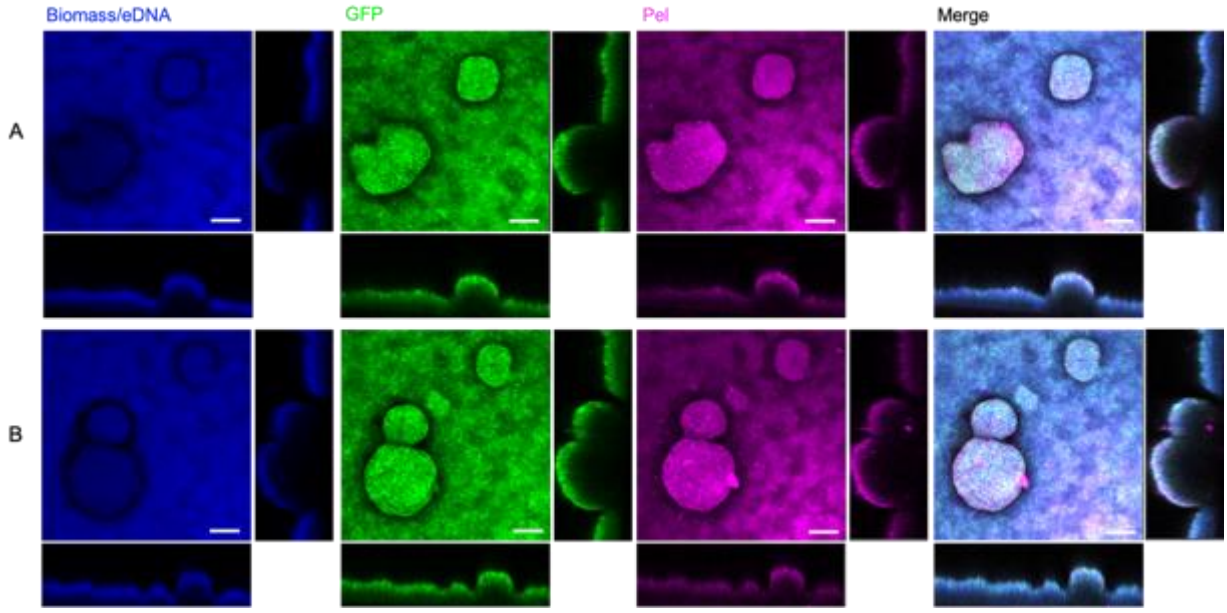


Representative confocal images are from PA14 *cdrA::gfp* biofilms (GFP signal is green) cultivated for 72 hours in the CBR under low shear (at 75 RPM) and stained with Hoechst for biomass/eDNA (blue) and the Pel-specific lectin WGA (magenta). Shown are top-down three-dimensional and side views of the biofilm Scale bar = 50 μm.

**Figure 3.16**
**Observation of macrocolony formation by PA14 *cdrA::gfp* after 72 hours under low shear at 75 RPM**

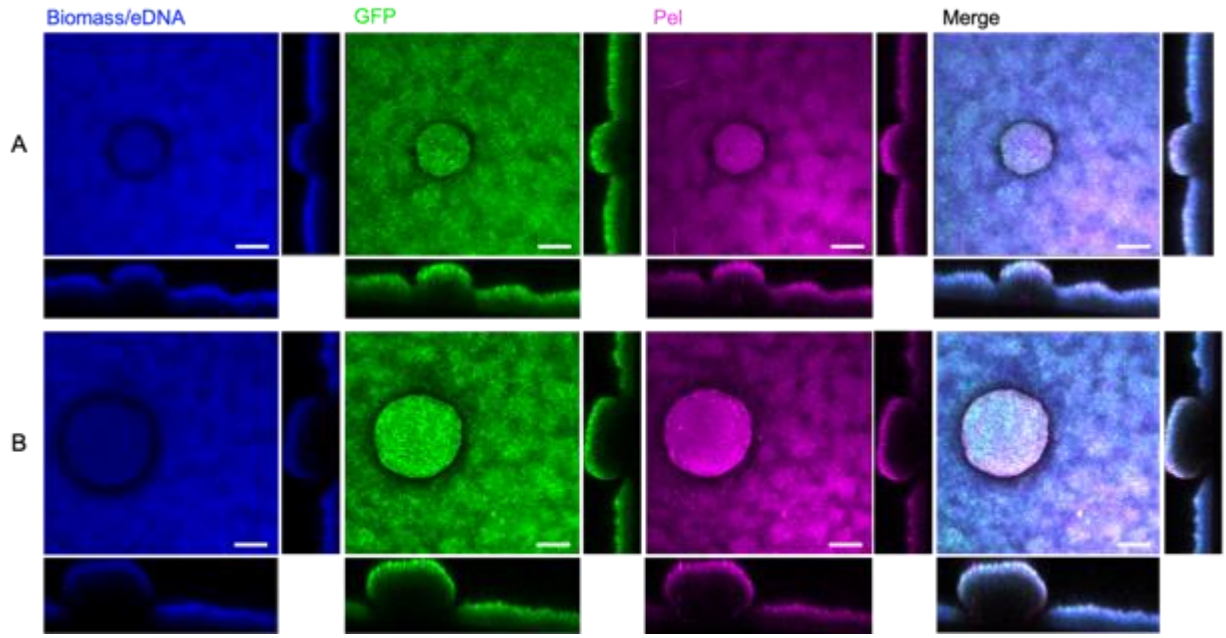


Representative confocal images are from PA14 *cdrA::gfp* biofilms (GFP signal is green) cultivated for 72 hours in the CBR under low shear (at 75 RPM) and stained with Hoechst for biomass/eDNA (blue) and the Pel-specific lectin WGA (magenta). Shown are top-down three-dimensional and side views of the biofilm Scale bar = 50 μm.

Mushroom-shaped macrocolonies were a recurrent architectural feature observed at 72 hours across different sample site locations on the coupons, and during independent runs of the CBR at 75 RPM. Under low shear conditions, the structural integrity of the macrocolonies is maintained, enabling the formation of a well-defined three-dimensional biofilm, which is in agreement with works in the literature that suggest that low shear forces result in thicker, multilayer biofilm structures (Rochex *et al.,* 2008; Rodesney *et al.,* 2017).

Fluorescence intensity profiles for Hoechst and GFP were well correlated throughout the basal biofilm at 72 hours, suggesting most cells were expressing equivalent quantities of *cdrA* to one another. Pel (as stained by WGA) production in the basal

biofilm appears equally distributed and cell-associated, as demonstrated by the fluorescence intensity profiles for Pel which also correlated well with Hoechst and GFP (Figures 3.17 and 3.18). This suggests that the basal biofilm is well-established and homogenous with respect to its composition. Due to the height of the biofilm features, Figures 3.17 and 3.18 are split; 3.17A and 3.18A show the basal layer and 3.17B and 3.18B the upper layers of the microcolonies. The outermost, or leading, edges of the basal layers were characterised by greater fluorescence intensities across all three channels, in comparison to other parts of the existing basal biofilm (Figures 3.17A and 3.18A, yellow arrows). Similarly to the other parts of the basal layer, the leading edges themselves exhibited good correlation between Hoechst, GFP and Pel fluorescence intensities. These leading edges may be representative of 'younger' cell populations that have colonised those particular surface areas more recently, and as a result could have increased *cdrA* expression and production of Pel to facilitate newer cell-surface and cell-cell interactions, resulting in lateral spreading of the biofilm (Figure 3.17A, grey arrows).

The emergence of three-dimensional macrocolony structures from the basal biofilm was frequently observed after 72 hours of biofilm growth (Figures 3.17 and 3.18). Structural cavities, located directly underneath the macrocolonies, appear at Z (i.e. the bottom of the biofilm), with negligible fluorescence intensity profiles across all three channels (Figures 3.17A at Z+4 μm and 3.18A up to a height Z+7 μm, red arrows). It is highly unlikely that the structural cavities represent areas completely void of bacterial cells and EPS, as this would suggest that the distinctive macrocolonies are able to form without any structural support from the basal biofilm. Instead, lack of visualisation within the cavities is likely due to poor laser penetration through the

entirety of the biofilm to its lowermost surface-associated layer, rather than poor penetration of Hoechst and WGA, the fluorescence intensity profiles for which were correlated to very low PA14 *cdrA::gfp* fluorescence. Furthermore, there is evidence of GFP-expressing cells and Pel production in the cavities when studying the representative CSLM slices (Figure 3.18A from Z to a height of Z+7 μm, pink arrows), with areas of localised and punctate concentration of Pel visible by eye.

**Figure 3.17A**
**Emergence of mushroom-shaped macrocolonies from PA14 *cdrA::gfp* basal biofilms formed after 72 hours at 75 RPM**

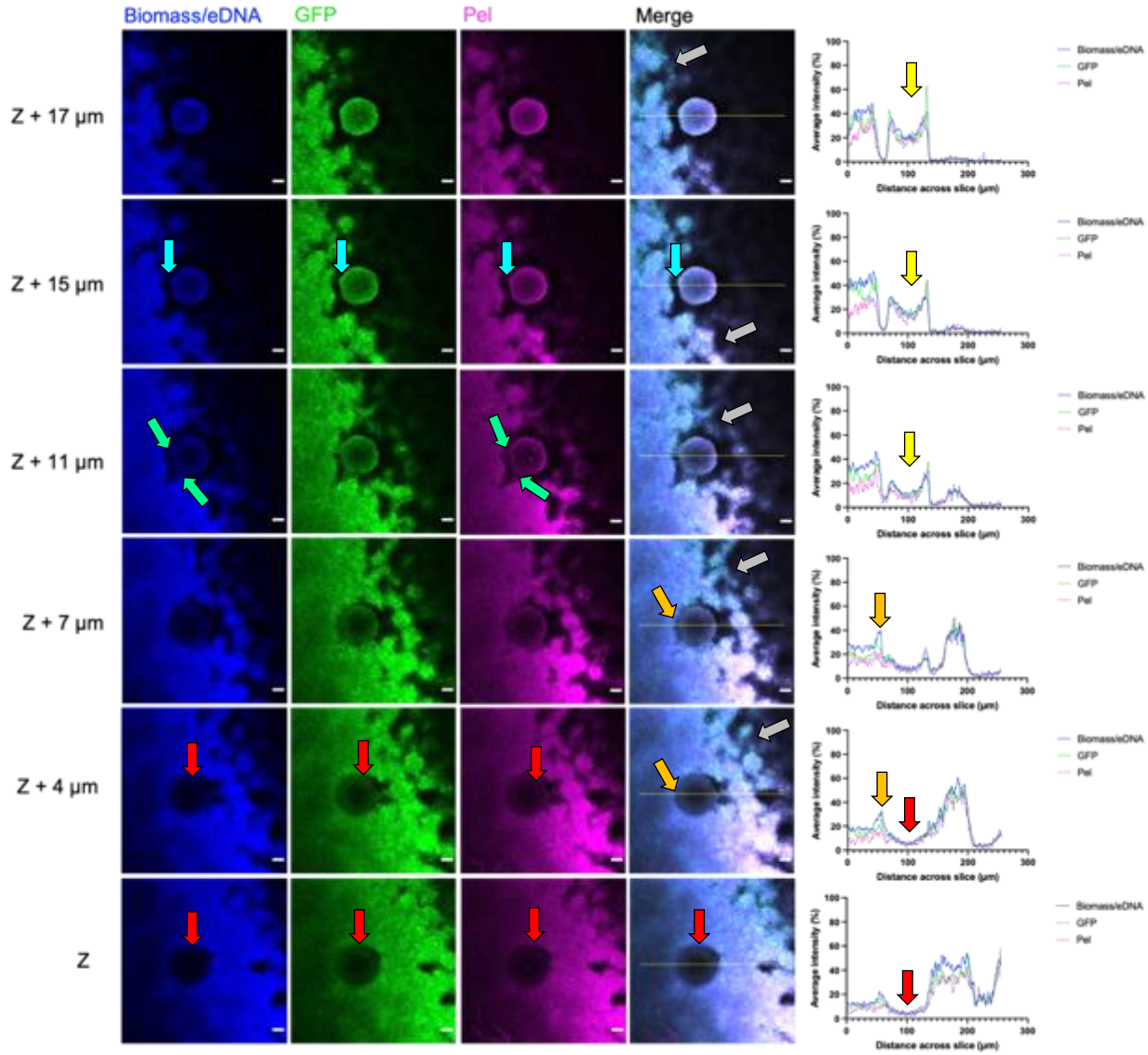


Representative confocal images are from PA14 *cdrA::gfp* biofilms (GFP signal is green) cultivated for 72 hours in the CBR under low shear (at 75 RPM) and stained with Hoechst for biomass/eDNA (blue) and the Pel-specific lectin WGA (magenta). Different z heights are shown for the same basal biofilm, with Z defined as the bottom layer closest to the coupon surface. Scale bar = 20 µm. Fiji was used to quantify fluorescent values in individual z-stack images: fluorescence signal intensity was normalised to the brightest pixel per coupon, and a five point moving average calculated. Yellow arrows show concave fluorescence intensity profiles for emerging macrocolonies. Grey arrows show the movement of the leading edge of the basal biofilm during lateral spreading. Red arrows show a cavity beneath the macrocolony in lower basal layers with negligible Hoechst, GFP and Pel fluorescence. Orange arrows show increased fluorescence intensities at the boundary layer between the forming macrocolony and basal biofilm. Green arrows show eDNA-Pel complexes, forming a 'bridge' between the macrocolony and adjacent basal layer. Cyan arrows show loss of the 'bridge' structure.

**Figure 3.18A.**

**Emergence of mushroom-shaped macrocolonies is homogenous across independent sampling sites after 72 hours under low shear at 75 RPM**

*(figure legend overleaf)*

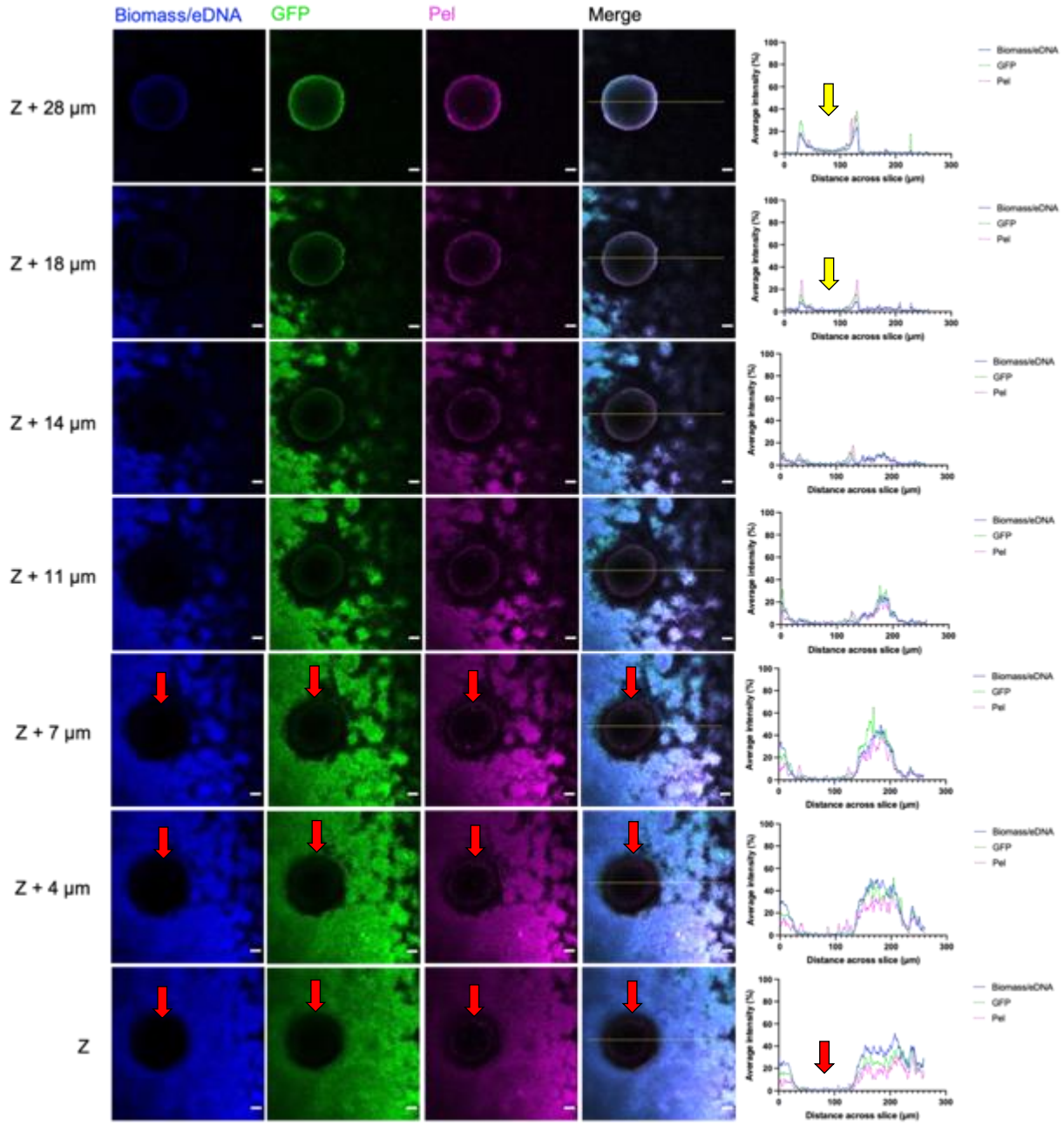

(*figure legend for* Figure 3.18A)

Representative confocal images are from PA14 *cdrA::gfp* biofilms (GFP signal is green) cultivated for 72 hours in the CBR under low shear (at 75 RPM) and stained with Hoechst for biomass/eDNA (blue) and the Pel-specific lectin WGA (magenta). Different z heights are shown for the same basal biofilm, with Z defined as the bottom layer closest to the coupon surface. Scale bar = 20 μm. Fiji was used to quantify fluorescent values in individual z-stack images: fluorescence signal intensity was normalised to the brightest pixel per coupon, and a five point moving average calculated. Yellow arrows show concave fluorescence intensity profiles for emerging macrocolonies. Red arrows show a cavity beneath the macrocolony in lower basal layers with negligible Hoechst, GFP and Pel fluorescence. Pink arrows show evidence of punctate Pel production within the cavity. Green arrows show further areas of punctate Pel fluorescence surrounding the boundary layer between the macrocolony and basal layer.

In Figure 3.17A, the boundary edge between the basal biofilm and the bottom of the macrocolony was observed to have slightly increased fluorescence intensities across all three channels (Z+7 μm, orange arrows), from which 'bridges' were seen forming between the macrocolony and the basal biofilm at a height of Z+11 μm, which could be composed of eDNA and Pel complexes that are cell-associated (Figure 3.17A, Z+11 μm, green arrows). The 'bridges' could thus be tethering part of the macrocolony to the rest of the biofilm, with Jennings *et al.,* (2015), previously demonstrating that Pel is able to colocalise with eDNA at the stalk of PA14 mushroom-shaped colony structures of flow-cell grown biofilms. By a height of Z+15 μm, this connecting 'bridge' is no longer visible, and the macrocolony appears discrete from the basal biofilm (Figure 3.17A, Z+15 μm, cyan arrows).

Figures 3.17B and 3.18B show the emergence of macrocolony structures above the biofilm, and are each a continuation of the same regions of the biofilms shown in Figures 3.17A and 3.18A respectively. Like basal biofilm formation under low shear at 75 RPM, macrocolony formation appears to be homogenous; irrespective of spatial location within the biofilm or the overall elevation of individual mushroom-shaped macrocolonies, as shown by the similarity in fluorescence intensity profiles across all three channels in both Figures 3.17B and 3.18B. Fluorescence intensities for Hoechst, GFP and Pel were well-correlated with one another in the mushroom macrocolonies, with the fluorescence intensities initially displaying a concave profile, indicative of increased biomass/eDNA, *cdrA* expression and production of Pel at the macrocolony periphery (Figures 3.17B and 3.18B, yellow arrows). Within the interior of the macrocolonies, localised concentrations of Pel were additionally observed (Figures 3.17B and 3.18B, grey arrows), resulting in punctate fluorescence intensities that did

not appear to be cell-associated or correlated to increased Hoechst staining (Figure 3.18B, red arrow).

With increasing height of the macrocolony, as shown in Figure 3.17B at a height of Z+21 μm, the fluorescence intensities of GFP and Pel at peripheral edges of the structure diverge: the as-viewed left-hand periphery exhibits increased *cdrA::gfp* fluorescence (orange arrows), whilst the as-viewed right-hand peripheral edge has an increased production of Pel which is maintained up to a height of Z+28 μm (pink arrows). Similar differences in the fluorescence intensities at the peripheral edges can be seen in Figure 3.18B. At a height of Z+43 μm, GFP and Pel fluorescence intensities are well-correlated and symmetrical at the peripheries (Figure 3.18B, green arrows). At a height of Z+48 μm, the as-viewed left-hand peripheral edge has increased PA14 *cdrA::gfp* fluorescence (Figure 3.18B, orange arrows) whilst at a height of and Z+53 μm the as-viewed right-hand peripheral edge exhibits increased *cdrA::gfp* fluorescence (Figure 3.18B, cyan arrows). As the apex of the macrocolony emerged, GFP expression was observed to increase within the interior of the structure, resulting in a punctate fluorescence intensity profile that did not correlate to greater Hoechst or Pel fluorescence intensities (Figure 3.18B, cerise arrows). Similarly in Figure 3.17B, punctate areas of increased *cdrA::gfp* fluorescence were observed at the structural apex at a height of Z+32 μm that did not correlate to either Hoechst or Pel fluorescence intensities (Figure 3.17B, cyan arrows).

PA14 cells with increased *cdrA* expression (and thus increased levels of intracellular c-di-GMP) may represent small cellular aggregates that, as suggested by Klausen *et al.,* (2003), are a motile subpopulation of cells that have formed a ‘cap’ on top of the

non-motile macrocolony population. Local consumption of nutrients within the biofilm is known to resultantly create nutrient gradients throughout the structure (DeBeer *et al.,* 1994; Picioreanu *et al.,* 1998). Thus, the apexes of macrocolonies, given their ascension from the basal biofilm and into the bulk fluid, may be surrounded by zones of higher nutrient concentrations that facilitate increased biomass accumulation and expansion of the three-dimensional structures as observed. Indeed, Figures 3.15 and 3.16, showing representative three-dimensional, top-down CLSM images, have similar areas of increased GFP and Pel fluorescence atop the mushroom-shaped macrocolonies that are visible by-eye.

**Figure 3.17B**

**Hoechst, GFP and Pel fluorescence increase across the interior of macrocolonies reaching their apexes**

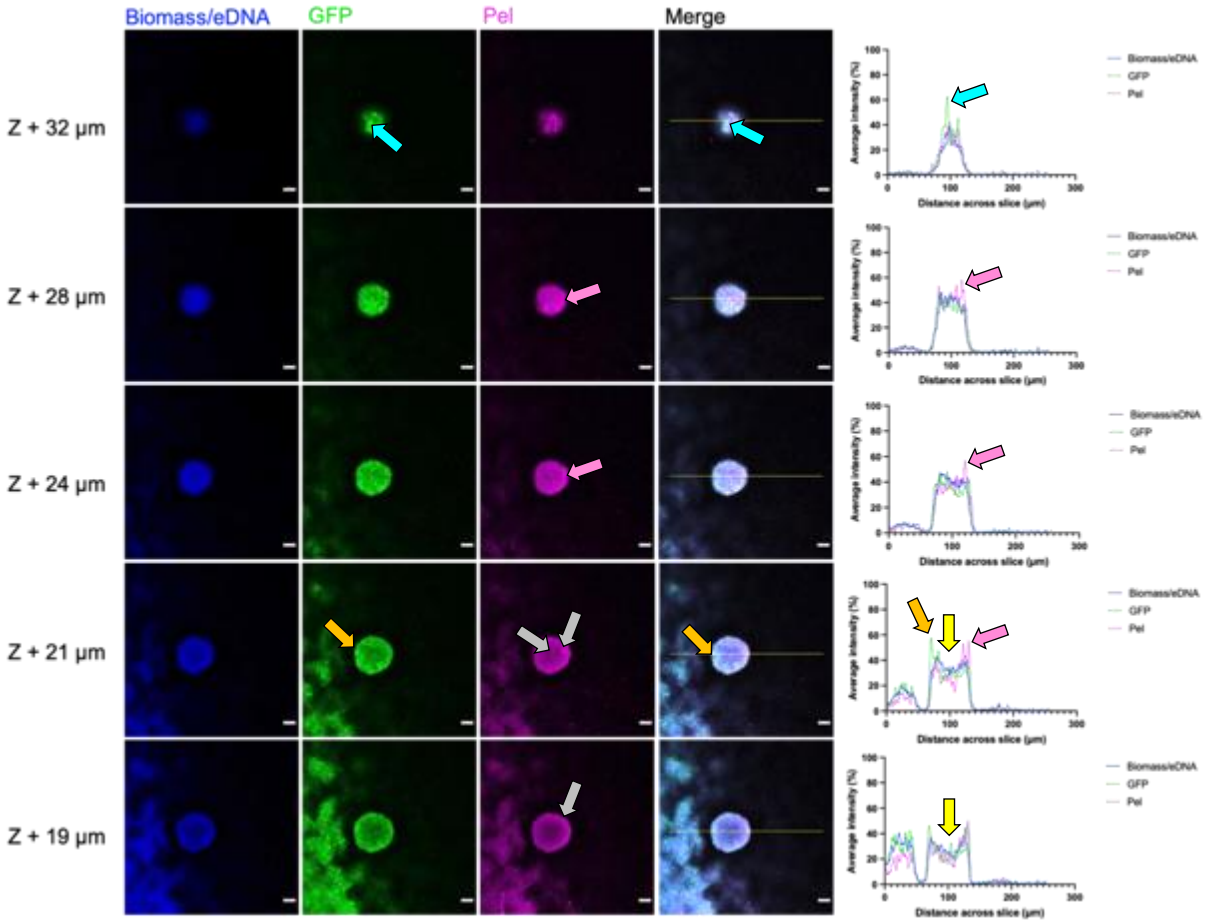


Representative confocal images are from PA14 *cdrA::gfp* biofilms (GFP signal is green) cultivated for 72 hours in the CBR under low shear (at 75 RPM) and stained with Hoechst for biomass/eDNA (blue) and the Pel-specific lectin WGA (magenta). Different z heights are shown for an emerging macrocolony structure, as a continuation of Figure 3.17A. Scale bar = 20 µm. Fiji was used to quantify fluorescent values in individual z-stack images: fluorescence signal intensity was normalised to the brightest pixel per coupon, and a five point moving average calculated. Yellow arrows show concave fluorescence intensity profiles for the emerging macrocolony. Grey arrows show localised and punctate concentrations of Pel within the macrocolony interior. Orange arrows show increased GFP fluorescence at as-viewed left-hand peripheral edge, whilst pink arrows show increased Pel fluorescence at the as-viewed right-hand side peripheral edge. Cyan arrows show punctate and increased GFP fluorescence of cell populations at the macrocolony apex.

**Figure 3.18B**
**Apical layers of macrocolonies formed after 72 hours under low shear at 75 RPM have increased GFP fluorescence**

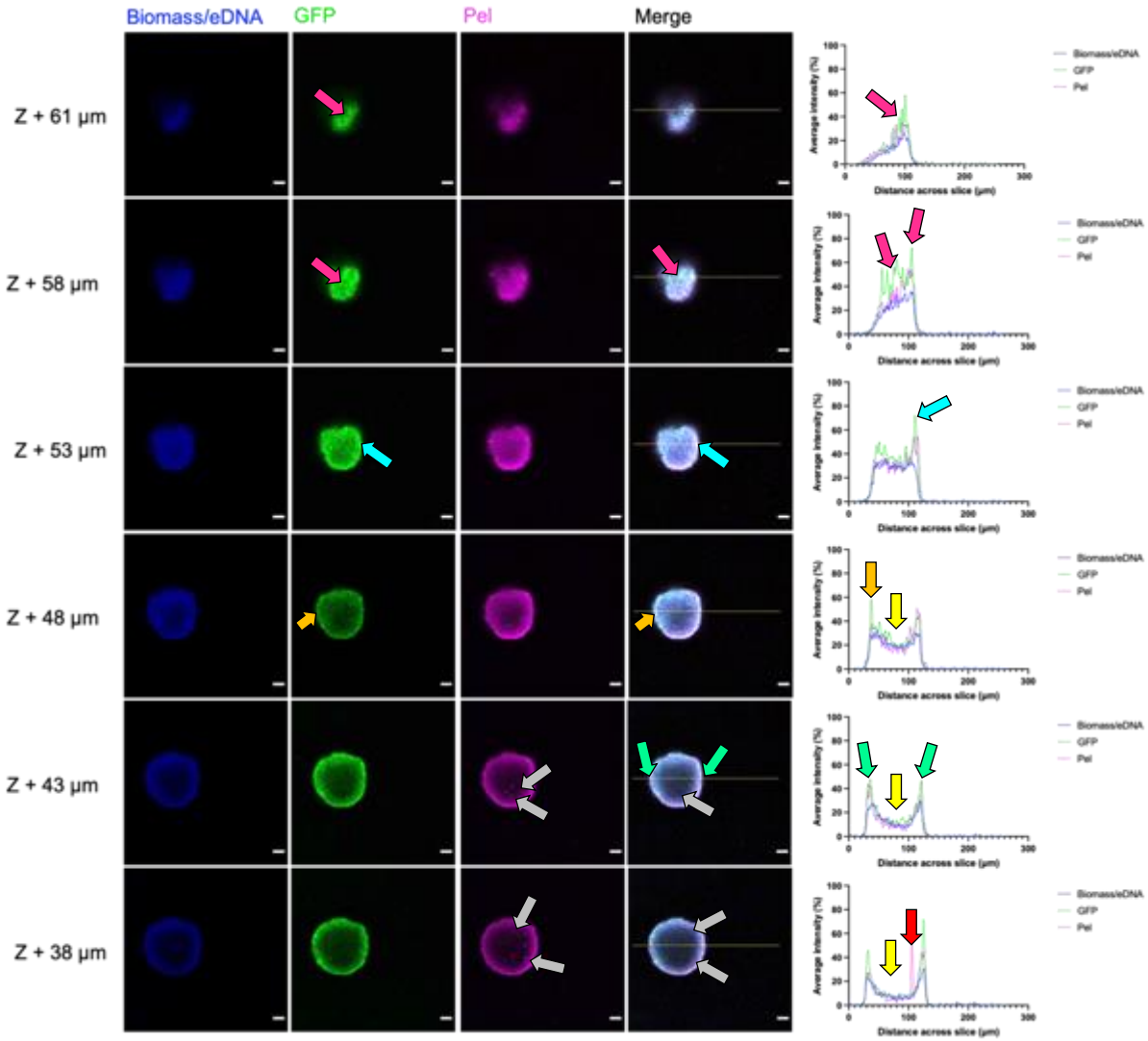


Representative confocal images are from PA14 *cdrA::gfp* biofilms (GFP signal is green) cultivated for 72 hours in the CBR under low shear (at 75 RPM) and stained with Hoechst for biomass/eDNA (blue) and the Pel-specific lectin WGA (magenta). Different z heights are shown for an emerging macrocolony structure, as a continuation of Figure 3.17A. Scale bar = 20 µm. Fiji was used to quantify fluorescent values in individual z-stack images: fluorescence signal intensity was normalised to the brightest pixel per coupon, and a five point moving average calculated. Yellow arrows show concave fluorescence intensity profiles for the emerging macrocolony. Grey arrows show localised and punctate concentrations of Pel within the macrocolony interior. Red arrow shows a punctate fluorescence intensity for Pel uncorrelated to Hoechst or GFP fluorescence. Green arrows show homogenous expression of GFP and fluorescence of Pel at the peripheries. Orange and cyan arrows show heterogenous GFP fluorescence at opposite as-viewed peripheral edges with increasing height. Cerise arrows show increased expression of GFP in apical cell populations, both at the macrocolony periphery and interior.

After 72 hours of growth under high shear at 350 RPM, PA14 *cdrA::gfp* biofilms were not observed to form mushroom-shaped macrocolonies, and instead appeared denser than those grown under low shear at 75 RPM, with an average height of just 30 – 40 μm. In general, high shear forces are believed to lead to the formation of biofilms that are thinner, with higher volumetric density and increased strength (Kwok *et al.,* 1998; Liu and Tay, 2002; Laspidou and Rittmann, 2004; Celmer *et al.,* 2008). In agreement with this is the fact that the PA14 biofilms formed under high shear at 350 RPM exhibited increased Hoechst, GFP and Pel fluorescence intensities in comparison to those formed under low shear at 75 RPM, in spite of their shorter overall heights in the z dimension. As with biofilm at 48 hours under high shear, a basal biofilm coherently covering the coupon surface was not observed at 72 hours, with biofilm structures and features remaining spatially-separated from one another (Figure 3.19).

**Figure 3.19**
**Biofilm formation after 72 hours under 350 RPM did not lead to macrocolony formation**

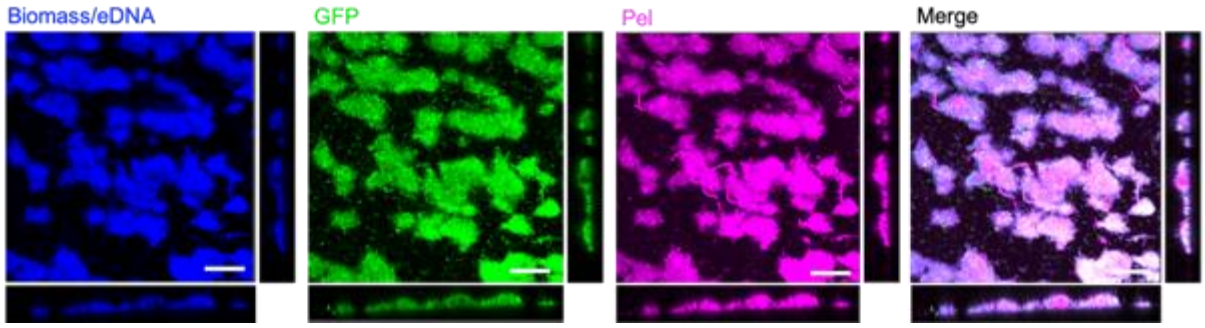


Representative confocal images are from PA14 *cdrA::gfp* biofilms (GFP signal is green) cultivated for 72 hours in the CBR under high shear (at 350 RPM) and stained with Hoechst for biomass/eDNA (blue) and the Pel-specific lectin WGA (magenta). Shown are top-down three-dimensional and side views of the biofilm Scale bar = 50 μm. The basal biofilm is composed of spatially-separated cell populations.

As previously seen after 48 hours of growth, PA14 biofilms formed under high shear also exhibited increased heterogeneity with respect to Hoechst, GFP and Pel fluorescence intensities (Figures 3.20 and 3.21). Figure 3.20 shows a representative

biofilm that is characterised by noticeably increased Pel production, with the exopolysaccharide appearing to completely encapsulate the PA14 *cdrA::gfp* cell populations (yellow arrows). The fluorescence intensities of Hoechst and GFP appear well-correlated to one another, although the intensity profiles appeared punctate, as a result of localised variation in the fluorescence intensities of adjacent subpopulations within the biofilm (Figure 3.20, grey arrows). Staining by WGA revealed several distinct morphologies for Pel, including the formation of fibre-like 'tendrils' that seemed to have a structural role; connecting parts of the basal biofilm to one another, even across areas of the coupon surface that appeared otherwise uncolonised by a basal layer (Figure 3.20, red arrows). The fibre-like 'tendrils' were maintained throughout the height of the biofilm, as either cell-associated or free Pel (Figure 3.20, orange arrows). Co-localisation of Hoechst staining in the 'tendrils' could also suggest that eDNA is complexed with Pel within these fibre-like structures, to increase their relative strength and ability to remain spatially fixed under high shear conditions (Figure 3.20, cyan arrows). Yang *et al.,* (2011), has previously demonstrated that Psl and Pel are important for facilitating interactions between subpopulations of cells during PA01 biofilm maturation, whilst others have observed eDNA forming fibre-like protrusions connecting adjacent microcolonies, believed to be involved in trail formation to guide cell movement during biofilm differentiation (Allesen-Holm *et al.,* 2006; Barken *et al.,* 2008; Gloag *et al.,* 2013).

**Figure 3.20**
**PA14:*cdrA::gfp* biofilm formation after 72 hours under 350 RPM is characterised by increased Pel production within spatially-separate cell populations**

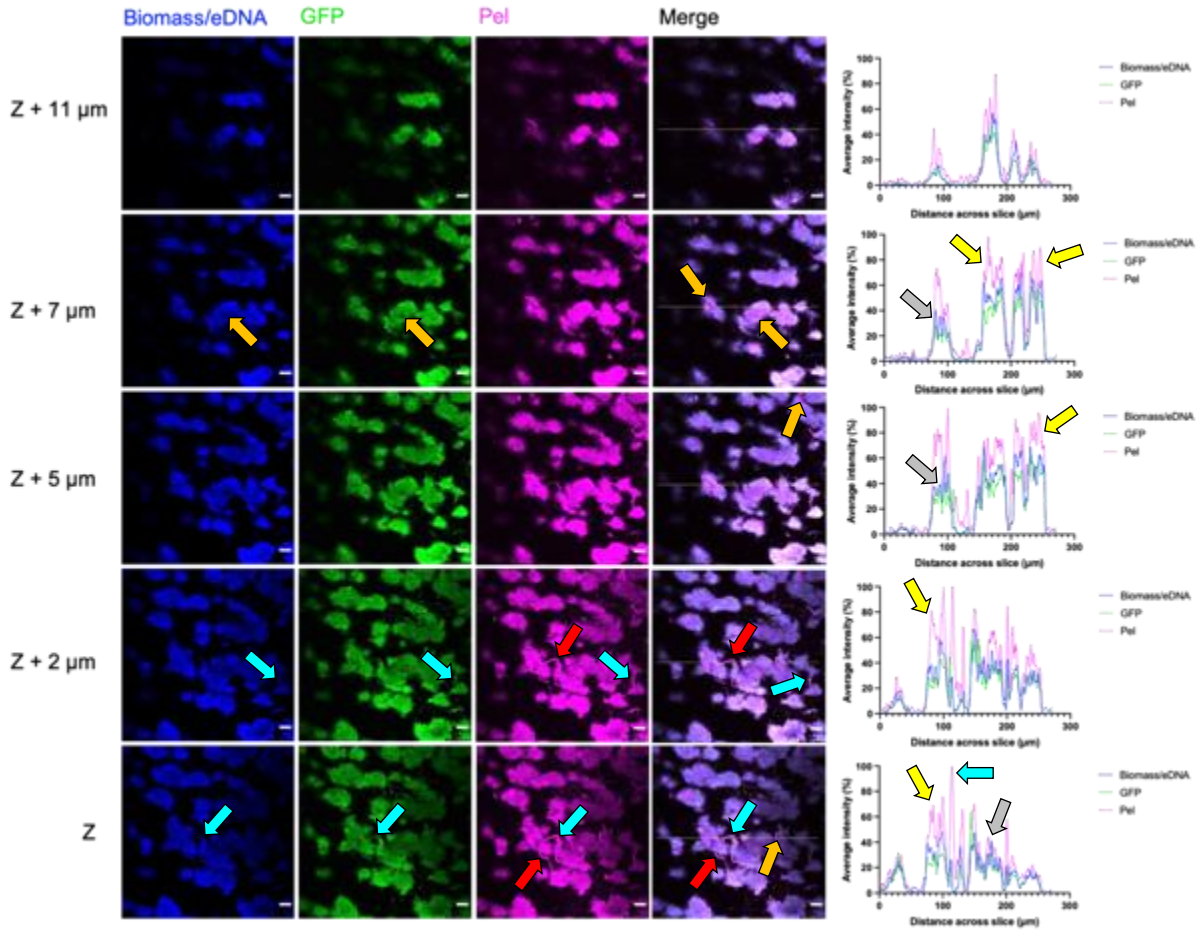


Representative confocal images are from PA14 *cdrA::gfp* biofilms (GFP signal is green) cultivated for 72 hours in the CBR under high shear (at 350 RPM) and stained with Hoechst for biomass/eDNA (blue) and the Pel-specific lectin WGA (magenta). Different z heights are shown for the same biofilm, with Z defined as the bottom layer closest to the coupon surface. Scale bar = 20 µm. Fiji was used to quantify fluorescent values in individual z-stack images: fluorescence signal intensity was normalised to the brightest pixel per coupon, and a five point moving average calculated. Yellow arrows show increased fluorescence intensities for Pel throughout the height of the biofilm, indicating encapsulation of cells by the exopolysaccharide (as further shown by the overall purple hue of the merged images). Grey arrows show punctate but well-correlated Hoechst and GFP fluorescence intensities. Red arrows show fibre-like 'tendril' formation of Pel projecting in-between adjacent cell populations. Orange arrows show both cell-associated and free structures of Pel maintained throughout the biofilm, including 'tendril' formation and aggregates of Pel in areas where cells are absent. Cyan arrows show co-localisation of fibres stained by Hoechst and WGA, suggestive of eDNA-Pel complexes.

In Figure 3.21, similarly punctate regions of increased Pel concentration were observed, with fluorescence intensities for such Pel aggerates uncorrelated to increased Hoechst and GFP fluorescence intensities (yellow arrows). At this particular sampling site however, the florescence intensities of Hoechst were greatest throughout the height of the biofilm: whilst well-correlated to GFP and Pel fluorescence intensities in certain structures (Figure 3.21, pink arrows), other areas of the biofilm exhibited increasing staining by Hoechst that did not correlate to either increased *cdrA::gfp* fluorescence, or WGA-staining of Pel (Figure 3.21, grey arrows).

Such areas could either have increased concentration of eDNA, or accumulation of biomass, with the latter suggestion supported by the merged CLSM images, which show individual PA14 cells at the leading edges of the biofilm (giving it a fringed appearance), and GFP-expressing cells atop the rest of the biofilm (Figure 3.21, cyan arrows). Gloag *et al.,* (2013), demonstrated that eDNA maintains coherent cell alignments at the leading edge of *Ps. a.* PAK strain biofilms, and promotes the formation of trails which facilitate the movement of individual cells or small cell clusters to the leading edge of the biofilm. Although defined trails were not observed, individual PA14:*cdrA::gfp* cells were found orientated in chain-like processions between biofilm structures, or attaching to the leading edge via the cell pole.

**Figure 3.21**

**Basal biofilm composition is heterogenous after 72 hours under high shear at 350 RPM**

*(figure legend overleaf)*

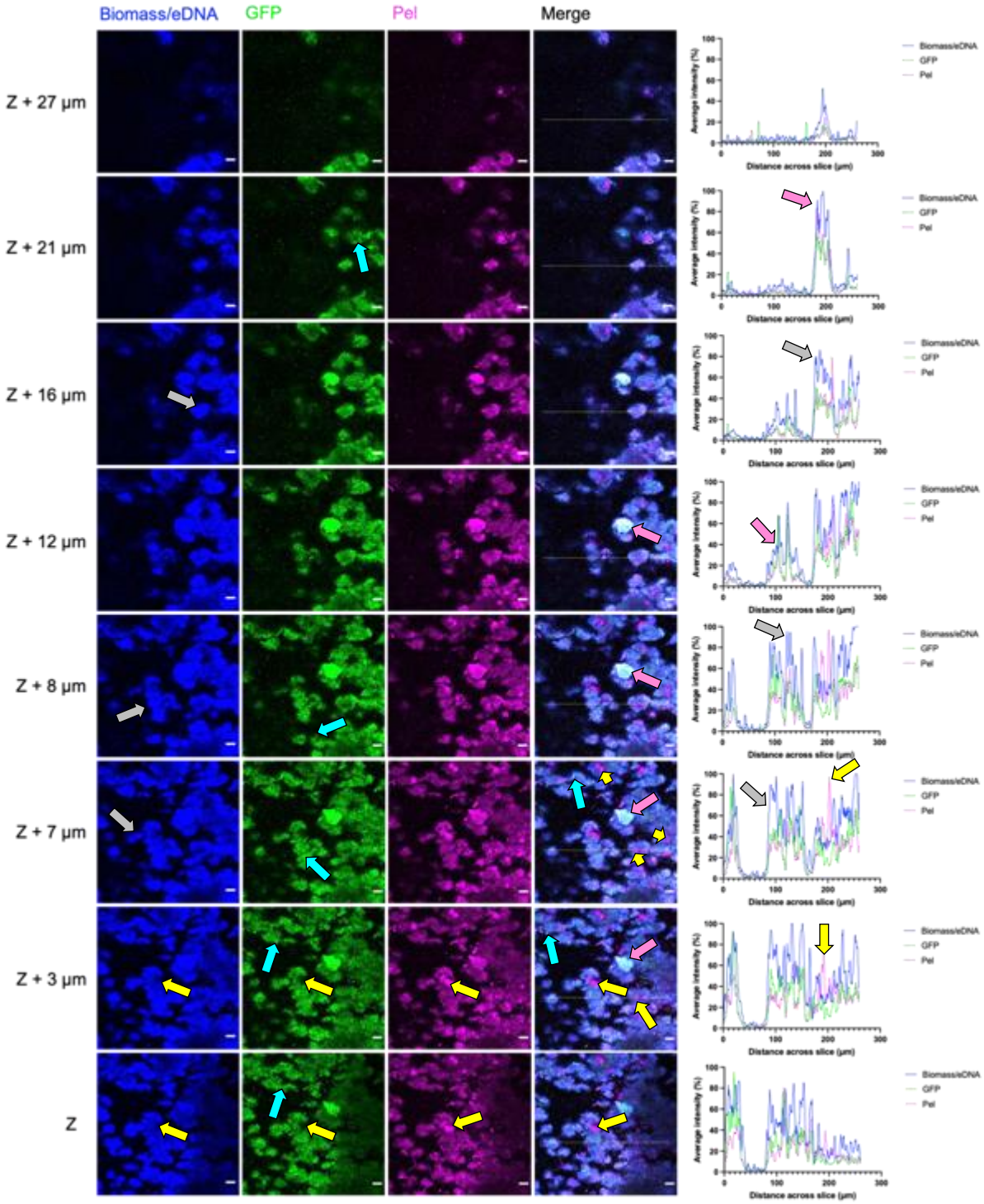

(*figure legend for* Figure 3.21)

Representative confocal images are from PA14:*cdrA::gfp* biofilms (GFP signal is green) cultivated for 72 hours in the CBR under high shear (at 350 RPM) and stained with Hoechst for biomass/eDNA (blue) and the Pel-specific lectin WGA (magenta). Different z heights are shown for the same biofilm, with Z defined as the bottom layer closest to the coupon surface. Scale bar = 20 μm. Fiji was used to quantify fluorescent values in individual z-stack images: fluorescence signal intensity was normalised to the brightest pixel per coupon, and a five point moving average calculated. Yellow arrows show areas with increased Pel fluorescence intensities for Pel aggregates, uncorrelated to Hoechst or GFP fluorescence. Pink arrows show areas of increased fluorescence intensities across all three channels, in a dense aggregate of cells and ECM material. Grey arrows show areas of the biofilm that exhibited increased and uncorrelated Hoechst fluorescence intensities. Cyan arrows shows small subpopulations of GFP-expressing cells atop different parts of the biofilm

Growth under high shear at 350 RPM did not result in the formation of typical mushroom-shaped macrocolonies, but there was a degree of uniformity with respect to the mature biofilm structures formed after 72 hours. Three-dimensional top-down CLSM images show that PA14 biofilms formed under high shear conditions comprise of distinct populations of bacterial cells (Figures 3.19 – 3.21); forming individual mounds that grow upwards in the vertical dimension (z), and do not appear to spread laterally to form a continuous basal biofilm as observed under low shear (in the x and y dimensions). The peripheral edges of these mounds are irregular, and maintained, fluid-filled channels that do not contain cellular or ECM material can be seen between individual mound structures.

### 3.3.4. Heterogeneity of mature PA14:*cdrA::gfp* biofilm structures is increased under high shear

Mushroom-shaped macrocolonies were once again frequently observed after growth under low shear at 75 RPM for 96 hours (Figures 3.22 and 3.23A), as well as subpopulations of PA14 cells with increased *cdrA::gfp* fluorescence forming aggregative structures atop the 'cap' region of the macrocolonies (Figures 3.22 and 3.23A, white arrows). Cells with greater *cdrA::gfp* fluorescence were also seen on top of the basal biofilm in a variety of structures, ranging from small aggregative clusters to those with a more complex three-dimensional architecture (Figures 3.22 and 3.23, yellow arrows).

Most notably, Pel was well distributed in both the basal biofilm and three-dimensional features, whereby staining by WGA revealed three distinct structural forms for the exopolysaccharide: throughout the height of mushroom-shaped macrocolony interior,

forming concentrated regions of punctate Pel (Figures 3.22 and 3.23A, cyan arrows); as a dense aggregative 'mat' of Pel forming across the basal biofilm (Figure 3.23, orange arrows), and observed forming a wide-reaching network of fibre-like Pel across the basal biofilm (Figures 3.22 and 3.23, grey arrows).

**Figure 3.22**
**Macrocolony formation after 96 hours under low shear at 75 RPM**

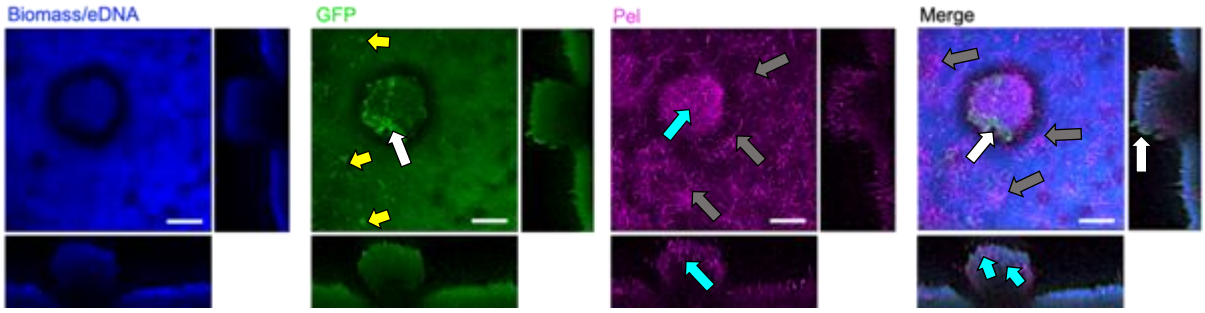


Representative confocal images are from PA14:*cdrA::gfp* biofilms (GFP signal is green) cultivated for 96 hours in the CBR under high shear (at 75 RPM) and stained with Hoechst for biomass/eDNA (blue) and the Pel-specific lectin WGA (magenta). Shown are top-down three-dimensional and side views of the macrocolony and biofilm. Scale bar = 50 μm. White arrows show a 'cap' structure composed of cells exhibiting increased GFP fluorescence atop the macrocolony. Yellow arrows show small, aggregative clustered cell populations with increased GFP fluorescence. Cyan arrows show punctate Pel production within the macrocolony interior. Grey arrows show a wide-reaching Pel fibre-like network across the biofilm.

**Figure 3.23**
**Different morphologies and functions of Pel in PA14:*cdrA::gfp* biofilms formed at 96 hours under low shear at 75 RPM**

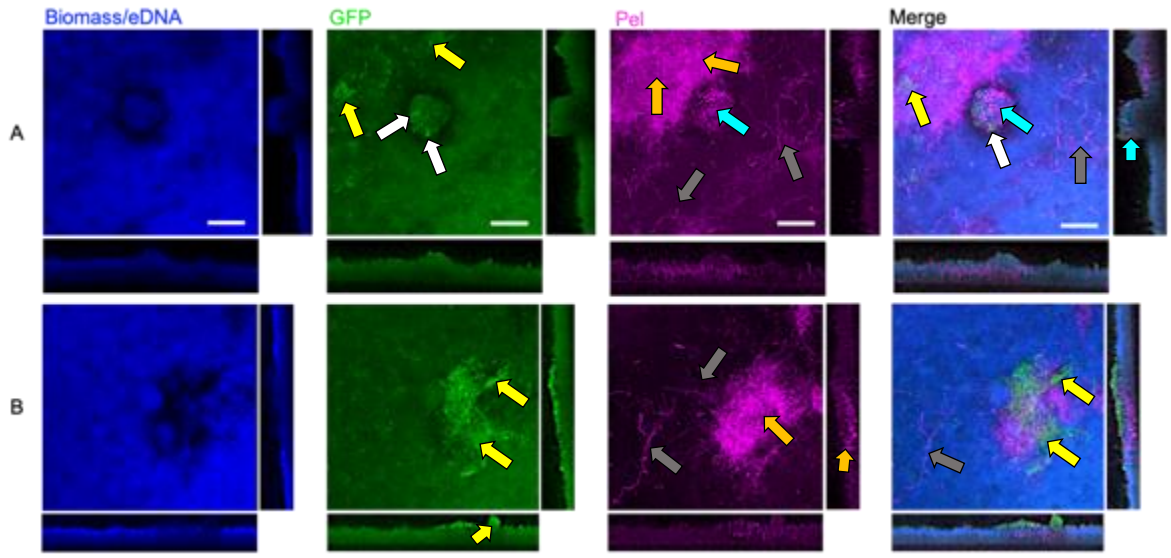


Representative confocal images are from PA14:*cdrA::gfp* biofilms (GFP signal is green) cultivated for 96 hours in the CBR under low shear (at 75 RPM) and stained with Hoechst for biomass/eDNA (blue) and the Pel-specific lectin WGA (magenta). Shown are top-down three-dimensional and side views of biofilms. Scale bar = 50 μm. A and B are from two independent sample sites from two different coupons. White arrows show a 'cap' structure composed of cells exhibiting increased GFP fluorescence atop the macrocolony. Yellow arrows show small, aggregative clustered cell populations with increased GFP fluorescence, forming a more complex three-dimensional structure in panel B. Cyan arrows Cyan arrows show punctate Pel production within the macrocolony interior in panel A. Orange arrows show dense, aggregative 'mats' of Pel. Grey arrows show a wide-reaching Pel fibre-like network across the biofilm.

In *Ps. a.* strain PA01, Zhao *et al.,* (2013), demonstrated that Psl trails can form upon a surface, which influences the motility of cells and their migration, whilst Wang *et al.,* (2013), independently reported that Psl can form a fibrous matrix via TFP-dependent migration, akin to spider web formation; connecting parts of the basal biofilm to one another and enabling transit of cells to areas of the growing biofilm. Given that PA14 has a deletion of *pslA* to *pslD* in its genome rendering the strain incapable of synthesising Psl (Friedman and Kolter, 2004a; 2004b), there is precedence perhaps for Pel to be able to adopt a variety of free or cell-associated forms with varying structures (and possibly properties) in order to facilitate maintenance of the both the basal biofilm and three-dimensional architecture over the course of its development.

The top-down three-dimensional biofilm in Figure 3.24 shows a dense ‘mat’ of Pel in an area with reduced Hoechst fluorescence, and subpopulations of cells with increased *cdrA* expression enmeshed within, and emerging above, the Pel ‘mat’. Slices at different heights of the biofilm (in the z dimension) reveal the leading edge of this part of the basal biofilm, and shows association of GFP-expressing cell populations with Pel (Figure 3.24, yellow arrows). As the leading edge retreated, GFP fluorescence was observed to increase in localised regions (Figure 3.24, white arrows), and by a height of Z+47 μm, aggregates of PA14:*cdrA::gfp* cells were seen forming at the leading edge and remained unstained by both Hoechst and WGA. This suggests that the subpopulations and aggregates with increased GFP fluorescence could be composed of cells that have recently migrated to the leading edge, and thus have become more recently sessile in comparison to cells within the established biofilm.

In agreement with this notion, the biofilm presented in Figure 3.23B also shows a population with increased GFP expression forming directly atop of the fibre-like network of Pel, further suggesting that Pel can recruit cells to the existing biofilm; facilitating both lateral bacterial migration within the basal biofilm, and vertical migration during differentiation of the biofilm to result in three-dimensional structures. Chew *et al.,* (2004), suggested that production of Pel within mature PA01 biofilms leads to formation an ECM with increased viscosity, resulting in a ‘looser’ and more malleable structure. If deformed in the presence of stress (such as shear), elastic structures are able to return to their original shape once the stress is removed; in contrast to viscous structures which are irreversibly deformed by stress and can ‘flow’ (Chew *et al.,* 2004). Therefore, formation of dense ‘mats’ of Pel as observed may

facilitate the lateral spreading of the basal biofilm and expansion of its boundary edges. The formation of dense ‘mats’ or fibre-like networks of Pel within the biofilm may also be important for the retention and transfer of nutrients throughout basal layers, in a similar way to alginate produced by mucoid *Ps. a.* strains (Sutherland, 2001).

**Figure 3.24**

**Pel networks maintain basal biofilm structure after 96 hours under low shear at 75 RPM**

*(figure legend overleaf)*

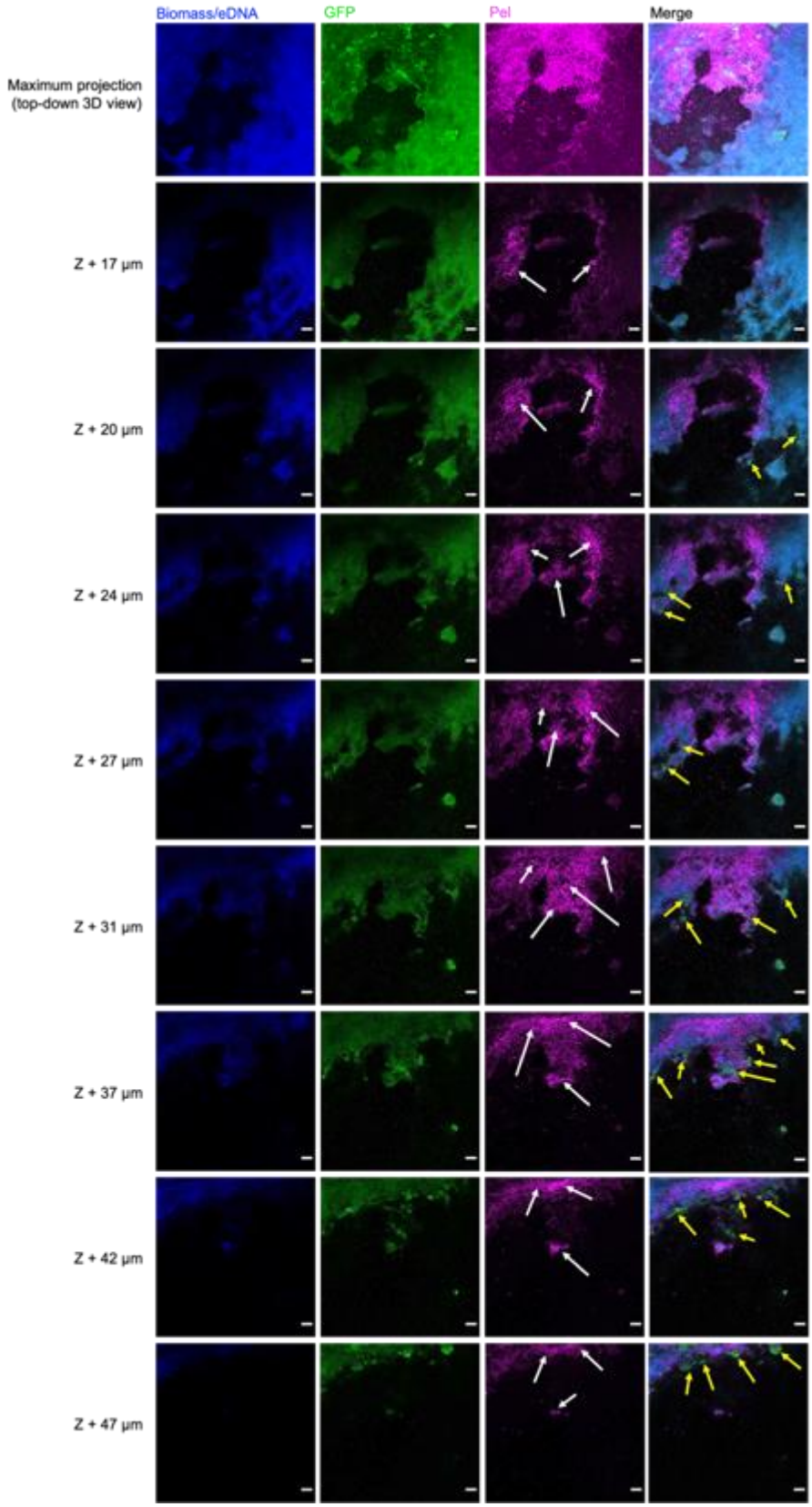

(*figure legend for 3.24*)

Representative confocal images are from PA14:*cdrA::gfp* biofilms (GFP signal is green) cultivated for 96 hours in the CBR under low shear (at 75 RPM) and stained with Hoechst for biomass/eDNA (blue) and the Pel-specific lectin WGA (magenta). Different z heights are shown for the same biofilm, with Z defined as the bottom layer closest to the coupon surface. Scale bar = 20 μm. Yellow arrows show association of cell populations with increased GFP fluorescence with the Pel 'mat'. White arrows show the leading edge retreating and co-localisation of cells with increased GFP fluorescence behind the leading edge of the biofilm.

Macrocolonies were frequently observed after 96 hours of growth under low shear at 75 RPM, and displayed comparable trends in fluorescence intensity profiles to those for mushroom-shaped structures formed after 72 hours of growth. In Figure 3.25A, from Z to a height of Z+7 μm, cavities beneath the three-dimensional structures were visible, and displayed negligible Hoechst, GFP and Pel fluorescence intensities in comparison to the surrounding basal biofilm (yellow arrows). Across all three channels, fluorescence intensities were well correlated in the basal biofilm: GFP and Pel fluorescence intensities were similar, whilst Hoechst fluorescence was greatest throughout the basal layers in Figure 3.25A, suggesting that the ECM in this particular sample site was composed more of eDNA than Pel. As shown by merge channels at Z and a height of Z+3 μm, Hoechst and Pel fluorescence was observed to co-localise (Figure 3.25A, white arrows), which could be indicative of eDNA-Pel complexes.

Emergence of the macrocolony began at a height of Z+17 μm, whereby two distinct structures (Figure 3.25A, i and ii) were observed. For the first feature (i), as captured by the top line drawn on the merge channel, Hoechst and Pel fluorescence intensities were similar and overall well-correlated to one another, whilst the fluorescence intensity of GFP was increased; indicative of increased *cdrA* expression within the feature in comparison to the basal biofilm. GFP fluorescence of this feature was punctate, with cellular subpopulations in feature i displaying a degree of heterogeneity in terms of local *cdrA* expression at both the feature periphery and its interior (Figure 3.25A, red arrows). Figure 3.25B demonstrates the emergence of feature i from the basal biofilm, to which it is attached (white arrows), which could be suggestive of active cell migration from the basal biofilm, resulting in the formation of the mushroom-shaped macrocolony structure (as captured by the bottom line drawn on the merge

channel, feature ii). In further support of this is the fact that feature i was observed to have a different morphology to the emerging, mushroom-shaped feature ii.

By contrast, the second feature emerging from the basal biofilm displayed concave fluorescence intensity profiles, with the peripheral edges of the feature having increased Hoechst, GFP and Pel fluorescence intensities in comparison to the feature's interior (Figure 3.25A, cyan arrows). This is in agreement with the work of Jennings *et al.,* (2015), who similarly observed increased staining of Pel at the periphery of biofilm structures such as mushroom-shaped macrocolonies, and proposed that the structural integrity of three-dimensional features is dependent upon the presence of exopolysaccharides at the peripheral edges.

At heights of Z+22 μm and Z+27 μm, the fluorescence intensities across all three channels continued to increase at the structure periphery, although the resultant concave fluorescence intensity profiles were heterogenous: whilst the as-viewed right-hand peripheral edge showed very good correlation between Hoechst, GFP and Pel fluorescence (Figure 3.25A, pink arrows), the as-viewed left-hand peripheral edge exhibited increased and well-correlated GFP and Pel fluorescence, but lower Hoechst fluorescence (Figure 3.25A, green arrows). The irregular fluorescence intensity profile is likely due to the fact that the as-viewed left-hand periphery is underdoing increased accumulation of cells and Pel as a result of cell migration from the basal biofilm, which resulted in an asymmetrical circumference for the feature.

**Figure 3.25A**

**Heterogenous periphery development during macrocolony formation after 96 hours under low shear at 75 RPM**

*(figure legend overleaf)*

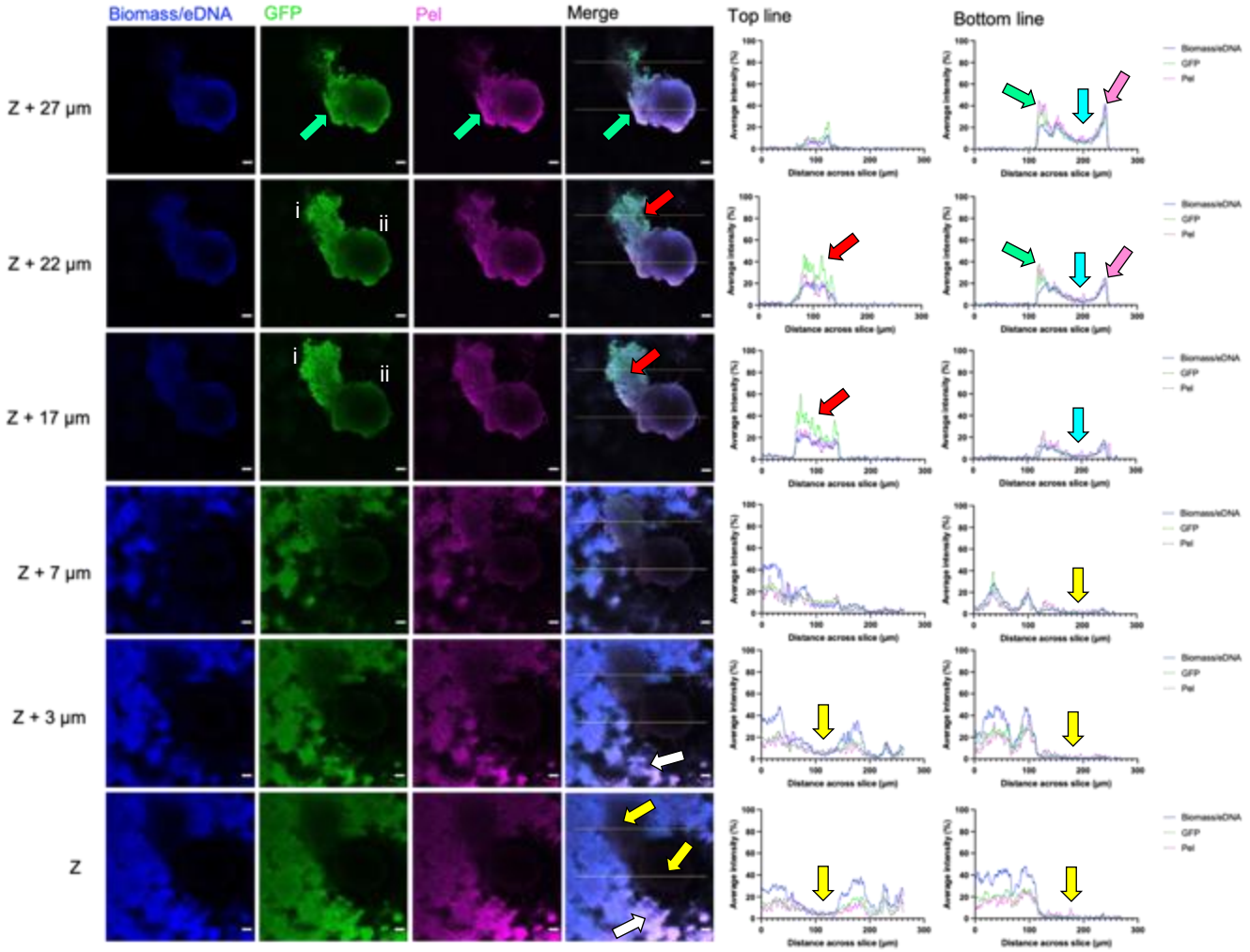

(*figure legend for* Figure 3.25A)

Representative confocal images are from PA14:*cdrA::gfp* biofilms (GFP signal is green) cultivated for 96 hours in the CBR under low shear (at 75 RPM) and stained with Hoechst for biomass/eDNA (blue) and the Pel-specific lectin WGA (magenta). Different z heights are shown for the same biofilm, with Z defined as the bottom layer closest to the coupon surface. Scale bar = 20 μm. Yellow arrows show cavities beneath three-dimensional architectures with negligible fluorescence intensities across all three channels. White arrows show areas in the basal that exhibited co-staining by Hoechst and WGA. Red arrows show heterogenous GFP expression of cells within feature i. Cyan arrows show concave fluorescence intensity profiles for feature ii, indicating increased staining and GFP expression at the periphery of the emerging macrocolony. Pink and arrows show well-correlated and homogenous fluorescence intensities at the as-viewed right-hand peripheral edge, whilst green arrows show the as-viewed left-hand periphery with increased GFP and Pel fluorescence intensities.

**Figure 3.25B**
**Development and maturation of macrocolonies may be facilitated by cell migration from the basal biofilm**

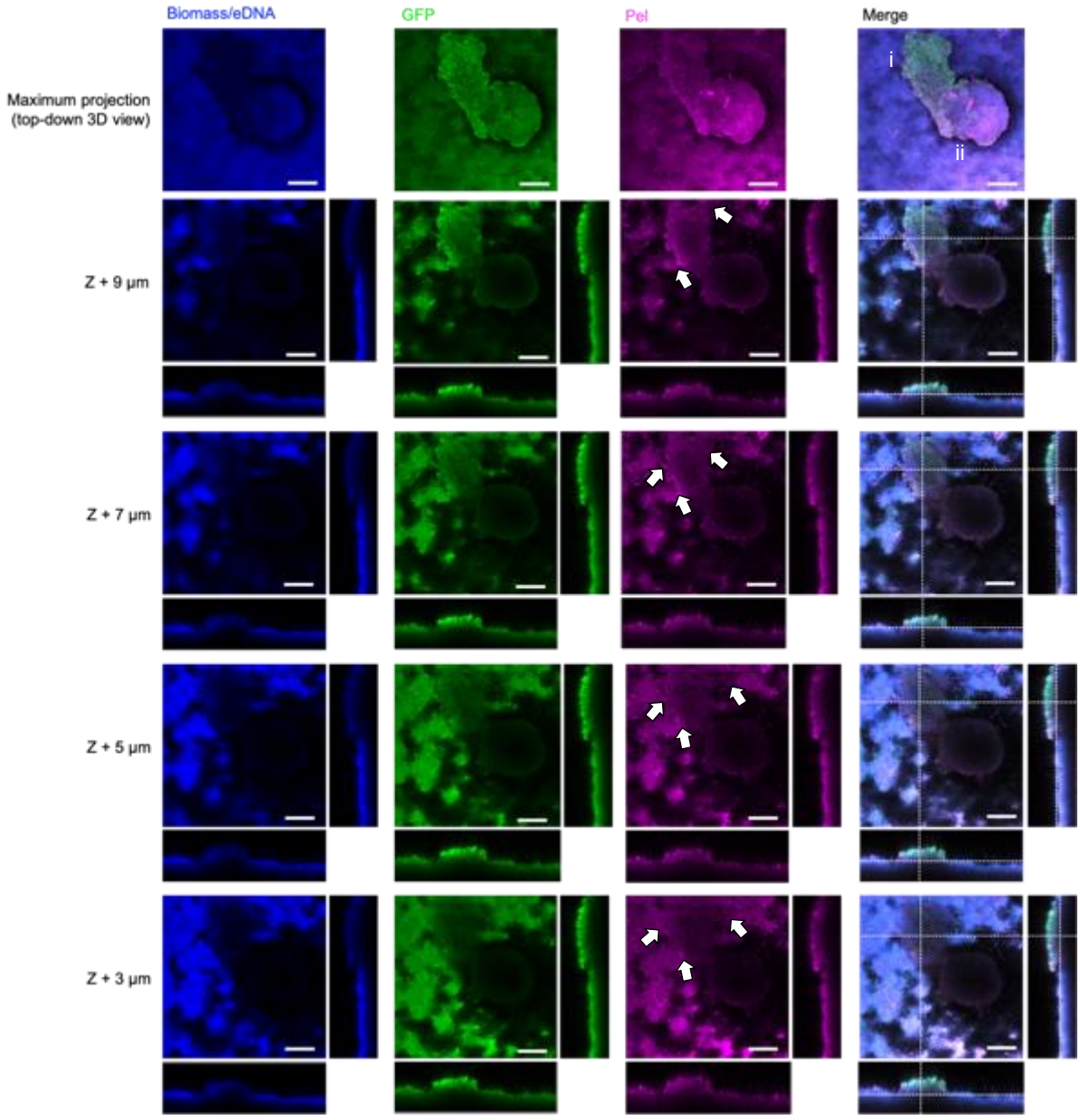


Representative confocal images are from PA14:*cdrA::gfp* biofilms (GFP signal is green) cultivated for 96 hours in the CBR under low shear (at 75 RPM) and stained with Hoechst for biomass/eDNA (blue) and the Pel-specific lectin WGA (magenta). Shown are the top-down three-dimensional maximum projection of the biofilm, as well are top-down z slices and side-views of the emerging macrocolony in, whereby is Z defined as the bottom layer closest to the coupon surface. Scale bar = 50 µm. White arrows show areas of Pel-mediated interactions between the basal biofilm and feature i (as denoted in the merge channel for maximum projection).

Continuous expression of *pel* was shown by Jennings *et al.,* (2015), to be required for sustained growth of PA14 biofilms (i.e. biomass accumulation), but not for maintenance of a basal biofilm's structure. In particular, Pel was shown to be crucial for sustaining cell-cell interactions in aggregative features, as PA14 *pel* mutant strains were unable to form stable aggregates (Jennings *et al.,* 2015). Figure 3.25C shows the emergence of the mushroom-shaped macrocolony structure (feature ii) above the biofilm, and is a continuation of the same biofilm shown in Figures 3.25A and 3.25B respectively.

At a height of Z+33 μm, fluorescence intensity profiles across all three channels are well-correlated, although the concave profile remained heterogenous, with increased GFP and Pel fluorescence localised to the as-viewed left-hand periphery of the structure (Figure 3.25C, yellow arrows). Punctate areas of Pel fluorescence were also observed across the macrocolony at this height, which were uncorrelated to either Hoechst or GFP fluorescence (Figure 3.25C, red arrows). At a height of Z+39 μm, fluorescence intensity profiles were more punctate, with the interior of the macrocolony structure exhibiting increased GFP and Pel fluorescence (Figure 3.25C, orange arrows). Fibre-like projections of Pel were additionally observed around the exterior of the feature, with punctate regions of Pel maintained with increasing height in the z dimension (Figure 3.57C, green arrows).

Indeed, from a height of Z+44 μm onwards, Pel fluorescence remained punctate, and was observed to have increased fluorescence intensities compared to those of Hoechst and GFP (Figure 3.25C, cyan arrows). Based on the fluorescence intensity profiles for Pel and the merge channels, Pel appeared to encapsulate the apical layers

of the macrocolony, forming fibre-like projections across the interior of the macrocolony apex (Figure 3.25C, cerise arrows). Encasement of the apex in Pel could maintain the developing macrocolony; protecting the mushroom-cap cell structure beneath to ensure its three-dimensional integrity is preserved. Crosslinking (or entanglement) of the Pel fibre-like projections could further enable the macrocolony apex to withstand any spatial or temporal changes to physical parameters in the bulk fluid. For example, Körstgens *et al.,* (2001), demonstrated that entanglement of alginate polymers, facilitated by the presence of $Ca^{2+}$ ions, increased the stability of mucoid *Ps. a.* biofilm structures.

**Figure 3.25C**
**Apical macrocolony layers formed by PA14:*cdrA::gfp* after 96 hours of growth under low shear at 75 RPM**

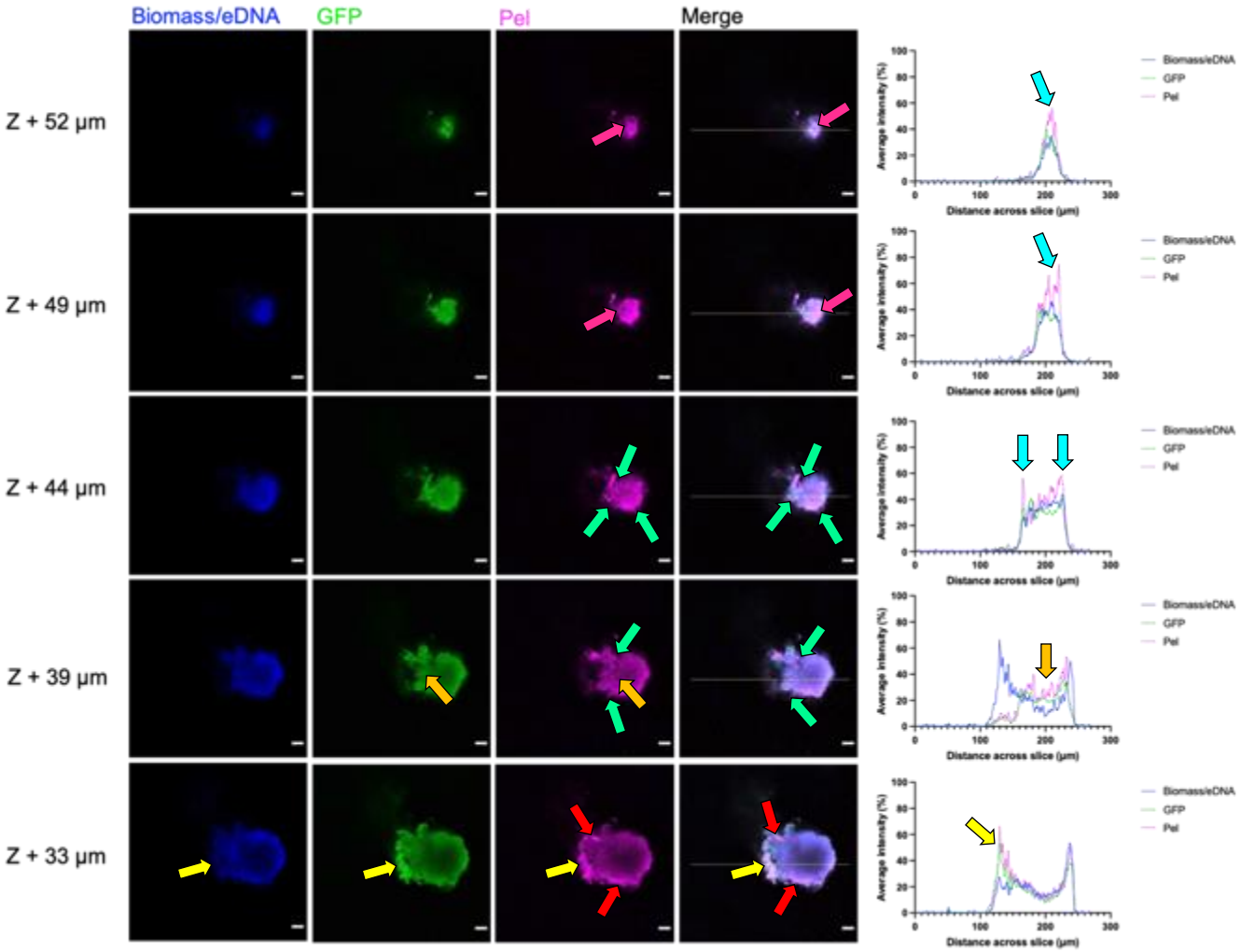


Representative confocal images are from PA14:*cdrA::gfp* biofilms (GFP signal is green) cultivated for 96 hours in the CBR under low shear (at 75 RPM) and stained with Hoechst for biomass/eDNA (blue) and the Pel-specific lectin WGA (magenta). Different z heights are a continuation of the emerging macrocolony from the same biofilm as shown in Figure 3.27A. with Z defined as the bottom layer closest to the coupon surface. Scale bar = 20 µm. Yellow arrows show heterogenous fluorescence intensities at the as-viewed left-hand periphery edge of the macrocolony. Red arrows show areas of the structure that exhibited increased Pel fluorescence uncorrelated to those of Hoechst or GFP. Orange arrows show increased GFP and Pel fluorescence intensities in the macrocolony interior. Green arrows show punctate regions of Pel maintained at the exterior of the macrocolony. Cyan arrows show increased production of WGA-stained Pel in the apical layers of the macrocolony. Cerise arrows show fibre-like projections of Pel across the interior of the macrocolony apex.

By 96 hours, PA14 biofilm formation under high shear at 350 RPM was characterised by multiple mounds that were highly variable in the x, y and z dimensions, resulting in an irregular biofilm topography (Figures 3.26 and 3.27). Biofilms formed after 96 hours of growth under high shear had an average height ranging between 70 – 150 μm, thus fluorescence intensity profiles for Hoechst, GFP and Pel were difficult to calculate, due to the reduced laser and stain penetration of the structures.

Similarly to the mounds formed after 72 hours, three-dimensional structures formed after 96 hours exhibited increased growth upwards in the vertical dimension (z), and appeared to remain spatially-separated from one another, rather than three-dimensional structures emerging from a defined basal layer as observed under high shear at 75 RPM. Mound formation across different areas of the coupon surface was heterogenous, with respect to the sizes of structures in the x and y dimensions, maximum height reached in the z dimension, and production of Pel throughout the biofilm (Figures 3.26 and 3.27). Figure 3.26 shows three different ‘tower-like’ biofilm architectures, composed of mounds growing irregularly and seemingly atop one another; varying in width (in the x dimension) from 20 μm (Figure 3.26, panels A and C, yellow arrows) up to > 250 μm (Figure 3.26, panels A and B, white arrows).

**Figure 3.26**

**Biofilm formation by PA14:*cdrA::gfp* after 96 hours under high shear at 350 RPM results in large mound formation**

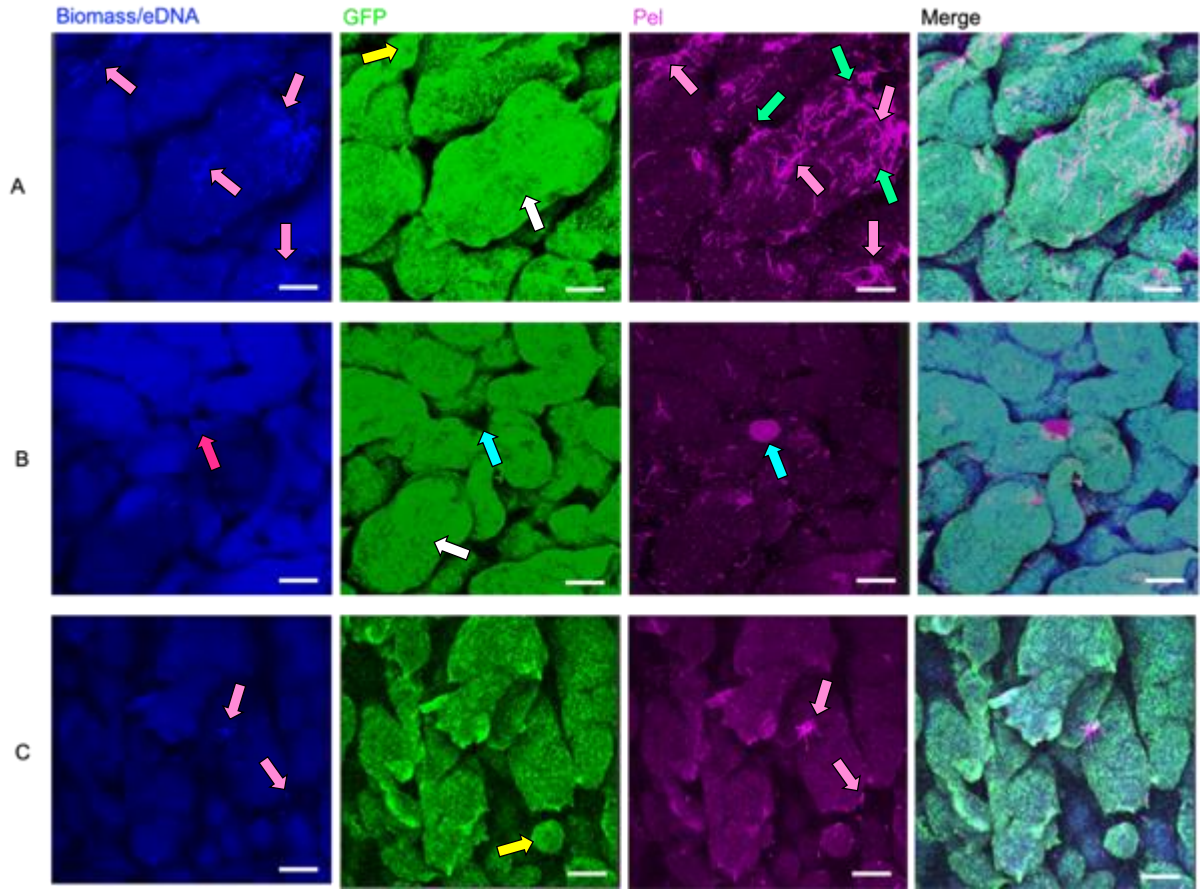


Representative confocal images are from PA14:*cdrA::gfp* biofilms (GFP signal is green) cultivated for 96 hours in the CBR under high shear (at 350 RPM) and stained with Hoechst for biomass/eDNA (blue) and the Pel-specific lectin WGA (magenta). Shown are top-down three-dimensional and side views of the macrocolony and biofilm. Scale bar = 50 μm. A, B and C represent different biofilms imaged during two independent CBR runs. Yellow arrows show mounds with maximal widths of approximately 20 μm whilst white arrows show neighbouring mounds exceeding widths of 250 μm (in the x dimension). Green arrows shown Pel fibre-like 'tendril' formation at a mound periphery. Pink arrows show similar Pel 'tendrils' also stained by Hoechst, indicative of eDNA-Pel 'tendril' complexes. Cyan arrows show an aggregative area of Pel in an area void of GFP-expressing cells. Cerise arrow show staining of a structure within the interior of the aggregate by Hoechst.

Staining by WGA revealed several distinct morphologies for Pel, including the formation of fibre-like ‘tendrils’ that seemed to have a structural role; aggregates composed of Pel ‘tendrils’ were observed at the periphery of mound structures, as well as protruding outwardly (Figure 3.26A, green arrows), maintaining critical cell-cell interactions in the developing mound. Areas with fibre-like ‘tendrils’ exhibited increased Pel fluorescence that were well correlated to ‘tendrils’ that similarly displayed increased Hoechst fluorescence (Figures 3.26A and 3.26C, pink arrows), suggesting that the ‘tendrils’ could be formed of Pel, or eDNA-Pel complexes. Punctate areas with increased Pel fluorescence was additionally observed, and did not appear cell-associated (Figure 3.26B, cyan arrows). eDNA appears to be localised to the interior of the Pel structure (Figure 3.26B, cerise arrows), once more suggesting that eDNA and Pel can interact within *Ps. a.* biofilms, which is in agreement with other works in the literature (Jennings *et al.,* 2015).

As shown by Figure 3.27, maximum heights reached by mounds was variable (Figure 3.27, yellow arrows), resulting in a lack of structural homogeneity. At a height of 35 μm, the apical layers of some mound structures were emerging, as demonstrated by their smaller dimensions in the x and y dimensions (Figure 3.27, white arrows), and increased GFP fluorescence at both the structure periphery and interior (Figure 3.27, red arrows). Punctate areas of Pel fluorescence were also observed at peripheral edges that had increased GFP fluorescence, as free rather than cell-associated Pel (Figure 3.27, cyan arrows). Also seen was an aggregate of Pel protruding approximately 30 μm above the apex of a ‘tower-like’ structure, which had minimal GFP fluorescence (suggesting there was not a cell population underneath), and well-

correlated Hoechst fluorescence at the aggregate's periphery, which could indicate co-localisation of eDNA and Pel (Figure 3.27, grey arrows).

**Figure 3.27**
**Mound features formed after 96 hours under high shear at 350 RPM exhibit variation in their maximal heights**

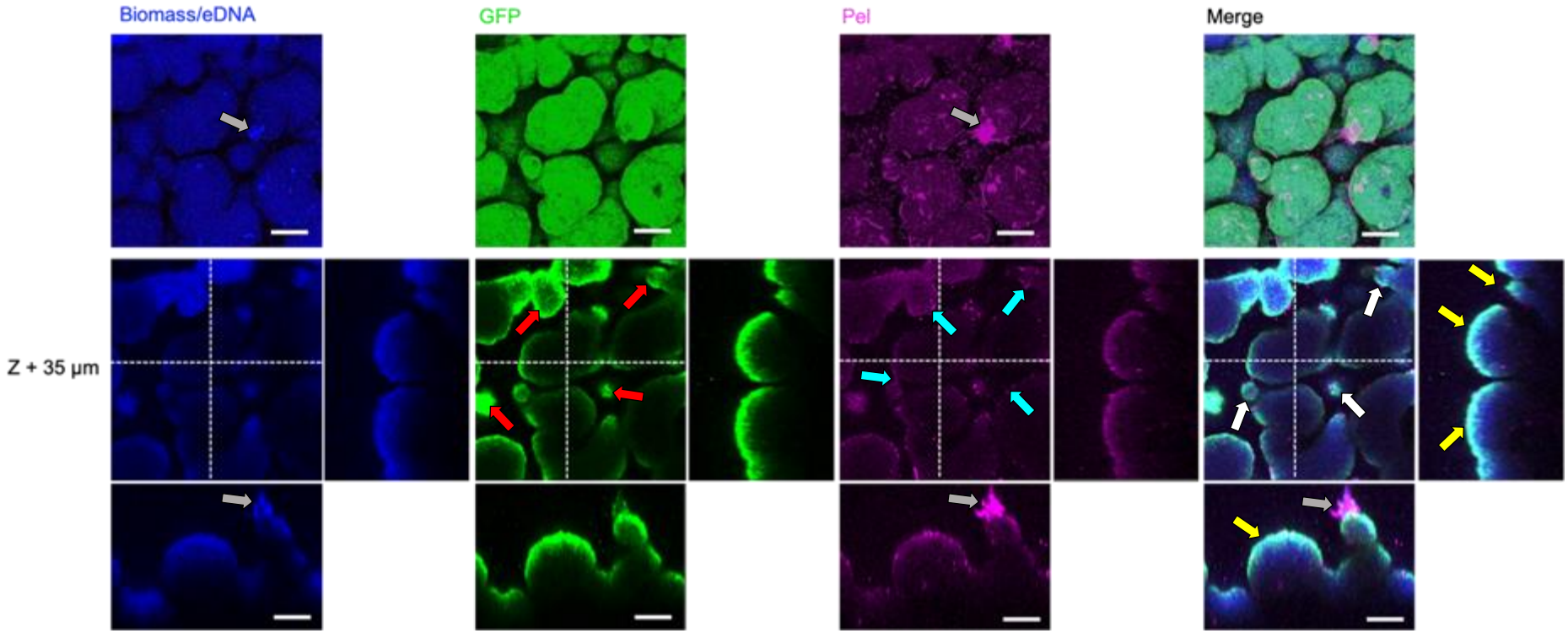


Representative confocal images are from PA14:*cdrA::gfp* biofilms (GFP signal is green) cultivated for 96 hours in the CBR under high shear (at 350 RPM) and stained with Hoechst for biomass/eDNA (blue) and the Pel-specific lectin WGA (magenta). Shown are top-down three-dimensional views of the mound structures, as side views at a height of Z+35 μm, with Z defined as the bottom layer closest to the coupon surface. Scale bar = 50 μm. Yellow arrows show variation in maximal height reached by mound structures. White arrows show the emergence of some mound apexes, characterised by increased GFP fluorescence across the mound interior and periphery, as shown by red arrows. Cyan arrows show punctate areas of Pel fluorescence around the exterior of the mound structures. Grey arrows show a large aggregate of Pel, co-stained by Hoechst, protruding from above the apex of a 'tower-like' structure.

As biofilms increase in size, the presence of gradients with respect to growth rate, metabolic activity and oxygen concentration will occur: the basal layers of the biofilm will have reduced metabolic activity, due to nutrient limitation or depravation (Walters *et al.,* 2003; Madsen *et al.,* 2007), whilst the apical layers of the biofilm continue to grow upwards into the bulk fluid, in order to gain access to nutrients and oxygen (Madsen *et al.,* 2007; Serra and Hengge, 2014). In agreement with this is the fact that the mounds exhibited increased Hoechst, GFP and Pel fluorescence at their growing apexes (Figure 3.28, white arrows) in comparison to the lower basal layers of the interior structure, which exhibited very little staining by Hoechst or WGA and negligible GFP fluorescence (Figure 3.28, red arrows). Water channels were additionally maintained throughout the height of the biofilm, resulting in spatial separation of the mound structures, in order to facilitate diffusion of nutrients and solutes to deeper layers of the biofilm (Figure 3.28, yellow arrows).

**Figure 3.28**

**Biofilm structures formed by PA14:*cdrA::gfp* after 96 hours under high shear at 350 RPM are highly heterogenous**

*(figure legend overleaf)*

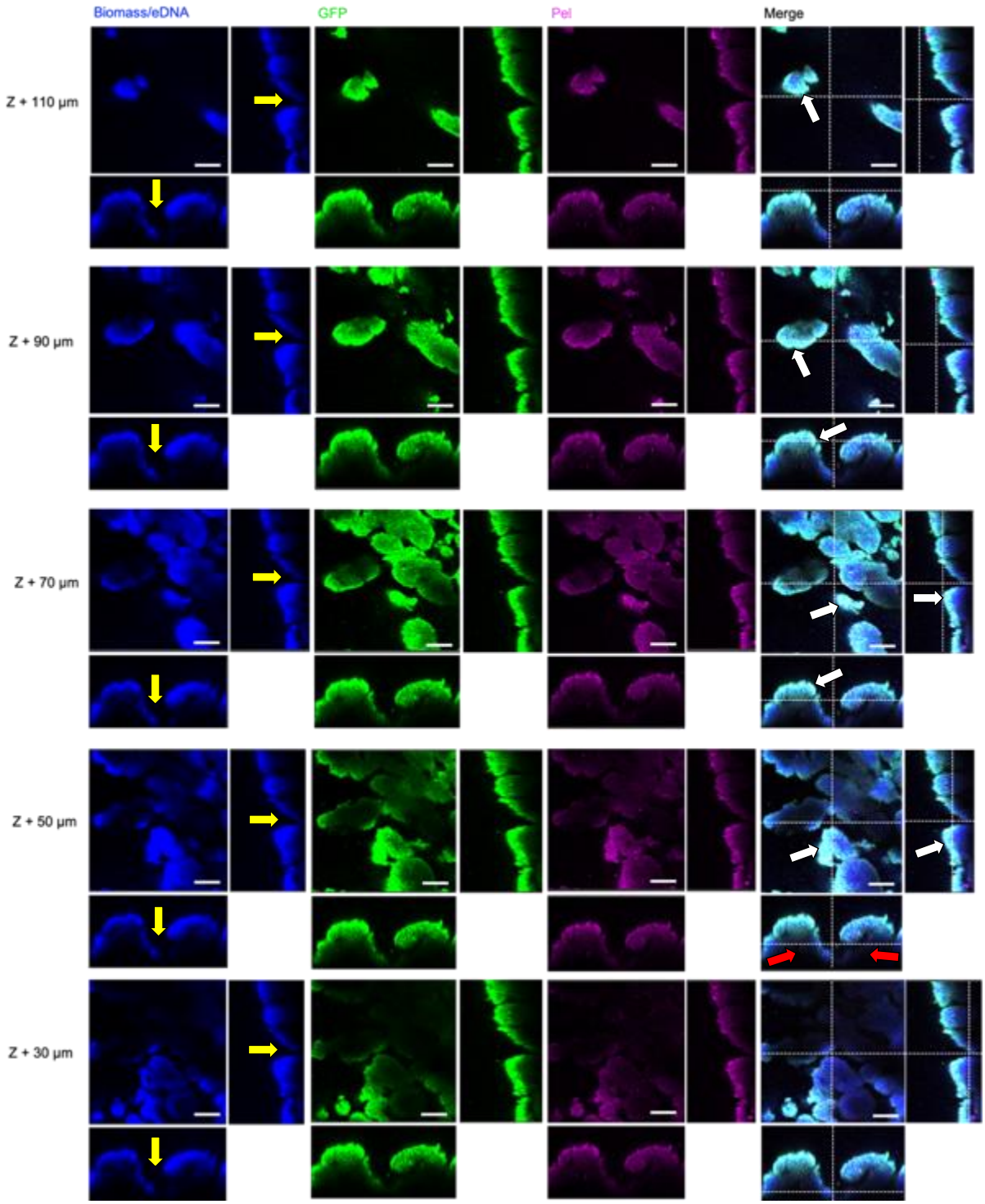

(*figure legend for* Figure 3.28)

Representative confocal images are from PA14:*cdrA::gfp* biofilms (GFP signal is green) cultivated for 96 hours in the CBR under high shear (at 350 RPM) and stained with Hoechst for biomass/eDNA (blue) and the Pel-specific lectin WGA (magenta). Shown are top-down top-down z slices and side-views of the mound structures with increasing biofilm height, with Z defined as the bottom layer closest to the coupon surface. Scale bar = 50 μm. White arrows show increased Hoechst, GFP and Pel fluorescence at the mound apexes. Red arrows show very little staining and/or poor laser penetration of the lowermost layers of the biofilm. Yellow arrows show maintained water channels between mound structures.

## 3.4. Discussion

The results presented in this chapter demonstrate that industrially-relevant low and high shear regimes, as modelled by the CBR at 75 versus 350 RPM respectively, have an impact upon PA14 biofilm formation, at all stages of development over a time period of 96 hours.

### 3.4.1. Biofilm formation under low shear conditions at 75 RPM

Growth under low shear at 75 RPM resulted the development of a confluent biofilm, composed of basal layers that exhibited homogeneity with respect to their structure and correlation of Hoechst, GFP and Pel fluorescence (Figures 3.5 – 3.7), which indicated that cell were all expressing equivalent amounts of *cdrA* to one another, and therefore comparable levels of intracellular c-di-GMP. The basal biofilm appeared to be composed of PA14:*cdrA::gfp* cells surrounded by an early ECM of eDNA and Pel, believed to be involved in the initiation of surface attachment and the formation of early *Ps. a.* biofilms (Whitchurch *et al.,* 2002; Vasseur *et al.,* (2005); Allensen-Holm *et al.,* 2006; Flemming and Wingender, 2010).

Several research groups have previously demonstrated that many strains of *Ps. a.*, including clinical isolates, produce large quantities of eDNA (Murakawa *et al.,* 1973a; 1973b; Hara and Ueda, 1981; Muto and Goto, 1986; Nemoto *et al.,* 2003), whilst Whitchurch *et al.,* (2002), were the first to propose that eDNA is requisite for the initial establishment of *Ps. a.* biofilms. Treatment of early PA01 biofilms with DNase I resulted in dissolution of preliminary structures, whilst mature PA01 biofilms were only slightly

affected, suggesting that eDNA facilitates initial cell-cell interactions in 'young' biofilms, by holding the cells together *in situ* (Whitchurch *et al.,* 2002; Allesen-Holm *et al.,* 2006). Others have further demonstrated that Pel mediates cell-cell interactions in *Ps. a.* biofilms, to serve as the primary structural scaffold upon which biofilm formation can occur (Colvin *et al.,* 2011; Yang *et al.,* 2011).

Colvin *et al.,* (2011), revealed that Pel is fundamental for the initiation and maintenance of cell-cell interactions within PA14 aggregates, and that expression of Pel positively influences daughter cell association with parental cells in a clonal population. A *pelB* mutant strain of PA14 was shown to result in loss of aggregate formation, due to dispersion of daughter cells (termed 'flyers') away from their parental cells in the absence of Pel (Colvin *et al.,* 2011). Continuous production of Pel is important for PA14 biofilm development – loss of *pel* expression results in biofilms that do not progress past the monolayer stage of growth, whilst overexpression of *pel* leads to continued accumulation of biomass and increased growth (Colvin *et al.,* 2011). Therefore, localised aggregates of Pel (and eDNA) may be indicative of areas of the biofilm that may develop into mature structures, such as micro- and macrocolonies.

Given that PA14 is incapable of making Psl, the strain must rely on Pel as its principal exopolysaccharide during matrix formation. Cooley *et al.,* (2013), showed that Pel promotes organisation of bacteria lying flat and symmetrically on a surface; Δ*pel* mutants formed disorganised piles of bacterial cells adhered to the surface and one another asymmetrically (i.e. standing on end rather than lying flat). It was therefore interesting to observe Pel fibre-like projections throughout the lower parts of the basal

layer, connecting local populations of adjacent cells and microcolonies to one another (Figures 3.6 and 3.8). In Figure 3.8 at a height of Z+10 μm, a definitive meshwork of Pel can be seen in a formation akin to a spider's web, with fibres radiating outwards from a central region that exhibited punctate Pel concentration. Whilst a similar morphology for Psl has been previously reported in the literature (Zhao *et al.,* (2013); Wang *et al.,* (2015)), to the author's knowledge there is no preceding description of Pel fibre-like network formation by PA14 as reported in this chapter.

TFP are believed to be involved in the development of microcolonies and macrocolonies, through the migration of cells to areas where aggregate formation is occurring (O'Toole and Kolter, 1998). In PA01, Psl forms a fibrous matrix via TFP-dependent migration; connecting parts of the basal biofilm to one another and enabling the translocation of cells to growing areas of the biofilm (Wang *et al.,* 2015). Zhao *et al.,* (2013), demonstrated that trails of Psl have a positive effect on the motility of cells that are in contact with the trails, resulting in increased cell-cell interactions as well as the formation of local, increased concentrations of Psl. Described by Zhao *et al.,* (2013), as 'elite' cells, PA01 cells associated with areas of accumulated Psl become the founding populations for initial microcolony formation. Chew *et al.,* (2014), suggested that 'younger' biofilms can be easily disrupted by shear forces, but the production of a matrix that is crosslinked or enmeshed was proposed to reduce detachment of surface-attached cells, and centralise growth newly-colonised sites. Thus, the Pel fibre-like networks observed could have an analogous function to those formed of Psl in PA01: to facilitate migration of cell subpopulations to developing areas of either the basal biofilm or emerging microcolonies. Dense aggregates comprised of

eDNA-Pel complexes were seen either existing as free eDNA-Pel agglomerates or encapsulating cell populations (Figures 3.8 and 3.9), which could also be indicative of 'elite' cell populations that will initial form microcolonies, and eventually develop into mature mushroom-shaped macrocolonies (Stoodley *et al.,* 2002; Klausen *et al.,* 2003).

Macrocolonies formed by PA14 under low shear conditions were observed at 72 and 96 hours, with defined and prototypical mushroom-shaped morphologies. Barken *et al.,* (2008), proposed that development of mushroom macrocolonies occurs via a sequential process, through which the 'stalk' is composed of founding microcolony cell populations that release eDNA, whilst motile subpopulations migrate to form the 'cap' structure atop the stalk, in agreement with the work of Klausen *et al.,* (2003). Data presented after 72 hours growth of PA14 under low shear supports this, as macrocolony formation appeared to be homogenous; fluorescence intensities across all three channels were extremely similar in terms of their profiles; across independent sampling sites, and irrespective of spatial location or the overall height of individual mushroom-shaped macrocolonies (Figures 3.15 and 3.16). Representative three-dimensional, top-down CLSM images (Figures 3.13 and 3.14) identified the presence of cell subpopulations with increased GFP and Pel fluorescence atop the mushroom-shaped macrocolonies observed, which could represent a recently developed 'cap' structure that is undergoing gene expression changes to become sessile.

Increased intracellular levels of c-di-GMP, as indicated through use of the c-di-GMP-dependent PA14:*cdrA::gfp* reporter strain, will result FleQ-mediated activation of *pel*, leading to increased Pel production (Baraquet *et al.,* 2012; Baraquet and Harwood,

2013; Su *et al.,* 2015). Post-translationally, c-di-GMP binding to PelD modulates its activity, resulting in increased synthesis of Pel polymers (Lee *et al.,* 2007). Pel is an essential component of mature PA14 biofilm structures (Colvin *et al.,* 2011; Ghafoor *et al.,* 2011), and likely facilitates and enhances cell-cell interactions between the non-motile populations of the macrocolony adjacent to the newly sessile 'cap' populations, to ensure that the integrity of the growing three-dimensional structure is maintained.

Figures 3.27A, 3.27B and 3.27C (at 96 hours) appear to show a mushroom-shaped macrocolony and large, migratory cell population emerging from the basal biofilm (Figure 3.27B), leading to the irregular accumulation of biomass along the macrocolony periphery, as shown by the heterogenous peaks of the resultant Hoechst, GFP and Pel fluorescence intensity profiles (Figures 3.27A and 3.27C). Concave fluorescence intensity profiles indicate the localisation of eDNA, Pel and cells with increased *cdrA* expression at the macrocolony exterior, which is in agreement with the work of Jennings *et al.,* (2015). The migratory cell population (denoted as 'feature i' in Figures 3.27A and 3.27C) exhibited increased GFP fluorescence intensities compared to the emerging macrocolony, and was observed to have a different morphology to the mushroom-shaped structure.

Cells residing within the basal layers and three-dimensional features of PA14 biofilms grown under low shear at 75 RPM maintained cell-cell interactions, as facilitated by the ECM components eDNA and Pel. There is evidence to suggest that QS is involved in biofilm formation and exopolysaccharide synthesis (Ueda and Wood, 2009), therefore it is feasible to suggest that intercellular communication, as mediated by

diffusion of QS autoinducers throughout the biofilm, could also have impacted upon structural maturation. The autoinducer 3-oxo-$C_{12}$-HSL, synthesised by the LasIR-QS system, leads to the formation of structured and established biofilms: *lasI* is expressed in a high proportion of cells during early biofilm formation (De Kievit *et al.,* 2001), and *lasI* mutant strains were shown by Davies *et al.,* (1998), to form flat, undifferentiated biofilms that did not undergo maturation, in spite of producing similar quantities of EPS in comparison to wild-types. The RhlIR-QS system was additionally shown by Sauer *et al.,* (2002), to undergo activation during *Ps. a.* biofilm maturation. AHL analogues, which inhibit QS, were further shown by Hentzer *et al.,* (2002) to results in perturbed biofilm development by flow-chamber grown *Ps. a.*, whilst Yang *et al.,* (2009), identified chlorzoxazone, nifuroxazide and salicylic acid as significant inhibitors of QS in PA01, leading to the formation of thinner, and less structured biofilms in comparison to the wild-type.

De Kievit *et al.,* (2001), found that *lasI* and *rhlI* gene activity was greater within lower layers of the biofilm (i.e. nearer to the adherent surface), and reduced with increasing height of the biofilm. In *Ps. a*, *lasI* and *rhlI* activation is autoregulated and sequential: *lasI* induced in response to 3-oxo-$C_{12}$-HSL, whilst maximal expression of *rhlI* requires both 3-oxo-$C_{12}$-HSL and $C_4$-HSL (De Kievit *et al.,* 2001; Waters and Bassler, 2005; Williams and Cámara, 2009). As PA14 biofilms grown under low shear at 75 RPM were composed of homogenous basal layers with maintained cell-surface and cell-cell interactions, diffusion of QS autoinducers and their accumulation in the basal layers may have been occurring to further control biofilm formation. The spatial organisation within these PA14 biofilms, in which basal layers were confluent, could further minimise

diffusion of autoinducers away from the cells, resulting in increased expression of QS genes, and subsequent transcription of genes under their control (De Kievit *et al.,* 2001; Waters and Bassler, 2005; Kostylev *et al.,* 2019).

The work of Sakuragi and Kolter, (2007), suggested that transcription of the *pel* operon is indirectly controlled by the LasIR QS system. A 20 bp sequence located upstream of *pelA* displayed similarity to the predicted LasR/RhlR binding motif, although deletion of this bp sequence did not alter quorum-dependent transcription (Whiteley and Greenberg, 2001), which could suggest that QS control of *pel* expression occurs via expression of as yet unidentified LasR/RhlR-regulated transcription factor (Sakuragi and Kolter, 2007). Regulation of these QS systems at the post-translational level also occurs, as the RNA binding protein RsmA has been shown to negatively regulate translation of *lasI* and *rhlI* (Pessi *et al.,* 2001). QS *lasIrhlI* and *psqA* mutant strains of *Ps. a.* were shown by Allensen-Holm *et al.,* (2006), to result in the formation of flat biofilms with decreased levels of eDNA and increased susceptibility to treatment using the anionic surfactant sodium dodecyl sulfate, suggesting that QS-mediated release of eDNA can increase the structural integrity of mature biofilm architecture.

### 3.4.2. Biofilm formation under high shear conditions at 350 RPM

Growth under high shear by contrast resulted in the formation of PA14 biofilms with considerably different architectures to those formed under low shear. Across every sampled timepoint, Hoechst, GFP and Pel fluorescence intensities exhibited increased heterogeneity, both spatially and temporally on a proximal (i.e. cell-cell or adjacent subpopulations of cells within the same coupon sampling site) and distal (i.e. cells

within different sampling sites on the same coupon, or from independent CBR runs) level. Initial surface colonisation was greater under high shear, with the formation of cell clusters and small, aggregative features frequently observed after 24 hours of growth (as shown by comparison of Figures 3.1 – 3.2 with Figures 3.3. – 3.4).

The work of several research groups has suggested that increased shear stress leads to increased residence time of bacterial cells at the substratum's interface with bulk fluid, resulting in more rapid cell association with the surface (Characklis, 1990; Donlan, 2002; Lecuyer *et al.,* 2011; Kharadi and Sundin, 2019). In contrast, others propose that high shear conditions lead to reduced attachment and maintenance of stable bacterial interactions with the surface, resulting in increased incidences of reversible compared to irreversible attachment (Ramsey and Whitley, 2004; Fonseca and Sousa, 2007; Park *et al.,* 2011).

Results presented in this chapter suggest that running the CBR at 350 RPM, an industrially-relevant high shear condition, results in increased initial attachment of PA14:*cdrA:gfp* cells. Increased mechanical shear has been previously identified as an environmental 'cue' that *Ps. a.* can mechanically sense; resulting in increased c-di-GMP synthesis and progression of the biofilm phenotype (Luo *et al.,* 2015; Rodesney *et al.,* 2017). In *Ps. a.*, the Wsp regulatory system is involved in surface-sensing and subsequent transduction of signals within the bacteria to regulate biofilm formation (Hickman *et al.,* 2005). Membrane-bound WspA is thought to sense surface-cell or cell-cell contacts in response to a as yet undetermined external signal, leading to phosphorylation of the response regulator WspR which then catalyses synthesis of c-

di-GMP (Hickman *et al.,* 2005; O'Connor *et al.,* 2012). WspR forms localised clusters in the cytoplasm, with WspR clustering enhanced in response to *Ps. a.* proliferation on a surface (Guvener and Harwood, 2007). Intracellular levels of c-di-GMP can be further modulated through increased activity of the membrane-bound DGC SadC: Luo *et al.,* (2015), identified PilY1 as a mechanosensory element that, upon contact with a surface, can induce SadC activity to result in increased intracellular concentrations of the second messenger.

Increased *cdrA* expression of PA14 *cdrA::gfp* cells within the biofilms formed under high shear at 350 RPM is indicative of higher intracellular levels of c-di-GMP, which in turn results in activation of the *pel* operon to increase Pel production (Baraquet *et al.,* 2012; Baraquet and Harwood, 2013; Su *et al.,* 2015). The binding of c-di-GMP to the inhibitory site of the effector protein PelD further enhances Pel biosynthesis, purportedly through eliciting a conformational change in PelD, which results in increased polymerisation and subsequent export of the polysaccharide (Lee *et al.,* 2007; Li *et al.,* 2012; Whitney *et al.,* 2012). Thus, the c-di-GMP-binding effector proteins FleQ and PelD respectively regulate synthesis of Pel at both the transcriptional and post-translational levels (Kathrios-Lanwermeyer *et al.,* 2021).

Increased c-di-GMP synthesis could therefore be an adaption of *Ps. a.* in response to growth under high shear conditions, to increase the production of ECM components such a Pel; enhancing the 'stickiness' of bacterial cells attaching to both the surface and to one another. In agreement with this is the observation that early biofilm formation during growth at 350 RPM resulted in increased Pel fluorescence intensities,

which could ensure adhered bacteria remain *in situ* and are not removed by the high shear regime. Moreover, high shear at 350 RPM appeared to induce the formation of aggregative structures which were characterised by increase fluorescence intensities across all three channels, most notably with respect to Pel (Figures 3.10 – 3.14). Although energetically costly to the bacterial cells, it is feasible to suggest that increased production of Pel is induced by high shear conditions at 350 RPM, to increase cohesion within the biofilm by maintaining cell-surface and cell-cell interactions, and protect the PA14 cells from risk of detachment under increased shear stress.

The arrangement of a biofilm's internal structure is believed to be governed by the velocity of the flow experienced during growth (Beyenal and Lewandowski 2002). Under high shear conditions, the magnitude of mechanical forces acting upon the biofilm is greater (Stoodley *et al.,* 1999; Nyguen *et al.,* 2005), resulting in increased shear stress. At 350 RPM, increased *cdrA* expression indicates increased intracellular levels of c-di-GMP, which will promote the sessility of PA14 cells through increased production of EPS such as Pel, both internally within the architecture of the biofilm and at the peripheral edges of the structure; enhancing the strength of the biofilm under adverse, high shear conditions. Increased Hoechst staining of PA14:*cdrA::gfp* biofilms formed under high shear at 350 RPM may also be indicative of increased biomass within the mounds, which would result in denser three-dimensional structures that are more resistant to the greater mechanical forces imposed upon them (Jackson *et al.,* 2001).

Pel has been shown by Colvin *et al.,* (2011), to be requisite for the initiation and maintenance of cell-cell interactions within PA14 aggregates, and to positively influence daughter cell association with parental cells in a clonal population. Increased Pel production in aggregates could therefore facilitate clonal growth of cell subpopulations, and increased cohesion within the developing structures. Co-localisation of staining by Hoechst (as shown in Figures 3.13 and 3.14) could be indicative of the presence of eDNA, which has been shown to further enhance cell-cell interactions in developing *Ps. a.* biofilm (Whitchurch *et al.,* 2002; Allensen-Holm *et al.,* 2006; Flemming and Wingender, 2010). Entwining of eDNA between cells can result in the development of stable clumps (Allensen-Holm *et al.,* 2006), suggesting that the aggregative phenotypes observed were as a result of both increased concentration and spatial organisation of eDNA and Pel within such structures. Merge channels for representative CSLM images also revealed encapsulation of aggregative features by Pel as well as increased Pel production throughout the height of basal-like biofilms (Figures 3.10 and 3.13). Pel encapsulation was not observed under low shear at 75 RPM, which may indicate that this morphology is induced in response to high shear stress. Several research groups have previously purported that aggregation is a protective mechanism; making cells encased within aggregative structures more resistant to chemical treatment and predation and enabling cooperative intercellular behaviours (Hense *et al.,* 2007; Friman *et al.,* 2013; McNally and Brown, 2015; Flemming *et al.,* 2016).

Alginate, the primary exopolysaccharide produced by mucoid strains of *Ps. a.*, is a capsular polysaccharide that forms a protective layer around a bacterium (Mann and

Wozniak, 2015). Biosynthesis of Pel is the least characterised out of the three *Ps. a.* exopolysaccharides, but analysis by Franklin *et al.,* (2011), suggested it is similar to to alginate synthesis. Modifications to alginate, post-polymerisation, have been shown to determine its functional properties (such as polymer viscosity and flexibility), occurring principally through O-acetylation of monomeric units (Skjåk-Bræk *et al.,* 1989; Baker *et al.,* 2014). Deacetylated alginate is associated with reduced exopolysaccharide viscosity and increased susceptibility to alginate lyase-mediated degradation (Skjåk-Bræk *et al.,* 1989; Boyd *et al.,* 1993; Boyd and Chakrabaty, 1994).

Modelling by Franklin *et al.,* (2011), predicted that PelA contains a TIM $\alpha/\beta$ barrel at its N-terminal that shares structural similarities with glycosidic hydrolases, and a carbohydrate esterase domain at the C-terminal (Urch *et al.,* 2009). Colvin *et al.,* (2013), demonstrated that PelA has deacetylase activity *in vitro*, and mutation of residues predicted to be required for deacetylation resulted in mutant *Ps. a.* strains with biofilm-deficient phenotypes. N-deacetylation of PGA is requisite for biofilm formation by a range of Gram positive and Gram negative bacteria (Agladze *et al.,* 2003), so it is feasible to suggest that PelA-mediated modification of Pel (which occurs at the periplasm) is similarly important for biofilm formation in PA14. Furthermore, PelA may also be involved in processing and/or clearance of Pel from the periplasm, analogous to the function of AlgL (alginate lyase) (Jain and Ohman, 2005). It is unknown whether PelA directly interacts with Pel, how many (and indeed which) moieties are potentially acetylated or deacetylated, and whether rates of acetylation/deacetylation are ‘fine-tuned’ by internal and external parameters. However, one can imagine that such modifications to Pel structure in response to

external stimuli, such as shear, would enable increased and varied functionality of the exopolysaccharide in response to a wider range of environmental conditions. Modification of Pel post-polymerisation could further enhance the survival of bacteria in adverse growth conditions by enabling them to adapt more rapidly to their environment, by producing multiple Pel morphologies.

In contrast to biofilm development under low shear, which resulted in the formation of a confluent and generally homogenous basal biofilm, biofilms formed under high shear at 350 RPM were characterised by spatially-separated and heterogenous cell populations that grew vertically, rather than spreading laterally. Interstitial voids were observed throughout biofilm structures across the x, y and z dimensions, and were hypothesised to be water channels rather than uncolonised or unstained areas of the coupon surface, due to the complete absence of GFP-expressing cells in the channels (Figures 3.18 and 3.19). The formation of interspersed water channels throughout a biofilm can increase transport and diffusion of solutes to areas of the structure that would otherwise experience nutrient limitation of depravation (Costerton *et al.,* 1994; Stoodley *et al.,* 1994; Lewandowski and Evans, 2000; Stewart *et al.,* 2003). Under high shear conditions, Hoechst, GFP and Pel fluorescence intensities were increased, indicative of greater nutrient consumption due to increased production of ECM components and accumulation of biomass, hypothesised to be through clonal cell division as a result of the spatial separation of microcolonies due to water channel formation. Therefore, maintenance of water channels is likely an important structural and survival feature of biofilm formation by PA14 under high shear at 350 RPM.

Production of EPS is energetically expensive, thus nutrient consumption during biofilm formation under high shear is likely to be increased. This could be why mature structures formed at 350 RPM remain spatially-separated from one another, as fluid-filled channels would enable the flow of nutrients to the biofilm to support the increased synthesis of ECM components. Concomitant to this, the formation of adjacent mounds that protrude into the bulk fluid may lead to increased surface area of the biofilm, furthering enabling acquisition of dissolved nutrient substrates. Costerton *et al.,* (2007), suggested that relatively flat and unstructured biofilms (such as the homogenous basal biofilms formed under low shear at 75 RPM) develop in more nutrient-rich conditions, whilst the formation of complex structures (such as those formed under high shear at 350 RPM) occurs if nutrients are scarce to maximise surface area and local fluid flow regimes. In support of this notion, biofilms grown under low fluid velocities display greater and more effective diffusion of substrates throughout their structures, whilst biofilms formed under high fluid velocities experience slower mass transfer rates of substrates due to increased biomass, resulting in nutrient depravation in lower layers (Cadieux *et al.,* 2009).

As a result of spatial separation, first observed in the basal biofilm formed after 48 hours of growth at 350 RPM, mound-like structures are likely to be composed of progeny cells, for which expression of Pel positively influences daughter cell association with parental cells in a clonal population (Colvin *et al.,* 2011). Increased accumulation of biomass in a localised area results in vertical rather than lateral growth occurring, in order to gain access to nutrients and oxygen for continued metabolic activity (Sønderholm *et al.,* 2018). Having spatially-separated, aggregative mounds

and interspersion of eDNA and Pel fibre-like ‘tendrils’ throughout the structure ensures that three-dimensional architecture is maintained under the high shear stress, in order to minimise the risk of sloughing of the biofilm (Bryers, 1988; Choi and Morgenroth, 2003). Spatial separation, rather than formation of a confluent basal biofilm, and the formation of large, complex structures that protrude into the bulk fluid moreover maximises the biofilm’s surface area when nutrients are scarce, enabling acquisition of dissolved nutrient substrates (Costerton *et al.,* 2007). However, increased shear stress is more likely to result in erosion or sloughing of structures that protrude too far into the surrounding fluid (Salek *et al.,* 2009). During sampling of coupons after 96 hours of growth at 350 RPM, aggregative clumps were visible in the CBR bulk fluid, and also observed during CLSM image acquisition, floating in the PBS-filled sampling dish. Outflow tubing was also observed to be colonised by sticky, surface-attached populations, suggesting that 350 RPM did result in sloughing of some structures which were then capable of colonising other surfaces with the CBR system.

The most notable difference between PA14:*cdrA::gfp* biofilm formation at 75 versus 350 RPM was the absence of mushroom-shaped macrocolonies under high shear conditions. Instead, mature biofilm formation under high shear was typified by continued growth in the z dimension, resulting in irregularly structured ‘mounds’ of varying shapes and sizes (Figures 3.26 – 3.28). Continued vertical growth was likely potentiated by increased nutrient consumption of the mounds, in order enabling acquisition of dissolved nutrient substrates in the bulk fluid (Madsen *et al.,* 2007; Serra and Hengge, 2014). Although water channels transport nutrients to areas within a biofilm, fluid cannot percolate through aggregated cells enmeshed in the ECM, which

prevents access of solutes to the interior cell populations within a dense, three-dimensional structure (de Beer *et al.,* 1997; Stewart, 2003). As a result of this, fluctuations in substrate availability due to limited diffusion through mature biofilm structures formed under high shear may have occurred, resulting in competition-based, rather than cooperative growth. Competition-based biofilm development would result in a 'rich get richer' mechanism, whereby cells at the apexes of taller mounds or tower-like structures formed after 96 hours would have better access to nutrients within the bulk fluid, at the expense of smaller mounds. Results presented in this chapter are in agreement with this notion, as the mounds exhibited increased Hoechst, GFP and Pel fluorescence at their growing apexes in comparison to the lower layers of the interior structure, which exhibited very little staining by Hoechst or WGA and negligible GFP fluorescence (Figure 3.28). Furthermore, in contrast to the stratified biofilms formed under low shear at 75 RPM, mounds formed after 96 hours of growth at 350 RPM appeared to grow atop of one another, suggesting that coordination of behaviour across the biofilm was not occurring. As a result of the high shear regime, QS autoinducers and other signalling molecules would likely be washed away, or unable to effectively diffuse throughout the mound-like structures, suggesting that biofilm formation under high shear is less community-driven.

### 3.4.3. Concluding remarks

Overall, the results of this chapter suggest that different shear regimes can affect population dynamics within PA14 biofilms, as well as ECM composition and function in adaptation to hydrodynamic conditions (Figures 3.29 and 3.30). Growth in the CBR under low shear at 75 RPM resulted in the formation of biofilms that followed the

accepted ‘biofilm lifestyle’ model; characterised by archetypal *Ps. a.* mushroom-shaped macrocolonies after maturation. Pel and eDNA production was observed across all stages of biofilm development, and in a variety of morphologies, including both cell-associated and free forms. Complex and expansive fibre-like networks of Pel and eDNA-Pel complexes were observed throughout basal biofilms formed under low shear, which has not been described before. Pel trails and networks may be deposited by PA14 cells in order to facilitate TFP-mediated migration of cells to different parts of the biofilm in a spatial and temporal manner. This could illustratively initiate microcolony and subsequent architectural development, whilst also facilitating expansion of the biofilm both vertically (through macrocolony formation), and laterally by spreading to increase surface colonisation, similar in function to the Psl trails PA01 is capable of depositing on surfaces (Wang *et al.,* 2013; Zhao *et al.,* 2013).

Growth in the CBR under high shear at 350 RPM contrariwise resulted in earlier and increased production of Pel, which is hypothesised to protect attached cells from risk of shear-induced detachment and increase both cell-surface and cell-cell interactions due to enhanced ‘stickiness’. Increased aggregation of early clusters and microcolonies was observed, which suggests that shear stress can induce structural (and likely functional) changes to Pel and eDNA morphologies, as bacteria adapt to the adverse environmental condition. Fibre-like networks of Pel were not seen under high shear, nor was the formation of a confluent basal biofilm. Instead, the biofilm was fragmented, with cell subpopulations isolated from one another due to the presence of maintained interstitial water channels. As a result, PA14 biofilm development under high shear was not coordinated between spatially-separated cell populations, leading

to competitive rather than cooperative structure differentiation and maturation. After 96 hours of growth at 350 RPM, mature mound structures were often in excess of 150 μm in height; however, growth in the z dimension would eventually be limited under high shear, due to the likelihood of erosion and sloughing of apical layers of the biofilm (which are not anchored into a well-defined basal biofilm), as well as increased nutrient depravation in the lowermost layers, which may also trigger biofilm dispersion.

**Figure 3.29**

**Overview schematic for PA14:*cdrA::gfp* biofilm formation under low shear at 75 RPM**

*(figure legend overleaf)*

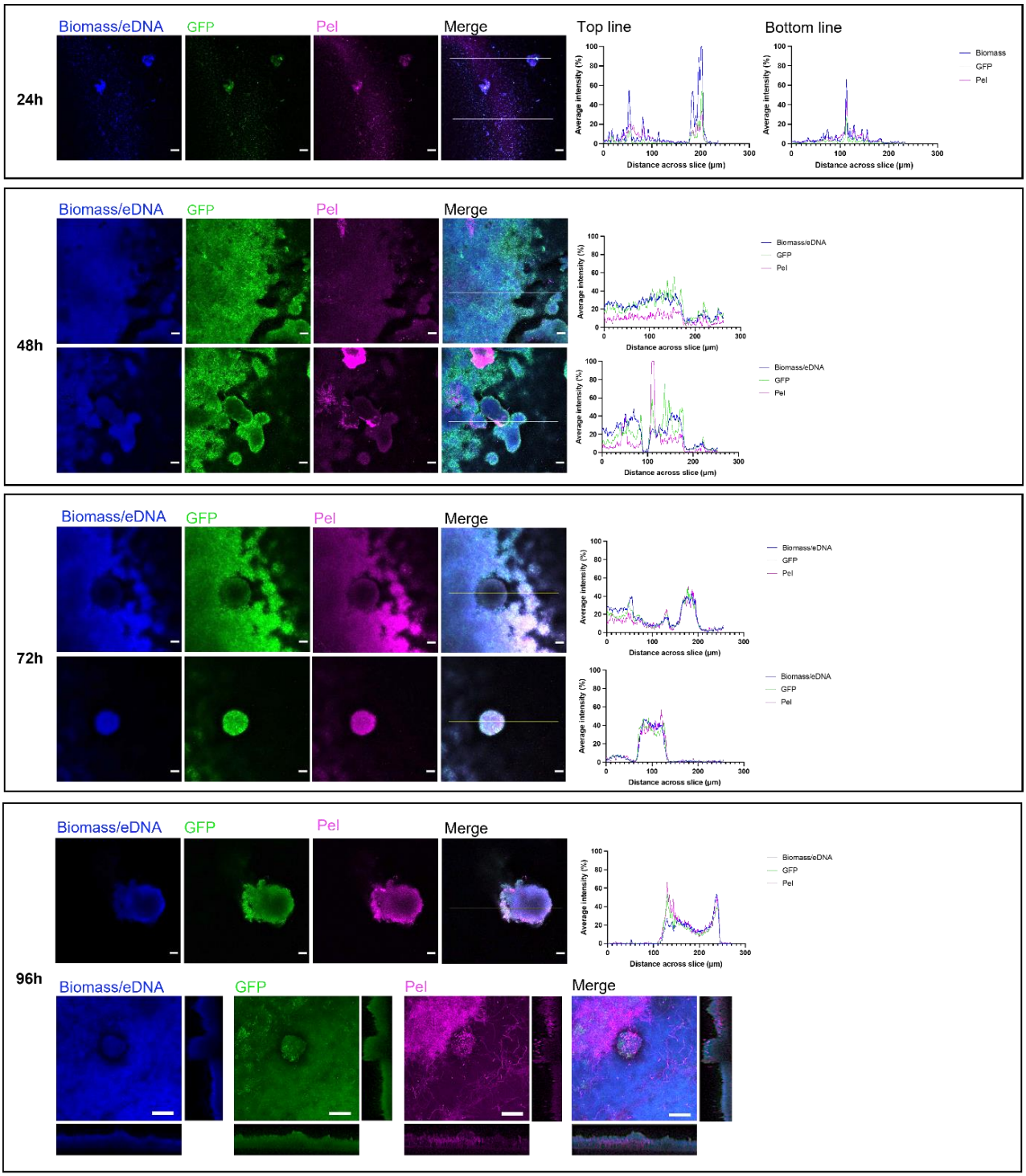

(*figure legend for* Figure 3.29)

Representative confocal images are from PA14:*cdrA::gfp* biofilms (GFP signal is green) cultivated for a total of 96 hours in the CBR under low shear (at 75 RPM) and stained with Hoechst for biomass/eDNA (blue) and the Pel-specific lectin WGA (magenta). Early biofilm formation (at 24 hours) was characterised by sparse colonisation of the coupon surface by a mixture of individual cells and small clusters, resulting in punctate and well-correlated fluorescence intensity profiles across all three channels. Surface colonisation at this stage was homogenous, with cells expressing comparable quantities of *cdrA* and likely exhibiting similar intracellular concentrations of c-di-GMP. By 48 hours, a basal biofilm had developed; displaying confluency and covering most of the coupon surface. Whilst Hoechst, GFP and Pel fluorescence intensities were generally well correlated with one another, some areas of the basal biofilms exhibited localised and increased Pel fluorescence intensities: forming either dense aggregates that encapsulated PA14:*cdrA::gfp* cell populations (thought to be indicative of areas of the biofilm that may be developing into more mature structures such as microcolonies), or fibre-like projections throughout the basal layers (which may promote further cell-surface and cell-cell interactions via the deposition of Pel trails to facilitate TFP-mediated migration of cells to different parts of the biofilm in a spatial and temporal manner). The development of mature biofilm structures (at 72 hours) was typical for *Ps. a.*, with mushroom-shaped macrocolonies observed emerging from the basal biofilm layers. Fluorescence intensity profiles for Hoechst, GFP and Pel remained well correlated throughout the basal biofilm and mushroom-shaped microcolony structures, indicating that eDNA and Pel were cell-associated, and contributing to the structural integrity of the three-dimensional macrocolonies. By the final timepoint of 96 hours, active cell migration from the basal biofilm to the ‘cap’ regions of the microcolonies was observed, with such areas characterised by increased GFP and Pel fluorescence. Pel remained well distributed in the basal biofilm layers, forming both dense aggregative ‘mats’ and wide-reaching networks of fibre-like Pel projecting throughout the basal biofilm; ensuring the maintenance of the basal biofilm and three dimensional architecture over the course of its development. Scale bar at 24, 48 and 72h = 20 µm; scale bar at 96 h = 50 µm.

**Figure 3.30**

**Overview schematic for PA14:*cdrA::gfp* biofilm formation under high shear at 350 RPM**

*(figure legend overleaf)*

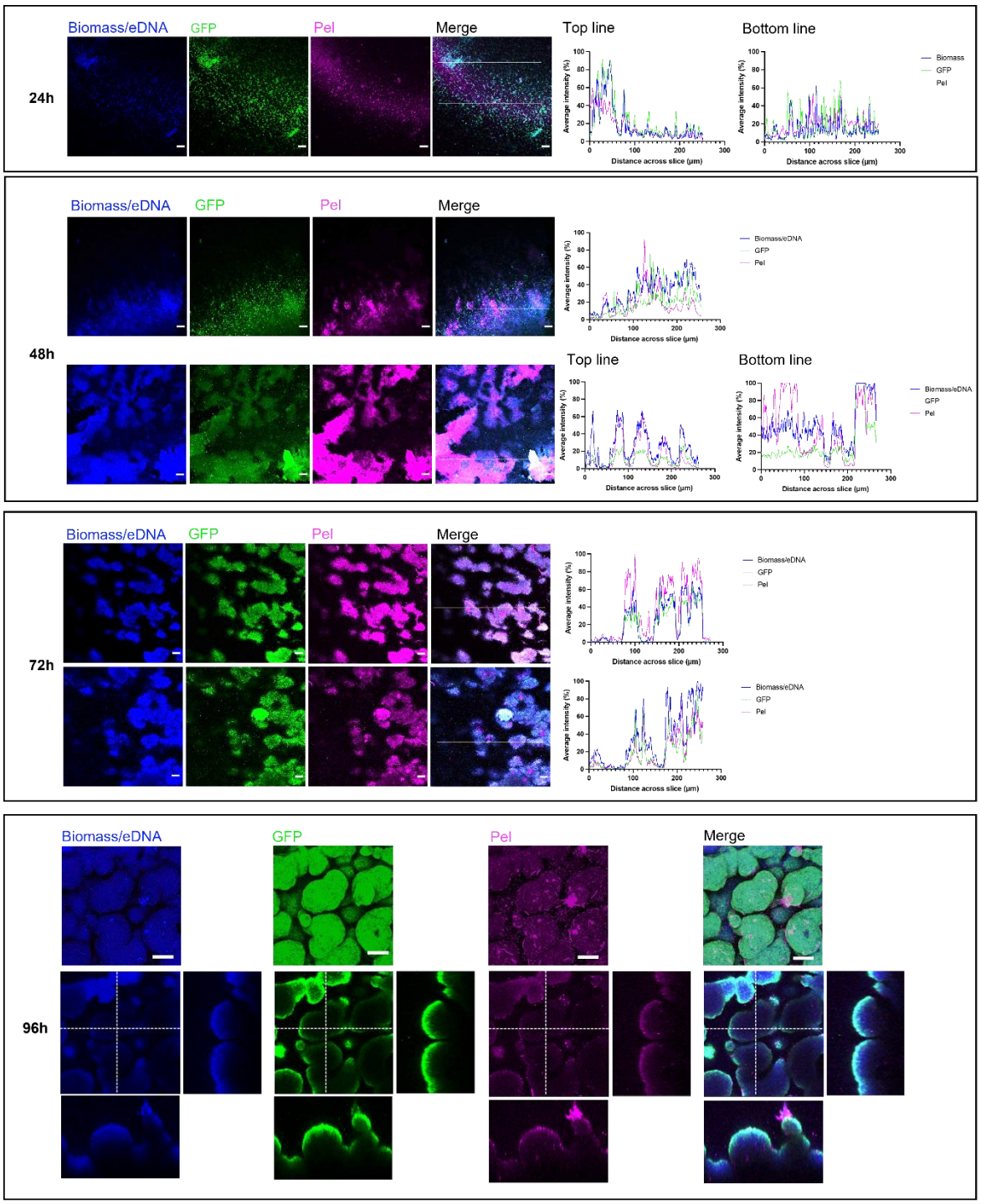

(*figure legend for* Figure 3.30)

Representative confocal images are from PA14:*cdrA::gfp* biofilms (GFP signal is green) cultivated for a total of 96 hours in the CBR under high shear (at 350 RPM) and stained with Hoechst for biomass/eDNA (blue) and the Pel-specific lectin WGA (magenta). Early biofilm formation (at 24 hours) was characterised by sparse colonisation of the surface overall, but occurred at an increased rate in comparison to growth under low shear at 75 RPM. Fluorescence intensity profiles across all three channels were punctate, and displayed increased heterogeneity, with individual cells and clusters exhibiting varying levels of *cdrA* expression (and therefore intracellular concentrations of c-di-GMP). By 48 hours, spatially-separate basal biofilms were observed across coupon surfaces; displaying increased heterogeneity with respect to Hoechst, GFP and Pel fluorescence. Most notably, Hoechst and Pel fluorescence intensities were generally greater than GFP fluorescence intensities, indicating that basal biofilms were composed of mostly eDNA and Pel, often encapsulating the PA14:*cdrA::gfp* surface-adhered cell populations in order to protect the bacteria from the high shear regime. GFP fluorescence was more heterogenous, indicating that individual cell populations were expressing differing quantities of *cdrA*. Clusters of cells aggregated together were observed, with increased GFP fluorescence (and thus greater intracellular levels of c-di-GMP in comparison to other areas of the basal biofilms). For such features, Hoechst, GFP and Pel fluorescence were well correlated with one another, indicating cells within these features were exhibiting increased production of eDNA and Pel, in order to remain attached to the basal biofilm underneath as well as each other. After 72 hours of growth, mushroom-shaped macrocolonies did not form under high shear conditions: instead, biofilm structures and features remained spatially-separated from one another, and fibre-like projections of Pel throughout basal biofilms was not observed. Instead, biofilm development at this stage was characterised by increased Pel production (as quantified by WGA), producing punctate fluorescence intensity profiles that were uncorrelated to Hoechst and GFP fluorescence. Fluorescence intensity profiles across all three channels remained heterogenous, with some features once again exhibiting increased and localised levels of *cdrA* expression in comparison to adjacent areas of the biofilm. By the final timepoint of 96 hours, three-dimensional mound-like structures were observed, and were irregular with respect to their sizes in the x and y dimensions; exhibiting increased growth vertically in the z dimension. These mounds adopted ‘tower’-like structures that appeared to grow atop of one another; lacking structural homogeneity. The structures remained spatially-separated, and exhibited increased Hoechst, GFP and Pel fluorescence intensities within the apical layers of the biofilm, likely as a result of competitive rather than cooperative growth due to increased nutrient consumption. Areas of the biofilm undergoing active growth had increased *cdrA* expression and eDNA and Pel production; ensuring the biofilm structures remained attached in response to the high shear regime by producing an ECM with increased ‘stickiness’. Scale bar at 24, 48 and 72h = 20 µm; scale bar at 96 h = 50 µm.

# Chapter 4: Biofilm formation by PA01 under low shear conditions at 75 RPM versus high shear conditions at 350 RPM

# Chapter 4: Biofilm formation by PA01 under low shear conditions at 75 RPM versus high shear conditions at 350 RPM

## 4.1. Introduction

An aim of the project was to compare initial attachment and development of *Ps. a*. PA01 and PA14 biofilms using the CDC biofilm reactor at low and high shear conditions. PA14 was studied first because, unlike strain PA01, it only generates one exopolysaccharide, Pel. Results presented in this chapter focus on PA01 biofilm formation under low and high shear conditions, and the effect different shear regimes had on Psl and Pel (which can both be synthesised by PA01).

## 4.2. Methodology

The CBR was used to investigate the effect of shear on biofilm formation by *Ps. a.* strains PA01 and PA14. Both strains were transformed with the p*cdrA::gfp* plasmid constructed by Rybtke *et al.,* (2012), which expresses GFP under control of the c-di-GMP-responsive *cdrA* promoter (Rybtke *et al.,* 2012; Nair *et al.,* 2016). Use of the *cdrA::gfp* reporter thusly enabled the visualisation of c-di-GMP throughout the biofilm structures as they developed over time, with the fluorescence intensity of GFP correlating directly to intracellular c-di-GMP levels. The CBR was operated as in chapter 3, except that PA01 p*cdrA::gfp* was used instead of PA14 p*cdrA::gfp*.

Biofilms were grown on the surfaces of PE coupons, which were removed at 24, 48, 72 and 96 hours for analysis by CLSM and flow cytometry. For CSLM, a 40X water immersion lens was used, due to the necessity of keeping biofilms hydrated during image acquisition. Hoechst 33342 was used to stain cellular and extracellular DNA, ConA (which binds to $\alpha$-mannopyranosyl and $\alpha$-glucopyranosyl residues) conjugated to tetramethylrhodamine (TRITC) was used to visualise the exopolysaccharide Psl, and WGA (which binds to *N*-acetylglucosaminyl residues) conjugated to Alexa Fluor 633 was used to visualise the exopolysaccharide Pel. The excitation and emission wavelengths used were as follows: Hoechst, 410 / 483 nm; GFP, 493 / 566 nm; ConA-TRITC, 493 / 566 nm; and WGA-Alexa633, 638 / 775 nm. When imaging PA01 biofilms, two sequential scans were completed to reduce the effect of fluorophore overlap: the first for Hoechst and ConA; the second for GFP and WGA.

Per coupon, 5 – 7 separate sample sites across the surface were imaged, with a Z-stack scan taken for each sample site, at a scanning distance of 1 – 2 $\mu$m between each Z-slice to capture the visible thickness of the biofilms. Two coupons were imaged per timepoint. Sectional and 3D rendered images of the biofilms were obtained using LasX software, whilst Fiji was used post-image acquisition to quantify fluorescent values in individual Z-stack images and generate fluorescence intensity profiles, enumerated from horizontal lines drawn across Z-stack slices of each sample site.

## 4.3. Results

### 4.3.1. Attachment of PA01 *cdrA::gfp* is dependent upon shear conditions

Initial colonisation of the coupon surfaces was sparse under both low and high shear conditions (at 75 and 350 RPM respectively) after 24 hours of growth, with a mixture of adhered single cells, cell clusters and three-dimensional features being observed. In contrast to the initial attachment of PA14 *cdrA::gfp* under low shear at 75 RPM, which was characterised by scarce surface colonisation by either individual cells and small clusters, initial attachment of PA01 *cdrA::gfp* under low shear conditions resulted in the formation of three-dimensional features that had an average height of 20 – 25 μm (Figures 4.1 and 4.2).

Hoechst, GFP, Psl and Pel fluorescence were more heterogenous with respect to individual PA01 features, which were the predominant form of surface colonisation at low shear under 75 RPM, rather than randomly attached single cells or clusters spatially isolated from one another as observed for PA14 under the same shear condition. Additionally, greater amounts of non-specific staining by ConA and WGA of the coupon surfaces occurred (Figures 4.1 and 4.2, white arrows), and as experienced with PA14, after 24 hours of growth it was challenging to expose the image such that small, faint features and large, bright features were both visible and not saturated. As a result of this, fluorescence intensity profiles were not calculated, as the analytical technique did not enable differentiation between specific staining of Psl or Pel, and non-specific staining of the uncolonised coupon surface. Instead, merge channels were used to infer colocalisation of EPS and PA01 cells with *cdrA::gfp* fluorescence.

In Figure 4.1 at Z μm, individual GFP-expressing PA01 cells can be seen adhering at the right-hand side of the feature, and appear to be organised such that they are orientated in the same direction to neighbouring cells (Figure 4.1, red arrows). Psl colocalisation with PA01:*cdrA::gfp* cells was observed from Z μm (Figure 4.1, pink arrows), and whilst fluorescence of ConA-stained Psl was punctate, it appeared cell-

**Figure 4.1**

**Psl promotes cell-surface and cell-cell interactions of PA01 *cdrA::gfp* after 24 hours under low shear at 75 RPM**

*(figure legend overleaf)*

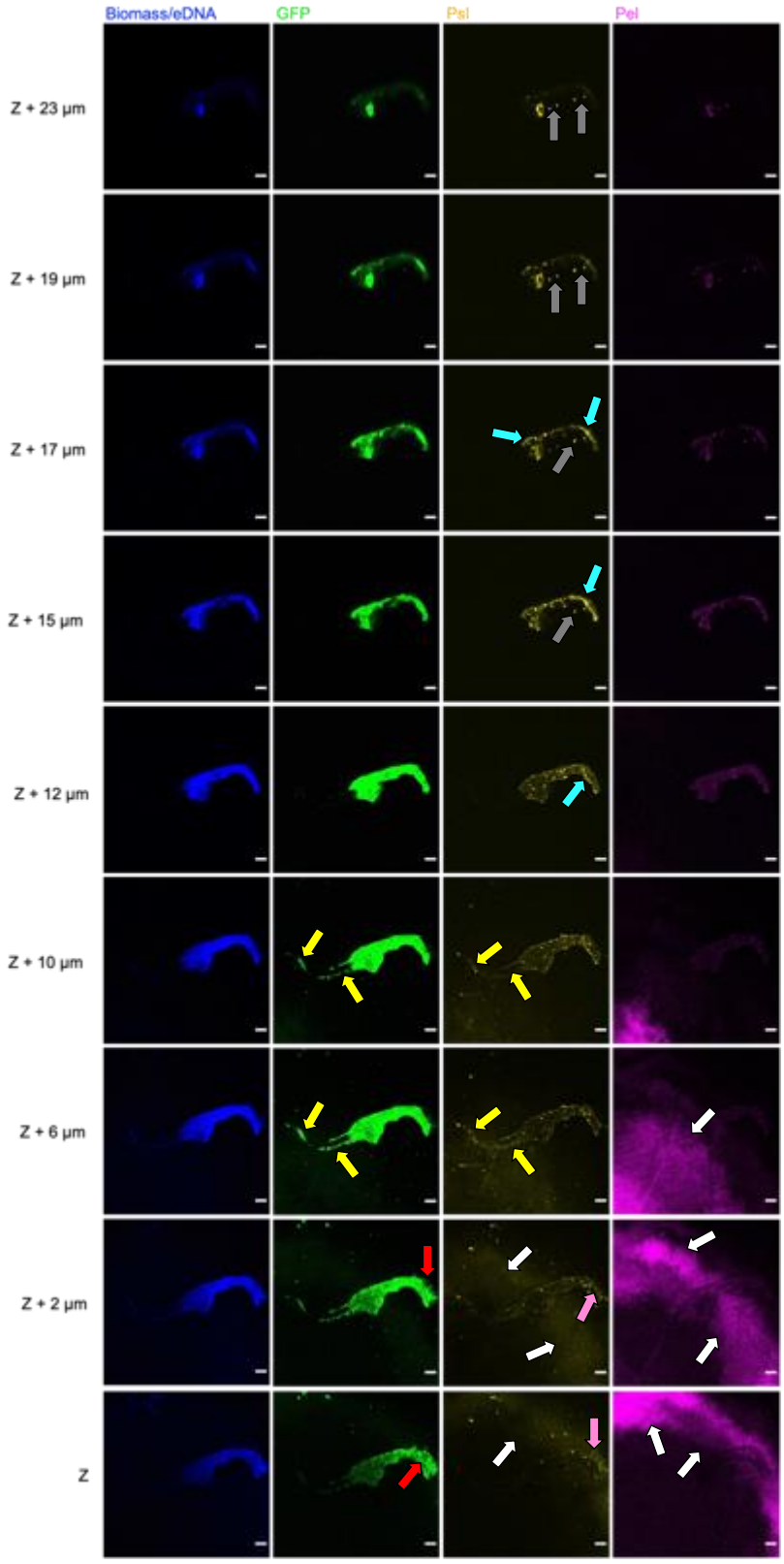

(*figure legend for* Figure 4.1)

Representative confocal images are from PA01 *cdrA::gfp* biofilms (GFP signal is green) cultivated for 24 hours in the CBR under low shear (at 75 RPM) and stained with Hoechst for biomass/eDNA (blue), the Psl-specific lectin ConA (yellow) and the Pel-specific lectin WGA (magenta). Different z heights are shown for the same sample area, with Z defined as the bottom layer closest to the coupon surface. Scale bar = 20 μm. White arrows show areas of non-specific staining of the coupon surface by ConA and Pel. Red arrows show attachment of individual PA01 cells to the periphery of the existing feature, whilst pink arrows show punctate areas of Psl co-localised with the attaching cells. Yellow arrows show the formation of Psl fibre-like trails on the coupon surface, to which GFP-expressing populations of cell clusters are associated. Cyan arrows show interior Psl fibres within the feature itself. Grey arrows show small non-cell associated, free Psl on the coupon surface, in-between the feature peripheries.

**Figure 4.2**

**Observation of microcolony-like features formed by PA01 *cdrA::gfp* after 24 hours under low shear at 75 RPM**

*(figure legend overleaf)*

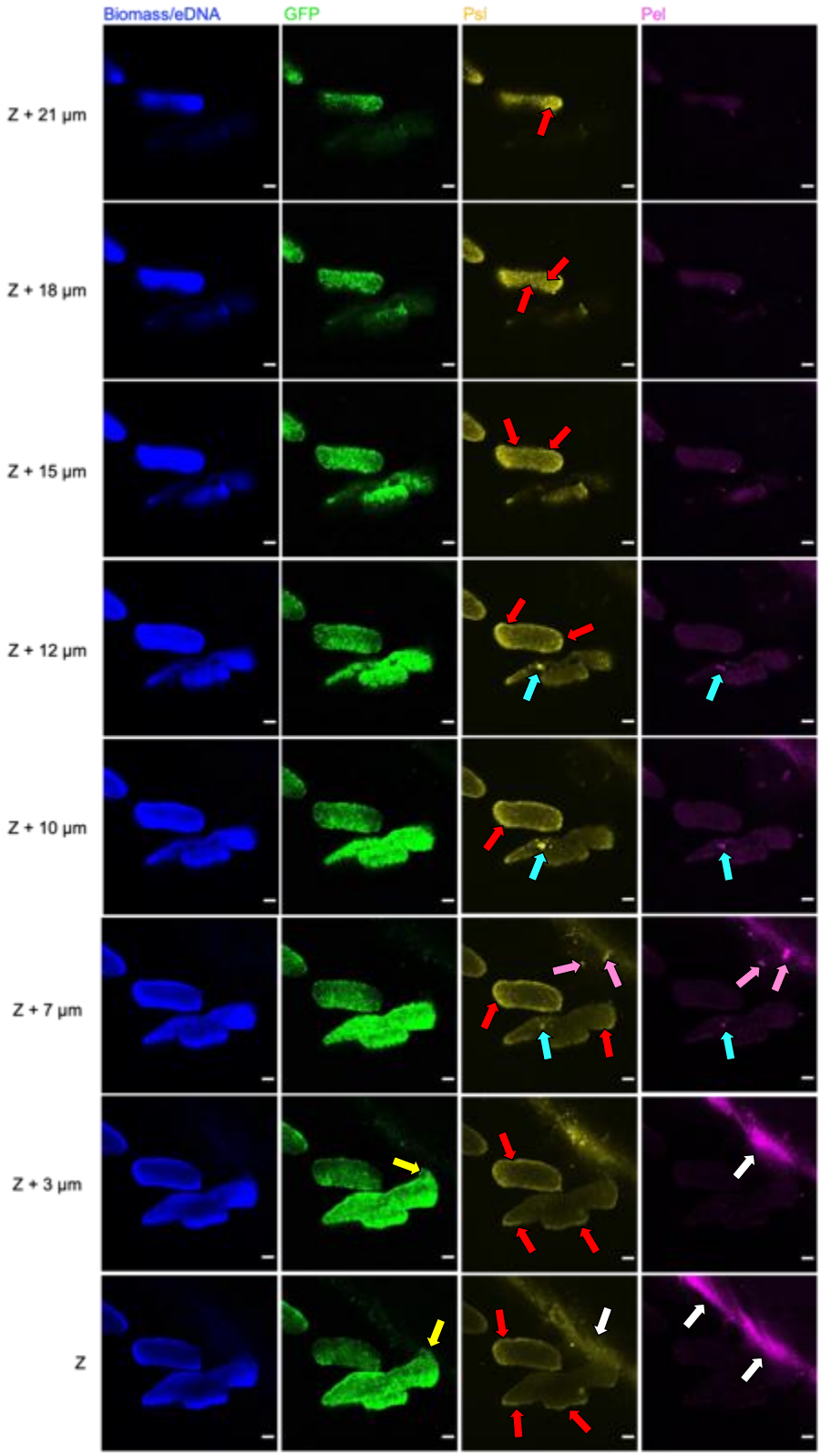

(*figure legend for* Figure 4.2)

Representative confocal images are from PA01 *cdrA::gfp* biofilms (GFP signal is green) cultivated for 24 hours in the CBR under low shear (at 75 RPM) and stained with Hoechst for biomass/eDNA (blue), the Psl-specific lectin ConA (yellow) and the Pel-specific lectin WGA (magenta). Different z heights are shown for the same sample area, with Z defined as the bottom layer closest to the coupon surface. Scale bar = 20 μm. White arrows show areas of non-specific staining of the coupon surface by ConA and Pel. Red arrows show accumulation of Psl at the peripheral edges of features, and within their interiors with increased height in the z dimension. Yellow arrows show attachment of individual PA01 cells to the periphery of an existing feature. Cyan arrows show aggregates of Psl and Pel at the boundary edges of feature cell populations, whilst pink arrows show aggregates of Psl and Pel attached to the coupon surface.

associated; interspersed between subpopulations within the feature. At heights of Z+6 μm and Z+10 μm, chains composed of individual PA01:*cdrA::gfp* cells were seen once again; orientated in the same direction as one another (and aligned parallel to the coupon surface rather than via cell poles), with Psl forming fibre-like trails and small aggregates associated with the cells (Figure 4.1, yellow arrows). Psl therefore appears to be important for facilitation of initial cell-surface interactions, as well as cell-cell interactions, which is in agreement with the work of Ma *et al.,* (2009), and their observation of Psl association with PA01 cells during early stages of biofilm development. Hoechst fluorescence was observed to be well correlated with *cdrA::gfp* fluorescence throughout the feature, which could suggest that eDNA is additionally important for cell-surface interactions and maintenance of coherent cell alignments, as previously reported by Allensen-Holm *et al.,* (2006), and Gloag *et al.,* (2013).

From a height of Z+12 μm upwards, fibre-like trails and punctate concentrations of Psl are clearly visible within the feature, providing a structural scaffold upon which cell-cell interactions could be facilitated (Figure 4.1, cyan arrows). This further suggests that Psl production is requisite for cell-cell interactions and cell-cell aggregation in developing PA01 biofilms. Degradation of Psl in the presence of cellulase was shown by Ma *et al.,* (2009), to result in loss of the Psl matrix in 'young' PA01 biofilms and consequently abolishment of the biofilm phenotype, which indicates that Psl is crucial for promoting initial cell-surface and cell-cell interactions that enable subsequent development and maturation of the ECM and biofilm structure.

Free aggregates of Psl that did not appear to be cell-associated were observed from a height of Z+15 μm upwards (Figure 4.1, grey arrows), which may facilitate recruitment of motile cells to the existing feature, and promote their subsequent surface attachment (Ma *et al.,* 2009). Irie *et al.,* (2012), reported that self-produced Psl can act as a signal that stimulates the activity of the DGCs SadC and SiaD, increasing intracellular c-di-GMP levels, thus free, non-cell associated Psl may also induce c-di-GMP synthesis of recruited planktonic cells, stimulating sessility and exopolysaccharide production. EPS are known to influence the local environment with respect to osmolarity, viscosity and ionic properties (Sutherland, 2001; Flemming and Wingender, 2010), and so free Psl may condition areas of the coupon surface to enhance cell attachment at existing, rather than uncolonised, sites.

In Figure 4.2, cell-association of Psl was observed and maintained throughout the height of the feature (Figure 4.2). Increased Psl fluorescence was initially observed at the peripheral edges of the microcolony features; with increasing height of the feature, Psl fluorescence in the interior and at the feature's poles became more homogenous, yet remained punctate (Figure 4.2, red arrows). Similarly to Figure 4.1, individual PA01 cells were observed to associate with the periphery of a feature at heights of Z and Z+3 μm (Figure 4.2, yellow arrows), although it is difficult to discern whether their recruitment involves Psl-mediated cell-cell interactions, due to non-specific staining of the coupon surface in this area.

Hoechst fluorescence was the most pronounced across all four channels in Figure 4.2, with staining of features largely diffuse. Whilst Hoechst and GFP fluorescence were

well correlated to one another throughout the height of the features, it was difficult to discern whether the increased intensities of Hoechst fluorescence observed were indicative of biomass accumulation in the microcolonies, the presence of eDNA within the feature matrix, or as a result of overexposure during image acquisition. In contrast, Pel fluorescence was the lowest across all four channels, which is in agreement with the consensus of the literature that PA01 utilises Psl, rather than Pel, as its primary exopolysaccharide (Ghafoor *et al.,* 2011; Yang *et al.,* 2001; Colvin *et al.,* 2012). Aggregates of exopolysaccharide were observed at boundary edges of features (Figure 4.2, cyan arrows) as well as across the coupon surface, in areas that displayed punctate but low GFP fluorescence of individually attached cells (Figure 4.2, pink arrows). Interestingly, such aggregates were stained by both ConA and WGA, and thus appeared to be composed of both Psl and Pel, which suggests that production of both exopolysaccharides can occur during early PA01 biofilm development, to maintain crucial cell-cell interactions within developing features. Yang *et al.,* (2011), have previously demonstrated that PA01 utilises production of Pel alongside Psl to facilitate compactness of biofilms as well as cell-cell association under certain conditions: therefore, responses to spatial and/or temporal conditions within the observed feature may have stimulated local production of both Psl and Pel.

Modelling by Lee *et al.,* (2020), determined that PA01 and PA14 use different strategies to initially colonise surfaces. EPS production was identified as the dominant mechanism of maintained surface adherence in PA01, whilst PA14 relied upon progressive upregulation and subsequent suppression of appendages such as flagella and TFP during initial cell-surface attachment. Early production of exopolysaccharides

by PA01 was suggested to enable cell lineages to commit to a surface at a faster rate and facilitate cell-cell interactions between neighbouring cell populations, leading to increased early biofilm formation by PA01 in comparison to PA14 (Lee *et al.,* 2020), as observed after 24 hours of growth in the CBR at 75 RPM (Figures 4.1 and 4.2 compared to Figures 3.1 and 3.2, Chapter 3).

In contrast to the observations of PA01 cells grown under low shear, high shear conditions at 350 RPM resulted in the formation of smaller features, which were more variable with respect to their size (in x, y and z dimensions), shape and relative proportions of Hoechst, GFP, Psl and Pel fluorescence. Whilst some of the features were of a comparable size to those formed under low shear, fluorescence intensities within the features differed based upon spatial location (Figures 4.3 – 4.5).

Greater adhesion of individual cells and cell clusters to the coupon surface was observed under high shear conditions (Figure 4.3, yellow arrows), which suggests that higher rates of shear resulted in increased accumulation of surface-associated bacteria, in agreement with the works of several research groups (Thomas *et al.,* 2002; Horn *et al.,* 2003) and results presented in Chapter 3. Aggregates of Psl and Pel were observed at sites of cell clustering (Figure 4.3, cyan arrows), with dense areas of associated PA01 cells localised in particular to Psl aggregates (light blue arrows). Co-localisation of Hoechst staining could suggest that the aggregate is composed of eDNA-Psl complexes, which have previously been shown result in the formation of a thick, ‘rope-like’ and radial web of eDNA-Psl fibres at the centre of pellicle biofilms to provide structural support to cell aggregates (Wang *et al.,* 2015).

**Figure 4.3.**
**Heterogenous development of PA01 *cdrA::gfp* features formed after 24 hours under high shear at 350 RPM**

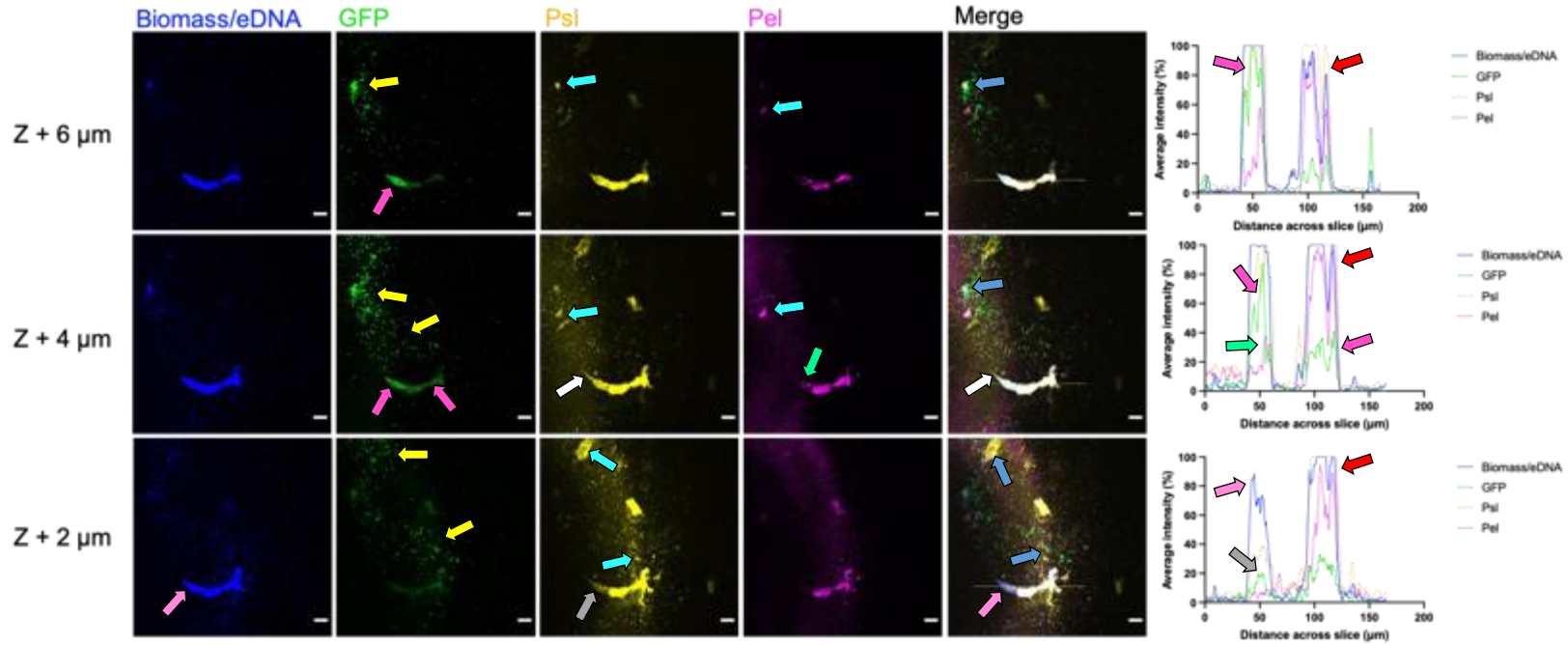


Representative confocal images are from PA01 *cdrA::gfp* biofilms (GFP signal is green) cultivated for 24 hours in the CBR under high shear (at 350 RPM) and stained with Hoechst for biomass/eDNA (blue), the Psl-specific lectin ConA (yellow) and the Pel-specific lectin WGA (magenta). Different z heights are shown for the same sample area, with Z defined as the bottom layer closest to the coupon surface. Scale bar = 20 µm. Yellow arrows show areas of clustering of GFP-expressing cells. Cyan arrows show punctate areas of Psl and Pel associated with the clustered cell populations. Light blue arrows shows cell localisation around Psl aggregates. Red arrows show well-correlated fluorescence intensities for Hoechst, Psl and Pel at the right-hand feature periphery. Pink arrows show spatially-increased Hoechst fluorescence at the left-hand side peripheral edge of the feature, whilst grey arrows show comparatively lower fluorescence intensities for GFP and Psl. Green arrows show an area of increased and punctate Pel. White arrows show a fibre-like projection of Psl extending from the feature, not-cell associated or co-localised with Hoechst and Pel. Cerise arrows show increased GFP fluorescence intensities at the left-hand peripheral edge, in comparison to the distal right-hand periphery.

The feature shown in Figure 4.3 is elongated in the x dimension, measuring 80 μm in width and only 20 μm in length, and exhibited heterogeneity with respect to fluorescence intensities across all four channels. Hoechst, Psl and Pel fluorescence intensities were well-correlated at the right-hand peripheral edge with increasing height in the z dimension (Figure 4.3, red arrows), which could be suggestive of a developing ECM composed of eDNA, Psl and Pel. GFP fluorescence intensities remained consistent throughout the feature height at this periphery, but lower than the fluorescence intensities of Hoechst, Psl and Pel; indicative that this area of the feature was predominantly ECM that was likely encapsulating the GFP-expressing cell population to protect the cells from the risk of sloughing or detachment induced by the high shear regime.

The left-hand side peripheral edge exhibited heterogeneity with increasing height in the z dimension. At a height of Z+2 μm, Hoechst fluorescence was greatest and staining across the structure by Hoechst diffuse (Figure 4.3, pink arrows). By contrast, Pel fluorescence intensities were negligible, whilst GFP and Psl fluorescence was correlated to Hoechst fluorescence, albeit at much lower fluorescence intensities respectively (Figure 4.3, grey arrows). Hoechst fluorescence was generally homogenous and staining diffuse; exhibiting increased fluorescence intensities across the entirety of the feature in comparison to the other three channels, which could suggest the presence of eDNA. *Ps. a.* is known to produce large quantities of eDNA (Murakawa *et al.,* 1973a; 1973b; Hara and Ueda, 1981; Muto and Goto, 1986; Nemoto *et al.,* 2003), to facilitate and maintain cell-cell interactions in ‘young’ biofilms, by holding the cells together *in situ* (Whitchurch *et al.,* 2002; Allesen-Holm *et al.,* 2006).

At a height of Z+4 μm, fluorescence intensities of GFP and Psl greatly increased, and were well-correlated with Hoechst fluorescence intensities across the left-hand periphery. Increased Pel fluorescence intensities at this peripheral edge were observed at a height of Z+6 μm, although staining of Pel was punctate throughout the feature interior (Figure 4.3, green arrows). This could suggest that the cell subpopulations that comprise the left-hand side of the feature are less established than those at the right-hand side of the feature. A thin, fibre-like projection of Psl can be seen protruding from the left-hand periphery at a height of Z+4 μm (white arrows), which may be facilitating the movement of spatially-close individual cells to the developing edge of the feature, as previously described by Zhao *et al.,* (2013). Increased GFP fluorescence in this part of the feature in comparison to the right-hand peripheral edge (Figure 4.3, cerise arrows) could therefore be indicative of cells that have become more recently sessile and are more metabolically active, increasing Psl production to remain both cell-surface and cell-cell associated.

Aggregative features were frequently observed across coupon surfaces during the same and independent CBR runs, suggesting that growth under high shear stress induces the formation of tightly-packed and cohesive structures, characterised by increased *cdrA* expression and GFP fluorescence, indicative of increased intracellular levels of c-di-GMP (Figure 4.4, yellow arrows). At a height of Z+3 μm, GFP fluorescence intensities were maximal, resulting in the plateauing of the line profile. Hoechst, Psl and Pel fluorescence were well-correlated, although the feature exhibited minimal staining of Pel by WGA, which appeared co-localised to chains of Psl or the interior of Psl aggregates (Figure 4.4, red arrows). As seen in Figure 4.3, individual GFP-expressing cells were observed to associate with the established feature,

**Figure 4.4**
**Recruitment of individual PA01 *cdrA::gfp* cells and small cell chains by Psl aggregates**

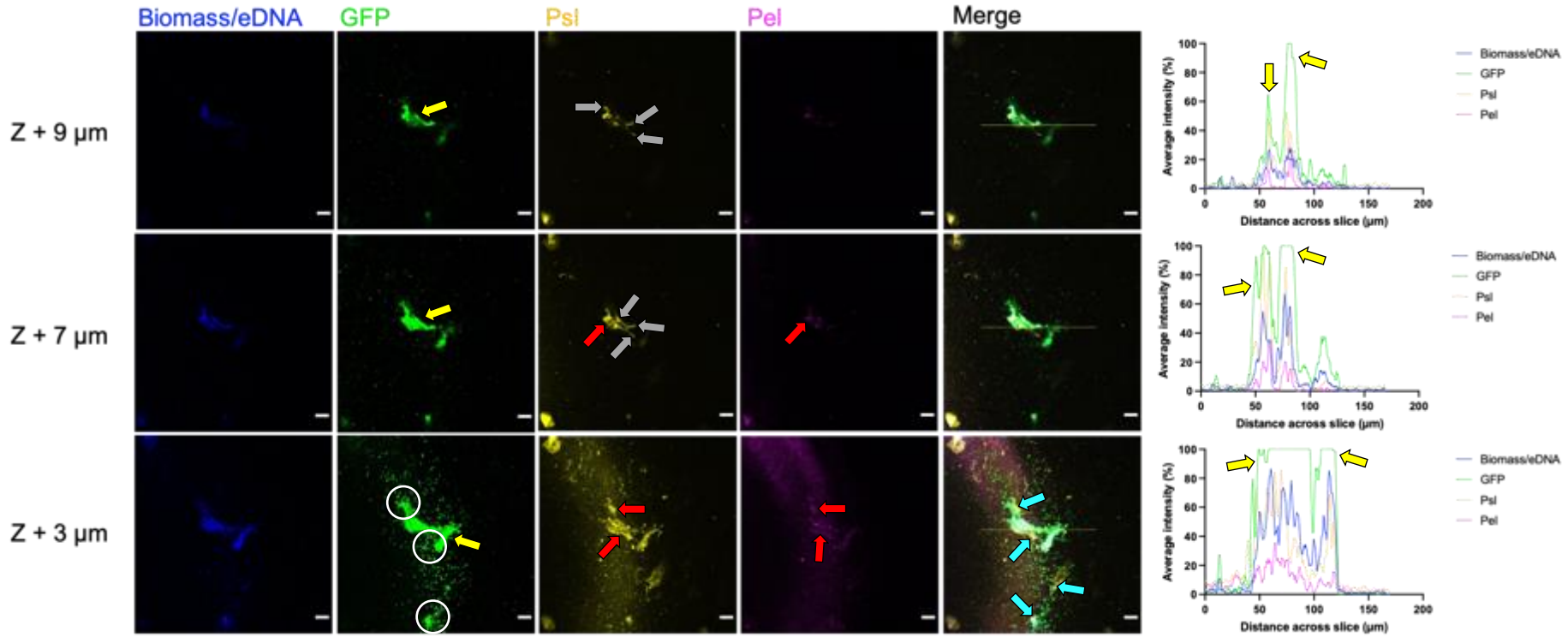


Representative confocal images are from PA01 *cdrA::gfp* biofilms (GFP signal is green) cultivated for 24 hours in the CBR under high shear (at 350 RPM) and stained with Hoechst for biomass/eDNA (blue), the Psl-specific lectin ConA (yellow) and the Pel-specific lectin WGA (magenta). Different z heights are shown for the same sample area, with Z defined as the bottom layer closest to the coupon surface. Scale bar = 20 µm. Yellow arrows show a dense cellular aggregate exhibiting increased GFP fluorescence intensities in comparison to the other three channels. Red arrows show minimal staining of Pel, which was found co-localised with areas of Psl accumulation. White circles show individual GFP-expressing cells associated with boundary edges of the feature and in a cell cluster, in similar orientations to one another. Cyan arrows show areas of free Psl surrounded by clustering cell populations. Grey arrows show interspersed and punctate regions of Psl in-between subpopulations of cells and within the interior of the feature.

seemingly organised in similar orientations to one another at the feature's edge (Z+3 μm, white circles). Concentrated areas of free Psl were seen at sites of individual cell association (Figure 4.4, cyan arrows), forming a fibre-like matrix structure enmeshing bacteria to the coupon surface, and promoting cell-cell interactions with the feature (Ma *et al.,* 2009).

Fibre-like projections of Psl were seen at heights of Z+7 and Z+9 μm, cell-associated and interspersed throughout the feature interior (Figure 4.4, grey arrows). Production of Psl is known to result in stiffer and more elastic matrices, which can 'spring' back to shape if deformed by mechanical shear (Chew *et al.,* 2014; Gloag *et al.,* 2018). Thus, increased, but localised concentrations of Psl within aggregative features may strengthen the ECM; maintaining its structural integrity through enhanced cell-cell interactions, and decreasing susceptibility of loss of biomass due to shear-induced erosion (Ma *et al.,* 2006; Ma *et al.,* 2012).

Features of heights > 10 μm in the z dimension were also observed after 24 hours of growth under high shear at 350 RPM (Figure 4.5). GFP fluorescence intensities were punctate throughout the height of the feature, and did not appear to correlate to Hoechst, Psl and Pel fluorescence intensities (Figure 4.5, yellow arrows). With increasing height of the feature, GFP and Psl fluorescence intensities were well-correlated but remained punctate, suggesting that cell-associated Psl is important for maintenance of developing structures and cell-cell interactions (Figure 4.5, light blue arrows). Expression of *cdrA* was therefore heterogenous, with subpopulations of cells within the feature exhibiting increased GFP fluorescence compared to spatially-

**Figure 4.5**

**Early feature development by PA01 *cdrA::gfp* after 24 hours under high shear at 350 RPM**

(*figure legend overleaf*)

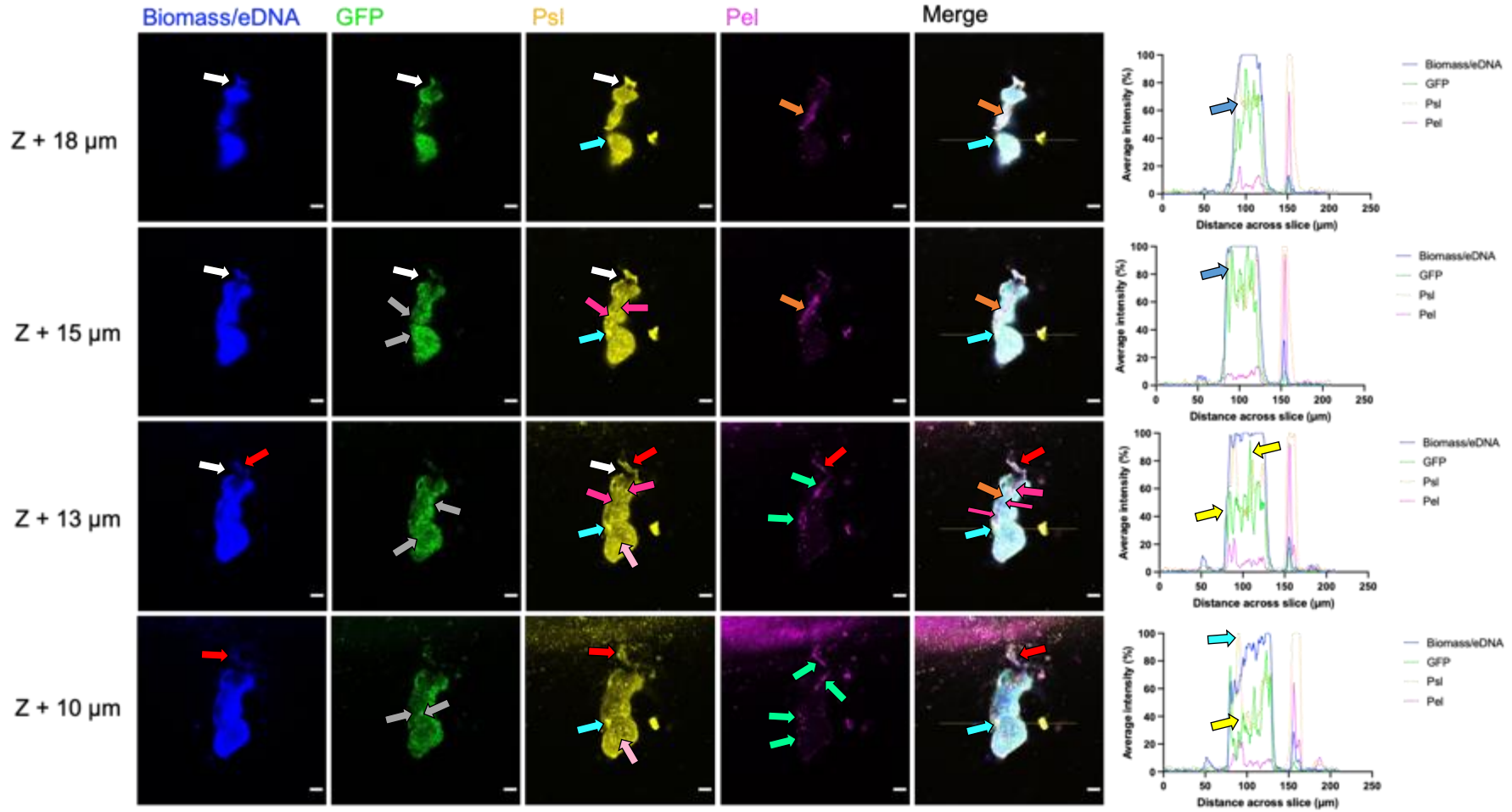

(*figure legend for* Figure 4.5)

Representative confocal images are from PA01 *cdrA::gfp* biofilms (GFP signal is green) cultivated for 24 hours in the CBR under high shear (at 350 RPM) and stained with Hoechst for biomass/eDNA (blue), the Psl-specific lectin ConA (yellow) and the Pel-specific lectin WGA (magenta). Different z heights are shown for the same sample area, with Z defined as the bottom layer closest to the coupon surface. Scale bar = 20 μm. Yellow arrows show heterogenous and punctate GFP fluorescence intensities throughout the feature, whilst light blue arrows show increased Psl fluorescence intensities with increasing height in the z dimension, which is well-correlated to GFP fluorescence intensity. Grey arrows show subpopulations of cells with increased GFP fluorescence in comparison to adjacent populations. Cyan arrows show a dense aggregate of Psl which is maintained vertically throughout the feature. Pink arrows show radial 'patterning' of Psl within the feature interior. Green arrows show punctate regions of Pel, in small aggregative structures spatially-separated from one another, or as complexed aggregates forming chains. Red arrows show co-localisation of Hoechst and Psl, forming fibre-like protrusions. White arrows show connection of the fibre-like protrusions to the rest of the feature. Orange arrows show a central area of Pel within the interior of the feature, akin to a 'backbone' or structural scaffold. Cerise arrows show small aggregates of Psl associating with parts of the Pel 'backbone'.

adjacent cell populations (Figure 4.5, grey arrows). At a height of Z+10 μm, a dense aggregate of Psl can be seen within the feature interior, maintained to a height of Z+15 μm (Figure 4.5, cyan arrows). This dense aggregate of Psl could be a nucleation centre, from which Psl chains and fibres can be synthesised and disseminated throughout the feature, as suggested by the radial 'pattern' of punctate Psl in the feature interior (Figure 4.5, pink arrows).

Although Pel fluorescence intensities were lowest, production of Pel exhibited spatial organisation throughout the feature. At a height of Z+10 μm, punctate regions of Pel can be seen localised to different areas of the feature periphery, either as individual aggregates or fibres composed of aggregates (Figure 4.5, green arrows). Co-localisation of punctate Psl aggregates and Hoechst fibres were also observed at heights of Z+10 and Z+13 μm (red arrows), suggesting that Psl, Pel and eDNA are capable of intertwining or complexing with one another; possibly to increase the 'stickiness' of the protruding structure, facilitating adherence to the coupon surface, as well as potentially enhancing recruitment or migration of individual cells to the feature periphery. By a height of Z+18 μm, GFP-expressing cells can be seen enmeshed in an eDNA-Psl dominated matrix, now connected to the rest of the feature (Figure 4.5, white arrows).

Of interest was the fact that the interior of the feature appeared to have a 'backbone' of Pel running down its length in the y dimension (Figure 4.5, orange arrows), with small aggregates of Psl observed to associate with the Pel 'backbone' structure (cerise arrows). Yang *et al.,* (2011), has previously demonstrated that both Psl and Pel are

important for facilitating interactions between subpopulations of cells during PA01 biofilm formation, thus under high shear conditions at 350 RPM, production of a Pel 'backbone' may maintain the structural integrity of the elongated feature. Colvin *et al.,* (2011), demonstrated that Pel is fundamental for the initiation and maintenance of cell-cell interactions within PA14 aggregates, and that expression of Pel positively influences daughter cell association with parental cells in a clonal population.

It is therefore feasible to suggest that PA01 may similarly employ Pel for retention of daughter cells under high shear conditions, with the arrangement of a biofilm's internal structure thought to be governed by the velocity of the flow experienced during growth (Beyenal and Lewandowski, 2002). Utilisation of the Pel 'backbone' by Psl to deposit aggregative trails (akin to breadcrumbs), may enable internal transit of cells to leading edges of larger features, rather than external migration of cells, which would be at risk of detachment and wash out under the higher shear regime. In agreement with this is the observation that the feature did not expand laterally in the x and y dimensions, but instead grew vertically in the z dimension, which could suggest it is comprised of clonal cell populations, maintained *in situ* by the ECM. Alternatively, as self-produced Psl can act as a signal to stimulate DGC activity and increase intracellular c-di-GMP levels (Irie *et al.,* 2012), interior aggregates of Psl may stimulate development of the biofilm above the Pel 'backbone', leading to spatially-specific accumulation of biomass and ECM components, facilitated by enhanced cell-cell interactions atop a robustly surface-adhered part of the structure.

4.3.2. Microcolony formation by PA01 does not occur under high shear conditions

After 48 hours of growth, biofilm formation under low shear at 75 RPM was typified by the development of a basal biofilm that covered most of the coupon surface (similarly to those formed by PA14 under low shear), with an average height for this layer of 15 – 20 μm. The formation of microcolonies was also frequently observed across different sampling sites, exhibiting variation in their shape and overall heights in the z dimension (Figures 4.6 and 4.7). Due to the height of the microcolonies, Figures 4.6 and 4.7 are split: 4.6A and 4.7A show the basal layers of the biofilm, whilst 4.6B and 4.7B show the upper layers of the microcolony structures.

Figure 4.6A shows a well-developed basal biofilm, within which lies a cavity directly underneath the emerging microcolony structure. From the bottom of the basal layer Z to a height of Z+7 μm, a dense aggregate of co-localised Psl and Pel was observed in the interior of the cavity, exhibiting increased fluorescence intensities in comparison to Psl and Pel fluorescence intensities in the basal biofilm (Figure 4.6A, red arrows). In particular, Pel was seen forming fibre-like structures around the cavity periphery (Figure 4.6A, yellow arrows), as well as in a stalk-like protrusion between the basal biofilm and the cavity (Figure 4.6A, grey arrows). Pel fluorescence was uncorrelated to Hoechst, GFP and Psl fluorescence, suggesting that it was free rather than cell-associated Pel, spatially-localised to part of the boundary between the basal biofilm and the cavity periphery.

Jennings *et al.,* (2015), have previously demonstrated that Pel can colocalise with eDNA in the stalks of microcolony structures, although the structural cavity in Figure

4.6A exhibited negligible Hoechst and GFP fluorescence intensities, in contrast to the work of Jennings *et al.,* (2015). The cavity of microcolony structures is likely to exhibit physiological differences to the basal biofilm, thus lack of Hoechst staining in the cavity may either indicate the absence of eDNA within the cavity interior, or occlusion of structural staining by Hoechst, due to the enhanced staining of the cavity aggregate by ConA and WGA. Jennings *et al.,* (2015), suggested that eDNA and Pel are capable of crosslinking via iconic bond formation in microcolony stalks, in a pH-dependent manner. Therefore, it is possible that the pH in the cavity interior shown in Figure 4.6A was such that Pel was not catatonically charged, and thus may have interacted with Psl via covalent interactions to form a heterogenous exopolysaccharide-based aggregate.

**Figure 4.6A** (*figure legend overleaf)*

**Emergence of a mushroom-shaped microcolony from a PA01 basal biofilm after 48 hours under low shear 75 RPM**

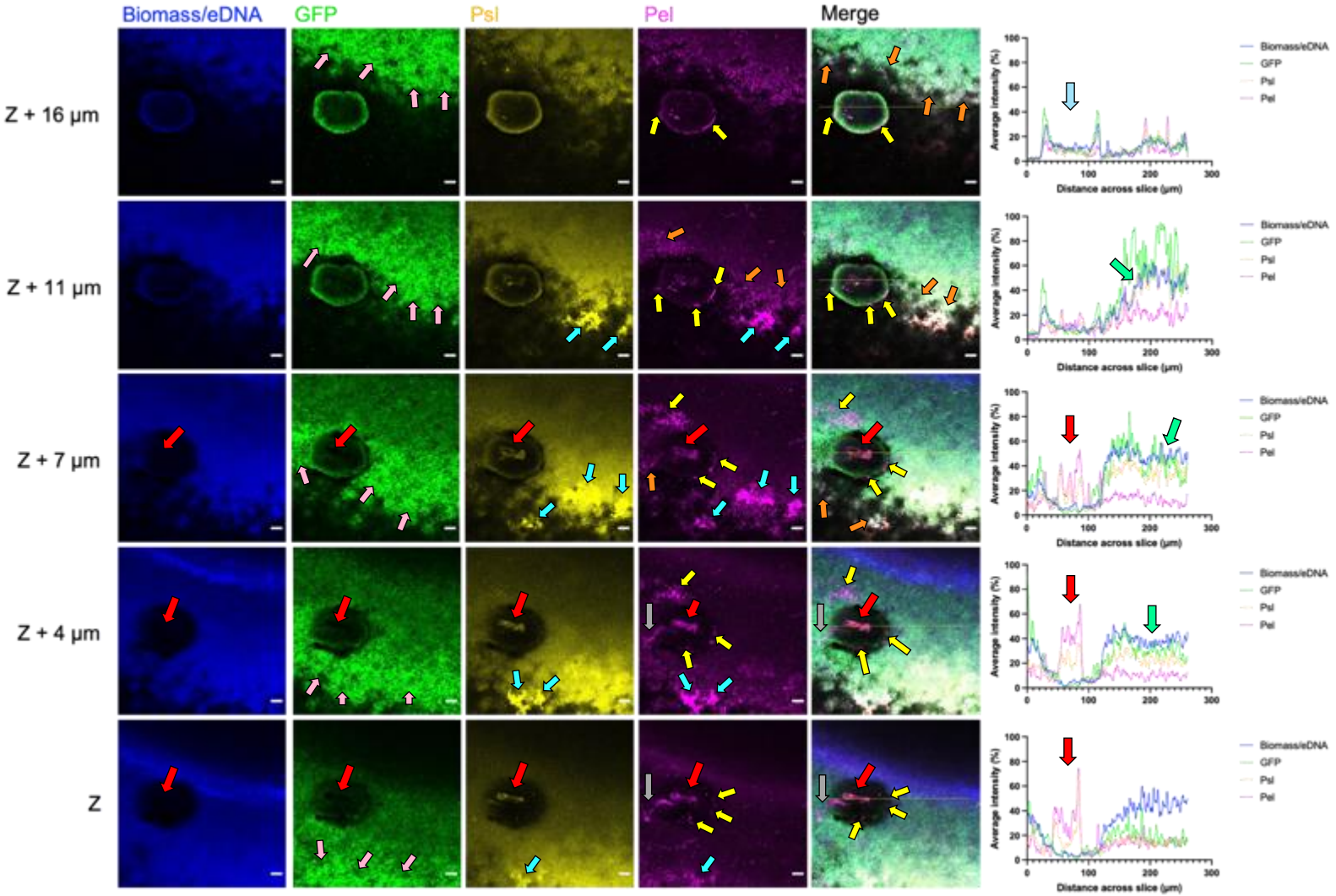

(*figure legend for* Figure 4.6A)

Representative confocal images are from PA01 *cdrA::gfp* biofilms (GFP signal is green) cultivated for 48 hours in the CBR under low shear (at 75 RPM) and stained with Hoechst for biomass/eDNA (blue), the Psl-specific lectin ConA (yellow) and the Pel-specific lectin WGA (magenta). Different z heights are shown for the same sample area, with Z defined as the bottom layer closest to the coupon surface. Scale bar = 20 μm. Red arrows show a cavity structure directly beneath the emerging microcolony, exhibiting increased Psl and Pel fluorescence intensities. Yellow arrows show fibre-like Pel production localised to the periphery of the cavity boundary, whilst grey arrows show a 'stalk'-like protrusion of Pel connecting the cavity interior to the basal biofilm. Cyan arrows show dense Psl and Pel aggregates. Pink arrows show the leading edge of the basal biofilm, characterised by increased GFP fluorescence as the leading edge retreated out of the field of view. Green arrows show well-correlated Hoechst and Psl fluorescence intensities across the basal biofilm. The light blue arrows shows a concave fluorescence intensity profile, typical of emerging microcolony structures.

**Figure 4.6B** *(figure legend overleaf)*

**Emergence of a protruding microcolony apex after 72 hours under low shear at 75 RPM**

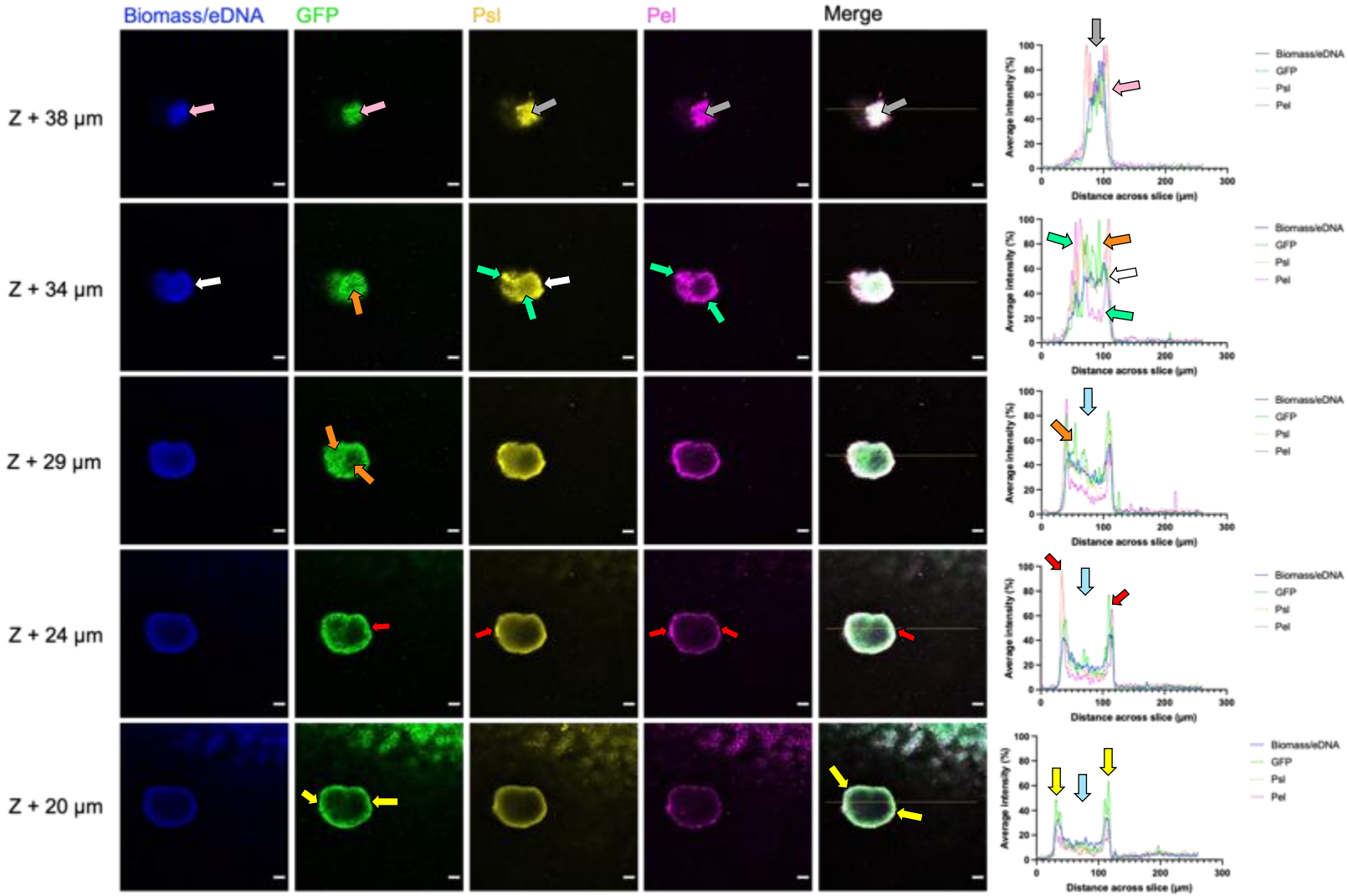

(*figure legend for* Figure 4.6B)

Representative confocal images are from PA01 *cdrA::gfp* biofilms (GFP signal is green) cultivated for 48 hours in the CBR under low shear (at 75 RPM) and stained with Hoechst for biomass/eDNA (blue), the Psl-specific lectin ConA (yellow) and the Pel-specific lectin WGA (magenta). Different z heights are shown for the same sample area, with Z defined as the bottom layer closest to the coupon surface. Scale bar = 20 μm. Light blue arrows show concave fluorescence intensity profiles for the emerging microcolony structure, indicative of enhanced peripheral rather than interior staining and GFP expression. Red arrows show heterogenous fluorescence intensities at the microcolony periphery, whilst yellow arrows show a more heterogenous fluorescence intensity profile across all four channels. Orange arrows show increased and punctate GFP fluorescence in localised areas of the microcolony interior. Green arrows show punctate and increased and localised fluorescence intensities for Psl and Pel within apical layers. White arrows show homogenous Hoechst and Psl fluorescence across the microcolony interior, whilst Pel fluorescence remained heterogenous. Pink arrows show increased Hoechst and GFP fluorescence intensities within the apex interior, whilst grey arrows show increased Psl and Pel fluorescence intensities in the interior, well-correlated to those of Hoechst and GFP.

4.6A exhibited negligible Hoechst and GFP fluorescence intensities, in contrast to the work of Jennings *et al.,* (2015). The cavity of microcolony structures is likely to exhibit physiological differences to the basal biofilm, thus lack of Hoechst staining in the cavity may either indicate the absence of eDNA within the cavity interior, or occlusion of structural staining by Hoechst, due to the enhanced staining of the cavity aggregate by ConA and WGA. Jennings *et al.,* (2015), suggested that eDNA and Pel are capable of crosslinking via iconic bond formation in microcolony stalks, in a pH-dependent manner. Therefore, it is possible that the pH in the cavity interior shown in Figure 4.6A was such that Pel was not catatonically charged, and thus may have interacted with Psl via noncovalent interactions to form a heterogenous exopolysaccharide-based aggregate.

At the outermost, or leading, edges of the basal layers, dense aggregates of co-localised Psl and Pel were similarly observed (Figure 4.6A, cyan arrows). GFP fluorescence was observed to increase as the leading edge retreated (Figure 4.6A, pink arrows), implying that Psl and Pel were functioning to maintain structural integrity at the leading edge of the basal biofilm. Whilst staining of Psl by ConA was diffuse across the basal layers, staining by WGA revealed Pel was more punctate throughout the basal biofilm; associated with the subpopulations of GFP-expressing cells at the leading edge (Figure 4.6A, orange arrows). Pel is thought to promote organisation of bacteria lying flat and symmetrically on a surface (Cooley *et al.,* 2013), thus its association with PA01 cell populations at the leading edge may also ensure maintenance of cohesive cell alignments during biomass accumulation.

Hoechst fluorescence across the basal biofilm was also diffuse, with Hoechst fluorescence intensities generally well-correlated to Psl fluorescence intensities (Figure 4.6A, green arrows), which suggests that eDNA and Psl were involved in cell-surface and cell-cell interactions within the basal layers. Allesen-Holm *et al.,* (2006), have previously shown that eDNA is able to promote distinct interactions between bacterial subpopulations, whilst Ma *et al.,* (2009), reported that Psl promotes cell-cell interactions and is well-distributed in flat biofilms. Production of an early ECM composed of eDNA and Psl, has been shown by several research groups to be involved in the initiation of surface attachment and the formation of early *Ps. a.* biofilms (Whitchurch *et al.,* 2002; Allensen-Holm *et al.,* 2006; Flemming and Wingender, 2010), leading to development of a stable basal layer from which three-dimensional structures can emerge.

Figure 4.6B show the emergence of the microcolony above the biofilm, and is a continuation of Figure 4.6A. From a height of Z+16 μm (Figure 4.7A) to a height of Z+29 μm, fluorescence intensity profiles across all four channels were concave, indicative of increased biomass/eDNA, *cdrA* expression and production of Psl and Pel at the feature periphery (Figures 4.6A and 4.6B, light blue arrows). The microcolony periphery exhibited heterogenous fluorescence intensities with respect to GFP, Psl and Pel with increasing height in the z dimension: at a height of Z+24 μm, the left-hand periphery was characterised by increased Psl and Pel accumulation, whilst the right-hand periphery exhibited increased GFP fluorescence (Figure 4.6B, red arrows). In comparison, at a height of Z+20 μm, fluorescence intensities at the peripheral edges

were more similar, and homogenous across all four channels (Figure 4.6B, yellow arrows).

GFP fluorescence intensities in the microcolony interior became more punctate and heterogenous with increasing feature height (Figure 4.6B, orange arrows), suggesting that subpopulations of cells were expressing different quantities of *cdrA* to neighbouring cell populations. The apical layers of the microcolony were characterised by similarly punctate fluorescence intensities for Psl and Pel (Figure 4.6B, green arrows). At a height of Z+34 μm, Pel fluorescence remained greatest at the periphery, whilst fluorescence of Hoechst and Psl were similar at the periphery and within the microcolony interior (Figure 4.6B, white arrows). At the feature apex (Z+38 μm), Psl and Pel fluorescence intensities were greatest at the peripheral edges, whilst Hoechst and GFP fluorescence intensities were highest in the microcolony interior (Figure 4.6B, pink arrows). Within the microcolony interior, Psl and Pel were observed to have more aggregative phenotypes, and displayed fluorescence intensities that were well-correlated with Hoechst and GFP fluorescence intensities (Figure 4.6B, grey arrows). Yang *et al.,* (2011), has previously demonstrated that Psl and Pel are important for facilitating interactions between subpopulations of cells during PA01 biofilm differentiation, thus increased Psl and Pel fluorescence in the microcolony interior of apical layers suggests that both exopolysaccharides are mediating cell-cell interactions and maintenance of structure's three-dimensional architecture, with specific rather than redundant functions.

Figure 4.7A shows another well-developed basal biofilm, within which is a structural cavity, that was equally observed to have an interior characterised by increased and well-correlated Psl and Pel fluorescence intensities, and negligible Hoechst and GFP fluorescence intensities (red arrows). From Z to a height of Z+3 μm, a fibre-like Psl network can be seen connecting the integral Psl-Pel cavity aggregate to the basal biofilm (Figure 4.7A, cyan arrows), to which individual PA01 cells can be seen associating with the fibre-like projections (Figure 4.7A, orange arrows). At a height of Z+6 μm, fibre-like structures of Psl and Pel can be seen surrounding the cavity's boundary edge and connecting to the neighbouring basal layer (Figure 4.7A, green arrows). As previously described, Irie *et al.,* (2012), demonstrated that Psl can act as a signal to increase c-di-GMP synthesis, thus a dense aggregate of Psl on the surface may denote a nucleation centre, that may recruit cells to the local area to stimulate biomass accumulation and microcolony development. Psl trails have been previously observed by Zhao *et al.,* (2013), and Wang *et al.,* (2013), and are believed to facilitate transit of cells to areas of the developing biofilm, by influencing their motility and migration.

Similar facilitation of cell migration during expansion of the biofilm can be seen from Z to a height of Z+6 μm, by globular-like aggregates of Psl and Pel forming a 'bridge' utilised by GFP-expressing PA01 cells to connect two spatially-separated parts of the basal biofilm (Figure 4.7A, pink arrows). The aggregates of Psl and Pel were observed to form a chain-like structure across the void between the basal layers, which was heterogenous in composition. Some aggregates appeared to have an interior of Pel surrounded by a peripheral Psl layer, whilst others comprised of Psl-Pel complexes

**Figure 4.7A**

**Formation of a Psl-Pel aggregate within microcolony cavities after 48 hours under low shear at 75 RPM**

*(figure legend overleaf)*

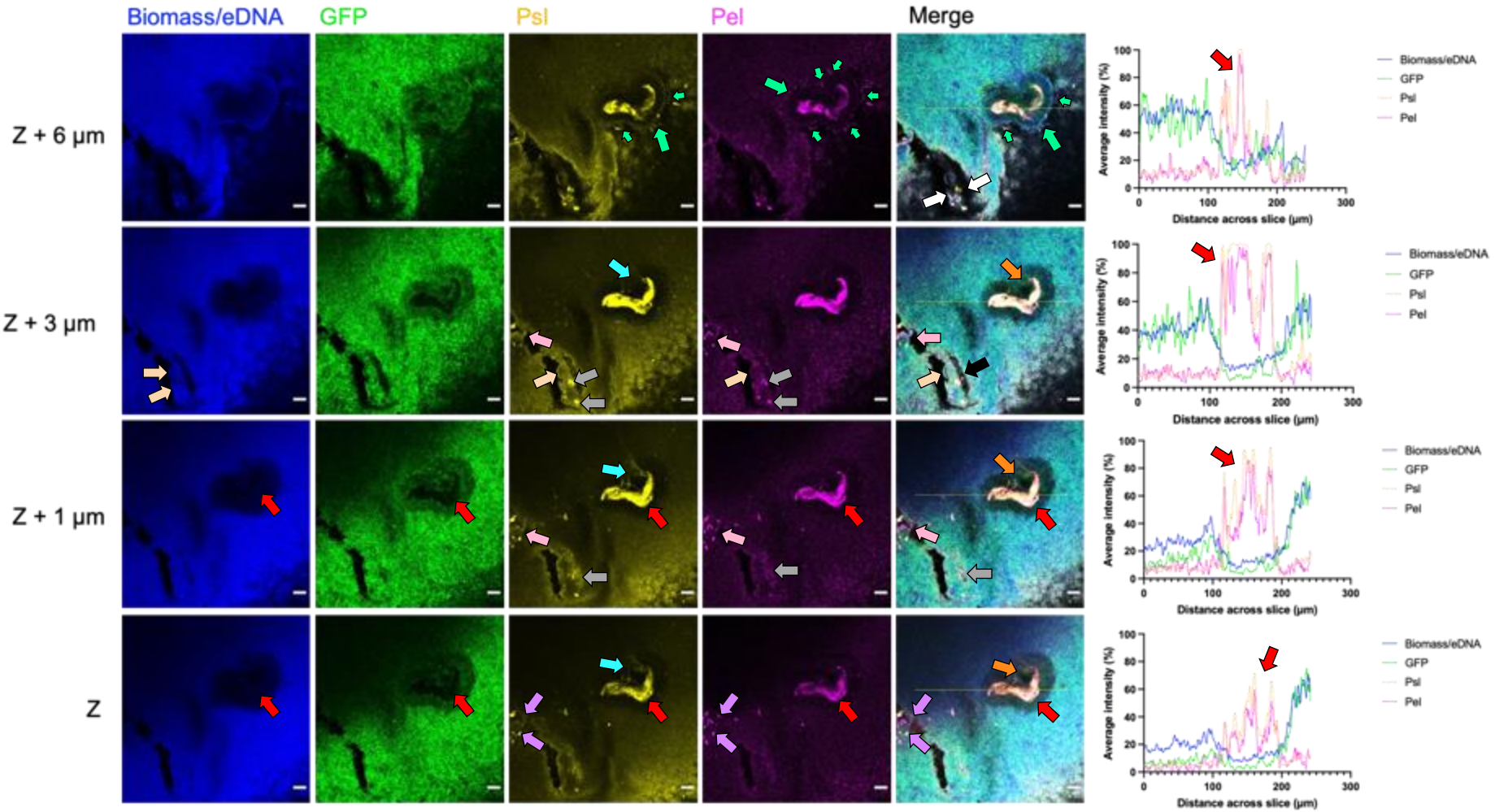

(*figure legend for* Figure 4.7A)

Representative confocal images are from PA01 *cdrA::gfp* biofilms (GFP signal is green) cultivated for 48 hours in the CBR under low shear (at 75 RPM) and stained with Hoechst for biomass/eDNA (blue), the Psl-specific lectin ConA (yellow) and the Pel-specific lectin WGA (magenta). Different z heights are shown for the same sample area, with Z defined as the bottom layer closest to the coupon surface. Scale bar = 20 μm. Red arrows show an area of increased Psl and Pel fluorescence in the interior of a cavity structure. Cyan arrows show a fibre-like Psl structure, connecting the cavity interior to the basal biofilm. Orange arrows show association of individual PA01 cells to the Psl-fibres. Green arrows show punctate Psl and Pel around the cavity periphery. Pink arrows show aggregates of Psl and Pel forming a 'bridge' connecting parts of the basal biofilm to one another. Lilac arrows show heterogenous composition of Psl and Pel aggregates. Grey arrows show local areas of increased Psl and Pel aggregate formation, whilst peach arrows show a eDNA-Psl-Pel fibre-like structure, localised to the boundary and peripheral edge between part of the basal biofilm and a subpopulation of cells. The black arrow shows cellular and ECM material within a void. White arrows show part of the basal biofilm now spatially-separated by two surrounding voids.

**Figure 4.7B** *(figure legend overleaf)*

**Emergence of mushroom-shaped macrocolonies is generally homogenous across independent sampling sites after 72 hours under low shear at 75 RPM**

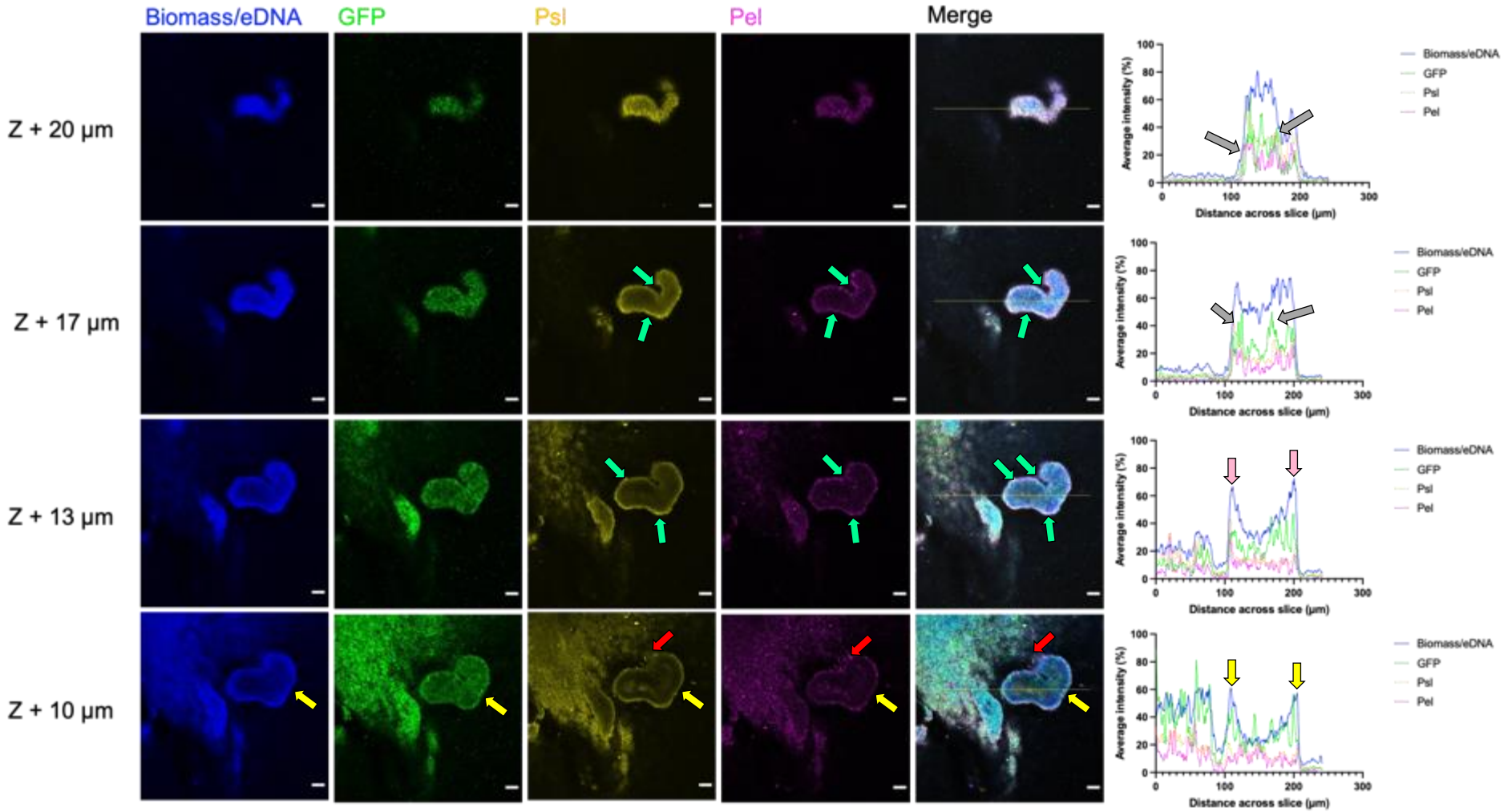

(*figure legend for* Figure 4.7B)

Representative confocal images are from PA01 *cdrA::gfp* biofilms (GFP signal is green) cultivated for 48 hours in the CBR under low shear (at 75 RPM) and stained with Hoechst for biomass/eDNA (blue), the Psl-specific lectin ConA (yellow) and the Pel-specific lectin WGA (magenta). Different z heights are shown for the same sample area, with Z defined as the bottom layer closest to the coupon surface. Scale bar = 20 μm. Yellow arrows show the emergence of the microcolony structure, and concave fluorescence intensity profile. Red arrows show fibre-like structures of Psl and Pel extending between the basal biofilm and microcolony periphery. Pink arrows show a concave fluorescence intensity profile, indicative of increased GFP expression and staining at the periphery, whilst grey arrows show punctate fluorescence intensities at the microcolony apex. Green arrows show heterogenous arrangement of Psl and Pel around the microcolony periphery.

and others just Pel (Figure 4.7A, lilac arrows). The ‘bridge’ structure was also stained by Hoechst, which could indicate the presence of eDNA, which was shown by Gloag *et al.,* (2012), to maintain coherent cell alignments during twitching motility-mediated growth of the biofilm.

Spatial localisation of small Psl and Pel aggregates within an area of the basal biofilm at Z was additionally seen; with increasing height in the z dimension aggregates became large, with a particularly punctate area of increased Psl and Pel fluorescence observed at the boundary and peripheral edge between part of the basal biofilm and a subpopulation of cells (Figure 4.7A, grey arrows), as well as the formation of fibre-like structures at the opposite boundary edge of the basal biofilm, which were composed of eDNA, Psl and Pel (Figure 4.7A, peach arrows). At a height of Z+3 μm, GFP-expressing cells and exopolysaccharide material can be seen in adjacent and emerging void, whilst by a height of Z+6 μm, the once-connected ECM is spatially-separated from the leading edge of the basal biofilm by two adjacent voids and contains very few enmeshed GFP-expressing cells (Figure 4.7A, white arrows).

Figure 4.7B show the emergence of the microcolony above the biofilm, and is a continuation of Figure 4.7A. At a height of Z+10 μm, the periphery of the emerging microcolony structure can be seen, and was observed to exhibit increased staining of the ECM by Hoechst, ConA and WGA in comparison to the microcolony interior (Figure 4.7B, yellow arrows). Fibre-like projections of Psl and Pel between the microcolony periphery and an area of the basal biofilm were seen, co-localised with fibres of eDNA (Figure 4.7B, red arrows), which were once again was likely facilitating the transit of

individual PA01 cells toward the microcolony periphery as previously described. Fluorescence intensities for the emerging microcolony displayed concave profiles to an extent (Figure 4.7B, pink arrows), and became noticeably more punctate with increasing height in the z dimension (Figure 4.7B, grey arrows). From a height of Z+13 μm, the fluorescence intensity of Hoechst was greatest and staining diffuse, consistent with consensus in the literature that eDNA is important during biofilm development and maintenance of cell-cell interactions (Whitchurch *et al.,* 2002; Wingender and Flemming, 2010).

The arrangement of Psl and Pel at the microcolony was noteworthy, as some peripheral areas exhibited increased accumulation of Psl, whilst other peripheral areas were observed to have increased accumulation of Pel, or co-localisation of both exopolysaccharides (Figure 4.7B, green arrows). Colvin *et al.,* (2011), classified PA01 as a 'Class II' matrix producer, producing Psl primarily and Pel at lower levels. This suggests that both Psl and Pel contribute to maintenance of the microcolony's three-dimensional architecture, perhaps through exopolysaccharide-mediated modulation of the periphery's rheological properties. Chew *et al.,* (2014), reported that production of a Psl-dominant matrix is more elastic and stronger when crosslinked; able to centralise growth to newly-colonised sites, whilst a Pel-dominant matrix is more viscous and exhibits less cross-linking. Therefore, having a heterogeneously-composed periphery may enable more dynamic remodelling of the ECM during maturation and spreading of the biofilm.

In contrast, PA01 biofilm development under high shear (at 350 RPM) was characterised by the development of spatially-separated basal biofilms (of an average < 25 μm in height) across the coupon surface; with cell populations divided by large voids, which could be suggestive of water channels (Figures 4.8 and 4.9). In contrast to biofilms formed after 48 hours under low shear at 75 RPM, basal biofilms formed under high shear conditions exhibited increased Hoechst and GFP fluorescence intensities, which were generally well-correlated to one another, irrespective of spatial location across the coupon surface as shown by resultant fluorescence intensity profiles. Pel fluorescence intensities were the lowest of the four channels, whilst Psl fluorescence intensities displayed heterogeneity, dependent on location within the biofilm.

In Figure 4.8 at a height of Z+4 μm, individual PA01 *cdrA::gfp* cells can be seen associating with part of the basal biofilm and forming small cell clusters *in situ* around the basal layer (Figure 4.8, yellow arrows). By a height of Z+8 μm, individual cells and clusters were assimilated with the local basal structures, which appeared denser and resulted in change of basal structure shape (Figure 4.8, white circles). Of interest was the fact that several basal structures were stained by Hoechst and ConA for Psl in areas lacking GFP-expressing cells, either as part of a basal aggregate (Figure 4.8, red arrows) or independently of established cell populations (Figure 4.8, pink arrows), with such regions easily noticeable on the merged z slice images. The former observation suggests a role for eDNA and Psl in maintaining cell-cell interactions between adjacent cell populations; facilitating biomass accumulation atop the eDNA-Psl ‘bridge’ and maintenance of the local basal structure during vertical expansion

**Figure 4.8**

**Basal biofilm composition is heterogenous after 48 hours under high shear at 350 RPM**

*(figure legend overleaf)*

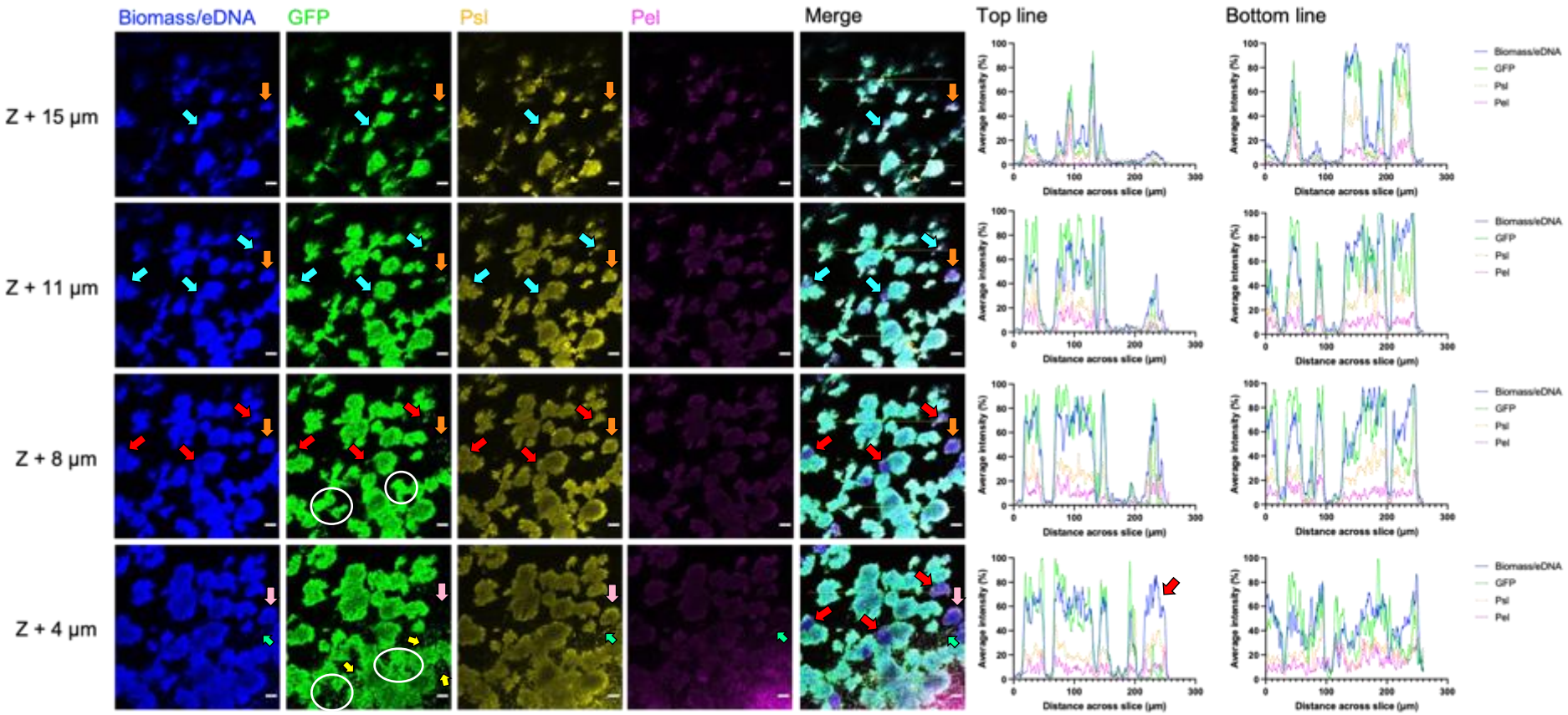

(*figure legend for* Figure 4.8)

Representative confocal images are from PA01 *cdrA::gfp* biofilms (GFP signal is green) cultivated for 48 hours in the CBR under high shear (at 350 RPM) and stained with Hoechst for biomass/eDNA (blue), the Psl-specific lectin ConA (yellow) and the Pel-specific lectin WGA (magenta). Different z heights are shown for the same sample area, with Z defined as the bottom layer closest to the coupon surface. Scale bar = 20 μm. Yellow arrows show individual PA01 *cdrA::gfp* cells can be seen associating with part of the basal biofilm. White circles show cell assimilation into existing basal structures with well-defined structures. Red and pink arrows show the formation of eDNA-Psl structures in areas lacking established GFP cell populations. Cyan and orange arrows show colonisation of these eDNA-Psl structures by cells that subsequently form clusters and their own subpopulations, associated with the ECM complex. Grey arrows show a fibre-like structure co-stained by Hoechst, ConA and WGA.

(Figure 4.8, cyan arrows). Non-cell associated eDNA and Psl complexes appear to be involved in recruitment and retention of PA01 cells to eDNA-Psl aggregate areas. This can be seen with increasing height in the z dimension: at a height of Z+8 μm, a few individual GFP-expressing cells were observed co-localised at the periphery of several eDNA-Psl complexes, whilst a heights of Z+11 μm and Z+15 μm, clusters of PA01 cells began to develop, leading to clonal colonisation of the eDNA-Psl complexes (Figure 4.8, orange arrows).

Wang *et al.,* (2015), reported that PA01 utilises a web of eDNA-Psl fibres to form a biofilm 'skeleton', which can structurally support the developing biofilm structure and facilitate its expansion, in agreement with the works of Wang *et al.,* (2013), and Zhao *et al.,* (2013), that demonstrated Psl trails can influence the migration of PA01 cells and surface exploration, leading to microcolony formation. Whilst a fibre-like structure composed of eDNA, Psl and Pel and surrounded by individual PA01 cells was observed at a height of Z+4 μm (Figure 4.8, green arrows), defined networks were not seen under high shear at 350 RPM. Thus, one could suggest that the formation of free eDNA-Psl complexes are induced in response to increased shear conditions, functioning as 'island' structures to which bacteria may be recruited and enmeshed, to protect 'younger' cell populations from the risk of detachment under high shear.

Figure 4.9 comprises another basal biofilm composed of spatially-separated cell populations. At a height of Z + 6 μm, individual PA01 *cdrA::gfp* cells can be seen associating with part of the basal biofilm and forming small cell clusters *in situ* around the basal layer (Figure 4.9, orange arrows); assimilated with the local basal populations

by a height of Z + 10 μm, resulting in the formation of well-defined structures (Figure 4.9, white circles). Similarly to Figure 4.8, independent eDNA-Psl structures were observed promoting attachment of individual PA01 cells, which subsequently developed into clustered populations; facilitating expansion of the local basal biofilm (Figure 4.9, red arrows). Under high shear conditions at 350 RPM, weakly-adhered cells are at increased risk of wash out and in competition with well-established cell populations for nutrients and space, thus adherence to an existing and cell-free ECM, rather than 'non-ECM-conditioned' coupon surfaces, likely provides immediate and enhanced cell-ECM and subsequent cell-cell interactions; promoting local growth and expansion of the biofilm.

**Figure 4.9**

**Spatial separation of PA01 cell subpopulations that comprise a basal biofilm after 48 hours under high shear at 350 RPM**

*(figure legend overleaf)*

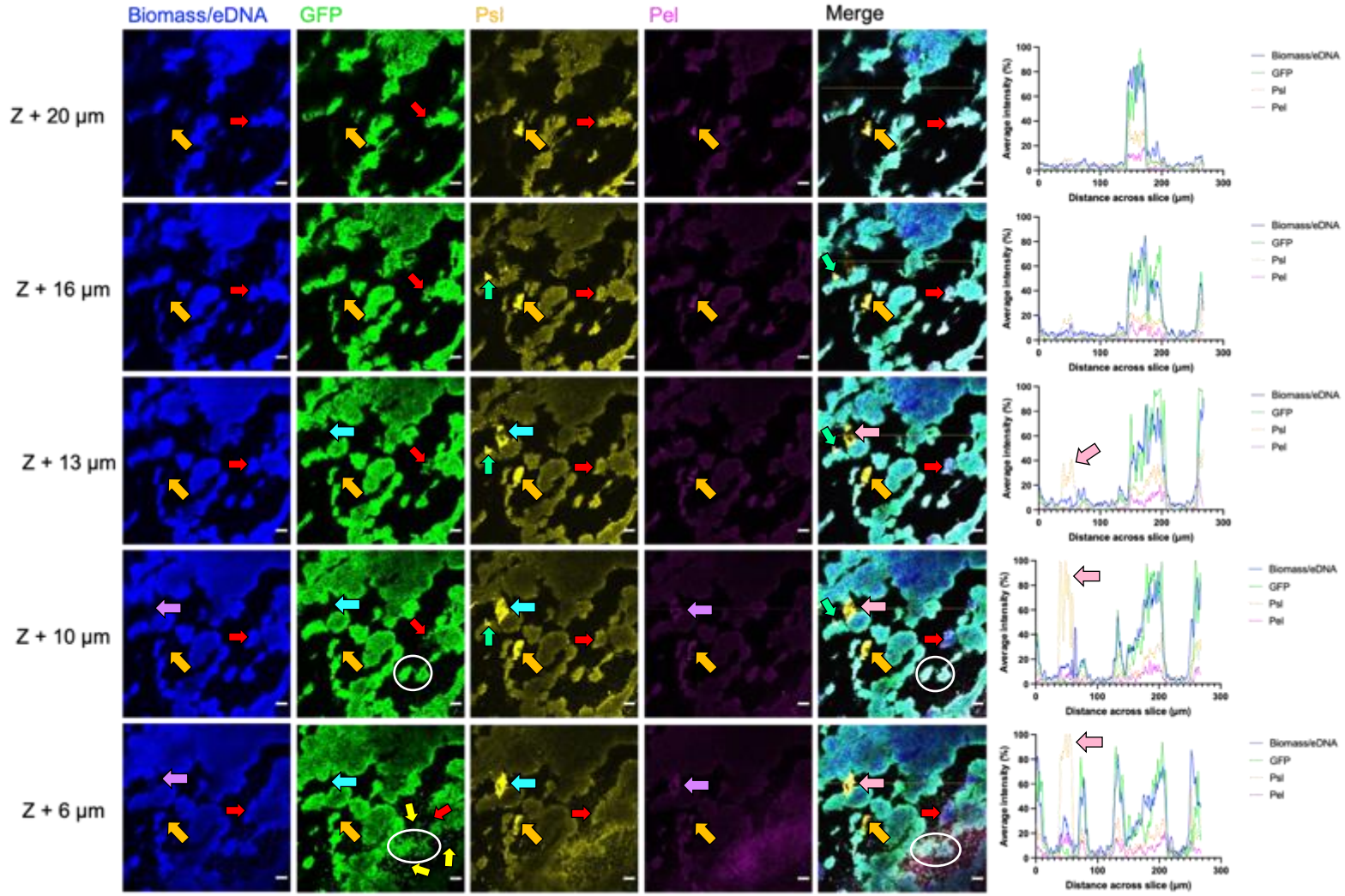

(*figure legend for* Figure 4.9)

Representative confocal images are from PA01 *cdrA::gfp* biofilms (GFP signal is green) cultivated for 48 hours in the CBR under high shear (at 350 RPM) and stained with Hoechst for biomass/eDNA (blue), the Psl-specific lectin ConA (yellow) and the Pel-specific lectin WGA (magenta). Different z heights are shown for the same sample area, with Z defined as the bottom layer closest to the coupon surface. Scale bar = 20 μm. Yellow arrows show individual PA01 *cdrA::gfp* cells can be seen associating with part of the basal biofilm. White circles show cell assimilation into existing basal structures with well-defined structures. Red arrows shows an area of non-cell associated eDNA-Psl facilitating the formation of a defined subpopulation of cells from individually-attached PA01 cells and clusters. Cyan arrows show a dense aggregate of free Psl between two-spatially separated basal structures, whilst pink arrows show the resultant increased fluorescence intensity profiles of this Psl aggregate. Lilac arrows show punctate co-staining of Psl aggregates by Hoechst and WGA. Green arrows show a secondary and adjacent area of Psl aggregation. Orange arrows show another non-cell associated Psl-Pel aggregate structure.

A dense aggregate of Psl polymers was seen forming a ‘tendril’-like ‘bridge’ between two separated areas of the basal biofilm, maintained over a height of 7 μm in the z dimension (Figure 4.9, cyan arrows). Resultantly, fluorescence intensities of Psl at this location were increased in comparison to the other three channels (Figure 4.9, pink arrows). At heights of Z+6 μm and Z+10 μm, there was evidence of punctate co-staining by Hoechst and WGA, which could suggest the presence of eDNA and Pel in the ‘tendril’-like structures (Figure 4.9, lilac arrows), although Psl was the predominant ECM component. Psl is an essential scaffolding constituent of PA01 biofilms, which promotes cellular interactions and maintains the structural integrity of the biofilm (Friedman and Kolter, 2004a; Jackson *et al.,* 2004; Matsukawa and Greenberg, 2004). Psl can also act as a signal to increase c-di-GMP synthesis (therefore increasing Psl production through a positive feedback loop) (Irie *et al.,* 2012), thus the ‘tendril’-like structure may have stimulated increased Psl production in the local biofilm area, as demonstrated by the emergence of secondary dense aggregate of Psl at one of the biofilm peripheries adjacent to the Psl ‘bridge’ (Figure 4.9, green arrows).

Indeed, Psl aggregates throughout the basal biofilm shown in Figure 4.9 were all non-cell associated. Another dense area of Psl was observed and exhibited punctate co-staining with WGA, indicative of the presence of Pel within the aggregate (Figure 4.9, orange arrows). Given that exopolysaccharide production is an energetically costly process, the production of a dense aggregate, free from cells, may provide the proximal subpopulation of cells with a competitive advantage during vertical growth over neighbouring populations. Previous work in the literature suggests that production of exopolysaccharides can ‘push’ progeny cells above surrounding and competing cell

populations; giving such cells a competitive advantage during biofilm growth (Xavier and Foster, 2007; Kim *et al.,* 2014). Thus, the Psl-Pel aggregative structure may serve as a site for further cell proliferation upon an well-developed and robust ECM; facilitating expansion of that particular basal structure and increased vertical growth atop the Psl-Pel aggregate under high shear conditions.

### 4.3.3. PA01 macrocolony formation does not occur under high shear conditions

After 72 hours of growth under low shear at 75 RPM, PA01:*cdrA::gfp* biofilms were characterised by a well-developed basal layer and the formation of mushroom-shaped macrocolony structures, typical of mature *Ps. a.* biofilms (O'Toole *et al.,* 2000; Klausen *et al.,* 2003). The basal biofilm was on average 20 – 25 μm in height, whilst the macrocolonies exhibited more variation in the individual heights they reached, as well as their respective sizes in the x and y dimensions (Figures 4.10 and 4.11).

**Figure 4.10**
**Macrocolony formation by PA01 *cdrA::gfp* after 72 hours under low shear at 75 RPM**

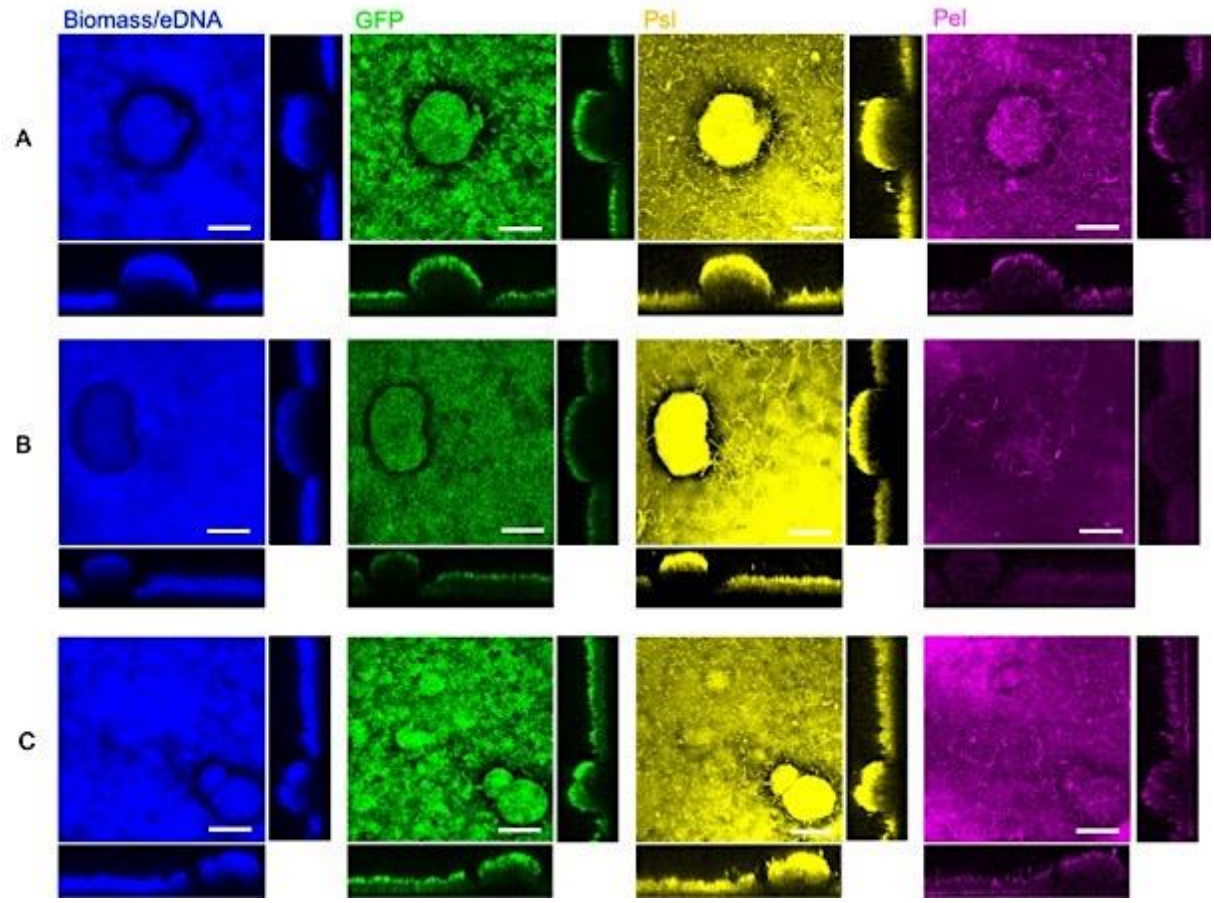


Representative confocal images are from PA01 *cdrA::gfp* biofilms (GFP signal is green) cultivated for 72 hours in the CBR under low shear (at 75 RPM) and stained with Hoechst for biomass/eDNA (blue), the Psl-specific lectin ConA (yellow) and the Pel-specific lectin WGA (magenta). Shown are top-down three-dimensional and side views of the biofilm Scale bar = 50 μm.

**Figure 4.11**

**Observation of Psl and Pel fibre-like networks throughout basal biofilms formed after 72 hours under low shear at 350 RPM**

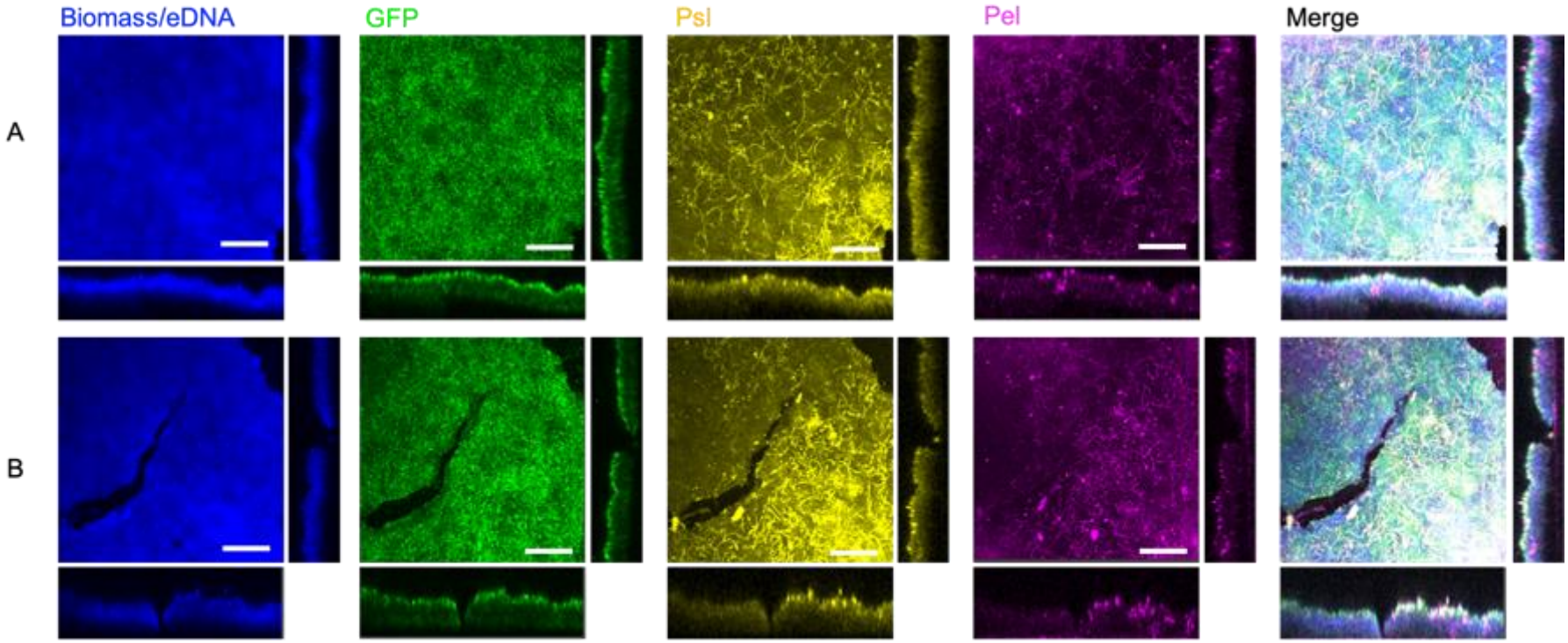


Representative confocal images are from PA01 *cdrA::gfp* biofilms (GFP signal is green) cultivated for 72 hours in the CBR under low shear (at 75 RPM) and stained with Hoechst for biomass/eDNA (blue), the Psl-specific lectin ConA (yellow) and the Pel-specific lectin WGA (magenta). Shown are top-down three-dimensional and side views of two biofilms observed during independent CBR runs. Scale bar = 50 μm

Similarly to growth of PA14:*cdrA::gfp* under low shear conditions at 75 RPM, mushroom-shaped macrocolonies were a recurrent architectural feature observed after 72 hours of PA01:*cdrA::gfp* biofilm growth (Figures 4.10 and 4.11). Consistently seen across different sample site locations on the coupons, and during independent runs of the CBR at 75RPM, the macrocolony structures formed by PA01 reached comparable heights on average in the z dimension to those formed by PA14 . Figure 4.12 shows a PA01:*cdrA::gfp* mushroom-shaped macrocolony, spilt into two figures due to macrocolony height; showing the structure's emergence from the basal biofilm (Figure 4.12A) and growth upwards into the surrounding bulk fluid (Figure 4.12B). In contrast to the generally homogenous basal biofilm formed by PA14:*cdrA::gfp* under low shear conditions after 72 hours, PA01:*cdrA::gfp* basal biofilms were more heterogenous, with respect to fluorescence intensities across all four channels with increasing height in the z dimension (Figure 4.12A). The intensity of Hoechst fluorescence in the lower layers of the biofilm (< Z+10 μm) was greatest, followed by Psl fluorescence intensity, whilst the fluorescence intensities of GFP and Pel were much lower and were not correlated to either Hoechst or Psl fluorescence Although not correlated to one another, the fluorescence intensity profiles for Hoechst and Psl were similar in terms of their respective line traces (i.e. peaks in the profile for Hoechst fluorescence corresponded to peaks in intensity profile for Psl fluorescence), suggesting that both eDNA and Psl are important for maintaining cell-cell interactions within the basal biofilm, as well its structural integrity.

**Figure 4.12A** *(figure legend overleaf)*

**Basal biofilm formation by PA01 exhibits spatial heterogeneity of Psl and Pel after 72 hours under low shear at 75 RPM**

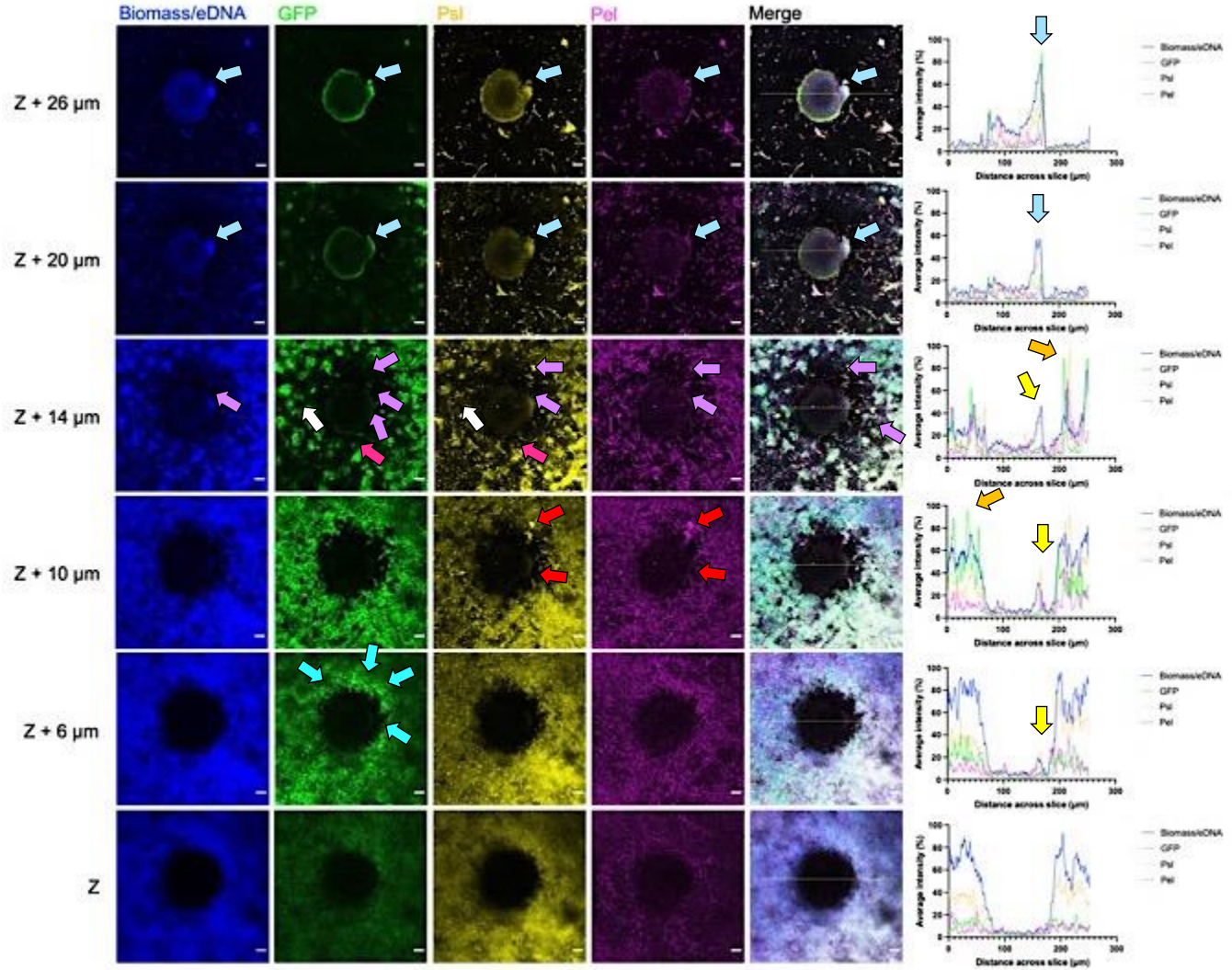

(*figure legend for* Figure 4.12A)

Representative confocal images are from PA01 *cdrA::gfp* biofilms (GFP signal is green) cultivated for 72 hours in the CBR under low shear (at 75 RPM) and stained with Hoechst for biomass/eDNA (blue), the Psl-specific lectin ConA (yellow) and the Pel-specific lectin WGA (magenta). Different z heights are shown for the same sample area, with Z defined as the bottom layer closest to the coupon surface. Scale bar = 20 μm. Orange arrows show areas of increased and punctate GFP fluorescence intensities, uncorrelated to increased Hoechst, Psl or Pel fluorescence intensities. Cyan arrows show an 'arc' composed of subpopulations of PA01 with increased GFP fluorescence in comparison to neighbouring basal cell populations. Red arrows show finger-like Psl and Pel protrusions from the basal biofilm towards to macrocolony cavity. Lilac arrows show GFP cells associating with finger-like fibres across the void between the basal biofilm and emerging macrocolony. Light blue arrows show heterogenous development of two opposite peripheral edges of the emerging macrocolony. Yellow arrows show a small peak in the fluorescence intensity profile across all four channels, which eventually forms the peripheral area identified by the light blue arrows. Cerise arrows show free Psl aggregate formation in areas lacking a GFP-expressing cell population, whilst white arrows show an example Psl association with other cell populations within the basal biofilm.

Upper layers of the basal biofilm, in contrast, were characterised by increased *cdrA* expression within cell subpopulations, resulting in punctate GFP fluorescence intensities from a height of Z+10 μm that were uncorrelated to Hoechst, Psl or Pel fluorescence intensities (Figure 4.12A, orange arrows). At a height of Z+6 μm, a localised area of increased *cdrA::gfp* fluorescence appeared to surround part of the structural cavity's circumference; forming an arc around the bottom of the emerging macrocolony (Figure 4.12A, cyan arrows). More widespread and increased GFP fluorescence across the basal biofilm was seen by a height of Z+10 μm, although it remained heterogenous; appearing both concentrated and localised to the boundary edge of the basal layer surrounding the macrocolony cavity.

The boundary edge had an irregular appearance, with subpopulations of PA01:*cdrA::gfp* cells observed protruding across a distance of approximately 20 μm (in the x and y dimensions) towards the structural cavity. Some protrusions also exhibited increased and punctate fluorescence of both Psl and Psl, which could indicate that the extending, 'finger-like' projections were composed of both PA01 cells and exopolysaccharide (Figure 4.12A, red arrows). Yang *et al.,* (2011), have previously demonstrated that Psl and Pel contribute to the formation of PA01 mushroom-shaped macrocolonies, as PA01Δ*pslBCD* and PA01Δ*pelA* mutants were unable to form differentiated, three-dimensional structures, with biofilm development only progressing to microcolony formation.

At sites from which protrusions extend, increased and localised production of Psl and Pel may thus facilitate the migration of bacterial cells from the basal biofilm towards

the site of macrocolony development; contributing to the formation of the three-dimensional structure. At a height of Z+14 μm, thin, 'tendril'-like structures can be seen attached to the right-hand side periphery of the macrocolony, composed of GFP-expressing cell populations that were also stained by Hoechst, ConA (for Psl) and WGA (for Pel) (Figure 4.12A, lilac arrows). Within the literature others have suggested that both eDNA (which is stained by Hoechst) and Psl are capable of forming eDNA-Psl heterologous fibres, that can function as a 'skeleton' to facilitate bacterial recruitment and migration from one area of the biofilm to another (Wang *et al.,* 2013; Wang *et al.,* 2015).

By a height of Z+20 μm, the peripheral edge of the emerging macrocolony is visible (Figure 4.12A), and appears irregular in circumference due to the formation of a 'mound' on its right-hand side, which could indicate an area composed of recently-migrated cells. At a height of Z+26 μm, fluorescence intensities across all four channels are greater in the developing 'mound' compared to the opposite peripheral edge (Figure 4.12A, light blue arrows), suggesting that macrocolony development may occur asymmetrically. There is evidence in the fluorescence intensity line profiles to support this notion: a small peak in the profile can be seen from a height of Z+6 μm, increasing in fluorescence intensity as the 'mound' emerges (Figure 4.12A, yellow arrows), seemingly emerging from in-between the 'finger'-like projections potentially involved in bacterial transit to enable macrocolony formation

Throughout the basal biofilm, Pel was predominantly organised into a fibre-like meshwork that extended both laterally and vertically throughout the basal layers of the

biofilm (Figure 4.12A, Pel channel). In contrast, Psl exhibited a variety of morphologies following staining by ConA, including regions with diffuse Psl associated with GFP-expressing cell populations (Figure 4.12A, cerise arrows), free aggregates with approximate diameters of 10 μm (Figure 4.12A, white arrows), and as punctate and localised smaller aggregates interspersed throughout the basal biofilm. Fibre-like structures were additionally observed spanning across cell-free areas, and exhibited co-localised staining by Hoechst, ConA (for Psl) and WGA (Pel). This suggests that as well as homogenous fibre-like networks forming (as seen most noticeably by Pel), heterogenous fibres can also be produced; comprised of eDNA, Psl and Pel, in a variety of combinations and different proportions to one another.

Previous studies have demonstrated that both Pel and Psl can co-localise with eDNA in *Ps. a.* biofilms, with Psl able to physically interact with eDNA via hydrogen bonding to generate fibres (Jennings *et al.,* 2015; Wang *et al.,* 2015). Such fibres may be produced to increase the structural stability of the biofilm (Di Martino, 2018); forming an extensive macro-network composed of eDNA, Psl and Pel fibre-like structures enmeshed throughout the basal layers. During the initial stages of biofilm development, formation of a Psl matrix results in a stiff and protective structure that mediates cell-surface and cell-cell interactions; keeping populations of cells adhered together *in situ* (Matsukawa *et al.,* 2005; Ma *et al.,* 2009; Byrd *et al.,* 2010).

Figure 4.12B shows the emergence of the mushroom-shaped macrocolony above the biofilm, and is each a continuation of the same biofilm shown in Figure 4.12A. Under low shear conditions at 75 RPM, mushroom-shaped macrocolony formation by PA14:*cdrA::gfp* in Chapter 3 appeared homogenous, as Hoechst, GFP and Pel fluorescence intensities were well-correlated to one another, irrespective of spatial location within the macrocolony (i.e. at the interior or periphery) or the overall elevation of individual mushroom-shaped macrocolonies. Macrocolony formation by PA01:*cdrA::gfp* under low shear was more heterogenous, with fluorescence intensity profiles across all four channels appearing uncorrelated to one another (Figure 4.12B).

At a height of Z+30 μm, fluorescence intensities across three channels initially displayed a concave profile, indicative of increased Hoechst, GFP and Psl fluorescence at the periphery of the macrocolony in comparison to the interior (Figure 4.12B). Pel localisation at the periphery was noticeably asymmetrical at some heights, with increased and punctate fluorescence present at either peripheral edge (Figure 4.12B, red arrows). The fluorescence intensity of peripheral Pel remained asymmetrical until a height of Z+50 μm, whereby increased Pel fluorescence was observed around the entire periphery of the macrocolony whilst the fluorescence intensity of Pel remained low throughout the macrocolony interior (Figure 4.12B, green arrows). With increasing height in the z dimension (up to Z+44 μm), the fluorescence intensity profile for GFP remained concave, thus peripheral cell populations had increased *cdrA* expression (indicative of greater intracellular c-di-GMP concentrations) in contrast to the macrocolony interior, which exhibited negligible GFP fluorescence.

**Figure 4.12B** *(figure legend overleaf)*

**Emergence of a PA01 macrocolony apex after 72 hours under low shear at 75 RPM**

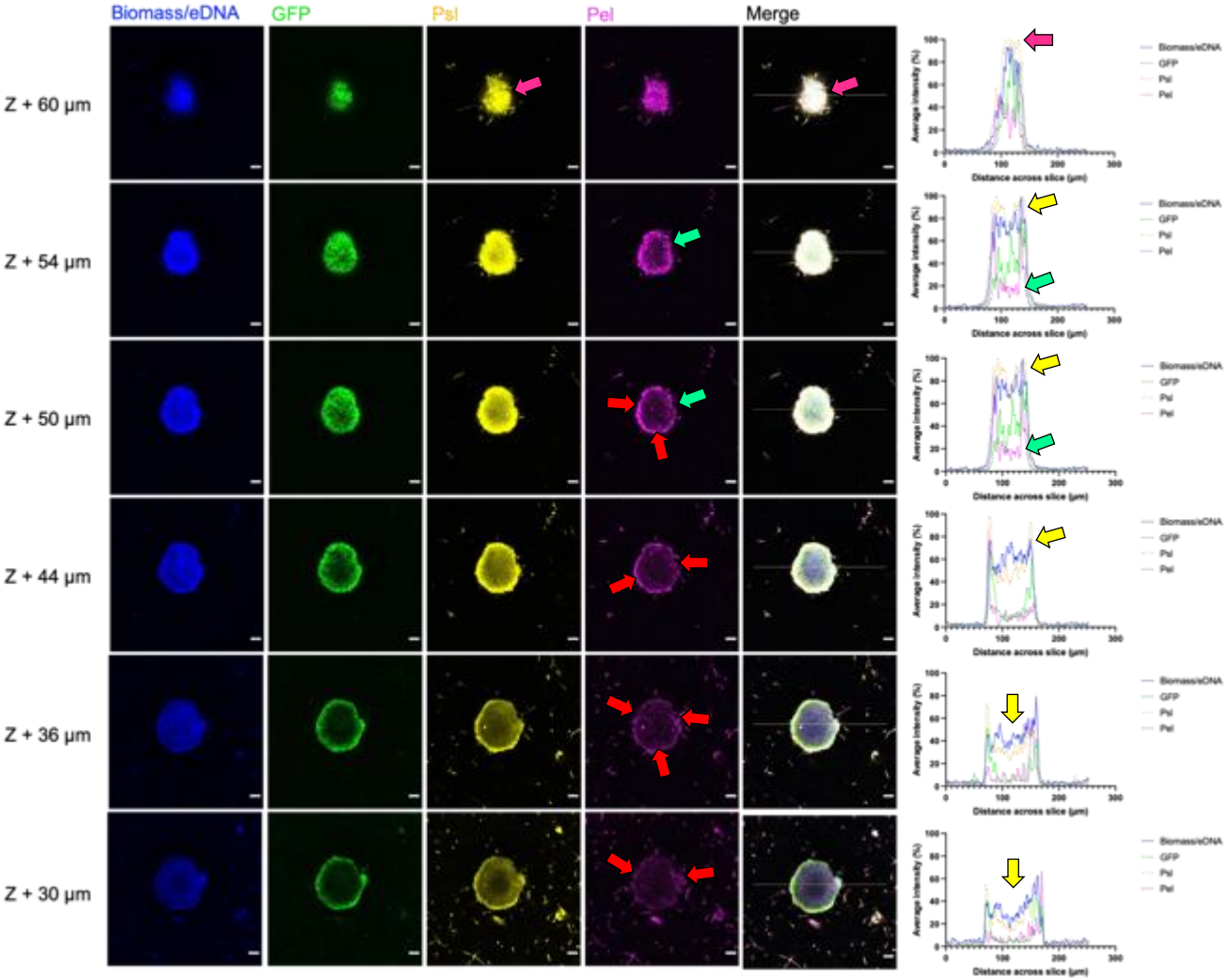

(*figure legend for* Figure 4.12B)

Representative confocal images are from PA01 *cdrA::gfp* biofilms (GFP signal is green) cultivated for 72 hours in the CBR under low shear (at 75 RPM) and stained with Hoechst for biomass/eDNA (blue), the Psl-specific lectin ConA (yellow) and the Pel-specific lectin WGA (magenta). Different z heights are shown for the same sample area, with Z defined as the bottom layer closest to the coupon surface. Scale bar = 20 μm. Red arrows show heterogenous, localised accumulation of Pel across different parts of the macrocolony periphery, whilst green arrows show negligible Pel fluorescence intensities in the macrocolony interior. Yellow arrows show increased staining of the macrocolony interior by Hoechst and Psl within increasing height in the z dimension. Cerise arrows show the macrocolony apex, completely surrounded by Psl.

Hoechst and Psl fluorescence intensities were not well-correlated, although their respective line profiles were similar; exhibiting parallel peaks and troughs within the fluorescence intensity profiles to one another. In contrast to localised Pel fluorescence at the macrocolony periphery, from a height of Z+44 μm onwards increased staining of the interior of the macrocolony by both Hoechst and ConA was observed, resulting in more uniform fluorescence intensities for both Hoechst and Psl across the whole macrocolony structure (Figure 4.12B, yellow arrows). Psl fluorescence was greater than that of Hoechst, GFP and Pel from a height of Z+50 μm onwards, suggesting that Psl was completely covering the apical cell populations of the macrocolony (Figure 4.12B, cerise arrows). This is similar to the work of Ma *et al.,* (2009), in which PA01 mushroom-shaped structures initially displayed minimal lectin staining of Psl within the interior and maximal staining at the periphery (as seen in Figure 4.12A), with Psl observed to surround the three-dimensional structure at its apex.

By 72 hours, PA01 biofilm formation under high shear at 350 RPM was characterised by multiple mounds that were highly variable in the x, y and z dimensions, resulting in an irregular ‘mound’-like biofilm topography (Figure 4.13), as previously seen after 96 hours of PA14 biofilm formation at 350 RPM (Chapter 3). PA01 biofilms formed after 72 hours of growth under high shear were characterised by increased GFP fluorescence, with an average height of 100 – 150 μm. Resultantly, fluorescence intensity profiles for Hoechst, GFP, Psl and Pel were difficult to calculate, due to the reduced laser and stain penetration of the structures.

**Figure 4.13**

**PA01 biofilms formed at 72 hours under 350 RPM exhibit increased vertical growth**

*(figure legend overleaf)*

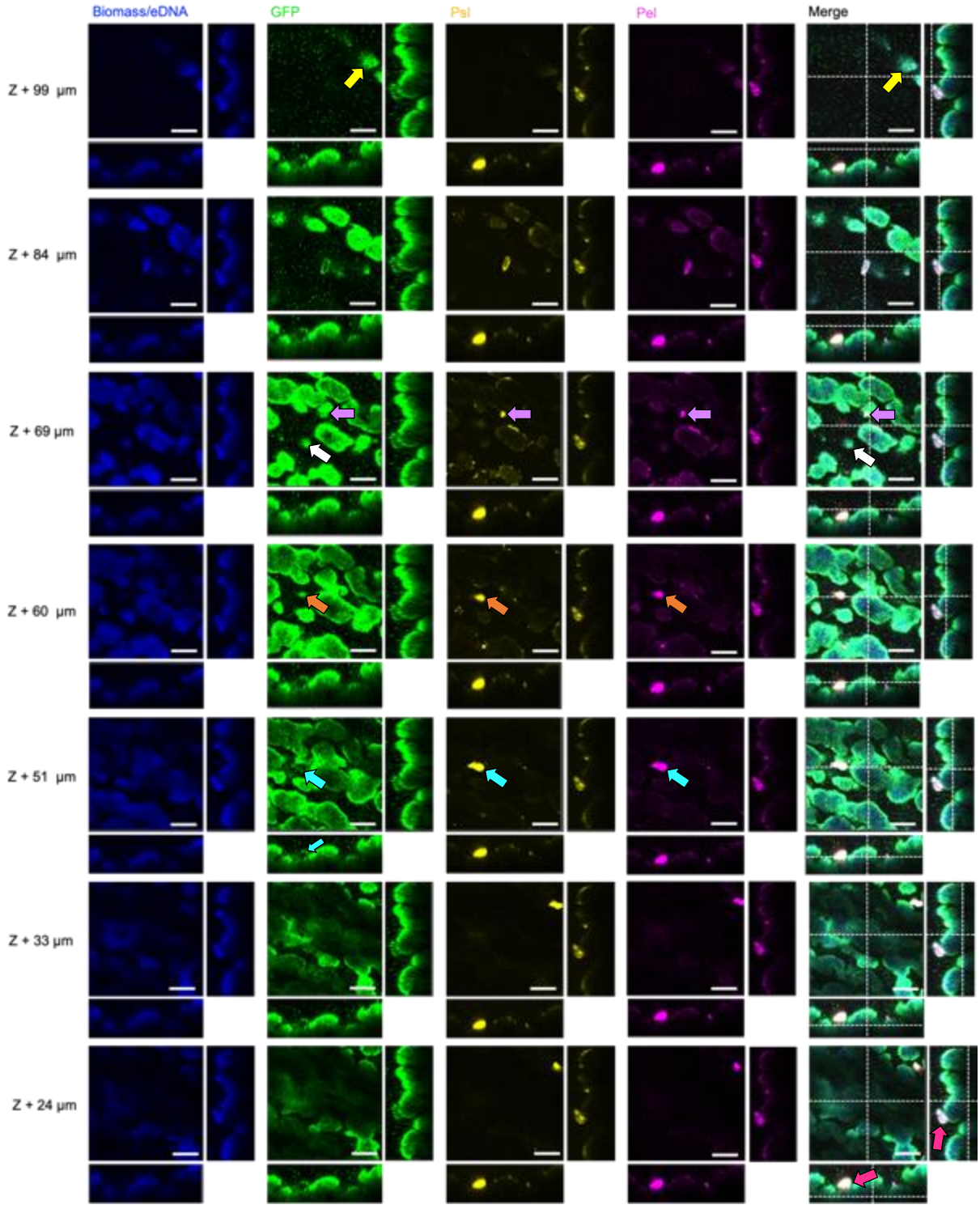

(*figure legend for* Figure 4.13)

Representative confocal images are from PA01 *cdrA::gfp* biofilms (GFP signal is green) cultivated for 72 hours in the CBR under high shear (at 350 RPM) and stained with Hoechst for biomass/eDNA (blue), the Psl-specific lectin ConA (yellow) and the Pel-specific lectin WGA (magenta). Different z heights are shown for the same sample area, with Z defined as the bottom layer closest to the coupon surface. Scale bar = 50 μm. White arrows and yellow arrows show mound apexes reaching different maximum heights to one another. Cyan arrows show a dense Psl and Pel co-aggregate, which is encapsulating a chain-like formation of individual PA01 cells. Orange arrows show the subsequent formation of a cell subpopulation associated with the Psl and Pel co-aggregate. Lilac arrows show another Psl-Pel aggregate associating with a specific and local subpopulation of cells. Cerise arrows show the the co-aggregate structure is mainly comprised of exopolysaccharide material and protrudes into the surround bulk fluid.

Figure 4.13 shows top-down z slices and side-views of the mound structures with increasing biofilm height, with Z defined as the bottom layer closest to the coupon surface. Maximum heights reached by mounds was variable, resulting in a lack of structural homogeneity. At a height of Z+69 μm, the apical layers of some mound structures were emerging, as demonstrated by their smaller dimensions in the x and y dimensions, and increased GFP fluorescence across structure periphery and interior (Figure 4.13, white arrows), whilst other mound apexes did not emerge for a further 30 μm in the z dimension (Figure 4.13, yellow arrows). Mounds exhibited increased Hoechst and GFP fluorescence at their growing apexes in comparison to the lower basal layers of the interior structure, which exhibited very little staining by Hoechst, ConA or WGA, and negligible GFP fluorescence.

This suggests that the basal layers of PA01 mound structures as shown in Figure 4.13 could have reduced metabolic activity, due to nutrient limitation or depravation (Walters *et al.,* 2003; Madsen *et al.,* 2007), whilst the apical layers of the biofilm continued to grow vertically into the bulk fluid, in order to gain access to nutrients and oxygen (Madsen *et al.,* 2007; Serra and Hengge, 2014). At 48 hours, PA01 biofilms under high shear at 350 RPM were already spatially-separated, and did not laterally spread to form a confluent and well-established basal biofilm, as seen under low shear at 75 RPM. Therefore, accumulation of biomass likely occurred through clonal cell division, resulting in neighbouring cell populations being in competition with one another for finite concentrations of nutrients in the surrounding environment. The formation of complex structures that protrude upwards into the bulk fluid would maximise the surface area of the biofilm when nutrients are scarce, enabling acquisition of dissolved

nutrient substrates (Costerton *et al.,* 2007), whilst also outcompeting neighbouring cell populations.

Staining of Psl by ConA and Pel by WGA was poor, therefore it was difficult to ascertain the functional roles of either exopolysaccharide in maintaining the structure and integrity of the mounds. Throughout the representative CLSM images shown in Figure 4.13, a dense co-aggregate of Psl and Pel can be seen from a height of Z+51 μm, localised to an area comprising a subpopulation of cells in an aggregate, immediately adjacent to a small population of GFP-expressing cells organised in a chain-like procession (Figure 4.13, cyan arrows). At a height of Z+60 μm, the Psl-Pel co-aggregate can be seen encapsulating a rounder cell structure (Figure 4.13, orange arrows), possibly to protect the PA01 cells from risk of detachment under high shear conditions. Other Psl-Pel complexes were additionally observed, and exhibited heterogeneity with respect to location within the mound structures and morphology of Psl and Pel.

Kragh *et al.,* (2016), used a combination of computer-simulated biofilm-formation and biofilm formation in flow cells to compare the relative fitness of individual *Ps. a.* cells versus cell aggregates during competition for nutrients. Aggregates were shown to have an advantage over individual cells when competition was high, due to their ability to rapidly grow upwards; gaining improved access to nutrients. Growth under high shear at 350 RPM in the CBR appeared to induce high levels of competition between neighbouring subpopulations of cells, which were frequently observed growing atop of one another; forming irregular three-dimensional structures in order to gain a fitness

advantage at the local, subpopulation level. Previous simulations have revealed that increased production of aggregative exopolysaccharides (such as Psl and Pel) may contribute to the increased fitness of producer populations (Xavier and Foster 2007), giving cells within apical layers of the biofilm a growth advantage, purported to be maintained through kin selection and its associated benefits (Hamilton, 1964).

Two Psl-Pel aggregates were co-localised with small populations of GFP-expressing PA01 cells (Figure 4.13, cyan arrows and lilac arrows). The two co-aggregative structures can be seen on representative side-views protruding into the surrounding bulk fluid (Figure 4.13, cerise arrows), forming predominantly ECM-composed mound apexes, which will protect associated cell populations from high shear conditions and may provide an aggregative scaffold, upon which vertical growth can continue. However, protrusion of 'tower'-like structures too far into the surrounding fluid under high shear conditions is likely to results in erosion or sloughing of the biofilm (Salek *et al.,* 2009), as illustrated by single PA01 GFP-expressing cells in the field of view, floating in the PBS-filled sampling dish (Figure 4.13, from a height of Z+60 μm).

4.3.4. Re-organisation of the macrocolony interior structure after 96 hours under low shear at 75 RPM

Mushroom-shaped macrocolonies were once again frequently observed after growth under low shear at 75 RPM for 96 hours, whilst the basal biofilm remained well-established and generally homogenous with respect to Hoechst, GFP, Psl and Pel fluorescence across the basal layers. Basal biofilms displayed increased heterogeneity

with respect to overall height in the z dimension, ranging on average from 10 – 30 μm in height.

Ma *et al.,* (2009), presented representative CLSM images of flow-cell grown PA01 biofilms showing the formation and differentiation of the Psl matrix at each stage of development in the prototypical *Ps. a.* biofilm lifestyle. Of interest was the fact that the macrocolony structure in Figure 4.14, grown for 96 hours under low shear at 75 RPM, exhibited similarities with respect to Psl morphologies observed by Ma *et al.,* (2009), to be involved in preparation for seeding dispersal and release of planktonic cells.

From a height of Z+15 μm, spatially-localised accumulation of Psl at the emerging macrocolony periphery was observed, in either dense aggregates or as linear chain-like structures (Figure 4.14, red arrows). Although staining of the macrocolony by Hoechst and WGA (for Pel) was limited, there is evidence of punctate Pel production co-localised to Psl at the periphery. Accumulation of Psl around the macrocolony periphery was initially seen in areas that exhibited slightly reduced GFP fluorescence in comparison to adjacent cell populations (Figure 4.14, pink arrows), with GFP fluorescence around the periphery more homogenous by a height of Z+32 μm (Figure 4.14, yellow arrows). Therefore, active synthesis of Psl in specific peripheral areas may maintain structural integrity of the macrocolony exterior, through enhanced cell-cell interactions, perhaps in response to localised changes in physiological parameters.

Of interest is the macrocolony interior, which was observed to be comprised of a Psl fibre-like matrix surrounding a secondary cavity (devoid of cells) from a height of Z+15

**Figure 4.14**

**Preparation of a PA01 macrocolony structure for seeding dispersal after 96 hours under low shear at 75 RPM**

*(figure legend overleaf)*

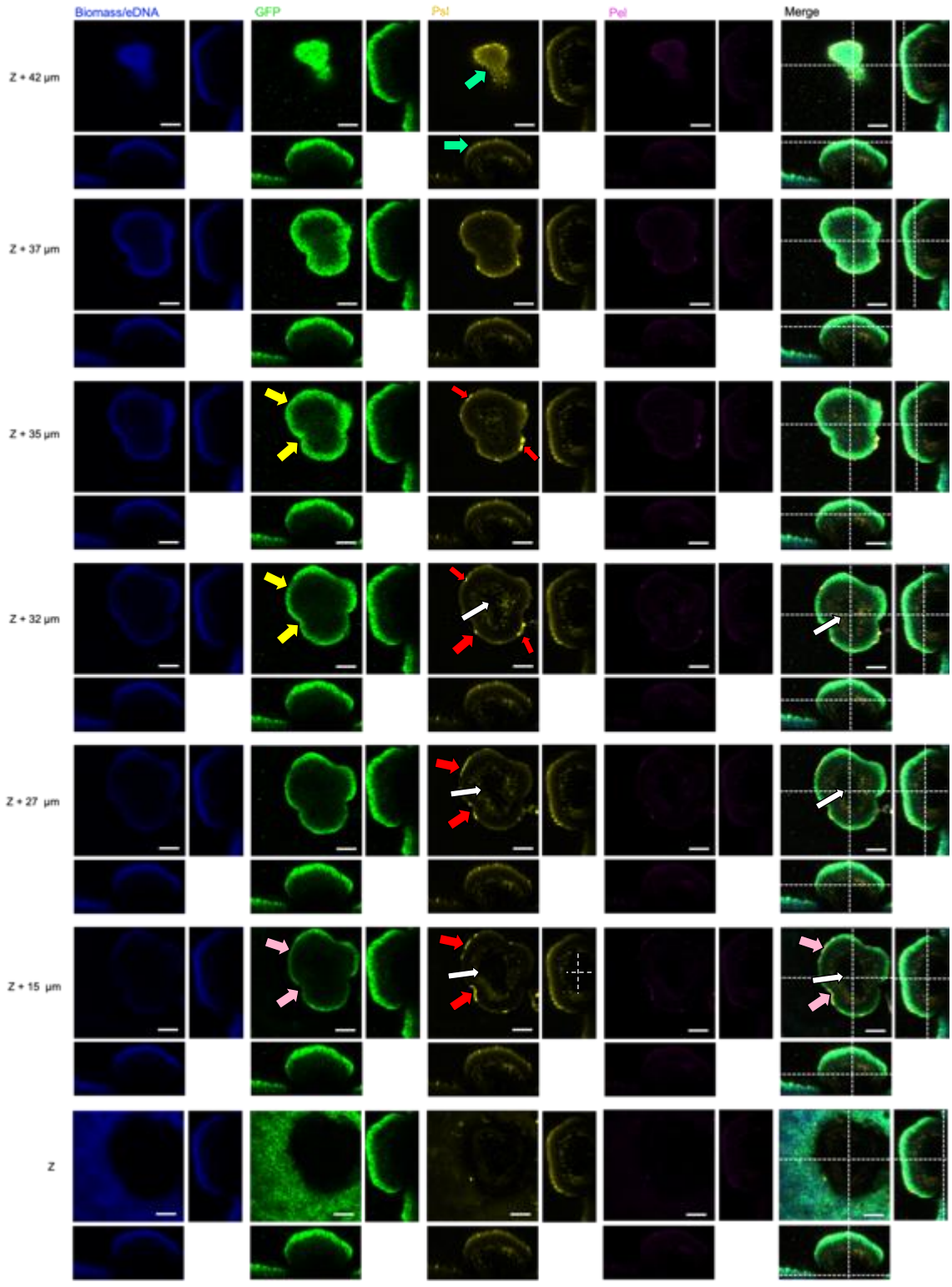

(*figure legend for* Figure 4.14)

Representative confocal images are from PA01 *cdrA::gfp* biofilms (GFP signal is green) cultivated for 96 hours in the CBR under low shear (at 75 RPM) and stained with Hoechst for biomass/eDNA (blue), the Psl-specific lectin ConA (yellow) and the Pel-specific lectin WGA (magenta). Different z heights are shown for the same sample area, with Z defined as the bottom layer closest to the coupon surface. Scale bar = 50 μm. Red arrows show spatial accumulation of Psl in specific regions of the macrocolony periphery. Pink arrows show areas of decreased GFP fluorescence co-localised to increased Psl accumulation, whilst yellow arrows show with increasing height the macrocolony circumference becoming more homogenous with respect to GFP expression. White arrows show the formation of a central void within the macrocolony interior, surrounding by an interior matrix of Psl. White dashed lines show the maximum dimensions of the central void. Green arrows show that macrocolony apex is covered in Psl, which may suggest the macrocolony is in preparation for seeding dispersal and disruption of apical ECM layers.

μm to Z+32 μm (Figure 4.14, white arrows). This is analogous to a Psl matrix structure seen by Ma *et al.,* (2009), formed by PA01 in preparation for active dispersion from the mature biofilm structure. CSLM by Ma *et al.,* (2009), showed that the preparation of a Psl matrix within the cavity interior preceded the appearance of swimming cells within the Psl-surrounded cavity, which itself was indicative of a mature structure undergoing active dispersion of PA01 cells. After dispersion, an empty hole remained, surrounded by the Psl fibre-like matrix which remained intact after cell dispersal (Ma *et al.,* 2009). Representative CSLM side-views of the Psl matrix within the macrocolony interior as shown in Figure 4.14 revealed the presence of an central area devoid of cellular or other ECM material; measuring approximately 100 μm in length and 60 μm in width (white dashed lines). In agreement with Ma *et al.,* (2009), this would suggest that organisation of the Psl matrix in this manner denotes that the macrocolony was undergoing structural modulation, in preparation for cell dispersal from the structure.

However, in contrast to Ma *et al.,* (2009), a defined hole within the apical ECM layers of the macrocolony were not observed, and the structure apex was intact; exhibiting homogenous Hoechst and GFP fluorescence and punctate accumulation of Psl across its exterior (Figure 4.14 at a height of Z+42 μm). At a height of Z+37 μm, the interior Psl matrix can be seen directly above the top of the central void, rather than surrounding it (Figure 4.14, green arrows), which further suggests that the macrocolony was preparing for, but not actively participating in, dispersion. Given the similarities to the observations of Ma *et al.,* (2009), it is feasible to suggest that Psl matrix may have been undergone further remodelling in the apical layers of the

macrocolony with increased time, in order to eventually form a continuous and unobstructed central void, from which dispersed cells could be released.

After 96 hours of growth under high shear at 350 RPM, PA01 biofilms reached an average height of 100 – 200 μm, making fluorescence intensity profiles for Hoechst, GFP, Psl and Pel difficult to calculate, due to the reduced laser and stain penetration of the structures. As such, inference of biofilm development at this stage was challenging, as demonstrated by Figures 4.15 and 4.16 which show towering, mound structures, the tallest of which are 150 μm and 135 μm in height (in the z dimension) respectively.

As previously observed after 72 hours of growth under high shear conditions, after 96 hours at 350 RPM a co-aggregate of dense Psl and Pel was observed; maintained vertically over a height of > 50 μm and protruding into the surrounding bulk fluid (Figure 4.16, white arrows). Increased Psl and Pel fluorescence of the aggregate was uncorrelated to either Hoechst or GFP fluorescence, which suggests that the co-aggregate structure was free rather than cell-associated, and composed predominantly from exopolysaccharides (Figure 4.16, cyan arrows). Such aggregates have not been described in the literature previously to the author's knowledge, and were not induced under low shear conditions in the CBR of 75 RPM.

**Figure 4.15**
**Mound formation by PA01 cell populations after 96 hours under high shear at 350 RPM is characterised by competitive vertical growth into the bulk fluid**

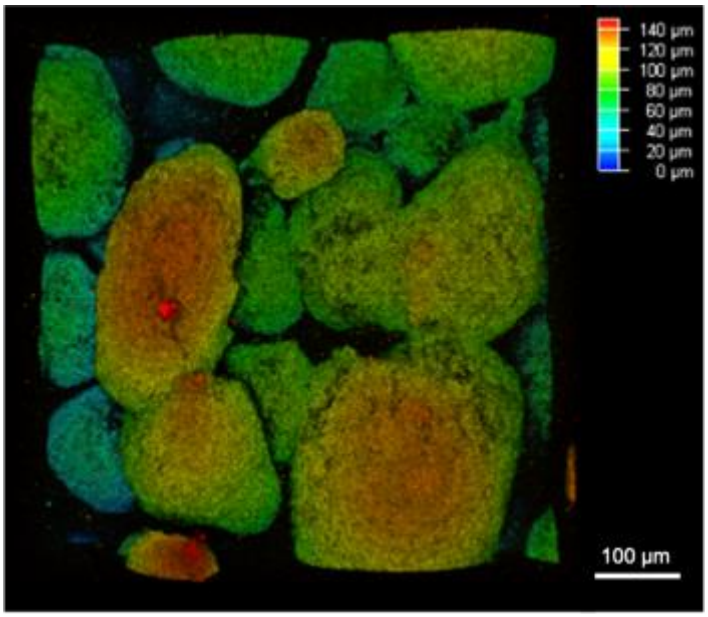


Representative top-down and maximum CSLM image, showing the variability in individual mound structure heights. The image is coloured coded to indicate areas of mound structures which are of a comparable height to one another, location of the tallest structures (in shares of orange and red) as well as the apexes of mound structures that have been outcompeted (in shades of blue). Scale bar = 100 μm.

Based on the maximum projection CLSM images (Figure 4.16), the dense Psl-Pel co-aggregate appeared elongated in the x dimension, with an approximate length of 50 μm and width of 20 μm. The co-aggregate was irregular in structure, with one periphery observed to have a narrower, tapered appearance; connecting the co-aggregate to an adjacent mound structure (Figure 4.16, orange arrows). The concentration and morphology of exopolysaccharides defines the immediate local environment that cell populations will be exposed to (Flemming, 2011), thus the dense Psl-Pel co-aggregate likely has a specific function, perhaps in relation to the neighbouring cell population it is connected to.

Charged or hydrophobic exopolysaccharides have been shown to facilitate sorption of organic compounds, enabling accumulation of nutrients from the surrounding environment, whilst additionally serving as reservoirs for carbon storage under metabolic conditions that result in unbalanced carbon to nitrogen ratios (Flemming, 2011). Exopolysaccharides enable retention and stabilisation of exoenzymes (which are at risk of being washed away under high shear conditions), such as hydrolases and lyases that have been shown to degrade *Ps. spp.* polysaccharide material into structures with lower molecular mass, for utilisation as an energy source as required (Laue *et al.,* 2006; Ude *et al.,* 2006; Flemming, 2011). Exopolysaccharides themselves are also likely to be a source of carbon and nitrogen for utilisation by cell populations, thus the dense aggregate of Psl-Pel may be involved in nutrient capture, accumulation and storage, which would be advantageous for the associated cell population under nutrient-limited and competitive growth conditions, as experienced under high shear at 350 RPM.

**Figure 4.16**
**Increased vertical height of PA01 mound structures after 96 hours under high shear at 350 RPM results in reduced laser and/or stain penetration through the biofilm**

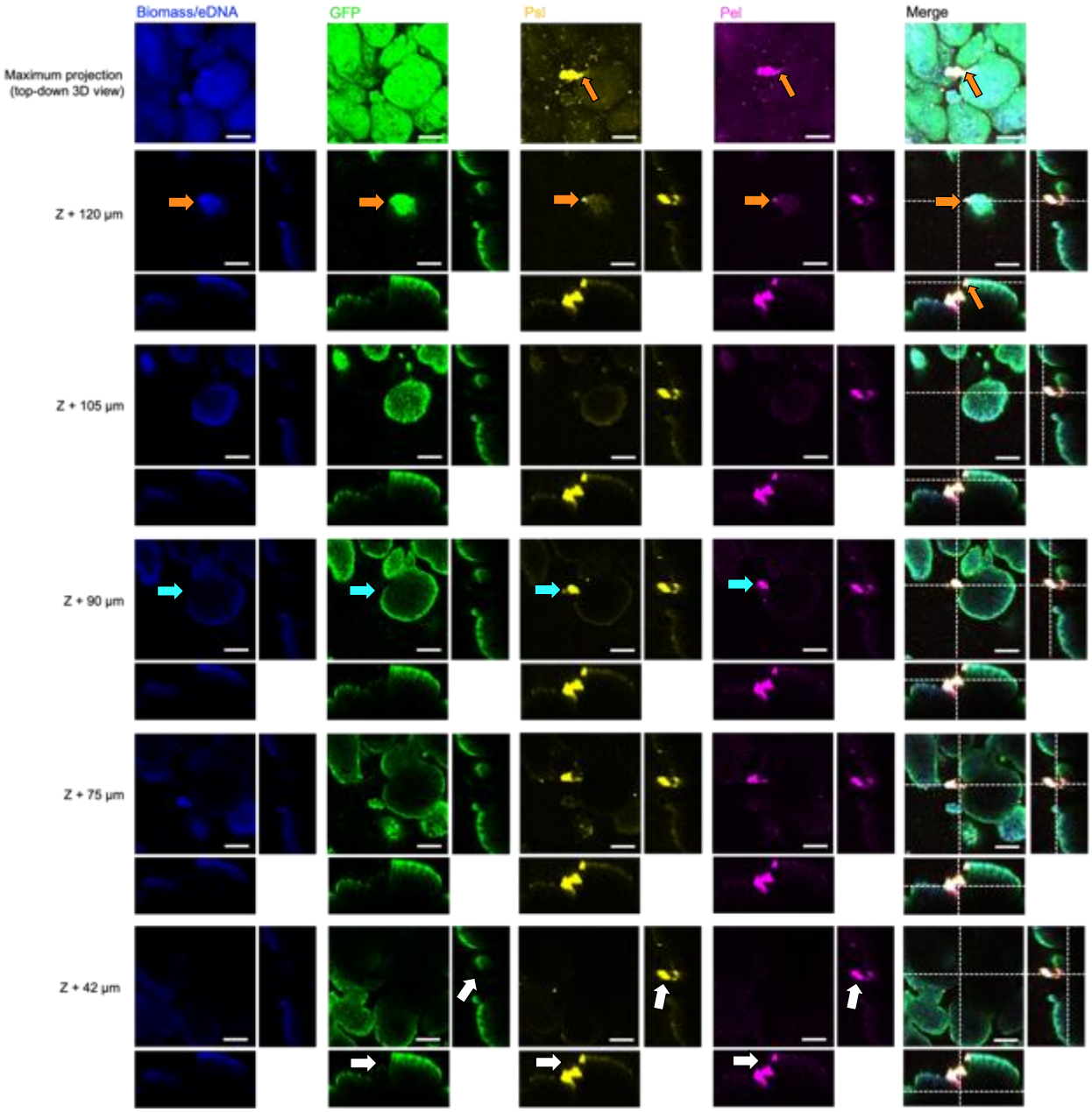


Representative confocal images are from PA01 *cdrA::gfp* biofilms (GFP signal is green) cultivated for 96 hours in the CBR under low shear (at 75 RPM) and stained with Hoechst for biomass/eDNA (blue), the Psl-specific lectin ConA (yellow) and the Pel-specific lectin WGA (magenta). Different z heights are shown for the same sample area, with Z defined as the bottom layer closest to the coupon surface. Scale bar = 50 µm. White arrows show a dense Psl and Pel co-aggregate of height in the z dimension of approximately 50 µm. Cyan arrows show the co-aggregate is independent of a GFP-expressing cell population. Orange arrows show a tapered part of the co-aggregate associating with a neighbouring mound structure at its apex.

## 4.4. Discussion

The results presented in this chapter demonstrate that industrially-relevant low and high shear regimes, as modelled by the CBR at 75 versus 350 RPM respectively, have an impact upon PA01 biofilm formation, across all stages of development over a time period of 96 hours.

### 4.4.1. Summary of chapter

Growth in the CBR under low shear at 75 RPM resulted in the formation of biofilms that followed the accepted 'biofilm lifestyle' model; characterised by archetypal *Ps. a.* mushroom-shaped macrocolony formation. Biofilm development under low shear resulted in the formation of a confluent basal biofilm, through which a fibre-like networks of Psl was observed (Figure 4.12), which may facilitate TFP-mediated migration of cells to different parts of the biofilm in a spatial and temporal manner, to initiate microcolony and subsequent architectural development, in agreement with the works of Wang *et al.,* (2013), and Zhao *et al.,* (2013). Staining of fibre-like networks by WGA indicated the additional presence of Pel, suggesting that both exopolysaccharides contribute to network formation in PA01 basal biofilms. Chew *et al.,* (2014), reported that a Psl-dominant matrix is more elastic and stronger when crosslinked; able to centralise growth to newly-colonised sites, whilst a Pel-dominant exhibits less cross-linking, resulting in a 'looser' and more malleable structure. Therefore, having a heterogeneously-composed fibre-like network may enable more dynamic remodelling of the ECM to facilitate lateral spreading of the biofilm and structural maturation (i.e. macrocolony development). Psl and Pel were often found co-

localised, forming heterogenous structures, which suggests possible synergy between the two exopolysaccharides. Yang *et al.,* (2011), has previously demonstrated that Psl and Pel are important for facilitating interactions between subpopulations of cells during PA01 biofilm differentiation, thus both exopolysaccharides are likely mediating cell-cell interactions and maintenance of structure's three-dimensional architecture, through specific rather than redundant functions contributing to biofilm formation. Colvin *et al.,* (2011), proposed that the ability to produce both Psl and Pel is advantageous; the exopolysaccharides are chemically and structurally distinct from one another, which likely influence the individual functions of Psl and Pel in PA01 biofilms, and enables the bacteria to respond to a wider range of environmental conditions (Friedman and Kolter, 2004a; Byrd *et al.,* 2009; Coulon *et al.,* 2010).

Growth in the CBR under high shear at 350 RPM by contrast resulted in earlier and increased production ECM matrix components, in order to protect attached cells from risk of shear-induced detachment and increase both cell-surface and cell-cell interactions due to enhanced 'stickiness'. Increased aggregation of early clusters and microcolonies was observed, which suggests that shear stress can induce structural (and likely functional) changes to Psl and Pel morphologies, as bacteria adapt to the adverse environmental condition. Fibre-like networks of eDNA, Psl and Pel were not seen under high shear, nor was the formation of a confluent basal biofilm. Instead, the biofilm was fragmented, leading to competitive rather than cooperative structure differentiation and maturation, due to increased nutrient consumption as a result of increased synthesis of ECM components. After 72 hours of growth at 350 RPM, mature PA01 mound structures were already in excess of 100 μm in height, and exhibited

degrees of erosion and sloughing of parts of the biofilm, as a result of increased shear stress and protrusion of towering mound structures too far into the surrounding fluid (Salek *et al.,* 2009).

### 4.4.2. Concluding remarks

The strength of shear fluid forces in a local environment can critically influence both microbial adhesion (Bucssher and van der Mei, 2006) and biofilm development (Stoodley *et al.,* 1999; Liu and Tay, 2002). Under low shear at 75 RPM, biofilm development by both PA01 and PA14 generally followed the accepted 'biofilm lifestyle' model, and observed morphologies for Psl and Pel were analogous to those in the literature (Ma *et al.,* 2009; Jennings *et al.,* 2015), in spite of the differences between experimental systems. For example, central void formation and modulation by a Psl matrix within a macrocolony interior was observed after 96 hours under low shear (Figures 4.7 and 4.13c). Ma *et al.,* (2009), grew PA01 biofilms in flow cells, and utilised a different Psl-specific lectin, but the morphology and organisation of the interior Psl matrix they observed was similar to the one shown in Figure 4.14. Inference of mature PA01 biofilm development (> 72 hours growth) and Psl and Pel morphologies induced by the high shear condition at 350 RPM was more challenging, due to the increased vertical growth of mound structures in the z dimension, that subsequently made analysis by CLSM difficult due to lack of laser and stain penetration of lower basal layers of biofilm structures. Nevertheless, it was apparent that high shear conditions induced the formation of more aggregative structures in comparison to low shear. Ultimately, shear conditions were shown to influence population dynamics within PA01 biofilms, as well as ECM composition and function in adaptation to hydrodynamic

conditions, in agreement with characterisation of PA14 biofilm formation under the same shear regimes as presented in Chapter 3.

# Chapter 5: Analysis of curli gene expression in the *Escherichia coli* strain K-12 PHL644

# Chapter 5: Analysis of curli gene expression in the *Escherichia coli* strain K-12 PHL644

Experimental work in this chapter was performed in conjunction with Stacey Golub and is published in: Leech J, Golub S, Allan W, Simmons MJH, Overton TW. (2020) Non-pathogenic *Escherichia coli* biofilms: effects of growth conditions and surface properties on structure and curli gene expression. *Arch Microbiol*. **202**:1517-1527. doi: 10.1007/s00203-020-01864-5.

## 5.1. Introduction

Multiple studies have previously demonstrated that *E. coli* biofilm formation can be greatly affected by both the type of growth medium used, and the components within the medium itself (Pratt and Kolter, 1998; Prigent-Combaret *et al.,* 2000; Naves *et al.,* 2008). Previous work in the Overton Laboratory has demonstrated that *E. coli* K-12 PHL644 was able to form more surface-associated biofilm in M63+ minimal medium compared to nutrient-rich LB broth when grown on PTFE-covered microscope slides in Duran bottles (Leech 2017). Furthermore, CLSM showed that biofilms grown in M63+ minimal medium were on average over three-fold thicker than those grown in LB broth (Leech, 2017).

Concentration of glucose is known to affect biofilm formation, through a process known as or catabolite repression (Jackson *et al.,* 2002; Hufnagel *et al.,* 2016). Catabolite repression describes the principal inhibitory effect of glucose on gene expression in

bacteria, whilst transient repression occurs after the addition of glucose to cells growing in the presence of other carbon sources (Ishizuka *et al.,* 1993; Tagami *et al.,* 1995). One of the most well-known global regulatory networks in *E. coli*, catabolite repression is mediated by the activity of the intracellular second messenger cAMP and the cAMP-receptor protein (CRP) (Gottesman, 1984; Jackson *et al.,* 2002; Ishizuka *et al.,* 2003). When cAMP is bound to CRP, the resulting complex has a high affinity and specificity for promoter regions of cAMP-regulated genes to either activate or repress their transcription (Jackson *et al.,* 2002). Examples of operons under control of the cAMP-CRP complex include *flhDC*, which encodes the activator protein that results in expression of flagellar components (Pratt and Kolter, 1998; Soutourina *et al.,* 1999) and *glgCAP*, which encodes for enzymes involved in the biosynthesis and degradation of glycogen (Romeo *et al.,* 1989; Romeo *et al.,* 1990; Jackson *et al.,* 2002).

In the presence of glucose, its transport across the bacterial membrane leads to dephosphorylation of the phosphoenolpyruvate-sugar phosphotransferase system, which prevents the activation of CyaA and consequently cAMP production (Jackson *et al.,* 2002; Ishizuka *et al.,* 2003). Makman and Sutherland, (1965), were the first to show that cAMP levels in *E. coli* respond to the presence or absence of glucose in growth medium, whilst Perlman *et al.,* (1969) demonstrated that the addition of exogenous cAMP to *E. coli* cultures grown in minimal medium overcame both catabolite and transient repression. In addition to eliciting an effect on cAMP, glucose has also been shown to decrease the expression of *crp*, leading to a decrease in CRP levels and subsequently the concentration of cAMP-CRP complexes available (Ishizuka *et al.,* 2003).

Although some studies have suggested that higher glucose concentrations can promote biofilm formation (Bühler *et al.,* 1998; Teodósio *et al.,*2011), others within the literature agree that the presence of glucose generally inhibits biofilm formation and the metabolism of alternative sugars (Makman and Sutherland, 1965; Tagami *et al.,* 1995; Jackson *et al.,* 2002; Ishizuka *et al.,* 2003). Previous research undertaken in the Overton Laboratory demonstrated that the standard recipe for M63+ minimal medium, which includes 10 mM glucose, resulted in the most biofilm formation by *E. coli* K-12 PHL644 (Leech, 2017).

Temperature is also known to affect *E. coli* biofilm formation (Barnhart and Chapman, 2006; Rühs *et al.,* 2013; Uhlich *et al.,* 2014). In *E. coli*, RNA polymerase is composed of a core enzyme (*E*) which can associate with a total of seven different sigma factors subunits ($\sigma$) to form the holoenzyme *E*$\sigma$ (Bougdour *et al.,* 2004). Encoded by the *rpoS* gene, the sigma factor $\sigma^s$ accumulates inside the cell in response to either the bacterium entering stationary phase, or exposure to stress conditions such as low pH, high osmolarity and high temperature (Small *et al.,* 1994; Ishihama, 2000; Hengge-Aronis, 2002; Robbe-Saule *et al.,* 2006). Accumulation of $\sigma^s$ and its association with the core enzyme of RNA polymerase thusly results in the transcription of genes fundamental for survival in stationary phase, or in response to environmental stress (Lange and Hengge-Aronis, 1991; Lelong *et al.,* 2007).

The thermosensitive regulatory protein Crl can stimulate the activity of $\sigma^s$; interacting directly with the sigma factor to control the binding of the holoenzyme *E*$\sigma^s$ to its target promoters (Bougdour *et al.,* 2004; Brombacher *et al.,* 2006; Robbe-Saule *et al.,* 2006).

Pratt and Silhavy, (1998), revealed that Crl stimulates $\sigma^s$ activity *in vivo* in stationary phase, whilst Bougdour *et al.,* (2004), demonstrated Crl binding to the $\sigma^s$ subunit *in vitro* and revealed that expression of Crl occurs in parallel to the presence of $\sigma^s$ within the cell. Crucially, Crl stimulates the transcription of the *cgsBA* promoter in a $\sigma^s$-dependent manner, resulting in the expression of curli subunits and secretion apparatus (Olsen *et al.,* 1993; Arnqvist *et al.,* 1994; Brombacher *et al.,* 2006). Work by Pratt and Silhavy, (1998), revealed that a *crl* null strain of *E. coli* resulted in a four-fold reduction in transcriptional activity of the *csgBA* promoter in comparison to the wild-type, and that mutations in *crl* successively affected all $\sigma^s$-regulated processes they analysed.

A temperature of 30 $^oC$ is known to induce both *crl* and $\sigma^s$ expression (Lelong *et al.,* 2007), whilst transcription of *csgBA* is activated by Crl at 30 $^oC$ but not at 37 $^oC$ (Bougdour *et al.,* 2004; Barnhart and Chapman, 2006; Brombacher *et al.,* 2006). Further to this, work by Gauldi *et al.,* 2008, suggested that *E. coli* K-12 grown at 32 $^oC$ produces more curli than at 37 $^oC$. Growth of *E. coli* K-12 PHL644 at 30 $^oC$ has previously been shown to be the optimal temperature for biofilm formation in the Duran bottle method (Leech, 2017).

The aim of this body of work was to evaluate the effect of physiological conditions have on curli expression in *E. coli* K-12, through use of an existing and established biofilm model in the Overton laboratory, in order to identify parameters that result in optimal curli expression.

## 5.2. Methodology

All experiments used the Duran bottle model to generate biofilms of transformed *E. coli* K-12 PHL644 cultures (containing the *csgB::gfp* reporter), which were incubated at 30 $^{o}$C and 70 RPM unless otherwise stated. At regular time intervals, 1 mL samples were taken from the top and bottom of the Duran bottles, comprised of planktonic culture and sedimented cells respectively. Growth was then analysed via spectrophotometry at $OD_{600}$ and GFP fluorescence of samples analysed via flow cytometry. All Duran bottles were prepared and inoculated in duplicate.

### 5.2.1 Investigation of the effect of rich versus minimal M63+ medium

To explore the effects of rich versus minimal medium on curli expression, *E. coli* K-12 PHL644 reporter cells were grown in either LB broth or M63+ minimal medium, for a total of 30 hours.

### 5.2.2. Investigation of the effect of glucose

To examine the effects of glucose concentration on curli expression, modifications to the M63+ minimal medium 'recipe' were made, as outlined in Table 5.1. In each case, the volume of water added was adjusted to give a total volume in the Duran bottles of 70 mL, with no other changes to the remaining medium components. Duran bottles were incubated for a total of 30 hours initially, and then for 56 hours in succeeding experiments.

**Table 5.1. Modifications to M63+ minimal medium to investigate the effect of different glucose concentrations on curli expression**

| Component | Concentration of stock solution | Desired final concentration | Volume added |
|---|---|---|---|
| D-glucose | 1 M | 0 mM | None |
| | | 1 mM | 70 μL |
| | | 10 mM * | 700 μL |
| | | 100 mM | 7 mL |

* 10 mM is the typical concentration of glucose in M63+ minimal medium.

### 5.2.3. Investigation of the effect of temperature

Preliminary work by Leech, (2017) demonstrated that biofilm formation by *E. col* K-12 PHL644 reporter cells was highest at 30 $^{o}$C, whilst Golub, (2019), showed that temperatures of 28 $^{o}$C and 30 $^{o}$C resulted in very similar curli expression profiles over a time period of 24 hours. In order to determine the optimal temperature for maximum curli expression, Duran bottles containing M63+ minimal medium were incubated at either 25 $^{o}$C, 28 $^{o}$C, 30 $^{o}$C or 37 $^{o}$C and 70 RPM, for a total of 56 hours.

## 5.3. Results

### 5.3.1. Curli expression is greater in M63+ minimal medium compared to LB broth

Building upon previous work in the Overton laboratory by Leech, (2017), in which analysis of biofilm formation by crystal violet staining indicated that M63+ minimal medium led to increased biofilm accretion than LB broth, the effect of minimal versus rich medium on curli expression was investigated. It was hypothesised that richer LB broth would result in faster growth of *E. coli* K-12 PHL644 but lower curli expression

based on previous work in the literature, whilst M63+ minimal medium would contrariwise result in higher curli expression and reduced growth of the bacteria.

Curli expression was found to be highest in the planktonic cell samples (taken from the top of the Duran bottles) grown in M63+ minimal medium (Figure 5.1). During the initial eight hours, there was little difference in *csgB::gfp* fluorescence of planktonic and sedimented cells (from the bottom of the Duran bottles) grown in M63+ minimal medium: at 8 hours, *csgB::gfp* fluorescence of sedimented cells was only 7% higher than the fluorescence of planktonic cells. From 24 hours onwards, curli expression of planktonic cells grown in M63+ minimum medium greatly increased, and *csgB::gfp* fluorescence was 1296% higher at 30 hours than it was at 2 hours. In comparison, over the same time course from 2 hours to 30 hours, the *csgB::gfp* fluorescence of sedimented cells grown in M63+ minimal medium increased by 180%. By 24 hours, *csgB::gfp* fluorescence of planktonic cells grown in M63+ minimal medium was additionally 60% greater than sedimented cells grown in the same Duran bottles, and by the final timepoint of 30 hours, *csgB::gfp* fluorescence of the planktonic cells was 80% higher than the sedimented cells.

Both planktonic and sedimented cells grown in LB broth had poor curli expression, with *csgB::gfp* fluorescence remaining similarly very low for both planktonic and sedimented cells across all timepoints. The effect of LB broth on curli expression was noticeable during even the earliest timepoints: at 2 hours, *csgB::gfp* fluorescence of planktonic cells grown in LB broth was 71% lower than the fluorescence of planktonic cells grown in M63+ minimal medium, whilst *csgB::gfp* fluorescence of LB broth-grown sedimented cells was 77% lower than the fluorescence of sedimented cells grown in M63+ minimal

medium (Figure 5.1.). There was little difference in *csgB::gfp* fluorescence between planktonic and sedimented cells grown in LB broth as time increased. At 24 hours, *csgB::gfp* fluorescence of planktonic cells was just 12% higher than that of sedimented cells, whilst by 30 hours, *csgB::gfp* fluorescence of the sedimented cells was greater than the fluorescence of the planktonic cells by 13%.

**Figure 5.1**
**Expression of *csgB* in planktonic (top) samples and sediment (bottom) samples in rich versus minimal medium**

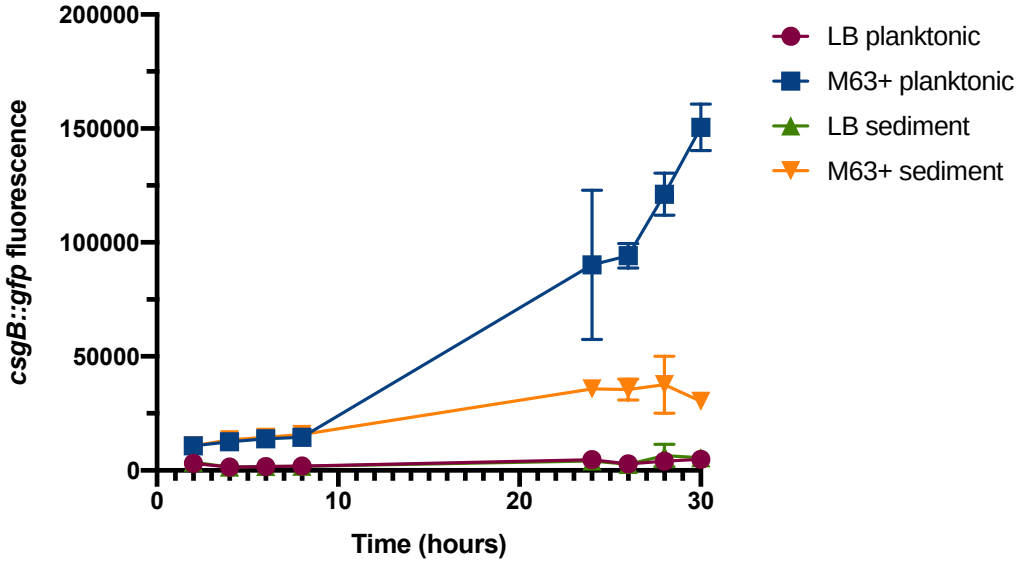


*E. coli* K-12 PHL644 transformed cells (carrying the *csgB::gfp* reporter) were grown in 70 mL of LB broth (rich medium) or in 70 mL M63+ minimal medium. GFP fluorescence of the reporter was measured by flow cytometry, with fluorescence values stated as arbitrary units as recorded by the BD Accuri C6 flow cytometer. Data shown are the mean ± standard deviation of the average GFP fluorescence of two independent cultures.

Curli expression was markedly higher in both the planktonic and sedimented cells grown in M63+ minimal medium compared to equivalent expression of curli by planktonic and sedimented cells grown in LB broth. By 24 hours, *csgB::gfp* fluorescence of planktonic cells grown in M63+ minimal medium was 95% higher than the fluorescence of LB broth-grown planktonic cells (Figure 5.2A), and *csgB::gfp*

fluorescence of sedimented cells grown in M63+ minimal medium was 88% higher than the fluorescence of sedimented cells grown in LB broth (Figure 5.2B). At the final timepoint of 30 hours, *csgB::gfp* fluorescence of planktonic cells grown in M63+ minimal medium was 97% greater than the fluorescence of LB broth-grown planktonic cells, whilst the *csgB::gfp* fluorescence of sedimented cells grown in M63+ minimal medium was 82% higher than that of LB broth-grown sedimented cells.

Flow cytometry histograms for each sample (Figure 5.3) indicated that cultures grown in LB broth were overall more heterogenous with respect to *csgB::gfp* fluorescence, and that both planktonic and sedimented cell populations were composed of a major population with low fluorescence at early timepoints, followed by the emergence of a second, “shoulder” cell population with slightly higher fluorescence from 24 hours onwards. In contrast, cultures grown in M63+ minimal medium were composed of two cell populations during early timepoints, which then developed into a single cell population with high *csgB::gfp* fluorescence from 24 hours onwards. For the final two timepoints however, sedimented cells grown in M63+ minimal medium displayed a shift from one cell population to two.

**Figure 5.2**
**Comparison of csgB expression in rich versus minimal medium**

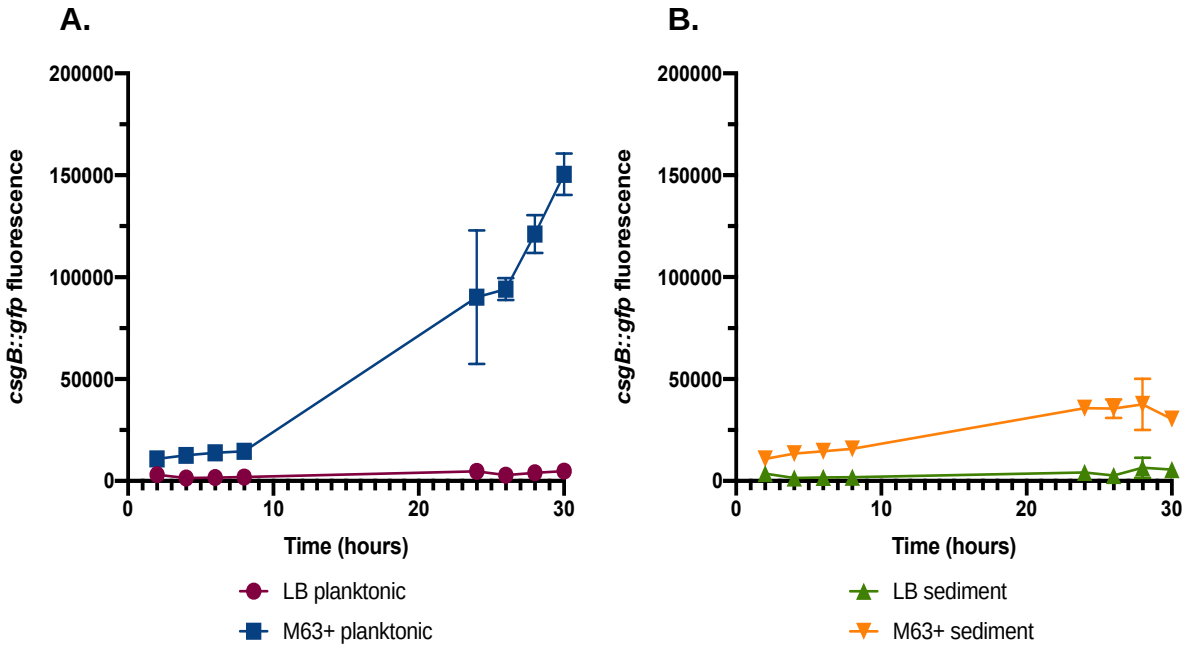


*E. coli* K-12 PHL644 transformed cells (carrying the *csgB::gfp* reporter) were grown in 70 mL of LB broth (rich medium) or in 70 mL M63+ minimal medium. GFP fluorescence of the reporter was measured by flow cytometry, with fluorescence values stated as arbitrary units as recorded by the BD Accuri C6 flow cytometer. Data shown are the mean ± standard deviation of the average GFP fluorescence of two independent cultures.

**Figure 5.3**

**Flow cytometry histograms corresponding to GFP fluorescence (recorded as FL1-A) under different growth medium, rich versus minimal**

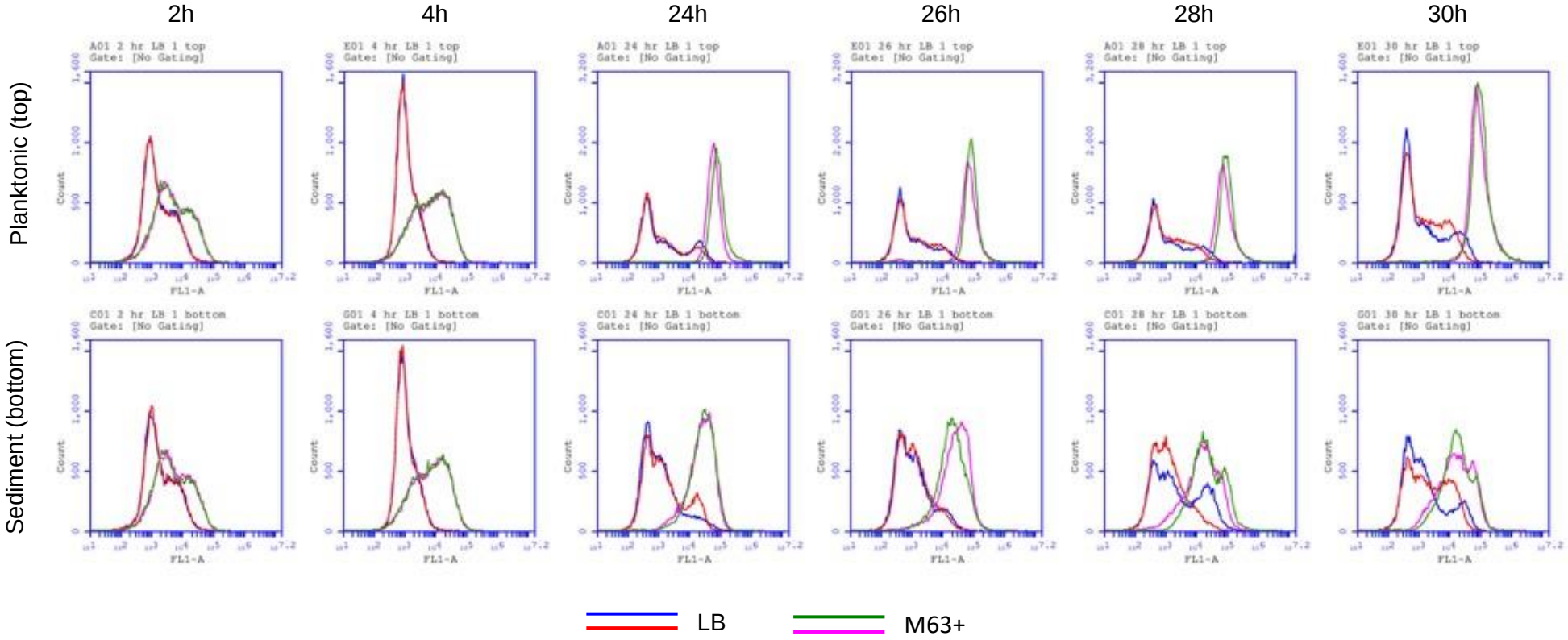


GFP fluorescence of the reporter was measured by flow cytometry, with fluorescence values stated as arbitrary units as recorded by the BD Accuri C6 flow cytometer. Histograms shown are the particle count versus the GFP fluorescence of two independent cultures (shown as different coloured traces).

5.3.2. Curli expression is greater in the presence of 10 mM glucose

Previous analysis of biofilm formation via crystal violet staining revealed that 10 mM glucose resulted in the greatest biofilm formation by *E. coli* K-12 PHL644 (Leech, 2017). A concentration of 10 mM is the standard concentration of glucose in M63+ minimal medium: it was hypothesised that lower concentrations of glucose at 0 mM and 1 mM would result in growth inhibition, whilst a higher glucose concentration of 100 mM would induce catabolite repression and resultantly lead to reduced biofilm formation.

Curli expression in the planktonic samples was overall highest in the presence of 10 mM glucose during later timepoints (Figure 5.4), which is in agreement with previously obtained crystal violet data (Leech, 2017). For the first 24 hours, curli expression was higher at glucose concentrations of both 0 mM and 1 mM. At 24 hours, *csgB::gfp* fluorescence was 29% higher in the absence of glucose (0 mM) than in the presence of 10 mM glucose, and *csgB::gfp* fluorescence 31% higher with 1 mM glucose compared to 10 mM glucose. From 24 hours onwards however, curli expression was greatest in M63+ minimal medium containing 10 mM glucose.

At the final timepoint of 56 hours, *csgB::gfp* fluorescence in the presence of 10 mM glucose was 33%, 13% and 74% higher than in the presence of 0 mM, 1 mM and 100 mM glucose respectively. Curli expression in planktonic samples was lowest in M63+ minimal medium supplemented with 100 mM glucose, across all timepoints. Over the time course of the experiment, the *csgB::gfp* fluorescence of planktonic cells grown in

10 mM glucose increased by 1418%, in comparison to the 300% increase in curli expression of planktonic cells grown in 100 mM glucose.

**Figure 5.4.**
**Expression of *csgB* in planktonic (top) samples under different glucose concentrations**

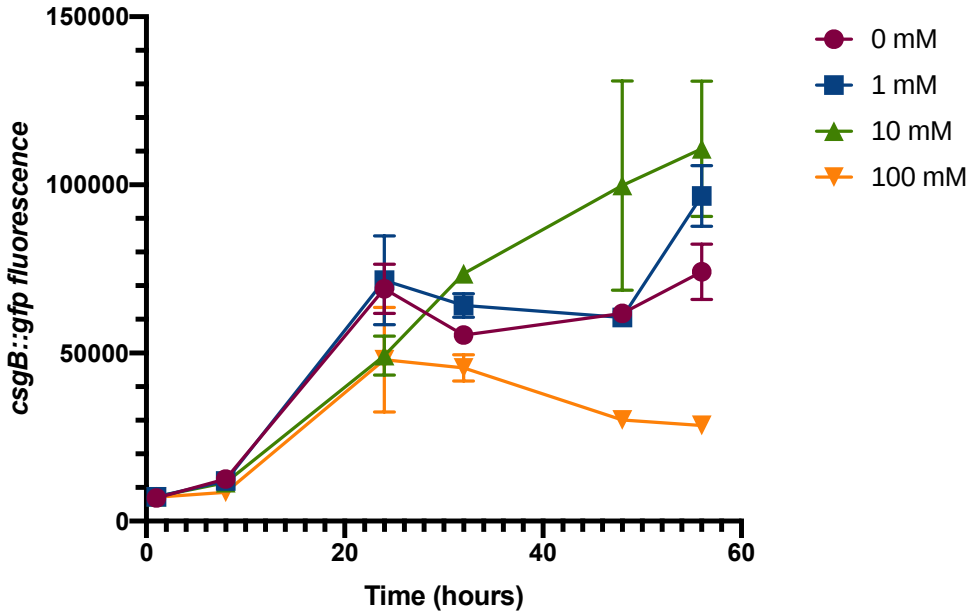


*E. coli* K-12 PHL644 transformed cells (carrying the *csgB::gfp* reporter) were grown in 70 mL M63+ minimal medium containing either 0, 1, 10 or 100 mM of glucose. GFP fluorescence of the reporter was measured by flow cytometry, with fluorescence values stated as arbitrary units as recorded by the BD Accuri C6 flow cytometer. Data shown are the mean ± standard deviation of the average GFP fluorescence of three independent cultures.

In comparison, curli expression in sedimented cells was lower than planktonic cultures taken from the top of the Duran bottles across all concentrations of glucose tested (Figure 5.5). In contrast to planktonic samples, in which the presence of 10 mM glucose resulted in the highest *csgB::gfp* fluorescence from 24 hours onwards, *csgB::gfp* fluorescence of sedimented cells was consistently highest in the absence of glucose, across all timepoints apart from at 56 hours. At 56 hours, *csgB::gfp* fluorescence in the presence of 1 mM glucose was 5%, 44% and 49% higher than in the presence of 0

mM, 10 mM and 100 mM glucose respectively. As with planktonic samples, expression of curli was the lowest in the presence of 100 mM glucose over time.

**Figure 5.5**
**Expression of *csgB* in sedimented (bottom) samples under different glucose concentrations**

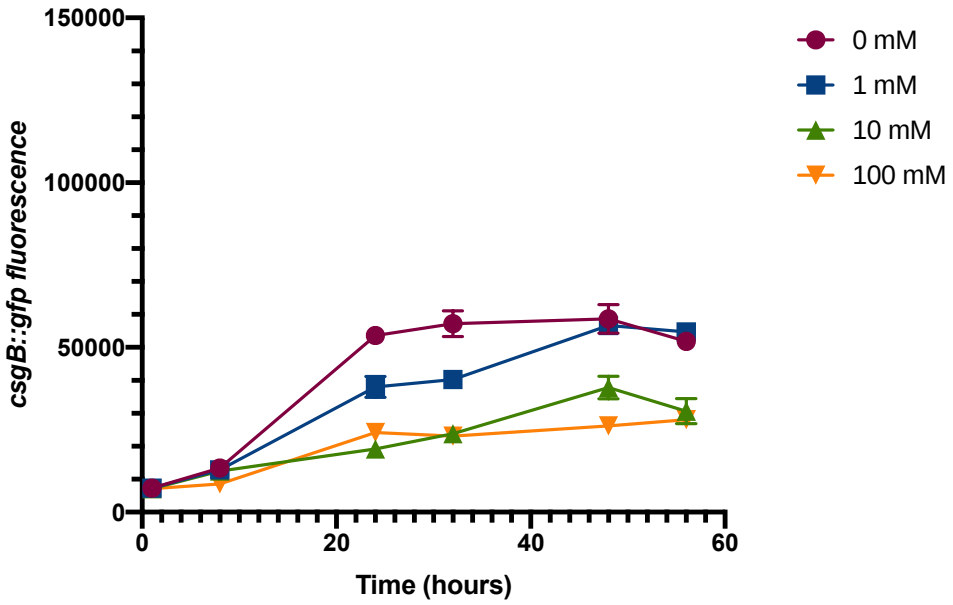


*E. coli* K-12 PHL644 transformed cells (carrying the *csgB::gfp* reporter) were grown in 70 mL M63+ minimal medium containing either 0, 1, 10 or 100 mM of glucose. GFP fluorescence of the reporter was measured by flow cytometry, with fluorescence values stated as arbitrary units as recorded by the BD Accuri C6 flow cytometer. Data shown are the mean ± standard deviation of the average GFP fluorescence of three independent cultures.

The greatest difference in *csgB::gfp* fluorescence between planktonic and sedimented cells was observed in the presence of 10 mM glucose: at 56 hours for instance, *csgB::gfp* fluorescence of the planktonic cells was 72% greater than the fluorescence of corresponding sedimented cells (Figure 5.6). Curli expression of planktonic and sedimented cells remained similar in the presence of 100 mM glucose across all timepoints, and at 56 hours, *csgB::gfp* fluorescence of the planktonic cells was only 1.6% greater than the fluorescence of the sedimented cells. A equivalent trend was observed in the absence of glucose, with *csgB::gfp* fluorescence of planktonic cells

being just 3% greater than the fluorescence of sedimented cells at 32 hours, and 5% greater in planktonic compared to sedimented cells at 48 hours.

When comparing curli expression of planktonic and sedimented cell samples for each concentration of glucose in turn, there was overall little difference in *csgB::gfp* fluorescence between the planktonic and sedimented cells in the absence of glucose (0 mM) (Figure 5.6). In the presence of 1 mM or 100 mM glucose, planktonic cells generally had increased curli expression, although the *csgB::gfp* fluorescence of planktonic and sedimented cells was comparable at later timepoints: at 48 hours, *csgB::gfp* fluorescence of planktonic cells was 6% greater than that of sedimented cells in the presence of 1 mM glucose, and 13% greater in the presence of 100 mM glucose respectively. Out of the four different glucose concentrations evaluated, the presence of 10 mM glucose was the only condition that resulted in distinctive curli expression between planktonic and sedimented cells (Figure 5.6).

As illustrated by Figures 5.4 and 5.5, *csgB::gfp* fluorescence of planktonic and sedimented cells was equivalently low for the first 8 hours across all glucose concentrations. Flow cytometry histograms (Figure 5.7) revealed that from 1 to 8 hours there were was a shift from a low fluorescence to a high fluorescence cell population, and that at 8 hours, two cell populations were present with differing levels of *csgB::gfp* fluorescence. From 24 hours onwards, flow cytometry histograms showed single cell populations with increased *csgB::gfp* fluorescence, as demonstrated by the shift of the histogram positions from the left-hand side towards the right-hand side of the plots.

**Figure 5.6**
**Comparison of *csgB* expression under different glucose concentrations**

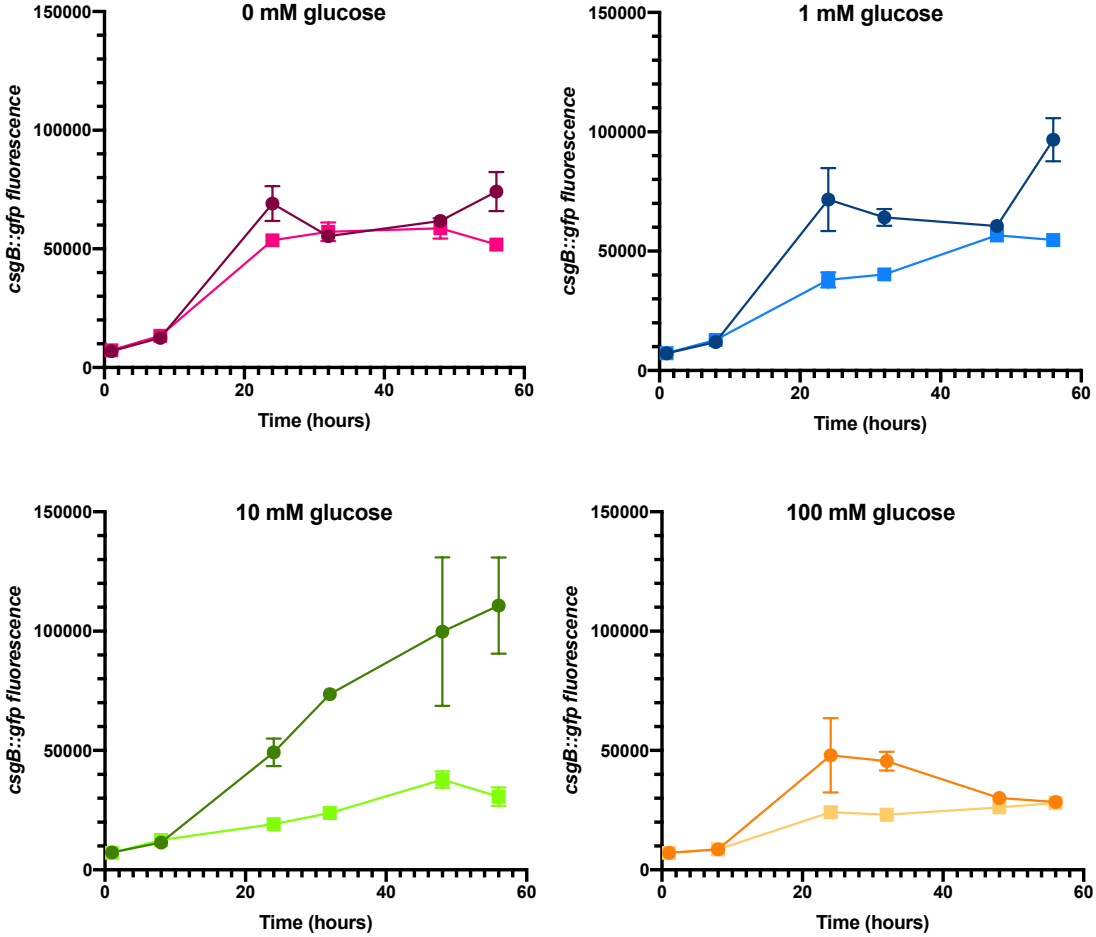


*E. coli* K-12 PHL644 transformed cells (carrying the *csgB::gfp* reporter) were grown in 70 mL M63+ minimal medium containing either 0, 1, 10 or 100 mM of glucose. For each graph, planktonic samples are shown in the darker shade, whilst sediment samples are shown in the lighter shade of the same colour. GFP fluorescence of the reporter was measured by flow cytometry, with fluorescence values stated as arbitrary units as recorded by the BD Accuri C6 flow cytometer. Data shown are the same as in Figures 5.3. and 5.4., representing the mean ± standard deviation of the average GFP fluorescence of three independent cultures.

**Figure 5.7**

**Flow cytometry histograms corresponding to GFP fluorescence (recorded as FL1-A) under different glucose concentrations**

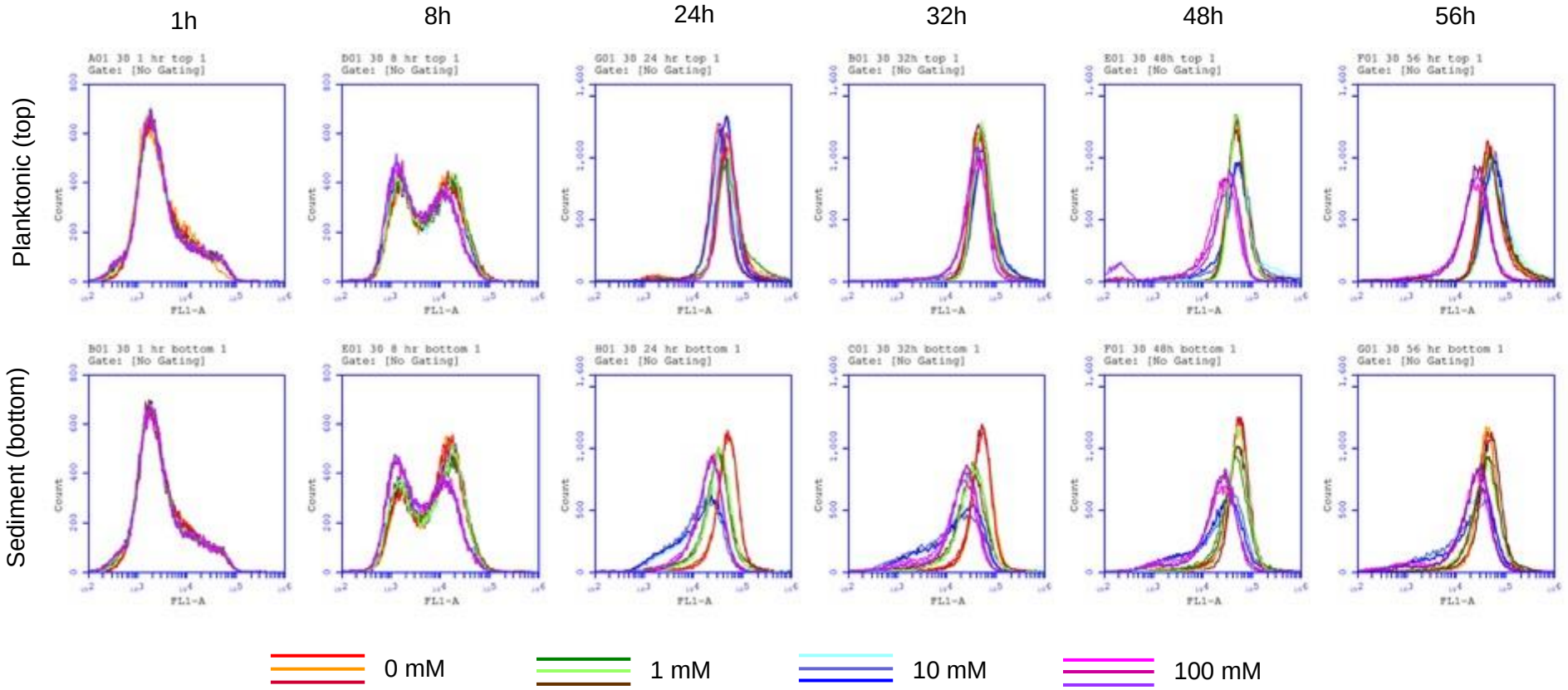


GFP fluorescence of the reporter was measured by flow cytometry, with fluorescence values stated as arbitrary units as recorded by the BD Accuri C6 flow cytometer. Histograms shown are the particle count versus the GFP fluorescence of three independent cultures (shown as different coloured traces).

5.3.3. Curli expression is temperature-regulated and greatest at 30 ºC

Earlier work in the Overton laboratory has demonstrated that a temperature of 30 ºC was the optimal temperature for *E. coli* K-12 PHL644 biofilm formation, as assessed by crystal violet assays (Leech, 2017). This is in agreement with previous work in the literature by Brombacher *et al.,* (2006) and Perrin *et al.,* (2009), although others have shown that maximal curli expression occurs below 30 ºC in different strains (Barnett and Chapman, 2006; White-Ziegler *et al.,* 2008). From this, it was hypothesised that a temperature of 37 ºC would reduce the transcription of *csgBA* due to thermoregulation of its activator, Crl, whilst a temperature of 30 ºC would result in the greatest expression of curli.

Curli expression was consistently highest in planktonic samples at a temperature of 30 ºC (Figure 5.8), which is in agreement with previous crystal violet data (Leech, 2017). Contrariwise, curli expression across all timepoints was lowest in planktonic cells incubated at 37 ºC. For the first 8 hours, *csgB::gfp* fluorescence was similarly low across all temperatures, but by 24 hours *csgB::gfp* fluorescence at 30 ºC was 42%, 24% and 76% higher than at 25 ºC, 28 ºC and 37 ºC respectively. By the final timepoint of 56 hours, the same trend was observed, with *csgB::gfp* fluorescence at 30 ºC being 54% and 79% higher than at 25 ºC and 37 ºC, and 15% higher than at 28 ºC. The largest increase in *csgB::gfp* fluorescence occurred at 28 ºC, with *csgB* expression being 69% higher at 56 hours than it was at the previous timepoint of 48 hours. In comparison, there was only a 11% increase in *csgB::gfp* fluorescence at 30 ºC from 48 hours to the final timepoint of 56 hours.

**Figure 5.8**
**Expression of *csgB* in planktonic (top) samples incubated at different temperatures**

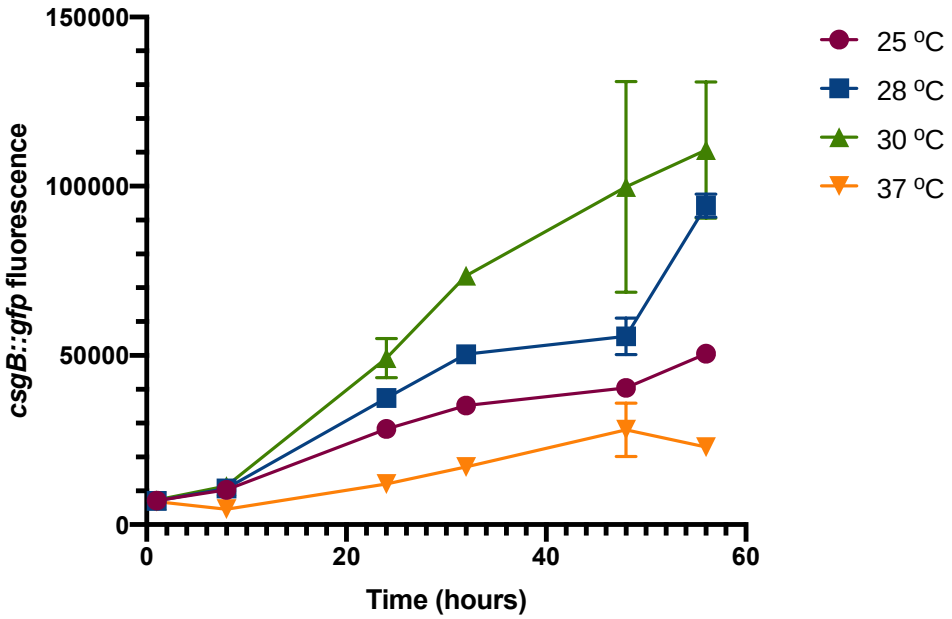


*E. coli* K-12 PHL644 transformed cells (carrying the *csgB::gfp* reporter) were grown in 70 mL M63+ minimal medium and incubated at 25 ºC, 28 ºC, 30 ºC or 37 ºC. GFP fluorescence of the reporter was measured by flow cytometry, with fluorescence values stated as arbitrary units as recorded by the BD Accuri C6 flow cytometer. Data shown are the mean ± standard deviation of the average GFP fluorescence of three independent cultures.

Across all temperatures, expression of curli in the sedimented cell samples was markedly reduced (Figure 5.9). Unlike in the planktonic cells, whereby a trend in highest to lowest *csgB::gfp* fluorescence at 30 ºC > 28 ºC > 25 ºC > 37 ºC was observed, the *csgB::gfp* fluorescence in sedimented cells remained similarly low when comparing *csgB* expression across the same temperature over time, and between different temperatures at the same timepoint. Overall however, *csgB::gfp* fluorescence of sedimented cells was greatest at 28 ºC and lowest at 37 ºC. By 24 hours, *csgB::gfp* fluorescence at 28 ºC was 2.8%, 25% and 55% higher than at 25 ºC, 30 ºC and 37 ºC respectively. At the final timepoint of 56 hours, *csgB::gfp* fluorescence of sedimented cells at 28 ºC remained the highest: 37%, 21% and 40% greater than *csgB::gfp* fluorescence at 25 ºC, 30 ºC and 37 ºC.

**Figure 5.9**
**Expression of *csgB* in sedimented (bottom) samples incubated at different temperatures**

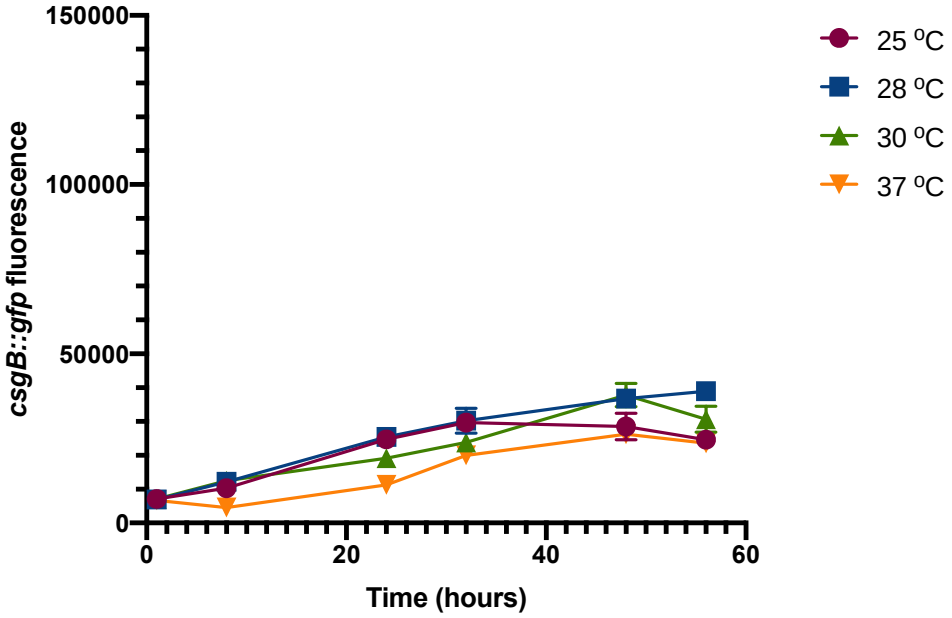


*E. coli* K-12 PHL644 transformed cells (carrying the *csgB::gfp* reporter) were grown in 70 mL M63+ minimal medium and incubated at 25 °C, 28 °C, 30 °C or 37 °C. GFP fluorescence of the reporter was measured by flow cytometry, with fluorescence values stated as arbitrary units as recorded by the BD Accuri C6 flow cytometer. Data shown are the mean ± standard deviation of the average GFP fluorescence of three independent cultures.

When comparing curli expression of planktonic and sedimented cell samples at each temperature, there was very little difference in *csgB::gfp* fluorescence between the planktonic and sedimented cells incubated at 37 °C (Figure 5.10). Planktonic cells had marginally higher *csgB::gfp* fluorescence at 37 °C, and by both 24 hours and 48 hours, the *csgB::gfp* fluorescence of planktonic samples was only 6% higher than that of the sedimented samples. At the final timepoint of 56 hours, *csgB* expression in planktonic and sedimented cells was even more similar, with the *csgB::gfp* fluorescence of sedimented cell samples being just 2.5% greater than that of the planktonic cells.

In contrast, the greatest difference in *csgB::gfp* fluorescence between planktonic and sedimented cells was observed at an incubation temperature of 30 $^{o}$C (Figure 5.10). At 24 hours for instance, *csgB::gfp* fluorescence of the planktonic cells was 61% greater than the fluorescence of corresponding sedimented cells whilst by 56 hours, *csgB::gfp* fluorescence was 72% greater in planktonic cells compared to sedimented cells. Out of the four different temperatures evaluated, incubation at 30 $^{o}$C was the only condition that resulted in distinctive curli expression between planktonic and sedimented cells.

Flow cytometry histograms (Figure 5.11) for planktonic and sedimented cell samples grown at 25 $^{o}$C, 28 $^{o}$C and 30 $^{o}$C displayed similar patterns: at 8 hours there were two cell populations with differing levels of *csgB::gfp* fluorescence, but from 24 hours onwards samples exhibited single cell populations with increased *csgB::gfp* fluorescence. In contrast, planktonic and sedimented cell samples grown at 37 $^{o}$C were composed of two cell populations across most timepoints, developing a distinct “shoulder” cell population with increased *csgB::gfp* fluorescence by 32 hours.

**Figure 5.10**
**Comparison of *csgB* expression incubated at different temperatures**

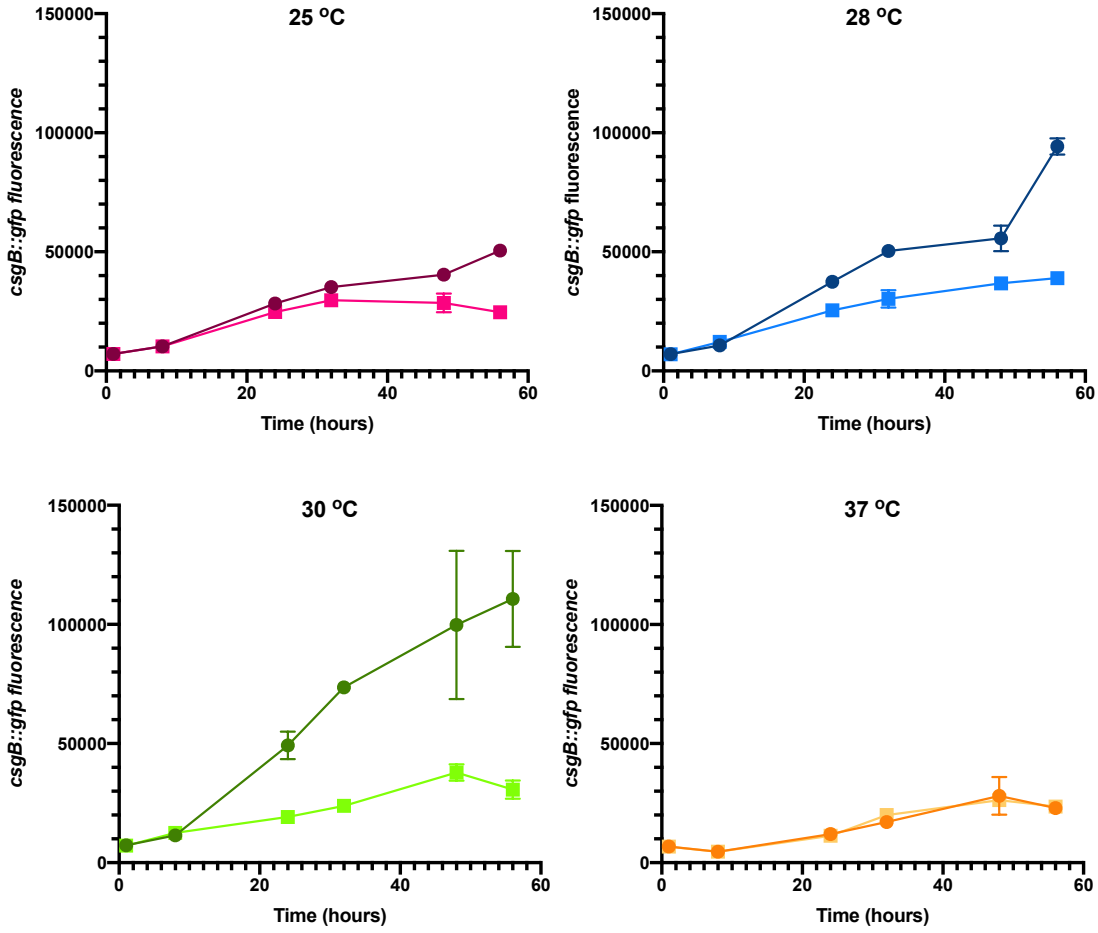


*E. coli* K-12 PHL644 transformed cells (carrying the *csgB::gfp* reporter) were grown in 70 mL M63+ minimal medium and incubated at 25 °C, 28 °C, 30 °C or 37 °C. For each graph, planktonic samples are shown in the darker shade, whilst sediment samples are shown in the lighter shade of the same colour. GFP fluorescence of the reporter was measured by flow cytometry, with fluorescence values stated as arbitrary units as recorded by the BD Accuri C6 flow cytometer. Data shown are the same as in Figures 5.9 and 5.10, representing the mean ± standard deviation of the average GFP fluorescence of three independent cultures.

**Figure 5.11**

**Flow cytometry histograms corresponding to GFP fluorescence (recorded as FL1-A) under different incubation temperatures**

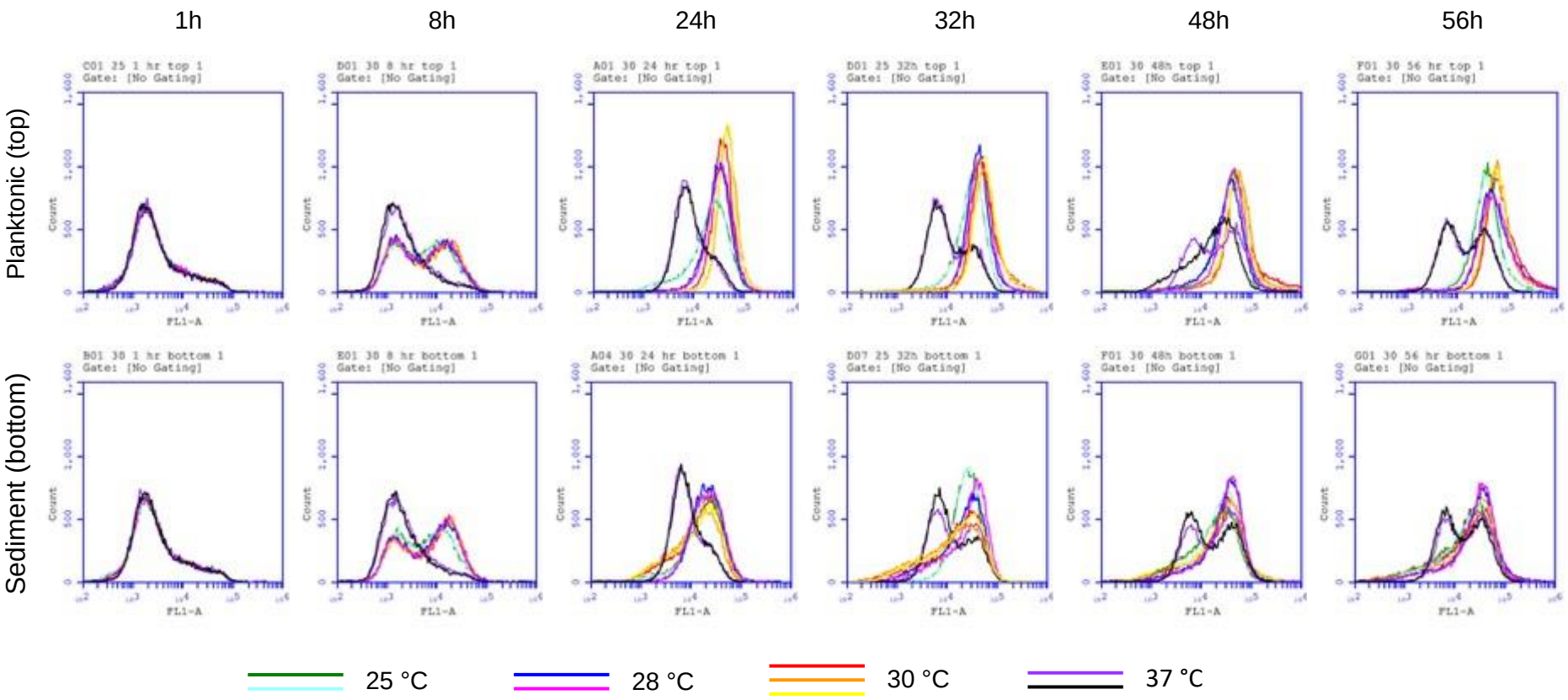


GFP fluorescence of the reporter was measured by flow cytometry, with fluorescence values stated as arbitrary units as recorded by the BD Accuri C6 flow cytometer. Histograms shown are the particle count versus the GFP fluorescence of two or three independent cultures (shown as different coloured traces).

## 5.4. Discussion

The aims of the body of work presented in this chapter was to investigate the effect of growth medium components and growth conditions on curli production by *E. coli* K-12 PHL644, and identify parameters that resulted in maximal expression of curli. Previous work in the Overton laboratory has demonstrated that curli is crucial for initial attachment to abiotic surfaces by *E. coli* K-12 PHL644 (Leech, 2017), and was in agreement with comparable studies in the literature that suggest that minimal medium, low glucose concentration and a temperature of 30 $^{o}$C result in increased curli expression (Barnhart and Chapman, 2006).

The effect of rich versus minimal medium on curli expression was determined first, over a time period of 30 hours. From the start of growth, *csgB::gfp* fluorescence was higher in cultures grown in M63+ minimal medium compared to those grown in LB broth (Figure 5.1.). A previous study by Brombacher *et al.,* (2006), which utilised an *E. coli* strain that overproduced CsgD, similarly found that minimal medium resulted in greater curli production than rich medium. Król *et al.,* (2019), demonstrated that *E. coli* K-12 biofilm formation is higher when cultures are grown in M9 minimal medium supplemented with glycerol rather than in LB broth. In *Salmonella*, curli is requisite for biofilm development, and expression of *csgB* and *csgD* has similarly been shown to be greater in minimal compared to rich media (Paytubi *et al.,* 2017).

In M63+ minimal medium, the *csgB::gfp* fluorescence of planktonic cell samples (taken from the tops of Duran bottles) was additionally greater than that of sedimented cell

samples (taken from the bottoms of Duran bottles) after 8 hours, whilst the fluorescence of both planktonic and sedimented cells grown in LB broth remained similarly very low across the time course of the experiment. The difference in *csgB* expression observed between planktonic and sedimented cell samples in M63+ minimal medium could be due to inhibition of curli via two factors: firstly, sedimented cells experiencing higher osmolarity as a result of entrained solutes (Tuson and Weibel, 2013), and secondly, as a result of intercellular communication via quorum sensing or contact dependence (Leech *et al.,* 2020). The conserved QS-regulator protein MsqR has been shown to induce curli expression via *crl* and increase motility through *crsA* (González Barrios *et al.,* 2006).

Low osmolarity is known to increase *csgD* expression through activation of the promoter OmpR, a response regulator that senses osmolarity via EnvZ, leading to expression of curli and increased biofilm formation (Jubelin *et al.,* 2005; Hou, *et al.,* 2014). A medium with high osmolarity by contrast leads to repression of *E. coli* genes, including *csgD* (Jubelin *et al.,* 2005). Conversely, under high osmolarity conditions, activation of the Cpx pathway results in phosphorylation of the transcriptional regulatory protein CpxR by the kinase CpxA, which binds to the *csgD* promoter, ceasing expression of CsgD and reducing curli-driven biofilm formation (Jubelin *et al.,* 2005; Ma and Wood, 2009; Dudin *et al.,* 2014).

Additionally, rich medium, such as LB broth, may contain components that can repress biofilm forming pathways (Jackson *et al.,* 2002; Hufnagel *et al.,* 2016). One such component is salt (NaCl), with Smith *et al.,* (2017), reporting that the formation of curli

is decreased in LB broth-grown cultures, due to the inhibitory effect the high salt concentration has on curli expression (i.e. osmolarity). Others in the literature are in agreement with this, demonstrating that both *Salmonella enterica* and enterohaemorrhagic *E. coli* biofilms were significantly greater in biomass when grown in LB broth with salt omitted, compared to standard LB medium (Han *et al.,* 2017). Furthermore, LB broth contains both peptone and yeast extracts, which have been shown to result in higher cell culture densities planktonically rather than in sessile communities such as a biofilm (Studier, 2005; Tsoligkas *et al.,* 2011).

Han *et al.,* (2017), reported that LB broth without salt resulted in more biofilm formation compared to standard LB medium due to its lower osmolarity, whilst Hou *et al.,* (2014), found that *E. coli* formed dense biofilms with a large concentration of extracellular fimbriae such as curli in response to low osmolarity ½ M9 minimal medium. As part of the publication that includes the work presented in this chapter, a colleague (Stacey Golub) measured the osmolarity of the LB broth and M63+ minimal medium used, and found that the osmolarity of LB broth approximately two-fold higher than that of M63+ minimal medium (Leech *et al.,* 2020). It is therefore likely that *csgB::gfp* fluorescence was highest in cultures grown in M63+ minimal medium as a combined result of its lower osmolarity and low salt concentration. This would stimulate curli expression, enhancing both cell-cell adhesion and adhesion to the abiotic test surface, resulting in greater biofilm formation (Pawar *et al.,* 2005).

The effect of glucose concentration on curli expression was determined through supplementation of M63+ minimal medium with either 0 mM, 1 mM, 10 mM (the typical

concentration of glucose in M63+ minimal medium), or 100 mM glucose. Although *csgB* expression was initially greater in the presence of 0 mM or 1 mM glucose, from 30 hours onwards *csgB::gfp* fluorescence was highest in the planktonic cells grown in the presence of 10 mM glucose, and lowest in planktonic cells grown in medium supplemented with 100 mM glucose (Figure 5.4). Furthermore, 10 mM glucose elicited the largest difference in *csgB::gfp* fluorescence between planktonic and sedimented cell samples from 8 hours onwards, whereas *csgB* expression was most similar between planktonic and sedimented cells in the presence of 0 mM glucose (Figure 5.6).

The role of glucose in catabolite repression is well documented in the literature (Gottesman, 1984; Jackson *et al.,* 2002; Brückner and Titgemeyer, 2002; Lengeler, 2013; Hufnagel *et al.,* 2016). Low glucose concentrations are known to stimulate cAMP production by CyaA, whilst catabolite repression is known to occur in response to high glucose concentrations (Ishizuka *et al.,* 2003). Glucose inhibits the activity of CyaA, thus leading to a reduction in intracellular cAMP levels. Consequentially, the concentration of cAMP-CRP complexes in the cell decreases, as does cAMP-CRP complex binding to promoter regions of cAMP-regulated genes. One such promoter region is *csgD*, the product of which (the master biofilm regulator, CsgD) is the main activator of *csgBA*, which encodes curli subunits (Zheng *et al.,* 2004; Hufnagel *et al.,* 2016). A genome-wide analysis of cAMP-CRP by Zheng *et al.,* (2004), demonstrated that 7% of the *E. coli* transcriptome is altered by CRP activation, including *csgD* and its transcription. Therefore, in the presence of 100 mM glucose, it is likely that catabolite repression of *csgD* expression (and consequently expression of *csgB*)

occurred to an extent, which could account for the lower *csgB::gfp* fluorescence of both planktonic and sedimented cell samples in comparison to the fluorescence of cell samples grown in the presence of 0 mM, 1 mM and 10 mM glucose.

The work of Jackson *et al.,* (2002), has previously demonstrated that addition of glucose to media has an inhibitory effect on biofilm formation by several *E. coli* K-12 strains including MC4100, which is the parental strain of *E. coli* K-12 PHL644. A concentration of 0.2% (v/v) glucose was found to significantly reduce biofilm formation by 30 – 95%, with the authors suggesting that suppression of biofilm development was at least partly-mediated by catabolite repression (Jackson *et al.,* 2002). Using *E. coli* K-12 BW25113, Domka *et al.,* (2006), found that the addition of 0.4% (v/v) glucose to LB medium resulted in the inhibition of biofilm formation, whilst in other biofilm-forming bacterial species such as *Bacillus subtilis*, glucose concentrations of 0.1% and 1% (both v/v) in medium has been shown to negatively affect biofilm formation (Stanley *et al.,* 2003). Thus, results presented in this chapter are in general agreement with other studies in the literature.

Growth in the presence of low glucose concentrations conversely results in increased cAMP synthesis, as bacteria adapt to the glucose-limited environment (Notley-McRobb *et al.,* 1997). It has been reported that copiotrophic bacteria (such as *E. coli* and *Ps. a.*) have increased adhesive properties in medium with low concentrations of carbon sources (Nikolaev and Plakunov, 2007), and in *Pseudomonas sp.* initial adhesion can be stimulated by low levels of nutrients, as a result of increased bacterial surface hydrophobicity (Chen *et al.,* 2005). This could explain why *csgB::gfp* fluorescence of

cells grown in the presence of 0 mM and 1 mM was higher during the first 24 hours, with increased curli production protecting cells from stress under nutrient-limited conditions. Indeed, such conditions have previously been shown to result in increased initial adherence and biofilm formation (Yang *et al.,* 2004; Reisner *et al.,* 2006; Naves *et al.,* 2008). This is in agreement with the work of Moreira *et al.,* (2013), demonstrating that initial biofilm formation over a period of 24 hours was greater at a low glucose concentration of 0.25 g/L compared to a glucose concentration of 1 g/L, for the *E. coli* JM109(DE3) strain.

Aside from glucose, the only other carbon source available in M63+ minimal medium is succinate (at a concentration of 10 mM), and in the presence of 0 mM or 1 mM glucose, conditions were carbon source limited. In spite of increased *csgB::gfp* fluorescence for the first 24 hours, planktonic growth of *E. coli* K-12 PHL644 (as measured by spectroscopy) remained low ($OD_{600}$ >0.2) across the 56 hours. This suggests that glucose concentrations of 0 mM and 1 mM were too low to support optimal growth of *E. coli* K-12 PHL644, resulting in a reduced growth rate, lower cell densities and consequently poor biofilm formation overall. Conversely, in the presence of 100 mM glucose, the rate of planktonic growth was initially greater, reaching an $OD_{600}$ of ~ 0.3 within the first 24 hours. However, from 32 hours onwards, planktonic growth in the presence of 100 mM glucose declined to an $OD_{600}$ >0.15, and curli production was similarly reduced.

Therefore, glucose abundance appears to be as detrimental to biofilm formation by *E. coli* K-12 PHL644 as glucose paucity – an observation previously observed in the

Overton Laboratory, in which crystal violet staining revealed that concentrations of 0 mM, 1 mM and 100 mM glucose had a negative effect on biofilm formation (Leech *et al.,* 2020). At lower glucose concentrations, biofilm formation is reduced due to inhibition of growth, resulting in reduced biomass whilst high glucose concentrations, such as 100 mM, are likely to induce catabolite repression and result in decreased biofilm formation. Out of the four glucose concentrations evaluated, a concentration of 10 mM glucose was thus the optimal for both growth of *E. coli* K-12 PHL644 and increased curli production, attachment and thus biofilm formation.

Finally, the effect of temperature was determined over a period of 56 hours. In planktonic cell samples, *csgB* expression was greatest at 30 $^{o}$C (Figure 5.8), which is in agreement with biofilm biomass data obtained in earlier experiments (Leech, 2017). Furthermore, in planktonic cell samples, *csgB::gfp* fluorescence was highest at 30 $^{o}$C, then 28 $^{o}$C, followed by 25 $^{o}$C and 37 $^{o}$C, corroborating previous reporter data in the literature (Brombacher *et al.,* 2006; Perrin *et al.,* 2009).

Barnhart and Chapman, (2006), suggested that maximum curli expression occurs at temperatures below 30 $^{o}$C, whilst a microarray analysis of *E.* coli K-12 by White-Ziegler *et al.,* (2008), revealed that all curli genes had significantly increased expression at 23 $^{o}$C in comparison to at 37 $^{o}$C. Furthermore, studies using human-pathogenic serotypes of *E. coli* isolated from ovine reservoirs (at 37 $^{o}$C *in vivo*) have also demonstrated that biofilm formation by Shiga toxin-producing *E. coli* is positively influenced by temperatures as low as 12 $^{o}$C and 20 $^{o}$C (Nesse *et al.,* 2014).This is in agreement with results presented in this chapter, as flow cytometry histograms (Figure 5.11) for 25 $^{o}$C,

28 $^{o}$C and 30 $^{o}$C are similar; showing one cell population with respect to *csgB::gfp* fluorescence in both planktonic and sedimented cell samples, whereas the flow cytometry histograms for 37 $^{o}$C are composed of two cell populations with varying *csgB* expression, and thus lower curli production overall.

Transcription of *csgBA* by Crl is known to occur at low but not high temperatures, as Crl expression is itself temperature-dependent (Bougdour *et al.,* 2004; Brombacher *et al.,* 2006; Lelong *et al.,* 2007). The Crl protein is thermosensitive and upregulates *csgBA* expression at 30 $^{o}$C via recruitment of $\sigma^{s}$ (Bougdour *et al.,* 2004; Brombacher *et al.,* 2006). At a temperature of 37 $^{o}$C, the activity of Crl is less efficient (Bougdour *et al.,* 2004), thus it is likely that *csgB* expression is reduced, which could account for the fact that *csgB::gfp* fluorescence of both planktonic and sedimented cell samples at 37 $^{o}$C were lower than at 25$^{o}$C, 28 $^{o}$C and 30 $^{o}$C. Work by Bougdour *et al.,* (2004), supports this observation: at 37 $^{o}$C, it was observed that Crl levels were low but detectable for the first 8 hours of growth in several *E. coli* K-12 strains, but after this Crl levels were approximately 30-fold higher at 30 $^{o}$C than at 37 $^{o}$C.

With the exception of growth at 37 $^{o}$C, *csgB::gfp* fluorescence differed between the two sampling sites, with *csgB* expression being greater in planktonic cells grown at 25 $^{o}$C, 28 $^{o}$C and 30 $^{o}$C compared to corresponding sedimented cell samples (Figure 5.10.). Interestingly, whilst incubation temperature resulted in distinct and different levels of *csgB::gfp* fluorescence in the planktonic cell samples, the fluorescence of sedimented cell samples was very similar, irrespective of incubation temperature (Figure 5.10.). Thus, thermoregulation of curli, as mediated by Crl, may be more important

planktonically. In sedimented cells, it is possible that signalling cascades were able to bypass temperature-dependent regulation, and resultantly downregulate expression of curli (Leech *et al.,* 2020). For example, work by Pratt and Silhavy, (1998), has previously suggested that in the *E.* coli strain MC4100, Crl is able to downregulate the level of $\sigma^S$ protein through a regulatory feedback loop, in which $\sigma^S$ is able to control its own expression.

Furthermore, there is evidence to suggest that the global regulatory protein H-NS (which regulates approximately 5% of the *E. coli* genome) is able to regulate $\sigma^S$ in response to changes in osmolarity and temperature (Barth *et al.,* 1995; Stella *et al.,* 2006). Whilst the *hns* gene is autoregulated in *E. coli* and intracellular levels of H-NS generally remain constant (Atlung and Ingmer, 1997), it has been reported that H-NS undergoes conformational changes in response to temperature (Ono *et al.,* 2005). Although the complex formed by $\sigma^S$ subunit binding to Crl is able to activate expression from the *csgBA* promoter and relieve H-NS-mediated repression of *csgA*, factors such as osmolarity and activity of the master biofilm regulator CsgD can also influence the complex's binding (Olsén *et al.,* 1993; Arnqvist *et al.,* 1994).

A model proposed by Gerstel *et al.,* (2004), has suggested that increased concentrations of H-NS are able to bind to *csgD* and thus repress expression of curli. Whilst Bougdour *et al.,* (2004) demonstrated that the *crl* promoter is itself not regulated by temperature, regulation of *csgBA* transcription has been shown to remain temperature-dependent in an *rpoS* and *hns* double mutant strain (Olsén *et al.,* 1993). This suggests that the activity of $\sigma^S$ and H-NS do not directly control curli expression

in response to temperature and osmolarity changes. Indeed, H-NS lacks an identifiable binding sequence, and is purported to activate or repress *csgD* expression in a manner that is dependent upon the bacterial strain and growth medium used (Olsén *et al.,* 1993; Gerstel *et al.,* 2004).

At low growth temperatures, expression of $\sigma^s$ is dependent upon the small regulatory RNA DsrA, which stabilises *rpoS* mRNA (Majdalani *et al.,* 1998). Interestingly, expression of *dsrA* is itself temperature-dependent, with work by Repoila and Gottesman, (2001), demonstrating that the half-life of *dsrA* RNA is significantly prolonged at 25 $^oC$ compared to at 37 $^oC$. Thus, both temperature-mediated mechanisms appear to act together: DsrA stimulates $\sigma^s$ expression at low but not high temperatures, whilst Crl enhances the activity of $\sigma^s$, leading to activation of the *csgBA* promoter and increased expression of the curli subunits (Repoila and Gottesman, 2001; Bougdour *et al.,* 2004).

Across all experimental subsets (LB broth versus M63+ minimal medium; different glucose concentrations, and different incubation temperatures), $OD_{600}$ values and *csgB::gfp* fluorescence appeared to have an inverse relationship: as $OD_{600}$ increased, FL1-A measurements (and thus curli expression) generally decreased. Curli expression in sedimented cell samples was consistently lower than in planktonic cell samples, which could suggest that planktonic cells were physically more adept at curli-mediated surface and cell-cell attachment, or alternatively that planktonic cells continued to increase curli expression over time in order to try and attach to any available surfaces within the Duran bottles.

Otto and Silhavy, (2002), suggested that curli expression in response to surface attachment occurs as a result of a sequential series of events, forming a three component pathway. Surface attachment is sensed initially by an outer membrane lipoprotein (NIpE), which activates the two component regulatory system CpxAR (Prigent-Combaret *et al.,* 2001). Activation of CpxAR represses both *csgB* and *csgD*, thus expression of curli is supressed (Ma and Wood, 2009; Dudin *et al.,* 2014). Alternatively, Kimkes and Heinemann, (2008), proposed that activation of the Rcs phosphorelay pathway in response surface attachment negatively regulates curli expression. Induction of the Rcs pathway occurs in response to damage to peptidoglycan polymers within the cell wall, illustratively as a result of desiccation or osmotic shock, and also regulates genes involved in biofilm formation (Laubacher and Ades, 2008). The Rcs pathway is known to downregulate genes associated with motility, such as flagella, as well as those that mediate cell adhesion to a surface, including curli (Prigent-Combaret *et al.,* 2000). Microarray analysis by Ferrieres and Clarke, (2003), revealed that RcsB, the response regulator in the Rcs pathway, represses the *csgDEFG* operon. Further work by Vianney *et al.,* (2005), is in agreement, demonstrating the RscB and RscA are moderate repressors of the *csgDEFG* operon and strong repressors of the *csgBA* operon. Phosphorylated RscB is able to form either homodimers, or heterodimers with the accessory protein RscA, to bind to DNA and modulate gene expression accordingly (Majdalani and Gottesman, 2005).

Furthermore, the Rsc pathway upregulates genes involved in colanic acid production (Huang *et al.,* 2006). Colanic acid is an integral EPS and constituent of the matrix of

mature *E. coli* biofilms: forming a protective capsular layer around cells, it is involved in maintenance of the three-dimensional structure of the biofilm (Prigent-Combaret *et al.,* 1999; Danese *et al.,* 2000). Thus, after attachment to a surface as mediated first by flagella and then by curli, the Rsc pathway likely downregulates their expression whilst upregulating colonic acid synthesis; modulating the changes in cell envelope composition required to form and maintain mature biofilm structures (Prigent-Combaret *et al.,* 2000; Lejeune, 2003; Vianney *et al.,* 2005).

The results presented in this chapter support this notion. Initial surface sensing and subsequent attachment as mediated by curli is reflected by high levels of *csgB::gfp* fluorescence in planktonic cell samples. As rates of surface and cell-cell attachment increased over time and cells settled to the bottom of the Duran bottles, it is likely that curli expression was downregulated concurrent to expression of other biofilm components (such as colonic acid synthesis) being upregulated, leading to decreased *csgB::gfp* fluorescence as observed for the sedimented cell samples.

When evaluating the Duran bottle method, there are several limitations to its experimental design, which could have affected the *csgB::gfp* fluorescence values obtained. It was noted when monitoring planktonic growth by sampling $OD_{600}$ that independent cultures of sedimented cells for each condition tested were widely variable as time progressed. As a result, error bars for each timepoint were very large, and it was difficult to ascertain the true effect of experimental conditions upon the sedimented cell samples (as illustrated by Figure 5.12). Spectroscopic measurements were used to evaluate both planktonic growth and settling of cultures, but removal of

samples from the sediment at each timepoint may have inadvertently affected $OD_{600}$ values obtained.

Figure 5.12. shows the comparison of the growth of *E. coli* K-12 PHL644 cultures in either LB broth or M63+ minimal medium, with samples taken from planktonic and sedimented cells. Whilst rate of cell growth in LB broth was observed to be greater than in M63+ minimal medium in planktonic samples over the full time course of the experiment (Figure 5.13.A), in sedimented cell samples the rate of cell growth was higher in LB broth for the first 8 hours only (Figure 5.13.B). From 24 hours onwards, the $OD_{600}$ values obtained for both sedimented cell samples in LB broth and M63+ minimal medium demonstrated a trend of sharply increasing and decreasing during subsequent sampling times. Illustratively, from 26 hours to 28 hours, the $OD_{600}$ value for sedimented cells grown in LB broth decreased by 61%, only to increase by 150% from 28 hours to 30 hours.

Removal of sediment (which can be observed with the naked eye) from a particular sampling site results in that location resultantly experiencing a decrease in cell concentration. Additionally, at 70 RPM, sedimented cells that have settled at the bottom of the Duran bottle are expected to remain *in situ*, as the rotational speed is relatively low, and thus would not cause sloughing off of cells from the sediment and their subsequent resettling. Conversely, if a different site was sampled at the next timepoint (for example, if one sample site was the centre of the bottom of the Duran bottle whilst the succeeding sample site was located more towards the bottle's edge), it could result in an increase in the resultant $OD_{600}$ value as the cell concentration in a

virgin area of the cell sediment would be higher than in an area previously disturbed by sampling. Furthermore, clumping of cells could result in spatial differences in cell concentrations; if a clump of cells was sampled, one would expect it to have a higher $OD_{600}$ than settled cells that are loosely associated with one another.

**Figure 5.12**
**Comparison of $OD_{600}$ values in planktonic (top) samples and sediment (bottom) samples in rich versus minimal medium**

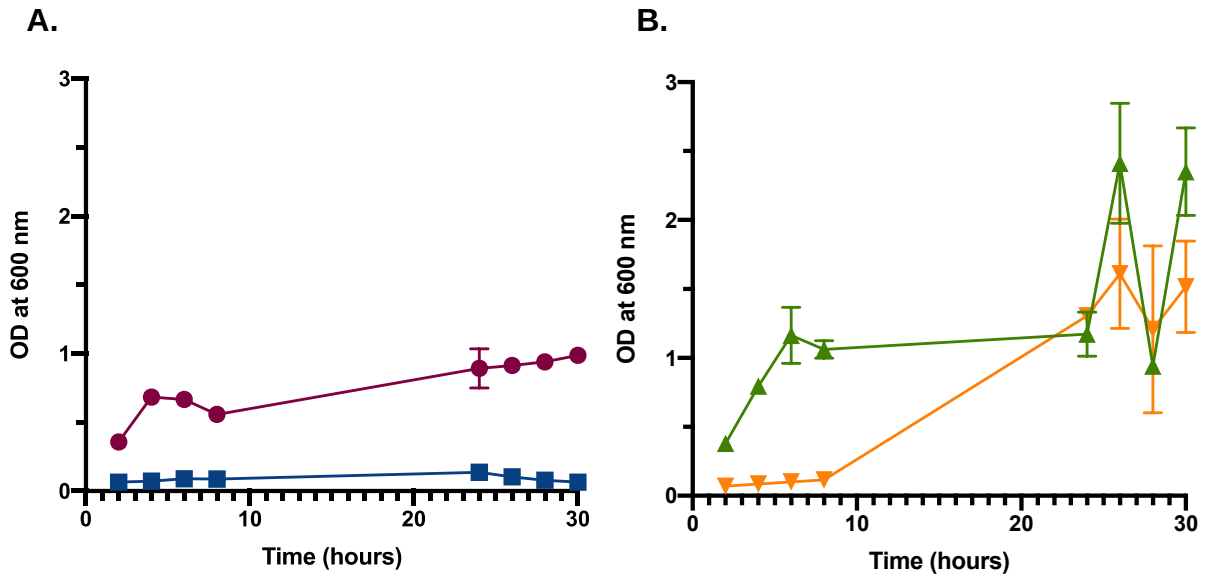


*E. coli* K-12 PHL644 transformed cells (carrying the *csgB::gfp* reporter) were grown in 70 mL of LB broth (rich medium) or in 70 mL M63+ minimal medium. Growth of cultures was measured by spectroscopy at 600 nm, with $OD_{600}$ values stated as arbitrary units. Data shown are the mean ± standard deviation of the average $OD_{600}$ of two independent cultures.

The use of Transwell plates in future experiments may help mitigate the limitations of the Duran bottle method as described above. Composed of a plastic Transwell insert support that is inlaid into a well plate, this technique offers semi-constant nutrient conditions, and two chambers separated by the insert (Cattò and Cappitelli, 2019). The Transwell insert has a semi-permeable membrane with a defined pore size, such as a

polytetrafluoroethylene membrane with a pore size of 0.4 μm (Jefferson *et al.,* 2005), upon which a biofilm can grow. Transwell plates have been used by numerous research groups to form and evaluate biofilms under a variety of physiological conditions, including but not limited to analysis of antibiotic penetration through a biofilm (Jefferson *et al.,* 2005); behaviour of mixed species biofilms (Standar *et al.,* 2010; Wu *et al.,* 2015); the effects of both natural and artificial anti-biofilm agents on biofilm development (Anderson *et al.,* 2014; Wang *et al.,* 2016; Bidossi *et al.,* 2018), and targeted disruption of EPS components within a biofilm (Powell *et al.,* 2018).

Kim *et al.,* (2012), used Transwell inserts of 12 mm diameter, with a membrane composed of polyester and pore size of 3 μm, and successfully demonstrated that *E. coli* biofilms could be grown on the membrane and analysed by numerous techniques, including crystal violet staining and microscopy. Samples from Transwell plates could similarly be analysed by spectroscopy and flow cytometry: planktonic cell samples would remain in the medium of the top chamber (above the insert), whilst removal of the insert itself would enable resuspension of the sedimented cell (or biofilm) samples formed upon the membrane. Crucially, due to the fact that the biofilm will form on the semi-permeable membrane, its location is fixed and distinct from the planktonic cells above as well as any pellicle formation at the air-liquid interface. Furthermore, multiple wells can easily be set up with independent cultures, and individual wells discretely sampled at timepoints without affecting conditions in the other wells. As a result, perturbation of the sedimented cells, as observed when repeatedly sampling from the same Duran bottles over time, and the resultant variation in $OD_{600}$ would not occur.

# Chapter 6: Conclusions and further work

# Chapter 6: Conclusions and further work

## 6.1. Conclusions

The results presented in Chapters 3 and 4 demonstrate that the CBR is a suitable experimental system for modelling industrial-relevant low and high shear conditions, and was show to generate reproducible and reliable data. Furthermore, different fluid shear regimes as modelled by the CBR (namely low shear at 75 RPM and high shear at 350 RPM) were shown to have act distinctive impacts upon biofilm formation by PA01 and PA14, across all stages of biofilm development analysed. Both strains responded similarly to shear, with respect to ECM morphologies observed and differentiation of three-dimensional architecture.

Under low shear at 75 RPM, biofilm development by both strains was generally characterised by: adherence to the coupon surface (at 24 hours); formation of a basal biofilm, composed of multiple and generally homogenous basal layers, from which microcolonies are emerging (at 48 hours); mushroom-shaped macrocolony development (at 72 hours); and formation of an expansive Psl and/or Pel fibre-like network through the basal biofilm during maturation (at 96 hours). PA01 biofilm formation occurred more quickly than that of PA14, with some PA01 macrocolonies observed preparing for seeding dispersal of motile cells, which is demarcated as the final stage of the 'biofilm lifestyle'. Overall, low shear conditions in the CBR did not appear to detrimentally affect formation of mature and differentiated *Ps. a.* biofilms.

By contrast, under high shear at 350 RPM biofilm development was defined by increased early adherence of both PA01 and PA14 to the coupon surface, and increased intracellular c-di-GMP levels (directly inferred from GFP fluorescence of *cdrA::gfp*), with attached cells of either strain predominantly forming either cell clusters or denser cellular aggregates surrounded by exopolysaccharide(s) and eDNA. Although energetically costly, increased production of the ECM components Psl and Pel, appeared to be induced in response to high shear conditions; enhancing the 'stickiness' of cell populations and promotion of the biofilm phenotype.

As the biofilms matured, vertical growth of cell populations occurred, whilst lateral spreading (and thus basal biofilm formation) did not. Psl and Pel were observed forming dense, 'tendril'-like structures, commonly protruding into parts of the bulk fluid to connect subpopulations of cells to one another. PA01 and PA14 both formed heterogenous fibres, composed of eDNA, Psl and Pel (for PA01), and eDNA and Pel (for PA14). Growth in the vertical dimension resulted in the formation of competing mound structures of heterogenous height, architecture and composition; consequently, evidence of detachment from parts of the biofilm was frequently observed during sampling. Furthermore, biofilm formation on the interior lumen of outflow tubing was also seen, akin to colonisation of secondary sites in industrial processing plants.

The influence of low and high shear conditions on Psl and Pel impacted upon observed morphologies for the exopolysaccharides, and growth in the CBR revealed a variety of both established structures for Psl and Pel, in agreement with the results of Ma *et al.,* (2009) and Jennings *et al.,* (2015), and novel morphologies, such as production of Pel

fibre-like structures by PA14, which has previously only been described occurring in PA01, mediated by Psl (Zhao *et al.,* 2013; Wang *et al.,* 2013; Wang *et al.,* 2015). The results presented in Chapter 3 and 4 offer a detailed insight into how PA01 and PA14 adapt to high shear regimes (as modelled in the CBR), through increased production of Psl, Pel and eDNA, which results in dominance of aggregative phenotypes and development of tall, irregularly-shaped 'tower'-like structures.

The results presented in Chapter 5 demonstrate that the Duran bottle model (which relied on natural biofilm formation over time) is a suitable experimental system for analysing the effects of different growth conditions and components of growth medium on curli gene expression by *E. coli* K-12 PHL644, and was able to generate reproducible and reliable data that has been published. Furthermore, through use of the Duran bottle method, parameters that resulted in maximal *csgB::gfp* fluorescence (and thus curli expression) were identified (namely growth in M63+ minimal medium rather than LB broth, a glucose concentration of 10 mM, and an incubation temperature of 30 $^{o}$C), which is in agreement with comparable studies in the literature (Jackson *et al.,* 2002; Barnhart and Chapman, 2006; Brombacher *et al.,* 2006).

## 6.2. Industrial Perspective

Bacterial colonisation and biofilm formation is a well-recognised problem in industry: the risk of microbial contamination and persistence of microorganisms in biofilms is known to have a widespread and detrimental impact upon production lines through corrosion and biofouling of working surfaces, as well as the risk of contamination of

raw materials and finished formulations. Whilst methods of biofilm control (including the use of biocides to disinfect surfaces, physical cleaning methods such as pigging or chemical treatments with detergents and disinfectants) can be successful, stagnation in low shear environments such as crevices, corners, dead zones and valves, or overall plant design can result in survival and accumulation of untreated biomass; increasing the risk of re-colonisation and biofilm proliferation of downstream processes and sites.

In manufacturing plants (such as those used by P&G), high shear conditions are essential during mixing of formulations and reagents; ensuring that a standardised mixture of ingredients is maintained for each batch of products, through the use of high-shear mixers operating under turbulent flow. Manufacturing environments that are likely to have more laminar-based flow regimes and operate under lower shear include connecting pipelines, crevices and corners, and bottling stations for the final product.

Through modelling of an industrially-relevant high shear condition (through use of the CBR and a stirring speed of 350 RPM), results presented in Chapters 3 and 4 revealed that biofilms produced by *Ps. a.* strains PA01 and PA14 were composed of increased ECM components, with bacteria exhibiting aggregative phenotypes and increased vertical growth of spatially-separated cell populations into the bulk fluid rather than lateral spreading and confluent colonisation of the entirety of the available coupon surface. Such structures, if allowed to form and subsequently mature in areas of P&G's manufacturing plants that experience similar high shear fluid flow regimes as the one modelled (i.e. turbulent flow with a Reynolds number of > $10^4$), could result in *in situ*

contamination of both working surfaces and ingredients, and over time corrosion of equipment materials themselves.

Furthermore, biofilm formation on the interior lumen of the CBR's outflow tubing was observed under high shear at 350 RPM, illustrating the risk of secondary site colonisation and subsequent continuation and persistence of the biofilm 'lifestyle'. It is feasible to imagine in manufacturing plants involving many different mixing vessels and transport pipelines operating under variable shear conditions (and in which they are a multitude of different surfaces bacteria can colonise and persist), that detached parts of a biofilm may travel downstream to areas with lower shear fluid flow, and either colonise new surfaces in crevices, dead zones and surrounding valves or utilise organic deposits on a surface (such as biomass left behind due to previous ineffective cleaning regimes) to re-colonise an area and persist through continued promotion of the biofilm 'lifestyle'

In industrial settings where multispecies biofilms, which are likely all heterogenous with respect to the proportions of each species residing in each individual biofilm, are present, different manufacturing sites may be colonised by an array of complex and differing communities, each with their own distinctive ECM conferring increased resistance against methods of removal. In addition, horizontal gene transfer within multispecies biofilms can further increase resistance of the bacterial population to antimicrobial treatments. A study by Lee *et al.,* (2013), revealed that whilst monospecies biofilms formed by *Ps. a.*, *Pseduomonas protegens* and *Klebsiella pneumoniae* had varying level of resistance towards the antibiotic tobramycin and the

anionic surfactant sodium dodecyl sulfate, with multispecies biofilms displayed resistance against both compounds. Rather than treatment with these compounds resulting in population shift to the more resistant species, the species composition of the multispecies biofilm was not affected, with Lee *et al.,* (2013), suggesting that the resistant species instead provided a protective effect to the whole community. Moreover, different species may reside in different locations within a multispecies biofilm, further exacerbating the difficulties in effective removal of the ECM and total biomass. Fazil *et al.,* (2009), illustratively demonstrated using fluorescent *in situ* hybridisation and CLSM that although *Ps. a.* and *Staphylococcus aureus* were present in the same chronic wound model, the two strains were spatially-separated and found on average 40 µm apart in different layers within the wound.

In industry, there has been an increased use of antimicrobial and microbial anti-biofilm enzymes, which can directly target microorganisms; interfere with and/or destroy the biofilm itself, or catalyse reactions that result in the production of antimicrobial compounds (Thallinger *et al.,* 2013). Subtilins, a type of proteolytic enzyme frequently used for the control of biofilms in industry, have been shown to effectively remove biofilms formed by *Ps. a.* and *Bascillus spp.*, and prevent co-aggregation of different species in multispecies biofilms (Marcato-Romain *et al.,* 2012). Polysaccharide-degrading enzymes, such as lysozyme can hydrolyse 1,4-β-linkages in the cell walls of Gram negative bacteria (Procter *et al.,* 1988), and could potentially be used against EPS featuring 1,4-β-linkages, such as Pel and alginate. In spite of their potential, the cost to produce such enzymes on an industrial scale is expensive, and successful application of the enzymes and their control of biofilm development is dependent upon

the environment in which treatment is required. Zanaroli *et al.,* (2011), demonstrated that a combination treatment composed of alpha-amylase, β-glucuronidase, glucose oxidase, dextranase, protease and pectinase was effective at removing biofilms from stainless steel coupons and dispensing lines, but the necessity of purchasing multiple enzymes required for use in combination with each other to prove most effective at removing biofilms, results in increased economic costs if each enzyme is expensively priced. Furthermore, similarly to the increased risk of microorganisms developing resistance to other antimicrobials (such as antibiotics) with continued use, there is evidence of resistance emerging against the proteolytic enzyme lysostaphin (which is often used to control multidrug resistant methicillin-resistant *Staphylococcus* aureus) both *in vitro* and *in vivo* (Strandén *et al.,* 1997; Climo *et al.,* 1998).

Consensus in the literature is that control and removal of biofilms in industry is most effective during earlier stages of biofilm formation, before the establishment of mature biofilm structures, characterised by their self-produced and protective ECM (Mah and O'Toole, 2001; Stewart and Costerton, 2001; Høiby *et al.,* 2010). Bacteria sequestered within mature biofilms are known to exhibit increased resistance and tolerance to biocidal, antimicrobial and enzymatic treatments, due to the reduced penetration and diffusion of such treatments through the biofilm. Consequently, microbial contamination in industry can lead to increased economic costs and manufacturing overheads, as a result of choice of treatment and its associated costs; the duration of each treatment (i.e. if chemical-based as this may need to be left on a surface to penetrate throughout the biofilm) and frequency of treatment required; if treatment requires additional energy (i.e. through pressure-jet washing, automated scrubbing or

increased temperatures during cleaning processes) (Gibson *et al.,* 2001), as well as ingredient instability, loss of product and increased wastage if formulations are contaminated. *In situ* application of biocidal treatments, or physical cleaning methods through use of brushes, may impact upon the surface topography of manufacturing equipment; if microscopic abrasions are left in equipment for example, bacteria transported via flow to such sites will be more readily colonised. As observed on older PE coupons for early, independent CBR runs, scratches left on the coupon surface after removal of biomass by scrubbing exhibited increased bacterial accumulation in comparison to smoother areas of the coupons (as visualised by increased lectin staining and GFP fluorescence) when re-used.

Based on the results presented in Chapters 3 and 4, which have described biofilm formation in the CBR by *Ps. a.* under industrially-relevant low and high shear stress regimes, mature biofilm formation upon working surfaces could occur in both low and high shear environments within 72 hours. There is therefore perhaps a precedence to keep manufacturing equipment and the environment in which it is housed as sterile as possible; reducing the risk of microbial contaminants entering the system at any vulnerable sites. In manufacturing plants, such as those used by P&G, the onus must be on ensuring that methods of sanitisation are as effective as possible to control surface-associated routes of contamination (i.e. through biofilm formation and their subsequent persistence) across all processes.

In manufacturing systems that are composed of several different processes, each requiring specific equipment and varying flow regimes, whole-system control regimes,

such as the circulation of fluid via clean-in-place systems which can be ran more regularly with minimal disruption due to their in-house design (Gibson *et al.,* 2001), and without the need for *in situ* application of biocides or disinfectants, may ensure that planktonic contaminants are effectively washed out of the system before they have a chance to adhere to surfaces or that or 'younger' biofilms lacking a well-defined ECM and mature structure, are more easily penetrated and removed. Sampling raw ingredients (including water) and formulations across the entire manufacturing system, and their analysis via spectroscopic methods to determine which microorganisms and ECM components (such as EPS and eDNA) are present, would further enable monitoring of the system over time and enable preparation for methods of control and removal.

## 6.3. Future work

This PhD project has characterised the roles of Psl and Pel in biofilm formation by PA01 and PA14, under shear conditions industrially-relevant to P&G. Furthermore, it has provided an insight into the ability of *Ps. a.* to utilise eDNA, Psl and Pel in different morphologies (which are likely to have different chemical properties) in response to increased shear stress. Through use of the CBR, low and high shear conditions at 75 and 350 RPM respectively, the effect of the following parameters on biofilm formation could each be investigated in turn, adapted as necessary in order to model industrially-relevant conditions:

1. Coupon material (for example, PE as used in this study versus stainless steel or polytetrafluoroethylene)

2. Residence time of bacteria in the CBR (for example, decreasing residence time would result in an increased rate of medium flow into and out of the reactor)
3. Use of industrial isolates of *Ps. a.* rather than reference strains
4. Medium, either concentration or composition (i.e. TSB versus minimal medium such as M9 or M63+)
5. Temperature (as suggested Sakuragi and Kolter, (2007), and Kim *et al.,* (2020), who reported expression of *pel* is thermoregulated)
6. Visualisation of other ECM components (such as proteins or rhamnolipids)

# References

# References


Ageorges, V., Schiavone, M., Jubelin, G., Caccia, N., Ruiz, P., Chafsey, I., Bailly, X., Dague, E., Leroy, S., Paxman, J., 2019. Differential homotypic and heterotypic interactions of antigen 43 (Ag43) variants in autotransporter-mediated bacterial autoaggregation. Scientific Reports 9, 1-19.

Agladze, K., Jackson, D., Romeo, T., 2003. Periodicity of cell attachment patterns during Escherichia coli biofilm development. J. Bacteriol. 185, 5632-5638.

Agladze, K., Wang, X., Romeo, T., 2005. Spatial periodicity of Escherichia coli K-12 biofilm microstructure initiates during a reversible, polar attachment phase of development and requires the polysaccharide adhesin PGA. J. Bacteriol. 187, 8237-8246.

Agostinho, A., Hartman, A., Lipp, C., Parker, A.E., Stewart, P.S., James, G.A., 2011. An in vitro model for the growth and analysis of chronic wound MRSA biofilms. J. Appl. Microbiol. 111, 1275-1282.

Ahmer, B.M., 2004. Cell-to-cell signalling in Escherichia coli and Salmonella enterica. Mol. Microbiol. 52, 933-945.

Aim, R.A., Hallinan, J.P., Watson, A.A., Mattick, J.S., 1996. Fimbrial biogenesis genes of Pseudomonas aeruginosa: pilW and pilX increase the similarity of type 4 fimbriae to the GSP protein-secretion systems and pilY1 encodes a gonococcal PilC homologue. Mol. Microbiol. 22, 161-173.

Allesen-Holm, M., Barken, K.B., Yang, L., Klausen, M., Webb, J.S., Kjelleberg, S., Molin, S., Givskov, M., Tolker-Nielsen, T., 2006. A characterization of DNA release in Pseudomonas aeruginosa cultures and biofilms. Mol. Microbiol. 59, 1114-1128.

Allison, J.S., Dawson, M., Drake, D., Montie, T.C., 1985. Electrophoretic separation and molecular weight characterization of Pseudomonas aeruginosa H-antigen flagellins. Infect. Immun. 49, 770-774.

Almeida, F.A.d., Pimentel-Filho, N.d.J., Pinto, U.M., Mantovani, H.C., Oliveira, L.L.d., Vanetti, M.C.D., 2017. Acyl homoserine lactone-based quorum sensing stimulates biofilm formation by Salmonella Enteritidis in anaerobic conditions. Arch. Microbiol. 199, 475-486.

Ammons, M.C.B., Ward, L.S., James, G.A., 2011. Anti-biofilm efficacy of a lactoferrin/xylitol wound hydrogel used in combination with silver wound dressings. International Wound Journal 8, 268-273.

An, D., Danhorn, T., Fuqua, C., Parsek, M.R., 2006. Quorum sensing and motility mediate interactions between Pseudomonas aeruginosa and Agrobacterium tumefaciens in biofilm cocultures. Proceedings of the National Academy of Sciences 103, 3828-3833.

Anderson, M.J., Parks, P.J., Peterson, M.L., 2013. A mucosal model to study microbial biofilm development and anti-biofilm therapeutics. J. Microbiol. Methods 92, 201-208.

Anyan, M.E., Amiri, A., Harvey, C.W., Tierra, G., Morales-Soto, N., Driscoll, C.M., Alber, M.S., Shrout, J.D., 2014. Type IV pili interactions promote intercellular association and

moderate swarming of Pseudomonas aeruginosa. Proc. Natl. Acad. Sci. U. S. A. 111, 18013-18018.

Aprikian, P., Interlandi, G., Kidd, B.A., Le Trong, I., Tchesnokova, V., Yakovenko, O., Whitfield, M.J., Bullitt, E., Stenkamp, R.E., Thomas, W.E., 2011. The bacterial fimbrial tip acts as a mechanical force sensor. PLoS Biol 9, e1000617.

Araújo, P.A., Malheiro, J., Machado, I., Mergulhão, F., Melo, L., Simões, M., 2016. Influence of flow velocity on the characteristics of Pseudomonas fluorescens biofilms. J. Environ. Eng. 142, 04016031.

Arnqvist, A., Olsén, A., Normark, S., 1994. σS-dependent growth-phase induction of the csgBA promoter in Escherichia coli can be achieved in vivo by σ70 in the absence of the nucleoid-associated protein H-NS. Mol. Microbiol. 13, 1021-1032.

Arora, S.K., Bangera, M., Lory, S., Ramphal, R., 2001. A genomic island in Pseudomonas aeruginosa carries the determinants of flagellin glycosylation. Proc. Natl. Acad. Sci. U. S. A. 98, 9342-9347.

Atlung, T., Ingmer, H., 1997. H-NS: a modulator of environmentally regulated gene expression. Mol. Microbiol. 24, 7-17.

Azeredo, J., Azevedo, N.F., Briandet, R., Cerca, N., Coenye, T., Costa, A.R., Desvaux, M., Di Bonaventura, G., Hébraud, M., Jaglic, Z., 2017. Critical review on biofilm methods. Crit. Rev. Microbiol. 43, 313-351.

Baker, P., Ricer, T., Moynihan, P.J., Kitova, E.N., Walvoort, M.T., Little, D.J., Whitney, J.C., Dawson, K., Weadge, J.T., Robinson, H., 2014. P. aeruginosa SGNH hydrolase-like proteins AlgJ and AlgX have similar topology but separate and distinct roles in alginate acetylation. PLoS Pathog 10, e1004334.

Bansal, T., Englert, D., Lee, J., Hegde, M., Wood, T.K., Jayaraman, A., 2007. Differential effects of epinephrine, norepinephrine, and indole on Escherichia coli O157: H7 chemotaxis, colonization, and gene expression. Infect. Immun. 75, 4597-4607.

Baraquet, C., Murakami, K., Parsek, M.R., Harwood, C.S., 2012. The FleQ protein from Pseudomonas aeruginosa functions as both a repressor and an activator to control gene expression from the pel operon promoter in response to c-di-GMP. Nucleic Acids Res. 40, 7207-7218.

Barends, T.R., Hartmann, E., Griese, J.J., Beitlich, T., Kirienko, N.V., Ryjenkov, D.A., Reinstein, J., Shoeman, R.L., Gomelsky, M., Schlichting, I., 2009. Structure and mechanism of a bacterial light-regulated cyclic nucleotide phosphodiesterase. Nature 459, 1015-1018.

Barken, K.B., Pamp, S.J., Yang, L., Gjermansen, M., Bertrand, J.J., Klausen, M., Givskov, M., Whitchurch, C.B., Engel, J.N., Tolker-Nielsen, T., 2008. Roles of type IV pili, flagellum-mediated motility and extracellular DNA in the formation of mature multicellular structures in Pseudomonas aeruginosa biofilms. Environ. Microbiol. 10, 2331-2343.

Barnhart, M.M., Chapman, M.R., 2006. Curli biogenesis and function. Annu. Rev. Microbiol. 60, 131-147.

Barth, M., Marschall, C., Muffler, A., Fischer, D., Hengge-Aronis, R., 1995. Role for the histone-like protein H-NS in growth phase-dependent and osmotic regulation of sigma S and many sigma S-dependent genes in Escherichia coli. J. Bacteriol. 177, 3455-3464.

Basu Roy, A., Sauer, K., 2014. Diguanylate cyclase NicD-based signalling mechanism of nutrient-induced dispersion by P seudomonas aeruginosa. Mol. Microbiol. 94, 771-793.

Beaussart, A., Baker, A.E., Kuchma, S.L., El-Kirat-Chatel, S., O'Toole, G.A., Dufrêne, Y.F., 2014. Nanoscale adhesion forces of Pseudomonas aeruginosa type IV pili. ACS Nano 8, 10723-10733.

Beloin, C., Roux, A., Ghigo, J., 2008. Escherichia coli biofilms. Bacterial Biofilms , 249-289.

Beloin, C., Valle, J., Latour-Lambert, P., Faure, P., Kzreminski, M., Balestrino, D., Haagensen, J.A., Molin, S., Prensier, G., Arbeille, B., 2004. Global impact of mature biofilm lifestyle on Escherichia coli K-12 gene expression. Mol. Microbiol. 51, 659-674.

Berne, C., Ducret, A., Hardy, G.G., Brun, Y.V., 2015. Adhesins involved in attachment to abiotic surfaces by Gram-negative bacteria. Microbial Biofilms , 163-199.

Besemer, K., Singer, G., Limberger, R., Chlup, A., Hochedlinger, G., Hödl, I., Baranyi, C., Battin, T.J., 2007. Biophysical controls on community succession in stream biofilms. Appl. Environ. Microbiol. 73, 4966-4974.

Beyenal, H., Lewandowski, Z., 2002. Internal and external mass transfer in biofilms grown at various flow velocities. Biotechnol. Prog. 18, 55-61.

Bharathi, P., Bhowmick, P., Shekar, M., Karunasagar, I., 2011. Biofilm formation by pure and mixed culture of Lactobacillus isolates on polystyrene surface in varying nutrient conditions. Biotechnol Bioinf Bioeng 1, 93-98.

Bhattacharjee, S., Basnet, M., Tufenkji, N., Ghoshal, S., 2016. Effects of rhamnolipid and carboxymethylcellulose coatings on reactivity of palladium-doped nanoscale zerovalent iron particles. Environ. Sci. Technol. 50, 1812-1820.

Biais, N., Ladoux, B., Higashi, D., So, M., Sheetz, M., 2008. Cooperative retraction of bundled type IV pili enables nanonewton force generation. PLoS Biol 6, e87.

Bidossi, A., De Grandi, R., Toscano, M., Bottagisio, M., De Vecchi, E., Gelardi, M., Drago, L., 2018. Probiotics Streptococcus salivarius 24SMB and Streptococcus oralis 89a interfere with biofilm formation of pathogens of the upper respiratory tract. BMC Infectious Diseases 18, 1-11.

Bjarnsholt, T., 2013. The role of bacterial biofilms in chronic infections. Apmis 121, 1-58.

Blair, D.F., 2003. Flagellar movement driven by proton translocation. FEBS Lett. 545, 86-95.

Blanc, V., Isabal, S., Sanchez, M., Llama-Palacios, A., Herrera, D., Sanz, M., León, R., 2014. Characterization and application of a flow system for in vitro multispecies oral biofilm formation. J. Periodont. Res. 49, 323-332.

Blount, Z.D., 2015. The natural history of model organisms: The unexhausted potential of E. coli. Elife 4, e05826.

Boles, B.R., McCarter, L.L., 2002. Vibrio parahaemolyticus scrABC, a novel operon affecting swarming and capsular polysaccharide regulation. J. Bacteriol. 184, 5946-5954.

Borlee, B.R., Goldman, A.D., Murakami, K., Samudrala, R., Wozniak, D.J., Parsek, M.R., 2010. Pseudomonas aeruginosa uses a cyclic-di-GMP-regulated adhesin to reinforce the biofilm extracellular matrix. Mol. Microbiol. 75, 827-842.

Bougdour, A., Lelong, C., Geiselmann, J., 2004. Crl, a low temperature-induced protein in Escherichia coli that binds directly to the stationary phase σ subunit of RNA polymerase. J. Biol. Chem. 279, 19540-19550.

Boulané-Petermann, L., 1996. Processes of bioadhesion on stainless steel surfaces and cleanability: a review with special reference to the food industry. Biofouling 10, 275-300.

Boyd, A., Chakrabarty, A., 1995. Pseudomonas aeruginosa biofilms: role of the alginate exopolysaccharide. Journal of Industrial Microbiology and Biotechnology 15, 162-168.

Boyd, A., Ghosh, M., May, T.B., Shinabarger, D., Keogh, R., Chakrabarty, A., 1993. Sequence of the algL gene of Pseudomonas aeruginosa and purification of its alginate lyase product. Gene 131, 1-8.

Boyd, A., Chakrabarty, A.M., 1994. Role of alginate lyase in cell detachment of Pseudomonas aeruginosa. Appl. Environ. Microbiol. 60, 2355-2359.

Branda, S.S., Vik, Å., Friedman, L., Kolter, R., 2005. Biofilms: the matrix revisited. Trends Microbiol. 13, 20-26.

Brok, R., Van Gelder, P., Winterhalter, M., Ziese, U., Koster, A.J., de Cock, H., Koster, M., Tommassen, J., Bitter, W., 1999. The C-terminal domain of the Pseudomonas secretin XcpQ forms oligomeric rings with pore activity. J. Mol. Biol. 294, 1169-1179.

Brombacher, E., Baratto, A., Dorel, C., Landini, P., 2006. Gene expression regulation by the curli activator CsgD protein: modulation of cellulose biosynthesis and control of negative determinants for microbial adhesion. J. Bacteriol. 188, 2027-2037.

Brombacher, E., Dorel, C., Zehnder, A.J., Landini, P., 2003. The curli biosynthesis regulator CsgD co-ordinates the expression of both positive and negative determinants for biofilm formation in Escherichia coli. Microbiology 149, 2847-2857.

Brooks, J.D., Flint, S.H., 2008. Biofilms in the food industry: problems and potential solutions. Int. J. Food Sci. Tech. 43, 2163-2176.

Brückner, R., Titgemeyer, F., 2002. Carbon catabolite repression in bacteria: choice of the carbon source and autoregulatory limitation of sugar utilization. FEMS Microbiol. Lett. 209, 141-148.

Bryers, J.D., 2008. Medical biofilms. Biotechnol. Bioeng. 100, 1-18.

Bryers, J.D., Drummond, F., 1998. Local macromolecule diffusion coefficients in structurally non-uniform bacterial biofilms using fluorescence recovery after photobleaching (FRAP). Biotechnol. Bioeng. 60, 462-473.

Bryers, J.D., Ratner, B.D., 2004. Bioinspired implant materials befuddle bacteria. ASM News-American Society for Microbiology 70, 232-232.

Bryers, J., Characklis, W., 1981. Early fouling biofilm formation in a turbulent flow system: overall kinetics. Water Res. 15, 483-491.

Buckingham-Meyer, K., Goeres, D.M., Hamilton, M.A., 2007. Comparative evaluation of biofilm disinfectant efficacy tests. J. Microbiol. Methods 70, 236-244.

Bühler, T., Ballestero, S., Desai, M., Brown, M., 1998. Generation of a reproducible nutrient-depleted biofilm of Escherichia coli and Burkholderia cepacia. J. Appl. Microbiol. 85, 457-462.

Burmølle, M., Webb, J.S., Rao, D., Hansen, L.H., Sørensen, S.J., Kjelleberg, S., 2006. Enhanced biofilm formation and increased resistance to antimicrobial agents and bacterial invasion are caused by synergistic interactions in multispecies biofilms. Appl. Environ. Microbiol. 72, 3916-3923.

Burns, J.L., Gibson, R.L., McNamara, S., Yim, D., Emerson, J., Rosenfeld, M., Hiatt, P., McCoy, K., Castile, R., Smith, A.L., 2001. Longitudinal assessment of Pseudomonas aeruginosa in young children with cystic fibrosis. J. Infect. Dis. 183, 444-452.

Burrows, L.L., 2012. Pseudomonas aeruginosa twitching motility: type IV pili in action. Annu. Rev. Microbiol. 66, 493-520.

Busscher, H.J., van der Mei, Henny C, 2006. Microbial adhesion in flow displacement systems. Clin. Microbiol. Rev. 19, 127-141.

Byrd, M.S., Pang, B., Mishra, M., Swords, W.E., Wozniak, D.J., 2010. The Pseudomonas aeruginosa exopolysaccharide Psl facilitates surface adherence and NF-κB activation in A549 cells. Mbio 1, e00140-10.

Byrd, M.S., Sadovskaya, I., Vinogradov, E., Lu, H., Sprinkle, A.B., Richardson, S.H., Ma, L., Ralston, B., Parsek, M.R., Anderson, E.M., 2009. Genetic and biochemical analyses of the Pseudomonas aeruginosa Psl exopolysaccharide reveal overlapping roles for polysaccharide synthesis enzymes in Psl and LPS production. Mol. Microbiol. 73, 622-638.

Cadieux, P., Wignall, G., Carriveau, R., 2009. Introduction to biofilms in urology. In: Anonymous , Biomaterials and Tissue Engineering in Urology. Elsevier, , pp. 3-41.

Caffrey, P., Owen, P., 1989. Purification and N-terminal sequence of the alpha subunit of antigen 43, a unique protein complex associated with the outer membrane of Escherichia coli. J. Bacteriol. 171, 3634-3640.

Cai, S.J., Inouye, M., 2002. EnvZ-OmpR interaction and osmoregulation in Escherichia coli. J. Biol. Chem. 277, 24155-24161.

Caiazza, N.C., Merritt, J.H., Brothers, K.M., O'Toole, G.A., 2007. Inverse regulation of biofilm formation and swarming motility by Pseudomonas aeruginosa PA14. J. Bacteriol. 189, 3603-3612.

Calfee, M.W., Coleman, J.P., Pesci, E.C., 2001. Interference with Pseudomonas quinolone signal synthesis inhibits virulence factor expression by Pseudomonas aeruginosa. Proc. Natl. Acad. Sci. U. S. A. 98, 11633-11637.

Campisano, A., Schroeder, C., Schemionek, M., Overhage, J., Rehm, B.H., 2006. PslD is a secreted protein required for biofilm formation by Pseudomonas aeruginosa. Appl. Environ. Microbiol. 72, 3066-3068.

Carter, M.Q., Feng, D., Li, H.H., 2019. Curli fimbriae confer shiga toxin-producing Escherichia coli a competitive trait in mixed biofilms. Food Microbiol. 82, 482-488.

Castelli, P., Caronno, R., Ferrarese, S., Mantovani, V., Piffaretti, G., Tozzi, M., Lomazzi, C., Rivolta, N., Sala, A., 2006. New trends in prosthesis infection in cardiovascular surgery. Surgical Infections 7, s-45-s-47.

Cattò, C., Cappitelli, F., 2019. Testing Anti-Biofilm Polymeric Surfaces: Where to Start? International Journal of Molecular Sciences 20, 3794.

Celmer, D., Oleszkiewicz, J., Cicek, N., 2008. Impact of shear force on the biofilm structure and performance of a membrane biofilm reactor for tertiary hydrogen-driven denitrification of municipal wastewater. Water Res. 42, 3057-3065.

Chandler, J.R., Heilmann, S., Mittler, J.E., Greenberg, E.P., 2012. Acyl-homoserine lactone-dependent eavesdropping promotes competition in a laboratory co-culture model. The ISME Journal 6, 2219-2228.

Chapman, M.R., Robinson, L.S., Pinkner, J.S., Roth, R., Heuser, J., Hammar, M., Normark, S., Hultgren, S.J., 2002. Role of Escherichia coli curli operons in directing amyloid fiber formation. Science 295, 851-855.

Characklis, W.G., 1981. Bioengineering report: fouling biofilm development: a process analysis. Biotechnol. Bioeng. 23, 1923-1960.

Chau, N.P.T., Pandit, S., Jung, J., Jeon, J., 2014. Evaluation of Streptococcus mutans adhesion to fluoride varnishes and subsequent change in biofilm accumulation and acidogenicity. J. Dent. 42, 726-734.

Chauhan, A., Sakamoto, C., Ghigo, J., Beloin, C., 2013. Did I pick the right colony? Pitfalls in the study of regulation of the phase variable antigen 43 adhesin. PLoS One 8, e73568.

Chen, A.I., Dolben, E.F., Okegbe, C., Harty, C.E., Golub, Y., Thao, S., Ha, D.G., Willger, S.D., O'Toole, G.A., Harwood, C.S., 2014. Candida albicans ethanol stimulates Pseudomonas aeruginosa WspR-controlled biofilm formation as part of a cyclic relationship involving phenazines. PLoS Pathog 10, e1004480.

Chen, M., Zhang, Z., Bott, T., 2005. Effects of operating conditions on the adhesive strength of Pseudomonas fluorescens biofilms in tubes. Colloids and Surfaces B: Biointerfaces 43, 61-71.

Chew, S.C., Kundukad, B., Seviour, T., van der Maarel, Johan RC, Yang, L., Rice, S.A., Doyle, P., Kjelleberg, S., 2014. Dynamic remodeling of microbial biofilms by functionally distinct exopolysaccharides. Mbio 5, e01536-14.

Chitnis, C.E., Ohman, D.E., 1990. Cloning of Pseudomonas aeruginosa algG, which controls alginate structure. J. Bacteriol. 172, 2894-2900.

Choi, Y., Morgenroth, E., 2003. Monitoring biofilm detachment under dynamic changes in shear stress using laser-based particle size analysis and mass fractionation. Water Science and Technology 47, 69-76.

Chou, F., Chou, H., Lin, Y., Yang, B., Lin, N., Weng, S., Tseng, Y., 1997. TheXanthomonas campestris gumDGene Required for Synthesis of Xanthan Gum Is Involved in Normal Pigmentation and Virulence in Causing Black Rot. Biochem. Biophys. Res. Commun. 233, 265-269.

Chou, S., Galperin, M.Y., 2016. Diversity of cyclic di-GMP-binding proteins and mechanisms. J. Bacteriol. 198, 32-46.

Chugani, S.A., Whiteley, M., Lee, K.M., D'Argenio, D., Manoil, C., Greenberg, E.P., 2001. QscR, a modulator of quorum-sensing signal synthesis and virulence in Pseudomonas aeruginosa. Proc. Natl. Acad. Sci. U. S. A. 98, 2752-2757.

Climo, M.W., Patron, R.L., Goldstein, B.P., Archer, G.L., 1998. Lysostaphin treatment of experimental methicillin-resistant Staphylococcus aureus aortic valve endocarditis. Antimicrob. Agents Chemother. 42, 1355-1360.

Cloete, T., 2003. Biofouling control in industrial water systems: What we know and what we need to know. Materials and Corrosion 54, 520-526.

Cloete, T.E., Jacobs, L., Brözel, V.S., 1998. The chemical control of biofouling in industrial water systems. Biodegradation 9, 23-37.

Coenye, T., De Prijck, K., De Wever, B., Nelis, H.J., 2008. Use of the modified Robbins device to study the in vitro biofilm removal efficacy of NitrAdine™, a novel disinfecting formula for the maintenance of oral medical devices. J. Appl. Microbiol. 105, 733-740.

Cohen, D., Mechold, U., Nevenzal, H., Yarmiyhu, Y., Randall, T.E., Bay, D.C., Rich, J.D., Parsek, M.R., Kaever, V., Harrison, J.J., Banin, E., 2015. Oligoribonuclease is a central feature of cyclic diguanylate signaling in Pseudomonas aeruginosa. Proc. Natl. Acad. Sci. U. S. A. 112, 11359-11364.

Colvin, K.M., Alnabelseya, N., Baker, P., Whitney, J.C., Howell, P.L., Parsek, M.R., 2013. PelA deacetylase activity is required for Pel polysaccharide synthesis in Pseudomonas aeruginosa. J. Bacteriol. 195, 2329-2339.

Colvin, K.M., Gordon, V.D., Murakami, K., Borlee, B.R., Wozniak, D.J., Wong, G.C., Parsek, M.R., 2011. The pel polysaccharide can serve a structural and protective role in the biofilm matrix of Pseudomonas aeruginosa. PLoS Pathog 7, e1001264.

Colvin, K.M., Irie, Y., Tart, C.S., Urbano, R., Whitney, J.C., Ryder, C., Howell, P.L., Wozniak, D.J., Parsek, M.R., 2012. The Pel and Psl polysaccharides provide Pseudomonas aeruginosa structural redundancy within the biofilm matrix. Environ. Microbiol. 14, 1913-1928.

Cookson, A.L., Cooley, W.A., Woodward, M.J., 2002. The role of type 1 and curli fimbriae of Shiga toxin-producing Escherichia coli in adherence to abiotic surfaces. International Journal of Medical Microbiology 292, 195-205.

Cooley, B.J., Thatcher, T.W., Hashmi, S.M., L'her, G., Le, H.H., Hurwitz, D.A., Provenzano, D., Touhami, A., Gordon, V.D., 2013. The extracellular polysaccharide Pel makes the attachment of P. aeruginosa to surfaces symmetric and short-ranged. Soft Matter 9, 3871-3876.

Correnti, J., Munster, V., Chan, T., Woude, M.v.d., 2002. Dam-dependent phase variation of Ag43 in Escherichia coli is altered in a seqA mutant. Mol. Microbiol. 44, 521-532.

Costerton, J.W., 2007. The Biofilm Primer, Springer Science & Business Media.

Costerton, J.W., 1999. Introduction to biofilm. Int. J. Antimicrob. Agents 11, 217-221.

Costerton, J.W., Geesey, G.G., Cheng, K., 1978. How bacteria stick. Sci. Am. 238, 86-95.

Costerton, J.W., Lewandowski, Z., DeBeer, D., Caldwell, D., Korber, D., James, G., 1994. Biofilms, the customized microniche. J. Bacteriol. 176, 2137-2142.

Coulon, C., Vinogradov, E., Filloux, A., Sadovskaya, I., 2010. Chemical analysis of cellular and extracellular carbohydrates of a biofilm-forming strain Pseudomonas aeruginosa PA14. PLoS One 5, e14220.

Cronan, J.E., 2014. Escherichia coli as an Experimental Organism. eLS, John Wiley and Sons Ltd (Ed.)., 1-7.

Culotti, A., Packman, A.I., 2014. Pseudomonas aeruginosa promotes Escherichia coli biofilm formation in nutrient-limited medium. PLoS One 9, e107186.

da Costa Lima, Jailton Lobo, Alves, L.R., de Araujo Jacome, Paula Regina Luna, Neto, J.P.B., Maciel, M.A.V., de Morais, Marcia Maria Camargo, 2018. Biofilm production by clinical isolates of Pseudomonas aeruginosa and structural changes in LasR protein of isolates non biofilm-producing. The Brazilian Journal of Infectious Diseases 22, 129-136.

Danese, P.N., Pratt, L.A., Dove, S.L., Kolter, R., 2000. The outer membrane protein, antigen 43, mediates cell-to-cell interactions within Escherichia coli biofilms. Mol. Microbiol. 37, 424-432.

Dasgupta, N., Arora, S.K., Ramphal, R., 2000. fleN, a gene that regulates flagellar number in Pseudomonas aeruginosa. J. Bacteriol. 182, 357-364.

Dasgupta, N., Wolfgang, M.C., Goodman, A.L., Arora, S.K., Jyot, J., Lory, S., Ramphal, R., 2003. A four-tiered transcriptional regulatory circuit controls flagellar biogenesis in Pseudomonas aeruginosa. Mol. Microbiol. 50, 809-824.

Davey, M.E., Caiazza, N.C., O'Toole, G.A., 2003. Rhamnolipid surfactant production affects biofilm architecture in Pseudomonas aeruginosa PAO1. J. Bacteriol. 185, 1027-1036.

Davies, D., 2003. Understanding biofilm resistance to antibacterial agents. Nature Reviews Drug Discovery 2, 114-122.

Davies, D.G., Parsek, M.R., Pearson, J.P., Iglewski, B.H., Costerton, J.W., Greenberg, E.P., 1998. The involvement of cell-to-cell signals in the development of a bacterial biofilm. Science 280, 295-298.

De Beer, D., Stoodley, P., Roe, F., Lewandowski, Z., 1994. Effects of biofilm structures on oxygen distribution and mass transport. Biotechnol. Bioeng. 43, 1131-1138.

De Keersmaecker, S.C., Sonck, K., Vanderleyden, J., 2006. Let LuxS speak up in AI-2 signaling. Trends Microbiol. 14, 114-119.

De Kievit, T.R., Gillis, R., Marx, S., Brown, C., Iglewski, B.H., 2001. Quorum-sensing genes in Pseudomonas aeruginosa biofilms: their role and expression patterns. Appl. Environ. Microbiol. 67, 1865-1873.

De Luna, Maria das Graças, Scott-Tucker, A., Desvaux, M., Ferguson, P., Morin, N.P., Dudley, E.G., Turner, S., Nataro, J.P., Owen, P., Henderson, I.R., 2008. The Escherichia coli biofilm-promoting protein Antigen 43 does not contribute to intestinal colonization. FEMS Microbiol. Lett. 284, 237-246.

De, N., Navarro, M.V., Wang, Q., Krasteva, P.V., Sondermann, H., 2010. Biophysical assays for protein interactions in the Wsp sensory system and biofilm formation. Meth. Enzymol. 471, 161-184.

De, N., Pirruccello, M., Krasteva, P.V., Bae, N., Raghavan, R.V., Sondermann, H., 2008. Phosphorylation-independent regulation of the diguanylate cyclase WspR. PLoS Biol 6, e67.

Dean, G.E., Macnab, R.M., Stader, J., Matsumura, P., Burks, C., 1984. Gene sequence and predicted amino acid sequence of the motA protein, a membrane-associated protein required for flagellar rotation in Escherichia coli. J. Bacteriol. 159, 991-999.

DeLisa, M.P., Wu, C., Wang, L., Valdes, J.J., Bentley, W.E., 2001. DNA microarray-based identification of genes controlled by autoinducer 2-stimulated quorum sensing in Escherichia coli. J. Bacteriol. 183, 5239-5247.

Déziel, E., Gopalan, S., Tampakaki, A.P., Lépine, F., Padfield, K.E., Saucier, M., Xiao, G., Rahme, L.G., 2005. The contribution of MvfR to Pseudomonas aeruginosa pathogenesis and quorum sensing circuitry regulation: multiple quorum sensing-regulated genes are modulated without affecting lasRI, rhlRI or the production of N-acyl-L-homoserine lactones. Mol. Microbiol. 55, 998-1014.

Di Martino, P., 2018. Extracellular polymeric substances, a key element in understanding biofilm phenotype. AIMS Microbiol. 4, 274-288.

Dietrich, G., Kurz, S., Hübner, C., Aepinus, C., Theiss, S., Guckenberger, M., Panzner, U., Weber, J., Frosch, M., 2003. Transcriptome analysis of Neisseria meningitidis during infection. J. Bacteriol. 185, 155-164.

Diggle, S.P., Matthijs, S., Wright, V.J., Fletcher, M.P., Chhabra, S.R., Lamont, I.L., Kong, X., Hider, R.C., Cornelis, P., Cámara, M., 2007. The Pseudomonas aeruginosa 4-quinolone signal molecules HHQ and PQS play multifunctional roles in quorum sensing and iron entrapment. Chem. Biol. 14, 87-96.

Diggle, S.P., Winzer, K., Chhabra, S.R., Worrall, K.E., Cámara, M., Williams, P., 2003. The Pseudomonas aeruginosa quinolone signal molecule overcomes the cell density-dependency of the quorum sensing hierarchy, regulates rhl-dependent genes at the onset of stationary phase and can be produced in the absence of LasR. Mol. Microbiol. 50, 29-43.

do Valle Gomes, Milene Zezzi, Nitschke, M., 2012. Evaluation of rhamnolipid and surfactin to reduce the adhesion and remove biofilms of individual and mixed cultures of food pathogenic bacteria. Food Control 25, 441-447.

Doggett, R.G., Harrison, G.M., Stillwell, R.N., Wallis, E.S., 1966. An atypical Pseudomonas aeruginosa associated with cystic fibrosis of the pancreas. J. Pediatr. 68, 215-221.

Domka, J., Lee, J., Bansal, T., Wood, T.K., 2007. Temporal gene-expression in Escherichia coli K-12 biofilms. Environ. Microbiol. 9, 332-346.

Domka, J., Lee, J., Wood, T.K., 2006. YliH (BssR) and YceP (BssS) regulate Escherichia coli K-12 biofilm formation by influencing cell signaling. Appl. Environ. Microbiol. 72, 2449-2459.

Donlan, R.M., 2002. Biofilms: microbial life on surfaces. Emerg. Infect. Dis. 8, 881-890.

Dorel, C., Vidal, O., Prigent-Combaret, C., Vallet, I., Lejeune, P., 1999. Involvement of the Cpx signal transduction pathway of E. coli in biofilm formation. FEMS Microbiol. Lett. 178, 169-175.

Douterelo, I., Jackson, M., Solomon, C., Boxall, J., 2016. Microbial analysis of in situ biofilm formation in drinking water distribution systems: implications for monitoring and control of drinking water quality. Appl. Microbiol. Biotechnol. 100, 3301-3311.

Doyle, T.B., Hawkins, A.C., McCarter, L.L., 2004. The complex flagellar torque generator of Pseudomonas aeruginosa. J. Bacteriol. 186, 6341-6350.

Duanis-Assaf, D., Duanis-Assaf, T., Zeng, G., Meyer, R.L., Reches, M., Steinberg, D., Shemesh, M., 2018. Cell wall associated protein TasA provides an initial binding component to extracellular polysaccharides in dual-species biofilm. Scientific Reports 8, 1-10.

Dudin, O., Geiselmann, J., Ogasawara, H., Ishihama, A., Lacour, S., 2014. Repression of flagellar genes in exponential phase by CsgD and CpxR, two crucial modulators of Escherichia coli biofilm formation. J. Bacteriol. 196, 707-715.

Dufrêne, Y.F., 2014. Atomic force microscopy in microbiology: new structural and functional insights into the microbial cell surface. Mbio 5, e01363-14.

Duncan, M.J., Mann, E.L., Cohen, M.S., Ofek, I., Sharon, N., Abraham, S.N., 2005. The distinct binding specificities exhibited by enterobacterial type 1 fimbriae are determined by their fimbrial shafts. J. Biol. Chem. 280, 37707-37716.

Elias, S., Banin, E., 2012. Multi-species biofilms: living with friendly neighbors. FEMS Microbiol. Rev. 36, 990-1004.

ENOMOTO, M., IINO, T., 1966. The comparison of normal and curly flagella in Salmonella abortus-equi by two-dimensional separation of peptides. The Japanese Journal of Genetics 41, 131-139.

Evans, M.L., Chapman, M.R., 2014. Curli biogenesis: order out of disorder. Biochimica Et Biophysica Acta (BBA)-Molecular Cell Research 1843, 1551-1558.

Evans, M.L., Chorell, E., Taylor, J.D., Åden, J., Götheson, A., Li, F., Koch, M., Sefer, L., Matthews, S.J., Wittung-Stafshede, P., 2015. The bacterial curli system possesses a potent and selective inhibitor of amyloid formation. Mol. Cell 57, 445-455.

Evans, L.R., Linker, A., 1973. Production and characterization of the slime polysaccharide of Pseudomonas aeruginosa. J. Bacteriol. 116, 915-924.

Faille, C., Brauge, T., Leleu, G., Hanin, A., Denis, C., Midelet, G., 2020. Comparison of the performance of the biofilm sampling methods (swab, sponge, contact agar) in the recovery of Listeria monocytogenes populations considering the seafood environment conditions. Int. J. Food Microbiol. 325, 108626.

Fazli, M., Bjarnsholt, T., Kirketerp-Møller, K., Jørgensen, B., Andersen, A.S., Krogfelt, K.A., Givskov, M., Tolker-Nielsen, T., 2009. Nonrandom distribution of Pseudomonas aeruginosa and Staphylococcus aureus in chronic wounds. J. Clin. Microbiol. 47, 4084-4089.

Feirer, N., Xu, J., Allen, K.D., Koestler, B.J., Bruger, E.L., Waters, C.M., White, R.H., Fuqua, C., 2015. A pterin-dependent signaling pathway regulates a dual-function diguanylate cyclase-phosphodiesterase controlling surface attachment in Agrobacterium tumefaciens. Mbio 6, e00156-15.

Fenchel, T., 2002. Microbial behavior in a heterogeneous world. Science 296, 1068-1071.

Ferrer, M.D., Mira, A., 2016. Oral biofilm architecture at the microbial scale. Trends Microbiol. 24, 246-248.

Ferrières, L., Clarke, D.J., 2003. The RcsC sensor kinase is required for normal biofilm formation in Escherichia coli K-12 and controls the expression of a regulon in response to growth on a solid surface. Mol. Microbiol. 50, 1665-1682.

Fick, R.B.,Jr, Sonoda, F., Hornick, D.B., 1992. Emergence and persistence of Pseudomonas aeruginosa in the cystic fibrosis airway. Semin. Respir. Infect. 7, 168-178.

Firth, N., Ippen-Ihler, K., Skurray, R.A., 1996. Structure and function of the F factor and mechanism of conjugation. Escherichia Coli and Salmonella: Cellular and Molecular Biology, 2nd Ed.ASM Press, Washington, DC , 2377-2401.

Fitzpatrick, F., Humphreys, H., O'gara, J., 2005. The genetics of staphylococcal biofilm formation—will a greater understanding of pathogenesis lead to better management of device-related infection? Clinical Microbiology and Infection 11, 967-973.

Flemming, H., 2011. Microbial biofouling: unsolved problems, insufficient approaches, and possible solutions. In: Anonymous , Biofilm Highlights. Springer, , pp. 81-109.

Flemming, H., Neu, T.R., Wozniak, D.J., 2007. The EPS matrix: the “house of biofilm cells”. J. Bacteriol. 189, 7945-7947.

Flemming, H., Wingender, J., 2010. The biofilm matrix. Nature Reviews Microbiology 8, 623-633.

Flemming, H., Wingender, J., Szewzyk, U., 2011. Biofilm Highlights, Springer Science & Business Media.

Flemming, H., Wingender, J., Szewzyk, U., Steinberg, P., Rice, S.A., Kjelleberg, S., 2016. Biofilms: an emergent form of bacterial life. Nature Reviews Microbiology 14, 563.

Floyd, K., Eberly, A., Hadjifrangiskou, M., 2017. Adhesion of bacteria to surfaces and biofilm formation on medical devices. In: Anonymous , Biofilms and Implantable Medical Devices. Elsevier, , pp. 47-95.

Fonseca, A., Sousa, J., 2007. Effect of shear stress on growth, adhesion and biofilm formation of Pseudomonas aeruginosa with antibiotic-induced morphological changes. Int. J. Antimicrob. Agents 30, 236-241.

Forero, M., Yakovenko, O., Sokurenko, E.V., Thomas, W.E., Vogel, V., 2006. Uncoiling mechanics of Escherichia coli type I fimbriae are optimized for catch bonds. PLoS Biol 4, e298.

Francis, N.R., Sosinsky, G.E., Thomas, D., DeRosier, D.J., 1994. Isolation, characterization and structure of bacterial flagellar motors containing the switch complex. J. Mol. Biol. 235, 1261-1270.

Franklin, M.J., Nivens, D.E., Weadge, J.T., Howell, P.L., 2011. Biosynthesis of the Pseudomonas aeruginosa extracellular polysaccharides, alginate, Pel, and Psl. Frontiers in Microbiology 2, 167.

Franklin, M.J., Ohman, D.E., 2002. Mutant analysis and cellular localization of the AlgI, AlgJ, and AlgF proteins required for O acetylation of alginate in Pseudomonas aeruginosa. J. Bacteriol. 184, 3000-3007.

Franklin, M.J., Ohman, D.E., 1993. Identification of algF in the alginate biosynthetic gene cluster of Pseudomonas aeruginosa which is required for alginate acetylation. J. Bacteriol. 175, 5057-5065.

Freestone, P.P., Haigh, R.D., Lyte, M., 2007. Specificity of catecholamine-induced growth in Escherichia coli O157: H7, Salmonella enterica and Yersinia enterocolitica. FEMS Microbiol. Lett. 269, 221-228.

Friedlander, R.S., Vogel, N., Aizenberg, J., 2015. Role of flagella in adhesion of Escherichia coli to abiotic surfaces. Langmuir 31, 6137-6144.

Friedlander, R.S., Vlamakis, H., Kim, P., Khan, M., Kolter, R., Aizenberg, J., 2013. Bacterial flagella explore microscale hummocks and hollows to increase adhesion. Proc. Natl. Acad. Sci. U. S. A. 110, 5624-5629.

Friedman, L., Kolter, R., 2004. Two Genetic Loci Produce Distinct Carbohydrate-Rich Structural Components of the Pseudomonas Aeruginosa Biofilm Matrix .

Friedman, L., Kolter, R., 2004. Genes involved in matrix formation in Pseudomonas aeruginosa PA14 biofilms. Mol. Microbiol. 51, 675-690.

Friman, V., Diggle, S.P., Buckling, A., 2013. Protist predation can favour cooperation within bacterial species. Biology Letters 9, 20130548.

Fuqua, W.C., Winans, S.C., Greenberg, E.P., 1994. Quorum sensing in bacteria: the LuxR-LuxI family of cell density-responsive transcriptional regulators. J. Bacteriol. 176, 269-275.

Fux, C., Shirtliff, M., Stoodley, P., Costerton, J.W., 2005. Can laboratory reference strains mirror 'real-world'pathogenesis? Trends Microbiol. 13, 58-63.

Gallagher, L.A., McKnight, S.L., Kuznetsova, M.S., Pesci, E.C., Manoil, C., 2002. Functions required for extracellular quinolone signaling by Pseudomonas aeruginosa. J. Bacteriol. 184, 6472-6480.

Gally, D.L., Leathart, J., Blomfield, I.C., 1996. Interaction of FimB and FimE with the fim switch that controls the phase variation of type 1 fimbriae in Escherichia coli K-12. Mol. Microbiol. 21, 725-738.

Garny, K., Horn, H., Neu, T.R., 2008. Interaction between biofilm development, structure and detachment in rotating annular reactors. Bioprocess and Biosystems Engineering 31, 619-629.

Geankoplis, C.J., 1993. Separation Process Principles. Prentice-Hall International, Inc., Upper Saddle River, NJ

Geesey, G., Richardson, W., Yeomans, H., Irvin, R., Costerton, J., 1977. Microscopic examination of natural sessile bacterial populations from an alpine stream. Can. J. Microbiol. 23, 1733-1736.

Gellatly, S.L., Hancock, R.E., 2013. Pseudomonas aeruginosa: new insights into pathogenesis and host defenses. Pathogens and Disease 67, 159-173.

Gerstel, U., Park, C., Römling, U., 2003. Complex regulation of csgD promoter activity by global regulatory proteins. Mol. Microbiol. 49, 639-654.

Ghafoor, A., Hay, I.D., Rehm, B.H., 2011. Role of exopolysaccharides in Pseudomonas aeruginosa biofilm formation and architecture. Appl. Environ. Microbiol. 77, 5238-5246.

Ghigo, J., 2001. Natural conjugative plasmids induce bacterial biofilm development. Nature 412, 442-445.

Gibson, H., Taylor, J., Hall, K., Holah, J., 1999. Effectiveness of cleaning techniques used in the food industry in terms of the removal of bacterial biofilms. J. Appl. Microbiol. 87, 41-48.

Gloag, E.S., German, G.K., Stoodley, P., Wozniak, D.J., 2018. Viscoelastic properties of Pseudomonas aeruginosa variant biofilms. Scientific Reports 8, 1-11.

Gloag, E.S., Turnbull, L., Huang, A., Vallotton, P., Wang, H., Nolan, L.M., Mililli, L., Hunt, C., Lu, J., Osvath, S.R., Monahan, L.G., Cavaliere, R., Charles, I.G., Wand, M.P., Gee, M.L., Prabhakar, R., Whitchurch, C.B., 2013. Self-organization of bacterial biofilms is facilitated by extracellular DNA. Proc. Natl. Acad. Sci. U. S. A. 110, 11541-11546.

Goeres, D.M., Hamilton, M.A., Beck, N.A., Buckingham-Meyer, K., Hilyard, J.D., Loetterle, L.R., Lorenz, L.A., Walker, D.K., Stewart, P.S., 2009. A method for growing a biofilm under low shear at the air–liquid interface using the drip flow biofilm reactor. Nature Protocols 4, 783.

Goeres, D.M., Loetterle, L.R., Hamilton, M.A., Murga, R., Kirby, D.W., Donlan, R.M., 2005. Statistical assessment of a laboratory method for growing biofilms. Microbiology 151, 757-762.

Goeres, D.M., 2006. Design of Model Reactor Systems for Evaluating Disinfectants Against Biofilm Bacteria, Montana State University.

González Barrios, A.F., Zuo, R., Hashimoto, Y., Yang, L., Bentley, W.E., Wood, T.K., 2006. Autoinducer 2 controls biofilm formation in Escherichia coli through a novel motility quorum-sensing regulator (MqsR, B3022). J. Bacteriol. 188, 305-316.

Goodman, A.L., Kulasekara, B., Rietsch, A., Boyd, D., Smith, R.S., Lory, S., 2004. A signaling network reciprocally regulates genes associated with acute infection and chronic persistence in Pseudomonas aeruginosa. Developmental Cell 7, 745-754.

Gottesman, S., 1984. Bacterial regulation: global regulatory networks. Annu. Rev. Genet. 18, 415-441.

Götz, F., 2002. Staphylococcus and biofilms. Mol. Microbiol. 43, 1367-1378.

Goulter, R., Gentle, I., Dykes, G., 2009. Issues in determining factors influencing bacterial attachment: a review using the attachment of Escherichia coli to abiotic surfaces as an example. Lett. Appl. Microbiol. 49, 1-7.

Govan, J.R., Deretic, V., 1996. Microbial pathogenesis in cystic fibrosis: mucoid Pseudomonas aeruginosa and Burkholderia cepacia. Microbiol. Rev. 60, 539-574.

Graham, M.V., Mosier, A.P., Kiehl, T.R., Kaloyeros, A.E., Cady, N.C., 2013. Development of antifouling surfaces to reduce bacterial attachment. Soft Matter 9, 6235-6244.

Gualdi, L., Tagliabue, L., Bertagnoli, S., Ierano, T., De Castro, C., Landini, P., 2008. Cellulose modulates biofilm formation by counteracting curli-mediated colonization of solid surfaces in Escherichia coli. Microbiology 154, 2017-2024.

Gupta, P., Sarkar, S., Das, B., Bhattacharjee, S., Tribedi, P., 2016. Biofilm, pathogenesis and prevention—a journey to break the wall: a review. Arch. Microbiol. 198, 1-15.

Güvener, Z.T., Harwood, C.S., 2007. Subcellular location characteristics of the Pseudomonas aeruginosa GGDEF protein, WspR, indicate that it produces cyclic-di-GMP in response to growth on surfaces. Mol. Microbiol. 66, 1459-1473.

Ha, D., O'Toole, G.A., 2015. c-di-GMP and its effects on biofilm formation and dispersion: a Pseudomonas aeruginosa review. Microbial Biofilms , 301-317.

Haagmans, W., van Der Woude, M., 2000. Phase variation of Ag43 in Escherichia coli: Dam-dependent methylation abrogates OxyR binding and OxyR-mediated repression of transcription. Mol. Microbiol. 35, 877-887.

Habimana, O., Heir, E., Langsrud, S., Åsli, A.W., Møretrø, T., 2010. Enhanced surface colonization by Escherichia coli O157: H7 in biofilms formed by an Acinetobacter calcoaceticus isolate from meat-processing environments. Appl. Environ. Microbiol. 76, 4557-4559.

Hadjifrangiskou, M., Gu, A.P., Pinkner, J.S., Kostakioti, M., Zhang, E.W., Greene, S.E., Hultgren, S.J., 2012. Transposon mutagenesis identifies uropathogenic Escherichia coli biofilm factors. J. Bacteriol. 194, 6195-6205.

Haiko, J., Westerlund-Wikström, B., 2013. The role of the bacterial flagellum in adhesion and virulence. Biology 2, 1242-1267.

Hall-Stoodley, L., Costerton, J.W., Stoodley, P., 2004. Bacterial biofilms: from the natural environment to infectious diseases. Nature Reviews Microbiology 2, 95-108.

Hall-Stoodley, L., Stoodley, P., 2005. Biofilm formation and dispersal and the transmission of human pathogens. Trends Microbiol. 13, 7-10.

Hamilton, W.D., 1964. The genetical evolution of social behaviour. II. J. Theor. Biol. 7, 17-52.

Hammar, M.r., Arnqvist, A., Bian, Z., Olsén, A., Normark, S., 1995. Expression of two csg operons is required for production of fibronectin-and congo red-binding curli polymers in Escherichia coli K-12. Mol. Microbiol. 18, 661-670.

Hammar, M., Bian, Z., Normark, S., 1996. Nucleator-dependent intercellular assembly of adhesive curli organelles in Escherichia coli. Proc. Natl. Acad. Sci. U. S. A. 93, 6562-6566.

Hanna, A., Berg, M., Stout, V., Razatos, A., 2003. Role of capsular colanic acid in adhesion of uropathogenic Escherichia coli. Appl. Environ. Microbiol. 69, 4474-4481.

Hansen, S.K., Rainey, P.B., Haagensen, J.A., Molin, S., 2007. Evolution of species interactions in a biofilm community. Nature 445, 533-536.

Hara, T., Ueda, S., 1981. A study on the mechanism of DNA excretion from P. aeruginosa KYU-1. Agric. Biol. Chem. 45, 2457-2461.

Hardie, K.R., Cooksley, C., Green, A.D., Winzer, K., 2003. Autoinducer 2 activity in Escherichia coli culture supernatants can be actively reduced despite maintenance of an active synthase, LuxS. Microbiology 149, 715-728.

Harris, S.L., Elliott, D.A., Blake, M.C., Must, L.M., Messenger, M., Orndorff, P.E., 1990. Isolation and characterization of mutants with lesions affecting pellicle formation and erythrocyte agglutination by type 1 piliated Escherichia coli. J. Bacteriol. 172, 6411-6418.

Harrison, F., Browning, L.E., Vos, M., Buckling, A., 2006. Cooperation and virulence in acute Pseudomonas aeruginosainfections. BMC Biology 4, 1-5.

Harrison, J.J., Turner, R.J., Ceri, H., 2007. A subpopulation of Candida albicans and Candida tropicalis biofilm cells are highly tolerant to chelating agents. FEMS Microbiol. Lett. 272, 172-181.

Hartl, D.L., Dykhuizen, D.E., 1984. The population genetics of Escherichia coli. Annu. Rev. Genet. 18, 31-68.

Hathroubi, S., Mekni, M.A., Domenico, P., Nguyen, D., Jacques, M., 2017. Biofilms: microbial shelters against antibiotics. Microbial Drug Resistance 23, 147-156.

Hay, I.D., Remminghorst, U., Rehm, B.H., 2009. MucR, a novel membrane-associated regulator of alginate biosynthesis in Pseudomonas aeruginosa. Appl. Environ. Microbiol. 75, 1110-1120.

He, J., Baldini, R.L., Deziel, E., Saucier, M., Zhang, Q., Liberati, N.T., Lee, D., Urbach, J., Goodman, H.M., Rahme, L.G., 2004. The broad host range pathogen Pseudomonas aeruginosa strain PA14 carries two pathogenicity islands harboring plant and animal virulence genes. Proc. Natl. Acad. Sci. U. S. A. 101, 2530-2535.

Heiniger, R.W., Winther-Larsen, H.C., Pickles, R.J., Koomey, M., Wolfgang, M.C., 2010. Infection of human mucosal tissue by Pseudomonas aeruginosa requires sequential and mutually dependent virulence factors and a novel pilus-associated adhesin. Cell. Microbiol. 12, 1158-1173.

Helmuth, R., Achtman, M., 1978. Cell-cell interactions in conjugating Escherichia coli: purification of F pili with biological activity. Proc. Natl. Acad. Sci. U. S. A. 75, 1237-1241.

Henderson, I.R., Meehan, M., Owen, P., 1997. Antigen 43, a phase-variable bipartite outer membrane protein, determines colony morphology and autoaggregation in Escherichia coli K-12. FEMS Microbiol. Lett. 149, 115-120.

Henderson, I.R., Owen, P., 1999. The major phase-variable outer membrane protein of Escherichia coli structurally resembles the immunoglobulin A1 protease class of exported protein and is regulated by a novel mechanism involving Dam and OxyR. J. Bacteriol. 181, 2132-2141.

Hengge, R., 2009. Principles of c-di-GMP signalling in bacteria. Nature Reviews Microbiology 7, 263-273.

Hengge-Aronis, R., 2002. Signal transduction and regulatory mechanisms involved in control of the σS (RpoS) subunit of RNA polymerase. Microbiology and Molecular Biology Reviews 66, 373-395.

Hengge-Aronis, R., Klein, W., Lange, R., Rimmele, M., Boos, W., 1991. Trehalose synthesis genes are controlled by the putative sigma factor encoded by rpoS and are involved in stationary-phase thermotolerance in Escherichia coli. J. Bacteriol. 173, 7918-7924.

Henikoff, S., Wallace, J.C., Brown, J.P., 1990. [7] Finding protein similarities with nucleotide sequence databases. Methods Enzymol. 1990;183:111-32.

Hense, B.A., Kuttler, C., Müller, J., Rothballer, M., Hartmann, A., Kreft, J., 2007. Does efficiency sensing unify diffusion and quorum sensing? Nature Reviews Microbiology 5, 230-239.

Hentzer, M., Riedel, K., Rasmussen, T.B., Heydorn, A., Andersen, J.B., Parsek, M.R., Rice, S.A., Eberl, L., Molin, S., Høiby, N., 2002. Inhibition of quorum sensing in Pseudomonas aeruginosa biofilm bacteria by a halogenated furanone compound. Microbiology 148, 87-102.

Hentzer, M., Wu, H., Andersen, J.B., Riedel, K., Rasmussen, T.B., Bagge, N., Kumar, N., Schembri, M.A., Song, Z., Kristoffersen, P., 2003. Attenuation of Pseudomonas aeruginosa virulence by quorum sensing inhibitors. Embo j. 22, 3803-3815.

Heras, B., Totsika, M., Peters, K.M., Paxman, J.J., Gee, C.L., Jarrott, R.J., Perugini, M.A., Whitten, A.E., Schembri, M.A., 2014. The antigen 43 structure reveals a molecular Velcro-like mechanism of autotransporter-mediated bacterial clumping. Proc. Natl. Acad. Sci. U. S. A. 111, 457-462.

Hickman, J.W., Tifrea, D.F., Harwood, C.S., 2005. A chemosensory system that regulates biofilm formation through modulation of cyclic diguanylate levels. Proc. Natl. Acad. Sci. U. S. A. 102, 14422-14427.

Hirayama, S., Nojima, N., Furukawa, S., Ogihara, H., Morinaga, Y., 2019. Steric microstructure of mixed-species biofilm formed by interaction between Lactobacillus plantarum ML11-11 and Saccharomyces cerevisiae. Biosci. Biotechnol. Biochem. 83, 2386-2389.

Hirota, N., Imae, Y., 1983. Na -driven flagellar motors of an alkalophilic Bacillus strain YN-1. J. Biol. Chem. 258, 10577-10581.

Høiby, N., 1975. Prevalence of mucoid strains of Pseudomonas aeruginosa in bacteriological specimens from patients with cystic fibrosis and patients with other diseases. Acta Pathologica Microbiologica Scandinavica Section B Microbiology 83, 549-552.

Høiby, N., Bjarnsholt, T., Givskov, M., Molin, S., Ciofu, O., 2010. Antibiotic resistance of bacterial biofilms. Int. J. Antimicrob. Agents 35, 322-332.

Høiby, N., Ciofu, O., Bjarnsholt, T., 2010. Pseudomonas aeruginosa biofilms in cystic fibrosis. Future Microbiology 5, 1663-1674.

Hooton, T.M., Bradley, S.F., Cardenas, D.D., Colgan, R., Geerlings, S.E., Rice, J.C., Saint, S., Schaeffer, A.J., Tambayh, P.A., Tenke, P., 2010. Diagnosis, prevention, and treatment of catheter-associated urinary tract infection in adults: 2009 International Clinical Practice Guidelines from the Infectious Diseases Society of America. Clinical Infectious Diseases 50, 625-663.

Horn, H., Reiff, H., Morgenroth, E., 2003. Simulation of growth and detachment in biofilm systems under defined hydrodynamic conditions. Biotechnol. Bioeng. 81, 607-617.

Hoštacká, A., Čižnár, I., Štefkovičová, M., 2010. Temperature and pH affect the production of bacterial biofilm. Folia Microbiol. (Praha) 55, 75-78.

Hou, B., Meng, X., Zhang, L., Tan, C., Jin, H., Zhou, R., Gao, J., Wu, B., Li, Z., Liu, M., 2014. TolC promotes ExPEC biofilm formation and curli production in response to medium osmolarity. BioMed Research International 2014.

Hou, J., Veeregowda, D.H., van de Belt-Gritter, B., Busscher, H.J., van der Mei, Henny C, 2018. Extracellular polymeric matrix production and relaxation under fluid shear and mechanical pressure in Staphylococcus aureus biofilms. Appl. Environ. Microbiol. 84, e01516-17.

Houari, A., Picard, J., Habarou, H., Galas, L., Vaudry, H., Heim, V., Di Martino, P., 2008. Rheology of biofilms formed at the surface of NF membranes in a drinking water production unit. Biofouling 24, 235-240.

Hu, M., Zhang, C., Mu, Y., Shen, Q., Feng, Y., 2010. Indole affects biofilm formation in bacteria. Indian J. Microbiol. 50, 362-368.

Huang, B., Whitchurch, C.B., Mattick, J.S., 2003. FimX, a Multidomain Protein Connecting EnvironmentalSignals to Twitching Motility in Pseudomonasaeruginosa. J. Bacteriol. 185, 7068-7076.

Huang, C., Lin, H., Yang, X., 2012. Industrial production of recombinant therapeutics in Escherichia coli and its recent advancements. Journal of Industrial Microbiology and Biotechnology 39, 383-399.

Huangyutitham, V., Güvener, Z.T., Harwood, C.S., 2013. Subcellular clustering of the phosphorylated WspR response regulator protein stimulates its diguanylate cyclase activity. Mbio 4, e00242-13.

Hueso-Gil, Á., Calles, B., de Lorenzo, V., 2020. The Wsp intermembrane complex mediates metabolic control of the swim-attach decision of Pseudomonas putida. Environ. Microbiol. 22, 3535-3547.

Hufnagel, D.A., Evans, M.L., Greene, S.E., Pinkner, J.S., Hultgren, S.J., Chapman, M.R., 2016. The catabolite repressor protein-cyclic AMP complex regulates csgD and biofilm formation in uropathogenic Escherichia coli. J. Bacteriol. 198, 3329-3334.

Hung, C., Marschall, J., Burnham, C.D., Byun, A.S., Henderson, J.P., 2014. The bacterial amyloid curli is associated with urinary source bloodstream infection. PLoS One 9, e86009.

Hunke, S., Keller, R., Müller, V.S., 2012. Signal integration by the Cpx-envelope stress system. FEMS Microbiol. Lett. 326, 12-22.

Irie, Y., Borlee, B.R., O'Connor, J.R., Hill, P.J., Harwood, C.S., Wozniak, D.J., Parsek, M.R., 2012. Self-produced exopolysaccharide is a signal that stimulates biofilm formation in Pseudomonas aeruginosa. Proc. Natl. Acad. Sci. U. S. A. 109, 20632-20636.

Ishihama, A., 2000. Functional modulation of Escherichia coli RNA polymerase. Annual Reviews in Microbiology 54, 499-518.

Ishizuka, H., Hanamura, A., Kunimura, T., Aiba, H., 1993. A lowered concentration of cAMP receptor protein caused by glucose is an important determinant for catabolite repression in Escherichia coli. Mol. Microbiol. 10, 341-350.

Itoh, Y., Rice, J.D., Goller, C., Pannuri, A., Taylor, J., Meisner, J., Beveridge, T.J., Preston III, J.F., Romeo, T., 2008. Roles of pgaABCD genes in synthesis, modification, and export of the Escherichia coli biofilm adhesin poly-β-1, 6-N-acetyl-D-glucosamine. J. Bacteriol. 190, 3670-3680.

Jackson, D.W., Suzuki, K., Oakford, L., Simecka, J.W., Hart, M.E., Romeo, T., 2002. Biofilm formation and dispersal under the influence of the global regulator CsrA of Escherichia coli. J. Bacteriol. 184, 290-301.

Jackson, G., Beyenal, H., Rees, W.M., Lewandowski, Z., 2001. Growing reproducible biofilms with respect to structure and viable cell counts. J. Microbiol. Methods 47, 1-10.

Jackson, K.D., Starkey, M., Kremer, S., Parsek, M.R., Wozniak, D.J., 2004. Identification of Psl, a Locus Encoding a Potential Exopolysaccharide that is Essential for Pseudomonas Aeruginosa PAO1 Biofilm Formation. J Bacteriol. 2004 Jul;186(14):4466-75

Jahid, I.K., Mizan, M.F.R., Myoung, J., Ha, S., 2018. Aeromonas hydrophila biofilm, exoprotease, and quorum sensing responses to co-cultivation with diverse foodborne pathogens and food spoilage bacteria on crab surfaces. Biofouling 34, 1079-1092.

Jain, S., Ohman, D.E., 2005. Role of an alginate lyase for alginate transport in mucoid Pseudomonas aeruginosa. Infect. Immun. 73, 6429-6436.

Jamal, M., Ahmad, W., Andleeb, S., Jalil, F., Imran, M., Nawaz, M.A., Hussain, T., Ali, M., Rafiq, M., Kamil, M.A., 2018. Bacterial biofilm and associated infections. Journal of the Chinese Medical Association 81, 7-11.

Jass, J., Roberts, S.K., Lappin-Scott, H.M., 2002. Microbes and enzymes in biofilms. Enzymes in the Environment.Activity, Ecology and Applications.Marcel Dekker Inc., New York, USA , 307-326.

Jefferson, K.K., 2004. What drives bacteria to produce a biofilm? FEMS Microbiol. Lett. 236, 163-173.

Jefferson, K.K., Goldmann, D.A., Pier, G.B., 2005. Use of confocal microscopy to analyze the rate of vancomycin penetration through Staphylococcus aureus biofilms. Antimicrob. Agents Chemother. 49, 2467-2473.

Jennings, L.K., Storek, K.M., Ledvina, H.E., Coulon, C., Marmont, L.S., Sadovskaya, I., Secor, P.R., Tseng, B.S., Scian, M., Filloux, A., 2015. Pel is a cationic exopolysaccharide that cross-links extracellular DNA in the Pseudomonas aeruginosa biofilm matrix. Proceedings of the National Academy of Sciences 112, 11353-11358.

Jennings, L.K., Storek, K.M., Ledvina, H.E., Coulon, C., Marmont, L.S., Sadovskaya, I., Secor, P.R., Tseng, B.S., Scian, M., Filloux, A., Wozniak, D.J., Howell, P.L., Parsek, M.R., 2015. Pel is a cationic exopolysaccharide that cross-links extracellular DNA in the Pseudomonas aeruginosa biofilm matrix. Proc. Natl. Acad. Sci. U. S. A. 112, 11353-11358.

JENSEN, E.T., KHARAZMI, A., HØIBY, N., COSTERTON, J.W., 1992. Some bacterial parameters influencing the neutrophil oxidative burst response to Pseudomonas aeruginosa biofilms. Apmis 100, 727-733.

Johannesson, B., Yamada, K., Hosokawa, Y., Mori, D., 2005. An approach for the evaluation of combined process of chloride penetration and carbonation by a multi-species model. Journal of Research-Taiheiyo Cement Corporation 148, 4.

Joo, H., Otto, M., 2012. Molecular basis of in vivo biofilm formation by bacterial pathogens. Chem. Biol. 19, 1503-1513.

Jørgensen, F., Bally, M., Chapon-Herve, V., Michel, G., Lazdunski, A., Williams, P., Stewart, G., 1999. RpoS-dependent stress tolerance in Pseudomonas aeruginosa. Microbiology 145, 835-844.

Joys, T.M., 1988. The flagellar filament protein. Can. J. Microbiol. 34, 452-458.

Jubelin, G., Vianney, A., Beloin, C., Ghigo, J., Lazzaroni, J., Lejeune, P., Dorel, C., 2005. CpxR/OmpR interplay regulates curli gene expression in response to osmolarity in Escherichia coli. J. Bacteriol. 187, 2038-2049.

Jude, B.A., Taylor, R.K., 2011. The physical basis of type 4 pilus-mediated microcolony formation by Vibrio cholerae O1. J. Struct. Biol. 175, 1-9.

Juhas, M., Wiehlmann, L., Huber, B., Jordan, D., Lauber, J., Salunkhe, P., Limpert, A.S., von Götz, F., Steinmetz, I., Eberl, L., 2004. Global regulation of quorum sensing and virulence by VqsR in Pseudomonas aeruginosa. Microbiology 150, 831-841.

Kansal, R., Rasko, D.A., Sahl, J.W., Munson, G.P., Roy, K., Luo, Q., Sheikh, A., Kuhne, K.J., Fleckenstein, J.M., 2013. Transcriptional modulation of enterotoxigenic Escherichia coli virulence genes in response to epithelial cell interactions. Infect. Immun. 81, 259-270.

Kaper, J.B., Sperandio, V., 2005. Bacterial cell-to-cell signaling in the gastrointestinal tract. Infect. Immun. 73, 3197-3209.

Kaplan, J.á., 2010. Biofilm dispersal: mechanisms, clinical implications, and potential therapeutic uses. J. Dent. Res. 89, 205-218.

Karatan, E., Watnick, P., 2009. Signals, regulatory networks, and materials that build and break bacterial biofilms. Microbiology and Molecular Biology Reviews 73, 310-347.

Katharios-Lanwermeyer, S., Whitfield, G.B., Howell, P.L., O'Toole, G., 2020. Pseudomonas aeruginosa uses c-di-GMP phosphodiesterases RmcA and MorA to regulate biofilm maintenance. mBio. 12(1):e03384-20.

Katouli, M., 2010. Population structure of gut Escherichia coli and its role in development of extra-intestinal infections. Iran. J. Microbiol. 2, 59-72.

Kazmierczak, B.I., Lebron, M.B., Murray, T.S., 2006. Analysis of FimX, a phosphodiesterase that governs twitching motility in Pseudomonas aeruginosa. Mol. Microbiol. 60, 1026-1043.

Kendall, M.M., Sperandio, V., 2007. Quorum sensing by enteric pathogens. Curr. Opin. Gastroenterol. 23, 10-15.

Kendall, M.M., Sperandio, V., 2014. Cell-to-Cell Signaling in Escherichia coli and Salmonella. EcoSal Plus 6, 10.1128/ecosalplus.ESP-0002-2013.

Kharadi, R.R., Sundin, G.W., 2019. Physiological and microscopic characterization of cyclic-di-GMP-mediated autoaggregation in Erwinia amylovora. Frontiers in Microbiology 10, 468.

Kiedrowski, M.R., Horswill, A.R., 2011. New approaches for treating staphylococcal biofilm infections. Ann. N. Y. Acad. Sci. 1241, 104-121.

Kikuchi, T., Mizunoe, Y., Takade, A., Naito, S., Yoshida, S., 2005. Curli fibers are required for development of biofilm architecture in Escherichia coli K-12 and enhance bacterial adherence to human uroepithelial cells. Microbiol. Immunol. 49, 875-884.

Kim, B.Y., Thyiam, G., Kang, J., Lee, S., Park, S., Kim, J., Abraham, M., 2012. Development of an Escherichia coli Biofilm Model on Transwell®. Korean Journal of Clinical Laboratory Science 44, 112-117.

Kim, J., Park, W., 2013. Indole inhibits bacterial quorum sensing signal transmission by interfering with quorum sensing regulator folding. Microbiology 159, 2616-2625.

Kim, L.H., Chong, T.H., 2017. Physiological responses of salinity-stressed Vibrio sp. and the effect on the biofilm formation on a nanofiltration membrane. Environ. Sci. Technol. 51, 1249-1258.

Kim, S., Li, X., Hwang, H., Lee, J., 2020. Thermoregulation of Pseudomonas aeruginosa biofilm formation. Appl. Environ. Microbiol. 86, e01584-20.

Kim, H.J., Boedicker, J.Q., Choi, J.W., Ismagilov, R.F., 2008. Defined spatial structure stabilizes a synthetic multispecies bacterial community. Proc. Natl. Acad. Sci. U. S. A. 105, 18188-18193.

Kim, W., Racimo, F., Schluter, J., Levy, S.B., Foster, K.R., 2014. Importance of positioning for microbial evolution. Proc. Natl. Acad. Sci. U. S. A. 111, E1639-47.

Kimkes, T.E., Heinemann, M., 2020. How bacteria recognise and respond to surface contact. FEMS Microbiol. Rev. 44, 106-122.

Kives, J., Guadarrama, D., Orgaz, B., Rivera-Sen, A., Vazquez, J., SanJose, C., 2005. Interactions in biofilms of Lactococcus lactis ssp. cremoris and Pseudomonas fluorescens cultured in cold UHT milk. J. Dairy Sci. 88, 4165-4171.

Klausen, M., Heydorn, A., Ragas, P., Lambertsen, L., Aaes-Jørgensen, A., Molin, S., Tolker-Nielsen, T., 2003. Biofilm formation by Pseudomonas aeruginosa wild type, flagella and type IV pili mutants. Mol. Microbiol. 48, 1511-1524.

Klemm, P., 1986. Two regulatory fim genes, fimB and fimE, control the phase variation of type 1 fimbriae in Escherichia coli. Embo j. 5, 1389-1393.

Klemm, P., Hjerrild, L., Gjermansen, M., Schembri, M.A., 2004. Structure-function analysis of the self-recognizing Antigen 43 autotransporter protein from Escherichia coli. Mol. Microbiol. 51, 283-296.

Kocharova, N., Hatano, K., Shaskov, A., Knirel, Y.A., Kochetkov, N., Pier, G., 1989. The structure and serologic distribution of an extracellular neutral polysaccharide from Pseudomonas aeruginosa immunotype 3. J. Biol. Chem. 264, 15569-15573.

Kojic, M., Venturi, V., 2001. Regulation of rpoS gene expression in Pseudomonas: involvement of a TetR family regulator. J. Bacteriol. 183, 3712-3720.

Kojima, S., Blair, D.F., 2004. The bacterial flagellar motor: structure and function of a complex molecular machine. Int. Rev. Cytol. 233, 93-135.

Körstgens, V., Flemming, H., Wingender, J., Borchard, W., 2001. Influence of calcium ions on the mechanical properties of a model biofilm of mucoid Pseudomonas aeruginosa. Water Science and Technology 43, 49-57.

Koseki, H., Yonekura, A., Shida, T., Yoda, I., Horiuchi, H., Morinaga, Y., Yanagihara, K., Sakoda, H., Osaki, M., Tomita, M., 2014. Early staphylococcal biofilm formation on solid orthopaedic implant materials: in vitro study. PloS One 9, e107588.

Kostakioti, M., Hadjifrangiskou, M., Hultgren, S.J., 2013. Bacterial biofilms: development, dispersal, and therapeutic strategies in the dawn of the postantibiotic era. Cold Spring Harb Perspect. Med. 3, a010306.

Kostylev, M., Kim, D.Y., Smalley, N.E., Salukhe, I., Greenberg, E.P., Dandekar, A.A., 2019. Evolution of the Pseudomonas aeruginosa quorum-sensing hierarchy. Proc. Natl. Acad. Sci. U. S. A. 116, 7027-7032.

Kragh, K.N., Hutchison, J.B., Melaugh, G., Rodesney, C., Roberts, A.E., Irie, Y., Jensen, P.Ø., Diggle, S.P., Allen, R.J., Gordon, V., 2016. Role of multicellular aggregates in biofilm formation. Mbio 7, e00237-16.

Król, J.E., Hall, D.C., Balashov, S., Pastor, S., Sibert, J., McCaffrey, J., Lang, S., Ehrlich, R.L., Earl, J., Mell, J.C., 2019. Genome rearrangements induce biofilm formation in Escherichia coli C–an old model organism with a new application in biofilm research. BMC Genomics 20, 1-18.

Kuchma, S.L., Griffin, E.F., O'Toole, G., 2012. Minor pilins of the type IV pilus system participate in the negative regulation of swarming motility. J. Bacteriol. 194, 5388-5403.

Kuchma, S., Ballok, A., Merritt, J., Hammond, J., Lu, W., Rabinowitz, J.D., O'Toole, G.A., 2010. Cyclic-Di-GMP-Mediated Repression of Swarming Motility by Pseudomonas Aeruginosa: The pilY1 Gene and its Impact on Surface-Associated Behaviors .

Kulasakara, H., Lee, V., Brencic, A., Liberati, N., Urbach, J., Miyata, S., Lee, D.G., Neely, A.N., Hyodo, M., Hayakawa, Y., Ausubel, F.M., Lory, S., 2006. Analysis of Pseudomonas aeruginosa diguanylate cyclases and phosphodiesterases reveals a role for bis-(3'-5')-cyclic-GMP in virulence. Proc. Natl. Acad. Sci. U. S. A. 103, 2839-2844.

Kulasekara, H.D., Ventre, I., Kulasekara, B.R., Lazdunski, A., Filloux, A., Lory, S., 2005. A novel two-component system controls the expression of Pseudomonas aeruginosa fimbrial cup genes. Mol. Microbiol. 55, 368-380.

Laganenka, L., Colin, R., Sourjik, V., 2016. Chemotaxis towards autoinducer 2 mediates autoaggregation in Escherichia coli. Nature Communications 7, 1-11.

Laganenka, L., Sourjik, V., 2018. Autoinducer 2-dependent Escherichia coli biofilm formation is enhanced in a dual-species coculture. Appl. Environ. Microbiol. 84, e02638-17.

Lam, J., Chan, R., Lam, K., Costerton, J.W., 1980. Production of mucoid microcolonies by Pseudomonas aeruginosa within infected lungs in cystic fibrosis. Infect. Immun. 28, 546-556.

Lappann, M., Claus, H., Van Alen, T., Harmsen, M., Elias, J., Molin, S., Vogel, U., 2010. A dual role of extracellular DNA during biofilm formation of Neisseria meningitidis. Mol. Microbiol. 75, 1355-1371.

Laspidou, C.S., Rittmann, B.E., 2004. Modeling the development of biofilm density including active bacteria, inert biomass, and extracellular polymeric substances. Water Res. 38, 3349-3361.

Latifi, A., Foglino, M., Tanaka, K., Williams, P., Lazdunski, A., 1996. A hierarchical quorum-sensing cascade in Pseudomonas aeruginosa links the transcriptional activators LasR and

RhIR (VsmR) to expression of the stationary-phase sigma factor RpoS. Mol. Microbiol. 21, 1137-1146.

Laubacher, M.E., Ades, S.E., 2008. The Rcs phosphorelay is a cell envelope stress response activated by peptidoglycan stress and contributes to intrinsic antibiotic resistance. J. Bacteriol. 190, 2065-2074.

Laue, H., Schenk, A., Li, H., Lambertsen, L., Neu, T.R., Molin, S., Ullrich, M.S., 2006. Contribution of alginate and levan production to biofilm formation by Pseudomonas syringae. Microbiology 152, 2909-2918.

Laverty, G., Gorman, S.P., Gilmore, B.F., 2014. Biomolecular mechanisms of Pseudomonas aeruginosa and Escherichia coli biofilm formation. Pathogens 3, 596-632.

Lawrence, J.R., Swerhone, G.D., Neu, T., 2000. A simple rotating annular reactor for replicated biofilm studies. J. Microbiol. Methods 42, 215-224.

Lecuyer, S., Rusconi, R., Shen, Y., Forsyth, A., Vlamakis, H., Kolter, R., Stone, H.A., 2011. Shear stress increases the residence time of adhesion of Pseudomonas aeruginosa. Biophys. J. 100, 341-350.

Ledgham, F., Ventre, I., Soscia, C., Foglino, M., Sturgis, J.N., Lazdunski, A., 2003. Interactions of the quorum sensing regulator QscR: interaction with itself and the other regulators of Pseudomonas aeruginosa LasR and RhlR. Mol. Microbiol. 48, 199-210.

Lee, C.K., Vachier, J., de Anda, J., Zhao, K., Baker, A.E., Bennett, R.R., Armbruster, C.R., Lewis, K.A., Tarnopol, R.L., Lomba, C.J., 2020. Social cooperativity of bacteria during reversible surface attachment in young biofilms: a quantitative comparison of Pseudomonas aeruginosa PA14 and PAO1. Mbio 11, e02644-19.

Lee, H., Chang, H., Venkatesan, N., Peng, H., 2008. Identification of amino acid residues important for the phosphomannose isomerase activity of PslB in Pseudomonas aeruginosa PAO1. FEBS Lett. 582, 3479-3483.

Lee, J., Jayaraman, A., Wood, T.K., 2007. Indole is an inter-species biofilm signal mediated by SdiA. BMC Microbiology 7, 1-15.

Lee, K.W.K., Periasamy, S., Mukherjee, M., Xie, C., Kjelleberg, S., Rice, S.A., 2014. Biofilm development and enhanced stress resistance of a model, mixed-species community biofilm. The ISME Journal 8, 894-907.

Lee, V.T., Matewish, J.M., Kessler, J.L., Hyodo, M., Hayakawa, Y., Lory, S., 2007. A cyclic-di-GMP receptor required for bacterial exopolysaccharide production. Mol. Microbiol. 65, 1474-1484.

Leech, J., 2017. Development of an *Escherichia coli* Biofilm Platform for use in Biocatalysis. PhD thesis, University of Birmingham, Birmingham, UK.

Leech, J., Golub, S., Allan, W., Simmons, M.J., Overton, T.W., 2020. Non-pathogenic Escherichia coli biofilms: effects of growth conditions and surface properties on structure and curli gene expression. Arch. Microbiol. 202, 1517-1527.

Leid, J.G., Willson, C.J., Shirtliff, M.E., Hassett, D.J., Parsek, M.R., Jeffers, A.K., 2005. The exopolysaccharide alginate protects Pseudomonas aeruginosa biofilm bacteria from IFN-gamma-mediated macrophage killing. J. Immunol. 175, 7512-7518.

Leimbach, A., Hacker, J., Dobrindt, U., 2013. E. coli as an all-rounder: the thin line between commensalism and pathogenicity. Between Pathogenicity and Commensalism , 3-32.

Lejeune, P., 2003. Contamination of abiotic surfaces: what a colonizing bacterium sees and how to blur it. Trends Microbiol. 11, 179-184.

Lelong, C., Aguiluz, K., Luche, S., Kuhn, L., Garin, J., Rabilloud, T., Geiselmann, J., 2007. The Crl-RpoS regulon of Escherichia coli. Molecular & Cellular Proteomics 6, 648-659.

Lembre, P., Lorentz, C., Di Martino, P., 2012. Exopolysaccharides of the biofilm matrix: a complex biophysical world. The Complex World of Polysaccharides , 371-392.

Lemon, K.P., Higgins, D.E., Kolter, R., 2007. Flagellar motility is critical for Listeria monocytogenes biofilm formation. J. Bacteriol. 189, 4418-4424.

Lemos, M., Mergulhão, F., Melo, L., Simões, M., 2015. The effect of shear stress on the formation and removal of Bacillus cereus biofilms. Food Bioprod. Process. 93, 242-248.

Lengeler, J., 2013. Catabolite Repression. Encyclopedia of Genetics, 2001, 281-284.https://www.sciencedirect.com/science/article/pii/B9780128012383024545

Leriche, V., Briandet, R., Carpentier, B., 2003. Ecology of mixed biofilms subjected daily to a chlorinated alkaline solution: spatial distribution of bacterial species suggests a protective effect of one species to another. Environ. Microbiol. 5, 64-71.

Lewandowski, Z., Evans, L., 2000. Structure and function of biofilms. Biofilms: Recent Advances in their Study and Control 1, 466.

Li, J., Attila, C., Wang, L., Wood, T.K., Valdes, J.J., Bentley, W.E., 2007. Quorum sensing in Escherichia coli is signaled by AI-2/LsrR: effects on small RNA and biofilm architecture. J. Bacteriol. 189, 6011-6020.

Li, K., Yang, G., Debru, A.B., Li, P., Zong, L., Li, P., Xu, T., Wu, W., Jin, S., Bao, Q., 2017. SuhB regulates the motile-sessile switch in Pseudomonas aeruginosa through the Gac/Rsm pathway and c-di-GMP signaling. Frontiers in Microbiology 8, 1045.

Liang, Z., 2015. The expanding roles of c-di-GMP in the biosynthesis of exopolysaccharides and secondary metabolites. Nat. Prod. Rep. 32, 663-683.

Linton, C., Sherriff, A., Millar, M., 1999. Use of a modified Robbins device to directly compare the adhesion of Staphylococcus epidermidis RP62A to surfaces. J. Appl. Microbiol. 86, 194-202.

Little, D.J., Whitney, J.C., Robinson, H., Yip, P., Nitz, M., Howell, P., 2012. Combining in situ proteolysis and mass spectrometry to crystallize Escherichia coli PgaB. Acta Crystallographica Section F: Structural Biology and Crystallization Communications 68, 842-845.

Little, D.J., Li, G., Ing, C., DiFrancesco, B.R., Bamford, N.C., Robinson, H., Nitz, M., Pomes, R., Howell, P.L., 2014. Modification and periplasmic translocation of the biofilm exopolysaccharide poly-beta-1,6-N-acetyl-D-glucosamine. Proc. Natl. Acad. Sci. U. S. A. 111, 11013-11018.

Liu, R., Zhu, J., Yu, Z., Joshi, D., Zhang, H., Lin, W., Yang, M., 2014. Molecular analysis of long-term biofilm formation on PVC and cast iron surfaces in drinking water distribution system. Journal of Environmental Sciences 26, 865-874.

Liu, W., Røder, H.L., Madsen, J.S., Bjarnsholt, T., Sørensen, S.J., Burmølle, M., 2016. Interspecific bacterial interactions are reflected in multispecies biofilm spatial organization. Frontiers in Microbiology , 1366.

Liu, W., Røder, H.L., Madsen, J.S., Bjarnsholt, T., Sørensen, S.J., Burmølle, M., 2016. Interspecific bacterial interactions are reflected in multispecies biofilm spatial organization. Frontiers in Microbiology , 1366.

Liu, W., Russel, J., Burmølle, M., Sørensen, S.J., Madsen, J.S., 2018. Micro-scale intermixing: a requisite for stable and synergistic co-establishment in a four-species biofilm. The ISME Journal 12, 1940-1951.

Liu, Y., Tay, J., 2002. The essential role of hydrodynamic shear force in the formation of biofilm and granular sludge. Water Res. 36, 1653-1665.

Liu, Z., Li, L., Fang, Z., Lee, Y., Zhao, J., Zhang, H., Chen, W., Li, H., Lu, W., 2021. The biofilm-forming ability of six Bifidobacterium strains on grape seed flour. Lwt 144, 111205.

Lopes, S.P., Ceri, H., Azevedo, N.F., Pereira, M.O., 2012. Antibiotic resistance of mixed biofilms in cystic fibrosis: impact of emerging microorganisms on treatment of infection. Int. J. Antimicrob. Agents 40, 260-263.

Ludensky, M., 2003. Control and monitoring of biofilms in industrial applications. Int. Biodeterior. Biodegrad. 51, 255-263.

Luo, Y., Zhao, K., Baker, A.E., Kuchma, S.L., Coggan, K.A., Wolfgang, M.C., Wong, G.C., O'Toole, G.A., 2015. A hierarchical cascade of second messengers regulates Pseudomonas aeruginosa surface behaviors. Mbio 6, e02456-14.

Ma, L., Conover, M., Lu, H., Parsek, M.R., Bayles, K., Wozniak, D.J., 2009. Assembly and development of the Pseudomonas aeruginosa biofilm matrix. PLoS Pathog 5, e1000354.

Ma, L., Jackson, K.D., Landry, R.M., Parsek, M.R., Wozniak, D.J., 2006. Analysis of Pseudomonas aeruginosa conditional psl variants reveals roles for the psl polysaccharide in adhesion and maintaining biofilm structure postattachment. J. Bacteriol. 188, 8213-8221.

Ma, L., Wang, S., Wang, D., Parsek, M.R., Wozniak, D.J., 2012. The roles of biofilm matrix polysaccharide Psl in mucoid Pseudomonas aeruginosa biofilms. FEMS Immunology & Medical Microbiology 65, 377-380.

Ma, Q., Wood, T.K., 2009. OmpA influences Escherichia coli biofilm formation by repressing cellulose production through the CpxRA two-component system. Environ. Microbiol. 11, 2735-2746.

Macnab, R.M., 1999. The bacterial flagellum: reversible rotary propellor and type III export apparatus. J. Bacteriol. 181, 7149-7153.

Madsen, J.S., Lin, Y., Squyres, G.R., Price-Whelan, A., de Santiago Torio, A., Song, A., Cornell, W.C., Sørensen, S.J., Xavier, J.B., Dietrich, L.E., 2015. Facultative control of matrix production optimizes competitive fitness in Pseudomonas aeruginosa PA14 biofilm models. Appl. Environ. Microbiol. 81, 8414-8426.

Magana, M., Sereti, C., Ioannidis, A., Mitchell, C.A., Ball, A.R., Magiorkinis, E., Chatzipanagiotou, S., Hamblin, M.R., Hadjifrangiskou, M., Tegos, G.P., 2018. Options and limitations in clinical investigation of bacterial biofilms. Clin. Microbiol. Rev. 31, e00084-16.

Mah, T.C., O'Toole, G.A., 2001. Mechanisms of biofilm resistance to antimicrobial agents. Trends Microbiol. 9, 34-39.

Majdalani, N., Gottesman, S., 2005. The Rcs phosphorelay: a complex signal transduction system. Annu. Rev. Microbiol. 59, 379-405.

Majdalani, N., Cunning, C., Sledjeski, D., Elliott, T., Gottesman, S., 1998. DsrA RNA regulates translation of RpoS message by an anti-antisense mechanism, independent of its action as an antisilencer of transcription. Proc. Natl. Acad. Sci. U. S. A. 95, 12462-12467.

Makman, R.S., Sutherland, E.W., 1965. Adenosine 3 ‘, 5 ‘-Phosphate in Escherichia coli. J. Biol. Chem. 240, 1309-1314.

Malone, J.G., Williams, R., Christen, M., Jenal, U., Spiers, A.J., Rainey, P., 2007. The structure–function relationship of WspR, a Pseudomonas fluorescens response regulator with a GGDEF output domain. Microbiology 153, 980-994.

Mann, E.E., Wozniak, D.J., 2012. Pseudomonas biofilm matrix composition and niche biology. FEMS Microbiol. Rev. 36, 893-916.

Manuel, C., Nunes, O., Melo, L., 2009. Unsteady state flow and stagnation in distribution systems affect the biological stability of drinking water. Biofouling 26, 129-139.

Manz, B., Volke, F., Goll, D., Horn, H., 2003. Measuring local flow velocities and biofilm structure in biofilm systems with magnetic resonance imaging (MRI). Biotechnol. Bioeng. 84, 424-432.

Marcato-Romain, C., Pechaud, Y., Paul, E., Girbal-Neuhauser, E., Dossat-Letisse, V., 2012. Removal of microbial multi-species biofilms from the paper industry by enzymatic treatments. Biofouling 28, 305-314.

March, J.C., Bentley, W.E., 2004. Quorum sensing and bacterial cross-talk in biotechnology. Curr. Opin. Biotechnol. 15, 495-502.

Marsden, A.E., Grudzinski, K., Ondrey, J.M., DeLoney-Marino, C.R., Visick, K.L., 2017. Impact of salt and nutrient content on biofilm formation by Vibrio fischeri. PLoS One 12, e0169521.

Mathee, K., Kharazmi, A., Høiby, N., 2002. Role of exopolysaccharide in biofilm matrix formation: the alginate paradigm. Molecular Ecology of Biofilms.Horizon Scientific Press, Norfolk, England , 23-55.

Matsukawa, M., Greenberg, E., 2004. Putative Exopolysaccharide Synthesis Genes Influence Pseudomonas Aeruginosa Biofilm Development. J Bacteriol (14):4449-56.

Matsukawa, M., Kunishima, Y., Takahashi, S., Takeyama, K., Tsukamoto, T., 2005. Bacterial colonization on intraluminal surface of urethral catheter. Urology 65, 440-444.

Mattick, J.S., 2002. Type IV pili and twitching motility. Annual Reviews in Microbiology 56, 289-314.

May, T., Okabe, S., 2008. Escherichia coli harboring a natural IncF conjugative F plasmid develops complex mature biofilms by stimulating synthesis of colanic acid and curli. J. Bacteriol. 190, 7479-7490.

McCoy, W., Bryers, J., Robbins, J., Costerton, J., 1981. Observations of fouling biofilm formation. Can. J. Microbiol. 27, 910-917.

McDonough, K.A., Rodriguez, A., 2012. The myriad roles of cyclic AMP in microbial pathogens: from signal to sword. Nature Reviews Microbiology 10, 27-38.

McGrath, S., Wade, D.S., Pesci, E.C., 2004. Dueling quorum sensing systems in Pseudomonas aeruginosa control the production of the Pseudomonas quinolone signal (PQS). FEMS Microbiol. Lett. 230, 27-34.

McKnight, S.L., Iglewski, B.H., Pesci, E.C., 2000. The Pseudomonas quinolone signal regulates rhl quorum sensing in Pseudomonas aeruginosa. J. Bacteriol. 182, 2702-2708.

McNally, L., Brown, S.P., 2015. Building the microbiome in health and disease: niche construction and social conflict in bacteria. Philosophical Transactions of the Royal Society B: Biological Sciences 370, 20140298.

Medina, G., Juárez, K., Soberón-Chávez, G., 2003. The Pseudomonas aeruginosa rhlAB operon is not expressed during the logarithmic phase of growth even in the presence of its activator RhlR and the autoinducer N-butyryl-homoserine lactone. J. Bacteriol. 185, 377-380.

Merighi, M., Lee, V.T., Hyodo, M., Hayakawa, Y., Lory, S., 2007. The second messenger bis-(3′-5′)-cyclic-GMP and its PilZ domain-containing receptor Alg44 are required for alginate biosynthesis in Pseudomonas aeruginosa. Mol. Microbiol. 65, 876-895.

Merritt, J.H., Brothers, K.M., Kuchma, S.L., O'toole, G.A., 2007. SadC Reciprocally Influences Biofilm Formation and Swarming Motility Via Modulation of Exopolysaccharide Production and Flagellar Function .

Merz, A.J., So, M., Sheetz, M.P., 2000. Pilus retraction powers bacterial twitching motility. Nature 407, 98-102.

Miller, E., Garcia, T., Hultgren, S., Oberhauser, A.F., 2006. The mechanical properties of E. coli type 1 pili measured by atomic force microscopy techniques. Biophys. J. 91, 3848-3856.

Miller, W.G., Leveau, J.H., Lindow, S.E., 2000. Improved gfp and inaZ broad-host-range promoter-probe vectors. Mol. Plant-Microbe Interact. 13, 1243-1250.

Moens, S., Vanderleyden, J., 1996. Functions of bacterial flagella. Crit. Rev. Microbiol. 22, 67-100.

Molin, S., Tolker-Nielsen, T., 2003. Gene transfer occurs with enhanced efficiency in biofilms and induces enhanced stabilisation of the biofilm structure. Curr. Opin. Biotechnol. 14, 255-261.

Momeni, B., Brileya, K.A., Fields, M.W., Shou, W., 2013. Strong inter-population cooperation leads to partner intermixing in microbial communities. Elife 2, e00230.

Monds, R.D., O'Toole, G.A., 2009. The developmental model of microbial biofilms: ten years of a paradigm up for review. Trends Microbiol. 17, 73-87.

Montanaro, L., Poggi, A., Visai, L., Ravaioli, S., Campoccia, D., Speziale, P., Arciola, C.R., 2011. Extracellular DNA in biofilms. Int. J. Artif. Organs 34, 824-831.

Moorthy, S., Keklak, J., Klein, E.A., 2016. Perspective: adhesion mediated signal transduction in bacterial pathogens. Pathogens 5, 23.

Moreira, C.G., Carneiro, S.M., Nataro, J.P., Trabulsi, L.R., Elias, W.P., 2003. Role of type I fimbriae in the aggregative adhesion pattern of enteroaggregative Escherichia coli. FEMS Microbiol. Lett. 226, 79-85.

Moreira, J.M., Gomes, L.C., Araújo, J.D., Miranda, J.M., Simões, M., Melo, L.F., Mergulhão, F.J., 2013. The effect of glucose concentration and shaking conditions on Escherichia coli biofilm formation in microtiter plates. Chemical Engineering Science 94, 192-199.

Moscoso, M., Claverys, J., 2004. Release of DNA into the medium by competent Streptococcus pneumoniae: kinetics, mechanism and stability of the liberated DNA. Mol. Microbiol. 54, 783-794.

Murakawa, T., 1973. Slime Production by Pseudomonas aeruginosa III. Purification of Slime and Its Physicochemical Properties. Jpn. J. Microbiol. 17, 273-281.

Murakawa, T., 1973. Slime Production by Pseudomonas aeruginosa: IV. Chemical Analysis of Two Varieties of Slime Produced by Pseudomonas aeruginosa. Jpn. J. Microbiol. 17, 513-520.

Muto, Y., Goto, S., 1986. Transformation by extracellular DNA produced by Pseudomonas aeruginosa. Microbiol. Immunol. 30, 621-628.

Nadal Jimenez, P., Koch, G., Thompson, J.A., Xavier, K.B., Cool, R.H., Quax, W.J., 2012. The multiple signaling systems regulating virulence in Pseudomonas aeruginosa. Microbiology and Molecular Biology Reviews 76, 46-65.

Nair, H.A., Periasamy, S., Yang, L., Kjelleberg, S., Rice, S.A., 2017. Real time, spatial, and temporal mapping of the distribution of c-di-GMP during biofilm development. J. Biol. Chem. 292, 477-487.

Navarro, M.V., De, N., Bae, N., Wang, Q., Sondermann, H., 2009. Structural analysis of the GGDEF-EAL domain-containing c-di-GMP receptor FimX. Structure 17, 1104-1116.

Naves, P., del Prado, G., Huelves, L., Gracia, M., Ruiz, V., Blanco, J., Dahbi, G., Blanco, M., del Carmen Ponte, M., Soriano, F., 2008. Correlation between virulence factors and in vitro biofilm formation by Escherichia coli strains. Microb. Pathog. 45, 86-91.

Nealson, K.H., Hastings, J.W., 1979. Bacterial bioluminescence: its control and ecological significance. Microbiol. Rev. 43, 496-518.

Nemoto, K., Hirota, K., Murakami, K., Taniguti, K., Murata, H., Viducic, D., Miyake, Y., 2003. Effect of Varidase (streptodornase) on biofilm formed by Pseudomonas aeruginosa. Chemotherapy 49, 121-125.

Nenninger, A.A., Robinson, L.S., Hultgren, S.J., 2009. Localized and efficient curli nucleation requires the chaperone-like amyloid assembly protein CsgF. Proc. Natl. Acad. Sci. U. S. A. 106, 900-905.

Nesse, L.L., Sekse, C., Berg, K., Johannesen, K.C., Solheim, H., Vestby, L.K., Urdahl, A.M., 2014. Potentially pathogenic Escherichia coli can form a biofilm under conditions relevant to the food production chain. Appl. Environ. Microbiol. 80, 2042-2049.

Newman, J.W., Floyd, R.V., Fothergill, J.L., 2017. The contribution of Pseudomonas aeruginosa virulence factors and host factors in the establishment of urinary tract infections. FEMS Microbiol. Lett. 364.

Nguyen, P.Q., Botyanszki, Z., Tay, P.K.R., Joshi, N.S., 2014. Programmable biofilm-based materials from engineered curli nanofibres. Nature Communications 5, 1-10.

Nguyen, V.T., Morgenroth, E., Eberl, H., 2005. A mesoscale model for hydrodynamics in biofilms that takes microscopic flow effects into account. Water Science and Technology 52, 167-172.

Nguyen, Y., Nguyen, N.X., Rogers, J.L., Liao, J., MacMillan, J.B., Jiang, Y., Sperandio, V., 2015. Structural and mechanistic roles of novel chemical ligands on the SdiA quorum-sensing transcription regulator. Mbio 6, e02429-14.

Nickel, J.C., Ruseska, I., Wright, J.B., Costerton, J.W., 1985. Tobramycin resistance of Pseudomonas aeruginosa cells growing as a biofilm on urinary catheter material. Antimicrob. Agents Chemother. 27, 619-624.

Nikolaev, Y.A., Plakunov, V., 2007. Biofilm—“City of microbes” or an analogue of multicellular organisms? Microbiology 76, 125-138.

Nivens, D.E., Ohman, D.E., Williams, J., Franklin, M.J., 2001. Role of alginate and its O acetylation in formation of Pseudomonas aeruginosa microcolonies and biofilms. J. Bacteriol. 183, 1047-1057.

Notley-McRobb, L., Death, A., Ferenci, T., 1997. The relationship between external glucose concentration and cAMP levels inside Escherichia coli: implications for models of phosphotransferase-mediated regulation of adenylate cyclase. Microbiology 143, 1909-1918.

Nowakowska, J., Landmann, R., Khanna, N., 2014. Foreign body infection models to study host-pathogen response and antimicrobial tolerance of bacterial biofilm. Antibiotics 3, 378-397.

O'Connor, J.R., Kuwada, N.J., Huangyutitham, V., Wiggins, P.A., Harwood, C.S., 2012. Surface sensing and lateral subcellular localization of WspA, the receptor in a chemosensory-like system leading to c-di-GMP production. Mol. Microbiol. 86, 720-729.

Ogasawara, H., Yamada, K., Kori, A., Yamamoto, K., Ishihama, A., 2010. Regulation of the Escherichia coli csgD promoter: interplay between five transcription factors. Microbiology 156, 2470-2483.

Oliveira, W., Silva, P., Silva, R., Silva, G., Machado, G., Coelho, L., Correia, M., 2018. Staphylococcus aureus and Staphylococcus epidermidis infections on implants. J. Hosp. Infect. 98, 111-117.

Olsén, A., Arnqvist, A., Hammar, M., rten, Sukupolvi, S., Normark, S., 1993. The RpoS sigma factor relieves H-NS-mediated transcriptional repression of csgA, the subunit gene of fibronectin-binding curli in Escherichia coli. Mol. Microbiol. 7, 523-536.

Ophir, T., Gutnick, D.L., 1994. A role for exopolysaccharides in the protection of microorganisms from desiccation. Appl. Environ. Microbiol. 60, 740-745.

Orndorff, P.E., Devapali, A., Palestrant, S., Wyse, A., Everett, M.L., Bollinger, R.R., Parker, W., 2004. Immunoglobulin-mediated agglutination of and biofilm formation by Escherichia coli K-12 require the type 1 pilus fiber. Infect. Immun. 72, 1929-1938.

Orr, M.W., Donaldson, G.P., Severin, G.B., Wang, J., Sintim, H.O., Waters, C.M., Lee, V.T., 2015. Oligoribonuclease is the primary degradative enzyme for pGpG in Pseudomonas aeruginosa that is required for cyclic-di-GMP turnover. Proc. Natl. Acad. Sci. U. S. A. 112, E5048-57.

O'Toole, G.A., Kolter, R., 1998. Flagellar and twitching motility are necessary for Pseudomonas aeruginosa biofilm development. Mol. Microbiol. 30, 295-304.

O'Toole, G.A., Kolter, R., 1998. Initiation of biofilm formation in Pseudomonas fluorescens WCS365 proceeds via multiple, convergent signalling pathways: a genetic analysis. Mol. Microbiol. 28, 449-461.

O'Toole, G., Kaplan, H.B., Kolter, R., 2000. Biofilm formation as microbial development. Annual Reviews in Microbiology 54, 49-79.

Otto, K., Silhavy, T.J., 2002. Surface sensing and adhesion of Escherichia coli controlled by the Cpx-signaling pathway. Proc. Natl. Acad. Sci. U. S. A. 99, 2287-2292.

Overhage, J., Schemionek, M., Webb, J.S., Rehm, B.H., 2005. Expression of the psl operon in Pseudomonas aeruginosa PAO1 biofilms: PslA performs an essential function in biofilm formation. Appl. Environ. Microbiol. 71, 4407-4413.

Palmer, J., Flint, S., Brooks, J., 2007. Bacterial cell attachment, the beginning of a biofilm. Journal of Industrial Microbiology and Biotechnology 34, 577-588.

Pande, S., Kaftan, F., Lang, S., Svatoš, A., Germerodt, S., Kost, C., 2016. Privatization of cooperative benefits stabilizes mutualistic cross-feeding interactions in spatially structured environments. The ISME Journal 10, 1413-1423.

Pannuri, A., Yakhnin, H., Vakulskas, C.A., Edwards, A.N., Babitzke, P., Romeo, T., 2012. Translational repression of NhaR, a novel pathway for multi-tier regulation of biofilm circuitry by CsrA. J. Bacteriol. 194, 79-89.

Park, A., Jeong, H., Lee, J., Kim, K.P., Lee, C., 2011. Effect of shear stress on the formation of bacterial biofilm in a microfluidic channel. BioChip Journal 5, 236.

Parsek, M.R., Greenberg, E., 2005. Sociomicrobiology: the connections between quorum sensing and biofilms. Trends Microbiol. 13, 27-33.

Parsek, M.R., Singh, P.K., 2003. Bacterial biofilms: an emerging link to disease pathogenesis. Annual Reviews in Microbiology 57, 677-701.

Partridge, J.D., Harshey, R.M., 2013. Swarming: flexible roaming plans. J. Bacteriol. 195, 909-918.

Pastar, I., Nusbaum, A.G., Gil, J., Patel, S.B., Chen, J., Valdes, J., Stojadinovic, O., Plano, L.R., Tomic-Canic, M., Davis, S.C., 2013. Interactions of methicillin resistant Staphylococcus aureus USA300 and Pseudomonas aeruginosa in polymicrobial wound infection. PloS One 8, e56846.

Paul, E., Ochoa, J.C., Pechaud, Y., Liu, Y., Liné, A., 2012. Effect of shear stress and growth conditions on detachment and physical properties of biofilms. Water Res. 46, 5499-5508.

Pawar, D., Rossman, M., Chen, J., 2005. Role of curli fimbriae in mediating the cells of enterohaemorrhagic Escherichia coli to attach to abiotic surfaces. J. Appl. Microbiol. 99, 418-425.

Payne, D.E., Boles, B.R., 2016. Emerging interactions between matrix components during biofilm development. Curr. Genet. 62, 137-141.

Paytubi, S., Cansado, C., Madrid, C., Balsalobre, C., 2017. Nutrient composition promotes switching between pellicle and bottom biofilm in Salmonella. Frontiers in Microbiology 8, 2160.

Pearson, J.P., Pesci, E.C., Iglewski, B.H., 1997. Roles of Pseudomonas aeruginosa las and rhl quorum-sensing systems in control of elastase and rhamnolipid biosynthesis genes. J. Bacteriol. 179, 5756-5767.

Pereira, M.O., Kuehn, M., Wuertz, S., Neu, T., Melo, L.F., 2002. Effect of flow regime on the architecture of a Pseudomonas fluorescens biofilm. Biotechnol. Bioeng. 78, 164-171.

Pérez, J.S., Porcel, E.R., López, J.C., Sevilla, J.F., Chisti, Y., 2006. Shear rate in stirred tank and bubble column bioreactors. Chem. Eng. J. 124, 1-5.

Periasamy, S., Nair, H.A., Lee, K.W., Ong, J., Goh, J.Q., Kjelleberg, S., Rice, S.A., 2015. Pseudomonas aeruginosa PAO1 exopolysaccharides are important for mixed species biofilm community development and stress tolerance. Frontiers in Microbiology 6, 851.

Perlman, R.L., Pastan, I., 1969. Pleiotropic deficiency of carbohydrate utilization in an adenyl cyclase deficient mutant of Escherichia coli. Biochem. Biophys. Res. Commun. 37, 151-157.

Perrin, C., Briandet, R., Jubelin, G., Lejeune, P., Mandrand-Berthelot, M., Rodrigue, A., Dorel, C., 2009. Nickel promotes biofilm formation by Escherichia coli K-12 strains that produce curli. Appl. Environ. Microbiol. 75, 1723-1733.

Pesci, E.C., Milbank, J.B., Pearson, J.P., McKnight, S., Kende, A.S., Greenberg, E.P., Iglewski, B.H., 1999. Quinolone signaling in the cell-to-cell communication system of Pseudomonas aeruginosa. Proc. Natl. Acad. Sci. U. S. A. 96, 11229-11234.

Pessi, G., Williams, F., Hindle, Z., Heurlier, K., Holden, M.T., Cámara, M., Haas, D., Williams, P., 2001. The global posttranscriptional regulator RsmA modulates production of virulence determinants and N-acylhomoserine lactones in Pseudomonas aeruginosa. J. Bacteriol. 183, 6676-6683.

Petrova, O.E., Cherny, K.E., Sauer, K., 2014. The Pseudomonas aeruginosa diguanylate cyclase GcbA, a homolog of P. fluorescens GcbA, promotes initial attachment to surfaces, but not biofilm formation, via regulation of motility. J. Bacteriol. 196, 2827-2841.

Petrova, O.E., Sauer, K., 2012. Sticky situations: key components that control bacterial surface attachment. J. Bacteriol. 194, 2413-2425.

Picioreanu, C., Van Loosdrecht, M.C., Heijnen, J.J., 1998. Mathematical modeling of biofilm structure with a hybrid differential-discrete cellular automaton approach. Biotechnol. Bioeng. 58, 101-116.

Pier, G.B., 1998. Pseudomonas aeruginosa: a key problem in cystic fibrosis. Asm News 64, 339-347.

Ping, L., 2010. The asymmetric flagellar distribution and motility of Escherichia coli. J. Mol. Biol. 397, 906-916.

Powell, L.C., Pritchard, M.F., Ferguson, E.L., Powell, K.A., Patel, S.U., Rye, P.D., Sakellakou, S., Buurma, N.J., Brilliant, C.D., Copping, J.M., 2018. Targeted disruption of the extracellular polymeric network of Pseudomonas aeruginosa biofilms by alginate oligosaccharides. NPJ Biofilms and Microbiomes 4, 1-10.

Pratt, L.A., Kolter, R., 1999. Genetic analyses of bacterial biofilm formation. Curr. Opin. Microbiol. 2, 598-603.

Pratt, L.A., Kolter, R., 1998. Genetic analysis of Escherichia coli biofilm formation: roles of flagella, motility, chemotaxis and type I pili. Mol. Microbiol. 30, 285-293.

Pratt, L.A., Silhavy, T.J., 1998. Crl stimulates RpoS activity during stationary phase. Mol. Microbiol. 29, 1225-1236.

Prigent-Combaret, C., Brombacher, E., Vidal, O., Ambert, A., Lejeune, P., Landini, P., Dorel, C., 2001. Complex regulatory network controls initial adhesion and biofilm formation in Escherichia coli via regulation of the csgD gene. J. Bacteriol. 183, 7213-7223.

Prigent-Combaret, C., Lejeune, P., 1999. [4] Monitoring gene expression in biofilms. Meth. Enzymol. 310, 56-79.

Prigent-Combaret, C., Prensier, G., Le Thi, T.T., Vidal, O., Lejeune, P., Dorel, C., 2000. Developmental pathway for biofilm formation in curli-producing Escherichia coli strains: role of flagella, curli and colanic acid. Environ. Microbiol. 2, 450-464.

Prigent-Combaret, C., Vidal, O., Dorel, C., Lejeune, P., 1999. Abiotic surface sensing and biofilm-dependent regulation of gene expression in Escherichia coli. J. Bacteriol. 181, 5993-6002.

Proctor, V.A., Cunningham, F., Fung, D.Y., 1988. The chemistry of lysozyme and its use as a food preservative and a pharmaceutical. Critical Reviews in Food Science & Nutrition 26, 359-395.

Purevdorj-Gage, B., Costerton, W., Stoodley, P., 2005. Phenotypic differentiation and seeding dispersal in non-mucoid and mucoid Pseudomonas aeruginosa biofilms. Microbiology 151, 1569-1576.

Qi, Y., Chuah, M.L.C., Dong, X., Xie, K., Luo, Z., Tang, K., Liang, Z., 2011. Binding of cyclic diguanylate in the non-catalytic EAL domain of FimX induces a long-range conformational change. J. Biol. Chem. 286, 2910-2917.

Qin, Z., Ou, Y., Yang, L., Zhu, Y., Tolker-Nielsen, T., Molin, S., Qu, D., 2007. Role of autolysin-mediated DNA release in biofilm formation of Staphylococcus epidermidis. Microbiology 153, 2083-2092.

Raina, S., Vizio, D.D., Odell, M., Clements, M., Vanhulle, S., Keshavarz, T., 2009. Microbial quorum sensing: a tool or a target for antimicrobial therapy? Biotechnol. Appl. Biochem. 54, 65-84.

Raivio, T.L., Silhavy, T.J., 1997. Transduction of envelope stress in Escherichia coli by the Cpx two-component system. J. Bacteriol. 179, 7724-7733.

Ramsey, D.M., Wozniak, D.J., 2005. Understanding the control of Pseudomonas aeruginosa alginate synthesis and the prospects for management of chronic infections in cystic fibrosis. Mol. Microbiol. 56, 309-322.

Ramsey, M.M., Whiteley, M., 2004. Pseudomonas aeruginosa attachment and biofilm development in dynamic environments. Mol. Microbiol. 53, 1075-1087.

Rao, F., Yang, Y., Qi, Y., Liang, Z., 2008. Catalytic mechanism of cyclic di-GMP-specific phosphodiesterase: a study of the EAL domain-containing RocR from Pseudomonas aeruginosa. J. Bacteriol. 190, 3622-3631.

Rashid, M.H., Kornberg, A., 2000. Inorganic polyphosphate is needed for swimming, swarming, and twitching motilities of Pseudomonas aeruginosa. Proc. Natl. Acad. Sci. U. S. A. 97, 4885-4890.

Rasmussen, B., 2000. Filamentous microfossils in a 3,235-million-year-old volcanogenic massive sulphide deposit. Nature 405, 676-679.

Reading, N.C., Rasko, D.A., Torres, A.G., Sperandio, V., 2009. The two-component system QseEF and the membrane protein QseG link adrenergic and stress sensing to bacterial pathogenesis. Proc. Natl. Acad. Sci. U. S. A. 106, 5889-5894.

Reichhardt, C., Jacobs, H.M., Matwichuk, M., Wong, C., Wozniak, D.J., Parsek, M.R., 2020. The versatile Pseudomonas aeruginosa biofilm matrix protein CdrA promotes aggregation through different extracellular exopolysaccharide interactions. J. Bacteriol. 202, e00216-20.

Reichhardt, C., Wong, C., Passos da Silva, D., Wozniak, D.J., Parsek, M.R., 2018. CdrA interactions within the Pseudomonas aeruginosa biofilm matrix safeguard it from proteolysis and promote cellular packing. Mbio 9, e01376-18.

Reisner, A., Haagensen, J.A., Schembri, M.A., Zechner, E.L., Molin, S., 2003. Development and maturation of Escherichia coli K-12 biofilms. Mol. Microbiol. 48, 933-946.

Reisner, A., Krogfelt, K.A., Klein, B.M., Zechner, E.L., Molin, S., 2006. In vitro biofilm formation of commensal and pathogenic Escherichia coli strains: impact of environmental and genetic factors. J. Bacteriol. 188, 3572-3581.

Ren, D., Bedzyk, L.A., Ye, R.W., Thomas, S.M., Wood, T.K., 2004. Stationary-phase quorum-sensing signals affect autoinducer-2 and gene expression in Escherichia coli. Appl. Environ. Microbiol. 70, 2038-2043.

Repoila, F., Gottesman, S., 2001. Signal transduction cascade for regulation of RpoS: temperature regulation of DsrA. J. Bacteriol. 183, 4012-4023.

Reysenbach, A., Cady, S.L., 2001. Microbiology of ancient and modern hydrothermal systems. Trends Microbiol. 9, 79-86.

Ribeiro, M., Monteiro, F.J., Ferraz, M.P., 2012. Infection of orthopedic implants with emphasis on bacterial adhesion process and techniques used in studying bacterial-material interactions. Biomatter 2, 176-194.

Rice, S.A., Tan, C.H., Mikkelsen, P.J., Kung, V., Woo, J., Tay, M., Hauser, A., McDougald, D., Webb, J.S., Kjelleberg, S., 2009. The biofilm life cycle and virulence of Pseudomonas aeruginosa are dependent on a filamentous prophage. The ISME Journal 3, 271-282.

Rickard, A.H., Gilbert, P., High, N.J., Kolenbrander, P.E., Handley, P.S., 2003. Bacterial coaggregation: an integral process in the development of multi-species biofilms. Trends Microbiol. 11, 94-100.

Riedel, K., Hentzer, M., Geisenberger, O., Huber, B., Steidle, A., Wu, H., Høiby, N., Givskov, M., Molin, S., Eberl, L., 2001. N-acylhomoserine-lactone-mediated communication between Pseudomonas aeruginosa and Burkholderia cepacia in mixed biofilms. Microbiology 147, 3249-3262.

Robbe-Saule, V., Jaumouillé, V., Prévost, M., Guadagnini, S., Talhouarne, C., Mathout, H., Kolb, A., Norel, F., 2006. Crl activates transcription initiation of RpoS-regulated genes involved in the multicellular behavior of Salmonella enterica serovar Typhimurium. J. Bacteriol. 188, 3983-3994.

Rocchetta, H.L., Pacan, J.C., Lam, J.S., 1998. Synthesis of the A-band polysaccharide sugar d-rhamnose requires Rmd and WbpW: identification of multiple AlgA homologues, WbpW and ORF488, in Pseudomonas aeruginosa. Mol. Microbiol. 29, 1419-1434.

Rochex, A., Godon, J., Bernet, N., Escudié, R., 2008. Role of shear stress on composition, diversity and dynamics of biofilm bacterial communities. Water Res. 42, 4915-4922.

Røder, H.L., Sørensen, S.J., Burmølle, M., 2016. Studying bacterial multispecies biofilms: where to start? Trends Microbiol. 24, 503-513.

Rodesney, C.A., Roman, B., Dhamani, N., Cooley, B.J., Katira, P., Touhami, A., Gordon, V.D., 2017. Mechanosensing of shear by Pseudomonas aeruginosa leads to increased levels of the cyclic-di-GMP signal initiating biofilm development. Proc. Natl. Acad. Sci. U. S. A. 114, 5906-5911.

Roehling, S., Astasov-Frauenhoffer, M., Hauser-Gerspach, I., Braissant, O., Woelfler, H., Waltimo, T., Kniha, H., Gahlert, M., 2017. In vitro biofilm formation on titanium and zirconia implant surfaces. J. Periodontol. 88, 298-307.

Romeo, T., Preiss, J., 1989. Genetic regulation of glycogen biosynthesis in Escherichia coli: in vitro effects of cyclic AMP and guanosine 5'-diphosphate 3'-diphosphate and analysis of in vivo transcripts. J. Bacteriol. 171, 2773-2782.

Römling, U., Galperin, M.Y., 2015. Bacterial cellulose biosynthesis: diversity of operons, subunits, products, and functions. Trends Microbiol. 23, 545-557.

Römling, U., Galperin, M.Y., Gomelsky, M., 2013. Cyclic di-GMP: the first 25 years of a universal bacterial second messenger. Microbiology and Molecular Biology Reviews 77, 1-52.

Ross, P., Weinhouse, H., Aloni, Y., Michaeli, D., Weinberger-Ohana, P., Mayer, R., Braun, S., De Vroom, E., Van der Marel, G., Van Boom, J., 1987. Regulation of cellulose synthesis in Acetobacter xylinum by cyclic diguanylic acid. Nature 325, 279-281.

Ross, P., Mayer, R., Benziman, M., 1991. Cellulose biosynthesis and function in bacteria. Microbiol. Rev. 55, 35-58.

Roux, D., Cywes-Bentley, C., Zhang, Y., Pons, S., Konkol, M., Kearns, D.B., Little, D.J., Howell, P.L., Skurnik, D., Pier, G.B., 2015. Identification of poly-N-acetylglucosamine as a major polysaccharide component of the Bacillus subtilis biofilm matrix. J. Biol. Chem. 290, 19261-19272.

Ruer, S., Stender, S., Filloux, A., de Bentzmann, S., 2007. Assembly of fimbrial structures in Pseudomonas aeruginosa: functionality and specificity of chaperone-usher machineries. J. Bacteriol. 189, 3547-3555.

Rühs, P.A., Böni, L., Fuller, G.G., Inglis, R.F., Fischer, P., 2013. In-situ quantification of the interfacial rheological response of bacterial biofilms to environmental stimuli. PLoS One 8, e78524.

Rumbaugh, K.P., Sauer, K., 2020. Biofilm dispersion. Nature Reviews Microbiology 18, 571-586.

Rusconi, R., Lecuyer, S., Guglielmini, L., Stone, H.A., 2010. Laminar flow around corners triggers the formation of biofilm streamers. Journal of the Royal Society Interface 7, 1293-1299.

Russo, F.D., Silhavy, T.J., 1991. EnvZ controls the concentration of phosphorylated OmpR to mediate osmoregulation of the porin genes. J. Mol. Biol. 222, 567-580.

Russotto, V., Cortegiani, A., Raineri, S.M., Giarratano, A., 2015. Bacterial contamination of inanimate surfaces and equipment in the intensive care unit. Journal of Intensive Care 3, 1-8.

Ryder, C., Byrd, M., Wozniak, D.J., 2007. Role of polysaccharides in Pseudomonas aeruginosa biofilm development. Curr. Opin. Microbiol. 10, 644-648.

Ryjenkov, D.A., Tarutina, M., Moskvin, O.V., Gomelsky, M., 2005. Cyclic diguanylate is a ubiquitous signaling molecule in bacteria: insights into biochemistry of the GGDEF protein domain. J. Bacteriol. 187, 1792-1798.

S Majik, M., T Parvatkar, P., 2014. Next generation biofilm inhibitors for Pseudomonas aeruginosa: synthesis and rational design approaches. Current Topics in Medicinal Chemistry 14, 81-109.

Sailer, F.C., Meberg, B.M., Young, K.D., 2003. β-Lactam induction of colanic acid gene expression in Escherichia coli. FEMS Microbiol. Lett. 226, 245-249.

Sakuragi, Y., Kolter, R., 2007. Quorum-sensing regulation of the biofilm matrix genes (pel) of Pseudomonas aeruginosa. J. Bacteriol. 189, 5383-5386.

Salek, M.M., Jones, S.M., Martinuzzi, R.J., 2009. The influence of flow cell geometry related shear stresses on the distribution, structure and susceptibility of Pseudomonas aeruginosa 01 biofilms. Biofouling 25, 711-725.

Santos, André Luis Souza dos, Galdino, A.C.M., Mello, T.P.d., Ramos, L.d.S., Branquinha, M.H., Bolognese, A.M., Columbano Neto, J., Roudbary, M., 2018. What are the advantages of living in a community? A microbial biofilm perspective! Memórias do Instituto Oswaldo Cruz 113.

Sastry, P.A., Finlay, B.B., Pasloske, B.L., Paranchych, W., Pearlstone, J.R., Smillie, L.B., 1985. Comparative studies of the amino acid and nucleotide sequences of pilin derived from Pseudomonas aeruginosa PAK and PAO. J. Bacteriol. 164, 571-577.

Sauer, F.G., Mulvey, M.A., Schilling, J.D., Martinez, J.J., Hultgren, S.J., 2000. Bacterial pili: molecular mechanisms of pathogenesis. Curr. Opin. Microbiol. 3, 65-72.

Sauer, K., Camper, A.K., Ehrlich, G.D., Costerton, J.W., Davies, D.G., 2002. Pseudomonas Aeruginosa Displays Multiple Phenotypes during Development as a Biofilm. J Bacteriol. (4):1140-54

Saur, T., Morin, E., Habouzit, F., Bernet, N., Escudié, R., 2017. Impact of wall shear stress on initial bacterial adhesion in rotating annular reactor. PloS One 12, e0172113.

Schembri, M.A., Dalsgaard, D., Klemm, P., 2004. Capsule shields the function of short bacterial adhesins. J. Bacteriol. 186, 1249-1257.

Schembri, M.A., Hjerrild, L., Gjermansen, M., Klemm, P., 2003. Differential expression of the Escherichia coli autoaggregation factor antigen 43. J. Bacteriol. 185, 2236-2242.

Schilling, J.D., Martin, S.M., Hunstad, D.A., Patel, K.P., Mulvey, M.A., Justice, S.S., Lorenz, R.G., Hultgren, S.J., 2003. CD14-and Toll-like receptor-dependent activation of bladder epithelial cells by lipopolysaccharide and type 1 piliated Escherichia coli. Infect. Immun. 71, 1470-1480.

Schindelin, J., Arganda-Carreras, I., Frise, E., Kaynig, V., Longair, M., Pietzsch, T., Preibisch, S., Rueden, C., Saalfeld, S., Schmid, B., 2012. Fiji: an open-source platform for biological-image analysis. Nature Methods 9, 676-682.

Schmidt, A.J., Ryjenkov, D.A., Gomelsky, M., 2005. The ubiquitous protein domain EAL is a cyclic diguanylate-specific phosphodiesterase: enzymatically active and inactive EAL domains. J. Bacteriol. 187, 4774-4781.

Schmidt, J., Müsken, M., Becker, T., Magnowska, Z., Bertinetti, D., Möller, S., Zimmermann, B., Herberg, F.W., Jänsch, L., Häussler, S., 2011. The Pseudomonas aeruginosa chemotaxis methyltransferase CheR1 impacts on bacterial surface sampling. PloS One 6, e18184.

Schuster, M., Hawkins, A.C., Harwood, C.S., Greenberg, E., 2004. The Pseudomonas aeruginosa RpoS regulon and its relationship to quorum sensing. Mol. Microbiol. 51, 973-985.

Schwartz, K., Stephenson, R., Hernandez, M., Jambang, N., Boles, B.R., 2010. The use of drip flow and rotating disk reactors for Staphylococcus aureus biofilm analysis. JoVE (Journal of Visualized Experiments) , e2470.

Semmler, A.B., Whitchurch, C.B., Mattick, J.S., 1999. A re-examination of twitching motility in Pseudomonas aeruginosa. Microbiology 145, 2863-2873.

Serra, D.O., Hengge, R., 2014. Stress responses go three dimensional–the spatial order of physiological differentiation in bacterial macrocolony biofilms. Environ. Microbiol. 16, 1455-1471.

Serra, D.O., Richter, A.M., Klauck, G., Mika, F., Hengge, R., 2013. Microanatomy at cellular resolution and spatial order of physiological differentiation in a bacterial biofilm. Mbio 4, e00103-13.

Shaw, T., Winston, M., Rupp, C.J., Klapper, I., Stoodley, P., 2004. Commonality of elastic relaxation times in biofilms. Phys. Rev. Lett. 93, 098102.

Shimada, T., Shimada, K., Matsui, M., Kitai, Y., Igarashi, J., Suga, H., Ishihama, A., 2014. Roles of cell division control factor SdiA: recognition of quorum sensing signals and modulation of transcription regulation targets. Genes to Cells 19, 405-418.

Shrout, J.D., Chopp, D.L., Just, C.L., Hentzer, M., Givskov, M., Parsek, M.R., 2006. The impact of quorum sensing and swarming motility on Pseudomonas aeruginosa biofilm formation is nutritionally conditional. Mol. Microbiol. 62, 1264-1277.

Silverman, P.M., Clarke, M.B., 2010. New insights into F-pilus structure, dynamics, and function. Integrative Biology 2, 25-31.

Simm, R., Morr, M., Kader, A., Nimtz, M., Römling, U., 2004. GGDEF and EAL domains inversely regulate cyclic di-GMP levels and transition from sessility to motility. Mol. Microbiol. 53, 1123-1134.

Singh, S., Singh, S.K., Chowdhury, I., Singh, R., 2017. Understanding the Mechanism of Bacterial Biofilms Resistance to Antimicrobial Agents. Open Microbiol. J. 11, 53-62.

Siryaporn, A., Kuchma, S.L., O'Toole, G.A., Gitai, Z., 2014. Surface attachment induces Pseudomonas aeruginosa virulence. Proc. Natl. Acad. Sci. U. S. A. 111, 16860-16865.

Skerker, J.M., Berg, H.C., 2001. Direct observation of extension and retraction of type IV pili. Proc. Natl. Acad. Sci. U. S. A. 98, 6901-6904.

Skjåk-Bræk, G., Zanetti, F., Paoletti, S., 1989. Effect of acetylation on some solution and gelling properties of alginates. Carbohydr. Res. 185, 131-138.

Sledjeski, D.D., Gottesman, S., 1996. Osmotic shock induction of capsule synthesis in Escherichia coli K-12. J. Bacteriol. 178, 1204-1206.

Smith, D.R., Price, J.E., Burby, P.E., Blanco, L.P., Chamberlain, J., Chapman, M.R., 2017. The production of curli amyloid fibers is deeply integrated into the biology of Escherichia coli. Biomolecules 7, 75.

Smyth, C.J., Marron, M.B., Twohig, J.M., Smith, S.G., 1996. Fimbrial adhesins: similarities and variations in structure and biogenesis. FEMS Immunology & Medical Microbiology 16, 127-139.

Son, M.S., Taylor, R.K., 2012. Growth and maintenance of Escherichia coli laboratory strains. Current Protocols in Microbiology 27, 5A. 4.1-5A. 4.9.

Sønderholm, M., Koren, K., Wangpraseurt, D., Jensen, P.Ø., Kolpen, M., Kragh, K.N., Bjarnsholt, T., Kühl, M., 2018. Tools for studying growth patterns and chemical dynamics of aggregated Pseudomonas aeruginosa exposed to different electron acceptors in an alginate bead model. NPJ Biofilms and Microbiomes 4, 1-11.

Sousa, A.M., Pereira, M.O., 2014. Pseudomonas aeruginosa diversification during infection development in cystic fibrosis lungs—a review. Pathogens 3, 680-703.

Soutourina, O., Kolb, A., Krin, E., Laurent-Winter, C., Rimsky, S., Danchin, A., Bertin, P., 1999. Multiple control of flagellum biosynthesis in Escherichia coli: role of H-NS protein and the cyclic AMP-catabolite activator protein complex in transcription of the flhDC master operon. J. Bacteriol. 181, 7500-7508.

Soutourina, O.A., Bertin, P.N., 2003. Regulation cascade of flagellar expression in Gram-negative bacteria. FEMS Microbiol. Rev. 27, 505-523.

Sperandio, V., Torres, A.G., Girón, J.A., Kaper, J.B., 2001. Quorum sensing is a global regulatory mechanism in enterohemorrhagic Escherichia coli O157: H7. J. Bacteriol. 183, 5187-5197.

Sperandio, V., Torres, A.G., Kaper, J.B., 2002. Quorum sensing Escherichia coli regulators B and C (QseBC): a novel two-component regulatory system involved in the regulation of flagella and motility by quorum sensing in E. coli. Mol. Microbiol. 43, 809-821.

Sperandio, V., Torres, A.G., Jarvis, B., Nataro, J.P., Kaper, J.B., 2003. Bacteria-host communication: the language of hormones. Proc. Natl. Acad. Sci. U. S. A. 100, 8951-8956.

Spoering, A.L., Lewis, K., 2001. Biofilms and planktonic cells of Pseudomonas aeruginosa have similar resistance to killing by antimicrobials. J. Bacteriol. 183, 6746-6751.

Srey, S., Jahid, I.K., Ha, S., 2013. Biofilm formation in food industries: a food safety concern. Food Control 31, 572-585.

Standar, K., Kreikemeyer, B., Redanz, S., Münter, W.L., Laue, M., Podbielski, A., 2010. Setup of an in vitro test system for basic studies on biofilm behavior of mixed-species cultures with dental and periodontal pathogens. PLoS One 5, e13135.

Stanley, N.R., Britton, R.A., Grossman, A.D., Lazazzera, B.A., 2003. Identification of catabolite repression as a physiological regulator of biofilm formation by Bacillus subtilis by use of DNA microarrays. J. Bacteriol. 185, 1951-1957.

Stapper, A.P., Narasimhan, G., Ohman, D.E., Barakat, J., Hentzer, M., Molin, S., Kharazmi, A., Høiby, N., Mathee, K., 2004. Alginate production affects Pseudomonas aeruginosa biofilm development and architecture, but is not essential for biofilm formation. J. Med. Microbiol. 53, 679-690.

Starkey, M., Hickman, J.H., Ma, L., Zhang, N., De Long, S., Hinz, A., Palacios, S., Manoil, C., Kirisits, M.J., Starner, T.D., 2009. Pseudomonas aeruginosa rugose small-colony variants have adaptations that likely promote persistence in the cystic fibrosis lung. J. Bacteriol. 191, 3492-3503.

Stella, S., Falconi, M., Lammi, M., Gualerzi, C.O., Pon, C.L., 2006. Environmental control of the in vivo oligomerization of nucleoid protein H-NS. J. Mol. Biol. 355, 169-174.

Stevenson, G., Lan, R., Reeves, P.R., 2000. The colanic acid gene cluster of Salmonella enterica has a complex history. FEMS Microbiol. Lett. 191, 11-16.

Stevenson, G., Andrianopoulos, K., Hobbs, M., Reeves, P.R., 1996. Organization of the Escherichia coli K-12 gene cluster responsible for production of the extracellular polysaccharide colanic acid. J. Bacteriol. 178, 4885-4893.

Stewart, P.S., Costerton, J.W., 2001. Antibiotic resistance of bacteria in biofilms. The Lancet 358, 135-138.

Stewart, P.S., Franklin, M.J., 2008. Physiological heterogeneity in biofilms. Nature Reviews Microbiology 6, 199-210.

Stoodley, P., DeBeer, D., Lewandowski, Z., 1994. Liquid flow in biofilm systems. Appl. Environ. Microbiol. 60, 2711-2716.

Stoodley, P., Lewandowski, Z., Boyle, J.D., Lappin-Scott, H.M., 1999. Structural deformation of bacterial biofilms caused by short-term fluctuations in fluid shear: An in situ investigation of biofilm rheology. Biotechnol. Bioeng. 65, 83-92.

Stoodley, P., Purevdorj-Gage, B., Costerton, J.W., 2005. Clinical significance of seeding dispersal in biofilms: a response. Microbiology 151, 3453-3453.

Stoodley, P., Sauer, K., Davies, D.G., Costerton, J.W., 2002. Biofilms as complex differentiated communities. Annual Reviews in Microbiology 56, 187-209.

Stranden, A.M., Ehlert, K., Labischinski, H., Berger-Bachi, B., 1997. Cell wall monoglycine cross-bridges and methicillin hypersusceptibility in a femAB null mutant of methicillin-resistant Staphylococcus aureus. J. Bacteriol. 179, 9-16.

Studier, F.W., 2005. Protein production by auto-induction in high-density shaking cultures. Protein Expr. Purif. 41, 207-234.

Su, T., Liu, S., Wang, K., Chi, K., Zhu, D., Wei, T., Huang, Y., Guo, L., Hu, W., Xu, S., 2015. The REC domain mediated dimerization is critical for FleQ from Pseudomonas aeruginosa to function as a c-di-GMP receptor and flagella gene regulator. J. Struct. Biol. 192, 1-13.

Sutherland, I.W., 2001. Biofilm exopolysaccharides: a strong and sticky framework. Microbiology 147, 3-9.

Suzuki, K., Wang, X., Weilbacher, T., Pernestig, A., Melefors, O., Georgellis, D., Babitzke, P., Romeo, T., 2002. Regulatory circuitry of the CsrA/CsrB and BarA/UvrY systems of Escherichia coli. J. Bacteriol. 184, 5130-5140.

Taga, M.E., Bassler, B.L., 2003. Chemical communication among bacteria. Proc. Natl. Acad. Sci. U. S. A. 100 Suppl 2, 14549-14554.

Tagami, H., Inada, T., Kunimura, T., Aiba, H., 1995. Glucose lowers CRP* levels resulting in repression of the lac operon in cells lacking cAMP. Mol. Microbiol. 17, 251-258.

Tal, R., Wong, H.C., Calhoon, R., Gelfand, D., Fear, A.L., Volman, G., Mayer, R., Ross, P., Amikam, D., Weinhouse, H., 1998. Three cdg operons control cellular turnover of cyclic di-GMP in Acetobacter xylinum: genetic organization and occurrence of conserved domains in isoenzymes. J. Bacteriol. 180, 4416-4425.

Tarutina, M., Ryjenkov, D.A., Gomelsky, M., 2006. An unorthodox bacteriophytochrome from Rhodobacter sphaeroides involved in turnover of the second messenger c-di-GMP. J. Biol. Chem. 281, 34751-34758.

Taylor, C.D., Wirsen, C.O., Gaill, F., 1999. Rapid microbial production of filamentous sulfur mats at hydrothermal vents. Appl. Environ. Microbiol. 65, 2253-2255.

Taylor, P.K., Yeung, A.T., Hancock, R.E., 2014. Antibiotic resistance in Pseudomonas aeruginosa biofilms: towards the development of novel anti-biofilm therapies. J. Biotechnol. 191, 121-130.

Telgmann, U., Horn, H., Morgenroth, E., 2004. Influence of growth history on sloughing and erosion from biofilms. Water Res. 38, 3671-3684.

Teodosio, J.S., Silva, F.C., Moreira, J.M., Simões, M., Melo, L.F., Alves, M.A., Mergulhão, F.J., 2013. Flow cells as quasi-ideal systems for biofouling simulation of industrial piping systems. Biofouling 29, 953-966.

Teodósio, J., Simões, M., Melo, L., Mergulhão, F., 2011. Flow cell hydrodynamics and their effects on E. coli biofilm formation under different nutrient conditions and turbulent flow. Biofouling 27, 1-11.

Teodósio, J., Simões, M., Mergulhao, F., 2012. The influence of nonconjugative Escherichia coli plasmids on biofilm formation and resistance. J. Appl. Microbiol. 113, 373-382.

Thallinger, B., Prasetyo, E.N., Nyanhongo, G.S., Guebitz, G.M., 2013. Antimicrobial enzymes: an emerging strategy to fight microbes and microbial biofilms. Biotechnology Journal 8, 97-109.

Thanassi, D.G., Hultgren, S.J., 2000. Multiple pathways allow protein secretion across the bacterial outer membrane. Curr. Opin. Cell Biol. 12, 420-430.

Thomas, W.E., Trintchina, E., Forero, M., Vogel, V., Sokurenko, E.V., 2002. Bacterial adhesion to target cells enhanced by shear force. Cell 109, 913-923.

Tolker-Nielsen, T., Molin, S., 2000. Spatial organization of microbial biofilm communities. Microb. Ecol. 40, 75-84.

Toutain, C.M., Caizza, N.C., Zegans, M.E., O'Toole, G.A., 2007. Roles for flagellar stators in biofilm formation by Pseudomonas aeruginosa. Res. Microbiol. 158, 471-477.

Toutain, C.M., Zegans, M.E., O'Toole, G.A., 2005. Evidence for two flagellar stators and their role in the motility of Pseudomonas aeruginosa. J. Bacteriol. 187, 771-777.

Tran, P.L., Hamood, A.N., de Souza, A., Schultz, G., Liesenfeld, B., Mehta, D., Reid, T.W., 2015. A study on the ability of quaternary ammonium groups attached to a polyurethane foam wound dressing to inhibit bacterial attachment and biofilm formation. Wound Repair and Regeneration 23, 74-81.

Tsai, Y., 2005. Impact of flow velocity on the dynamic behaviour of biofilm bacteria. Biofouling 21, 267-277.

Tsoligkas, A.N., Winn, M., Bowen, J., Overton, T.W., Simmons, M.J., Goss, R.J., 2011. Engineering biofilms for biocatalysis. Chembiochem 12, 1391-1395.

Tümmler, B., Kiewitz, C., 1999. Cystic fibrosis: an inherited susceptibility to bacterial respiratory infections. Mol. Med. Today 5, 351-358.

Tuson, H.H., Weibel, D.B., 2013. Bacteria–surface interactions. Soft Matter 9, 4368-4380.

Ude, S., Arnold, D.L., Moon, C.D., Timms-Wilson, T., Spiers, A.J., 2006. Biofilm formation and cellulose expression among diverse environmental Pseudomonas isolates. Environ. Microbiol. 8, 1997-2011.

Ueda, A., Wood, T.K., 2009. Connecting quorum sensing, c-di-GMP, pel polysaccharide, and biofilm formation in Pseudomonas aeruginosa through tyrosine phosphatase TpbA (PA3885). PLoS Pathog 5, e1000483.

Uhlich, G.A., Chen, C., Cottrell, B.J., Nguyen, L., 2014. Growth media and temperature effects on biofilm formation by serotype O157: H7 and non-O157 Shiga toxin-producing Escherichia coli. FEMS Microbiol. Lett. 354, 133-141.

Ulett, G.C., Valle, J., Beloin, C., Sherlock, O., Ghigo, J., Schembri, M.A., 2007. Functional analysis of antigen 43 in uropathogenic Escherichia coli reveals a role in long-term persistence in the urinary tract. Infect. Immun. 75, 3233-3244.

Urch, J.E., Hurtado-Guerrero, R., Brosson, D., Liu, Z., Eijsink, V.G., Texier, C., van Aalten, D.M., 2009. Structural and functional characterization of a putative polysaccharide deacetylase of the human parasite Encephalitozoon cuniculi. Protein Science 18, 1197-1209.

Valentini, M., Filloux, A., 2016. Biofilms and cyclic di-GMP (c-di-GMP) signaling: lessons from Pseudomonas aeruginosa and other bacteria. J. Biol. Chem. 291, 12547-12555.

Vallet, I., Olson, J.W., Lory, S., Lazdunski, A., Filloux, A., 2001. The chaperone/usher pathways of Pseudomonas aeruginosa: identification of fimbrial gene clusters (cup) and their involvement in biofilm formation. Proc. Natl. Acad. Sci. U. S. A. 98, 6911-6916.

Van Delden, C., Iglewski, B.H., 1998. Cell-to-cell signaling and Pseudomonas aeruginosa infections. Emerging Infectious Diseases 4, 551.

Van der Woude, Marjan W, Henderson, I.R., 2008. Regulation and function of Ag43 (flu). Annu. Rev. Microbiol. 62.

Van Houdt, R., Aertsen, A., Moons, P., Vanoirbeek, K., Michiels, C.W., 2006. N-acyl-L-homoserine lactone signal interception by Escherichia coli. FEMS Microbiol. Lett. 256, 83-89.

Van Loosdrecht, M.C., Picioreanu, C., Heijnen, J.J., 1997. A more unifying hypothesis for biofilm structures. FEMS Microbiol. Ecol. 24, 181-183.

Vasseur, P., Vallet-Gely, I., Soscia, C., Genin, S., Filloux, A., 2005. The pel genes of the Pseudomonas aeruginosa PAK strain are involved at early and late stages of biofilm formation. Microbiology 151, 985-997.

Veerachamy, S., Yarlagadda, T., Manivasagam, G., Yarlagadda, P.K., 2014. Bacterial adherence and biofilm formation on medical implants: a review. Proc. Inst. Mech. Eng. Part H J. Eng. Med. 228, 1083-1099.

Vendeville, A., Winzer, K., Heurlier, K., Tang, C.M., Hardie, K.R., 2005. Making'sense'of metabolism: autoinducer-2, LuxS and pathogenic bacteria. Nature Reviews Microbiology 3, 383-396.

Venturi, V., 2006. Regulation of quorum sensing in Pseudomonas. FEMS Microbiol. Rev. 30, 274-291.

Vergidis, P., Patel, R., 2012. Novel approaches to the diagnosis, prevention, and treatment of medical device-associated infections. Infect. Dis. Clin. North Am. 26, 173-186.

Vianney, A., Jubelin, G., Renault, S., Dorel, C., Lejeune, P., Lazzaroni, J.C., 2005. Escherichia coli tol and rcs genes participate in the complex network affecting curli synthesis. Microbiology 151, 2487-2497.

Vidal, O., Longin, R., Prigent-Combaret, C., Dorel, C., Hooreman, M., Lejeune, P., 1998. Isolation of an Escherichia coli K-12 mutant strain able to form biofilms on inert surfaces: involvement of a new ompR allele that increases curli expression. J. Bacteriol. 180, 2442-2449.

Vieira, M., Melo, L., 1999. Intrinsic kinetics of biofilms formed under turbulent flow and low substrate concentrations. Bioprocess Eng. 20, 369-375.

Vishwakarma, V., 2020. Impact of environmental biofilms: Industrial components and its remediation. J. Basic Microbiol. 60, 198-206.

Von Bodman, S.B., Willey, J.M., Diggle, S.P., 2008. Cell-cell communication in bacteria: united we stand. J. Bacteriol. 190, 4377-4391.

Vonderviszt, F., Namba, K., 2008. Structure, function and assembly of flagellar axial proteins. Fibrous Proteins , 58-76.

Wade, D.S., Calfee, M.W., Rocha, E.R., Ling, E.A., Engstrom, E., Coleman, J.P., Pesci, E.C., 2005. Regulation of Pseudomonas quinolone signal synthesis in Pseudomonas aeruginosa. J. Bacteriol. 187, 4372-4380.

Wagner, V.E., Bushnell, D., Passador, L., Brooks, A.I., Iglewski, B.H., 2003. Microarray analysis of Pseudomonas aeruginosa quorum-sensing regulons: effects of growth phase and environment. J. Bacteriol. 185, 2080-2095.

Waldron, D.E., Owen, P., Dorman, C.J., 2002. Competitive interaction of the OxyR DNA-binding protein and the Dam methylase at the antigen 43 gene regulatory region in Escherichia coli. Mol. Microbiol. 44, 509-520.

Wallecha, A., Correnti, J., Munster, V., van der Woude, M., 2003. Phase variation of Ag43 is independent of the oxidation state of OxyR. J. Bacteriol. 185, 2203-2209.

Walters III, M.C., Roe, F., Bugnicourt, A., Franklin, M.J., Stewart, P.S., 2003. Contributions of antibiotic penetration, oxygen limitation, and low metabolic activity to tolerance of Pseudomonas aeruginosa biofilms to ciprofloxacin and tobramycin. Antimicrob. Agents Chemother. 47, 317-323.

Walters, M., Sperandio, V., 2006. Quorum sensing in Escherichia coli and Salmonella. International Journal of Medical Microbiology 296, 125-131.

Wang, R., 2019. Biofilms and meat safety: a mini-review. J. Food Prot. 82, 120-127.

Wang, R., Kalchayanand, N., Schmidt, J.W., Harhay, D.M., 2013. Mixed biofilm formation by Shiga toxin–producing Escherichia coli and Salmonella enterica serovar Typhimurium enhanced bacterial resistance to sanitization due to extracellular polymeric substances. J. Food Prot. 76, 1513-1522.

Wang, S., Liu, X., Liu, H., Zhang, L., Guo, Y., Yu, S., Wozniak, D.J., Ma, L.Z., 2015. The exopolysaccharide Psl–eDNA interaction enables the formation of a biofilm skeleton in P seudomonas aeruginosa. Environmental Microbiology Reports 7, 330-340.

Wang, S., Parsek, M.R., Wozniak, D.J., Ma, L.Z., 2013. A spider web strategy of type IV pili-mediated migration to build a fibre-like Psl polysaccharide matrix in P seudomonas aeruginosa biofilms. Environ. Microbiol. 15, 2238-2253.

Wang, S., Yu, S., Zhang, Z., Wei, Q., Yan, L., Ai, G., Liu, H., Ma, L.Z., 2014. Coordination of swarming motility, biosurfactant synthesis, and biofilm matrix exopolysaccharide production in Pseudomonas aeruginosa. Appl. Environ. Microbiol. 80, 6724-6732.

Wang, X., Dubey, A.K., Suzuki, K., Baker, C.S., Babitzke, P., Romeo, T., 2005. CsrA post-transcriptionally represses pgaABCD, responsible for synthesis of a biofilm polysaccharide adhesin of Escherichia coli. Mol. Microbiol. 56, 1648-1663.

Wang, X., Preston III, J.F., Romeo, T., 2004. The pgaABCD locus of Escherichia coli promotes the synthesis of a polysaccharide adhesin required for biofilm formation. J. Bacteriol. 186, 2724-2734.

Wang, Y., Hong, X., Liu, J., Zhu, J., Chen, J., 2020. Interactions between fish isolates Pseudomonas fluorescens and Staphylococcus aureus in dual-species biofilms and sensitivity to carvacrol. Food Microbiol. 91, 103506.

Wang, Y.A., Yu, X., Silverman, P.M., Harris, R.L., Egelman, E.H., 2009. The structure of F-pili. J. Mol. Biol. 385, 22-29.

Wang, Z., Xiang, Q., Yang, T., Li, L., Yang, J., Li, H., He, Y., Zhang, Y., Lu, Q., Yu, J., 2016. Autoinducer-2 of Streptococcus mitis as a target molecule to inhibit pathogenic multi-species biofilm formation in vitro and in an endotracheal intubation rat model. Frontiers in Microbiology 7, 88.

Waters, C.M., Bassler, B.L., 2005. Quorum sensing: cell-to-cell communication in bacteria. Annu. Rev. Cell Dev. Biol. 21, 319-346.

Watnick, P.I., Kolter, R., 1999. Steps in the development of a Vibrio cholerae El Tor biofilm. Mol. Microbiol. 34, 586-595.

Watnick, P., Kolter, R., 2000. Biofilm, city of microbes. J. Bacteriol. 182, 2675-2679.

Wei, Q., Ma, L.Z., 2013. Biofilm matrix and its regulation in Pseudomonas aeruginosa. International Journal of Molecular Sciences 14, 20983-21005.

Weigel, W., Demuth, D., 2016. Qse BC, a two-component bacterial adrenergic receptor and global regulator of virulence in Enterobacteriaceae and Pasteurellaceae. Molecular Oral Microbiology 31, 379-397.

Wenzel, R.P., 2007. Health care–associated infections: major issues in the early years of the 21st century. Clinical Infectious Diseases 45, S85-S88.

Westall, F., de Wit, M.J., Dann, J., van der Gaast, S., de Ronde, C.E., Gerneke, D., 2001. Early Archean fossil bacteria and biofilms in hydrothermally-influenced sediments from the Barberton greenstone belt, South Africa. Precambrian Res. 106, 93-116.

Whitchurch, C.B., Tolker-Nielsen T FARagas, P.,C., Ragas, P.C., Mattick, J.S., 2002. Extracellular DNA required for bacterial biofilm formation. Science 295, 1487.

White, A., Gibson, D., Kim, W., Kay, W., Surette, M., 2006. Thin aggregative fimbriae and cellulose enhance long-term survival and persistence of Salmonella. J. Bacteriol. 188, 3219-3227.

Whiteley, M., Greenberg, E., 2001. Promoter specificity elements in Pseudomonas aeruginosa quorum-sensing-controlled genes. J. Bacteriol. 183, 5529-5534.

White-Ziegler, C.A., Um, S., Perez, N.M., Berns, A.L., Malhowski, A.J., Young, S., 2008. Low temperature (23 C) increases expression of biofilm-, cold-shock-and RpoS-dependent genes in Escherichia coli K-12. Microbiology 154, 148-166.

Whitfield, C., Roberts, I.S., 1999. Structure, assembly and regulation of expression of capsules in Escherichia coli. Mol. Microbiol. 31, 1307-1319.

Whitney, J.C., Colvin, K.M., Marmont, L.S., Robinson, H., Parsek, M.R., Howell, P.L., 2012. Structure of the cytoplasmic region of PelD, a degenerate diguanylate cyclase receptor that regulates exopolysaccharide production in Pseudomonas aeruginosa. J. Biol. Chem. 287, 23582-23593.

Williams, P., 2007. Quorum sensing, communication and cross-kingdom signalling in the bacterial world. Microbiology 153, 3923-3938.

Williams, P., Cámara, M., 2009. Quorum sensing and environmental adaptation in Pseudomonas aeruginosa: a tale of regulatory networks and multifunctional signal molecules. Curr. Opin. Microbiol. 12, 182-191.

Wilson, D.R., Beveridge, T.J., 1993. Bacterial flagellar filaments and their component flagellins. Can. J. Microbiol. 39, 451-472.

Wilton, M., Charron-Mazenod, L., Moore, R., Lewenza, S., 2016. Extracellular DNA acidifies biofilms and induces aminoglycoside resistance in Pseudomonas aeruginosa. Antimicrob. Agents Chemother. 60, 544-553.

Winsor, G.L., Griffiths, E.J., Lo, R., Dhillon, B.K., Shay, J.A., Brinkman, F.S., 2016. Enhanced annotations and features for comparing thousands of Pseudomonas genomes in the Pseudomonas genome database. Nucleic Acids Res. 44, D646-D653.

Winzer, K., Falconer, C., Garber, N.C., Diggle, S.P., Camara, M., Williams, P., 2000. The Pseudomonas aeruginosa lectins PA-IL and PA-IIL are controlled by quorum sensing and by RpoS. J. Bacteriol. 182, 6401-6411.

Wood, T.L., Gong, T., Zhu, L., Miller, J., Miller, D.S., Yin, B., Wood, T.K., 2018. Rhamnolipids from Pseudomonas aeruginosa disperse the biofilms of sulfate-reducing bacteria. NPJ Biofilms and Microbiomes 4, 1-8.

Wood, T.K., Barrios, A.F.G., Herzberg, M., Lee, J., 2006. Motility influences biofilm architecture in Escherichia coli. Appl. Microbiol. Biotechnol. 72, 361-367.

Wozniak, D.J., Wyckoff, T.J., Starkey, M., Keyser, R., Azadi, P., O'Toole, G.A., Parsek, M.R., 2003. Alginate is not a significant component of the extracellular polysaccharide matrix of PA14 and PAO1 Pseudomonas aeruginosa biofilms. Proc. Natl. Acad. Sci. U. S. A. 100, 7907-7912.

Wu, C., Lin, C., Wu, C., Peng, W., Lee, M., Tsai, Y., 2015. Inhibitory effect of Lactobacillus salivarius on Streptococcus mutans biofilm formation. Molecular Oral Microbiology 30, 16-26.

Xavier, K.B., Bassler, B.L., 2005. Regulation of uptake and processing of the quorum-sensing autoinducer AI-2 in Escherichia coli. J. Bacteriol. 187, 238-248.

Xavier, K.B., Miller, S.T., Lu, W., Kim, J.H., Rabinowitz, J., Pelczer, I., Semmelhack, M.F., Bassler, B.L., 2007. Phosphorylation and processing of the quorum-sensing molecule autoinducer-2 in enteric bacteria. ACS Chemical Biology 2, 128-136.

Xavier, J.B., Foster, K.R., 2007. Cooperation and conflict in microbial biofilms. Proc. Natl. Acad. Sci. U. S. A. 104, 876-881.

Yamamoto, K., Hirao, K., Oshima, T., Aiba, H., Utsumi, R., Ishihama, A., 2005. Functional characterization in vitro of all two-component signal transduction systems from Escherichia coli. J. Biol. Chem. 280, 1448-1456.

Yang, L., Barken, K.B., Skindersoe, M.E., Christensen, A.B., Givskov, M., Tolker-Nielsen, T., 2007. Effects of iron on DNA release and biofilm development by Pseudomonas aeruginosa. Microbiology 153, 1318-1328.

Yang, L., Hu, Y., Liu, Y., Zhang, J., Ulstrup, J., Molin, S., 2011. Distinct roles of extracellular polymeric substances in Pseudomonas aeruginosa biofilm development. Environ. Microbiol. 13, 1705-1717.

Yang, L., Rybtke, M.T., Jakobsen, T.H., Hentzer, M., Bjarnsholt, T., Givskov, M., Tolker-Nielsen, T., 2009. Computer-aided identification of recognized drugs as Pseudomonas aeruginosa quorum-sensing inhibitors. Antimicrob. Agents Chemother. 53, 2432-2443.

Yao, Y., Martinez-Yamout, M.A., Dickerson, T.J., Brogan, A.P., Wright, P.E., Dyson, H.J., 2006. Structure of the Escherichia coli quorum sensing protein SdiA: activation of the folding switch by acyl homoserine lactones. J. Mol. Biol. 355, 262-273.

Zanaroli, G., Negroni, A., Calisti, C., Ruzzi, M., Fava, F., 2011. Selection of commercial hydrolytic enzymes with potential antifouling activity in marine environments. Enzyme Microb. Technol. 49, 574-579.

Zhang, G., Gurtu, V., Kain, S.R., 1996. An enhanced green fluorescent protein allows sensitive detection of gene transfer in mammalian cells. Biochem. Biophys. Res. Commun. 227, 707-711.

Zhao, K., Tseng, B.S., Beckerman, B., Jin, F., Gibiansky, M.L., Harrison, J.J., Luijten, E., Parsek, M.R., Wong, G.C., 2013. Psl trails guide exploration and microcolony formation in Pseudomonas aeruginosa biofilms. Nature 497, 388-391.

Zheng, D., Constantinidou, C., Hobman, J.L., Minchin, S.D., 2004. Identification of the CRP regulon using in vitro and in vivo transcriptional profiling. Nucleic Acids Res. 32, 5874-5893.

Zhu, J., Yan, Y., Wang, Y., Qu, D., 2019. Competitive interaction on dual-species biofilm formation by spoilage bacteria, Shewanella baltica and Pseudomonas fluorescens. J. Appl. Microbiol. 126, 1175-1186.

Zijnge, V., van Leeuwen, M Barbara M, Degener, J.E., Abbas, F., Thurnheer, T., Gmür, R., M. Harmsen, H.J., 2010. Oral biofilm architecture on natural teeth. PloS One 5, e9321.

Zimmerli, W., Trampuz, A., Ochsner, P.E., 2004. Prosthetic-joint infections. N. Engl. J. Med. 351, 1645-1654.

Zobell, C.E., 1943. The Effect of Solid Surfaces upon Bacterial Activity. J. Bacteriol. 46, 39-56.

Zogaj, X., Nimtz, M., Rohde, M., Bokranz, W., Römling, U., 2001. The multicellular morphotypes of Salmonella typhimurium and Escherichia coli produce cellulose as the second component of the extracellular matrix. Mol. Microbiol. 39, 1452-1463.

Zweig, M., Schork, S., Koerdt, A., Siewering, K., Sternberg, C., Thormann, K., Albers, S., Molin, S., van der Does, C., 2014. Secreted single-stranded DNA is involved in the initial phase of biofilm formation by N eisseria gonorrhoeae. Environ. Microbiol. 16, 1040-1052.